GENESIS OF THE IGNEOUS ROCK SUITE OF GRENADA, LESSER ANTILLES

Alastair Macleod Graham M.A.(Cantab)

Thesis submitted for the degree of

Doctor of Philosophy

University of Edinburgh

1980

DECLARATION

I hereby declare that this thesis has been composed by myself, and that the work contained is my own, except where specifically stated.

Alastair Graham

28.i.80

ABSTRACT

The Grenada igneous rock suite comprises extrusive rocks, coarse-grained, gabbroic cumulate blocks, and peridotite nodules. The extrusive rocks include a variety of basalts and basaltic andesites, together with andesites and dacites. Two basaltic series are distinguished in major and trace element chemistry. The generally microphyric, M-series basalts include picritic types close in composition to primary partial melts of peridotite. The porphyritic, C-series basalts have major element chemistry consistent with derivation by olivine fractionation from these primitive compositions.

The major element variation is explicable by fractionation of phenocryst phases. Ne-normative M-series parents fractionated olivine, clinopyroxene, and spinel at high pressures, producing Hy-normative derivatives. Both basaltic series are parental to andesites, amphibole fractionation being restricted to the origin of these evolved magmas. Trace element abundances are highly variable, and cannot be products of variable partial melting and crystallisation processes, a heterogeneous source being required. Different sources are required for the two basaltic series. Combined chemical data and published isotopic analyses are interpreted in a model of variable contamination of the mantle source by a component, rich in water and incompatible elements, derived from the subducted lithosphere. This component may include a contribution from sediments as well as from subducted oceanic crust.

Olivine-bearing cumulates have mineral assemblages and compositions indicative of equilibrium crystallisation from M-series magmas, producing basaltic andesite residua. Olivine-free cumulates equilibrated with andesitic residual liquids. Combined thermodynamic calculations and experimental studies indicate cumulate crystallisation at 0.5 to 6 kbar and 900°-1000°C, at high oxygen and water activities.

Peridotite nodules in M-series basalts are interpreted as accidental inclusions of depleted mantle material.

Comparison of the chemical data with those from other islands in the Lesser Antilles and other arcs suggests that, although differing in trace element and isotopic compositions, probably as a result of differing source chemistries, many island arc suites are products of fractionation of picritic magmas. The eruption of these in Grenada may reflect unusual thermal characteristics in the underlying mantle, or unusually high melt water contents.

CONTENTS

CONTENTS (cont.)

CONTENTS (cont.)

CONTENTS (cont.)

CONTENTS (cont.)

TABLES

TABLES (cont.)

FIGURES

FIGURES (cont.)

PLATES

CHAPTER 1

INTRODUCTION

1.1 Regional geological setting and petrological studies

The island of Grenada lies at the southernmost end of the Lesser Antilles island arc, which forms the eastern boundary to the Caribbean Sea (Figure 1.1.1). The arc itself is composite, comprising an older, outer arc (Limestone Caribbees) and a younger, inner arc (Volcanic Caribbees). Islands of the older arc contain volcanic rocks of Eocene to Miocene age, together with minor sedimentary and intrusive rocks, which are capped by Miocene limestones. Islands of the younger arc are composed of Miocene to Recent volcanic rocks (Briden et al., 1979). South of Martinique the two arcs are superimposed, and outcrop is dominated by the Miocene to Recent volcanics.

To the west of the Lesser Antilles arc lies the Grenada Basin, which is itself bounded to the west by the Aves Ridge. Granitic rocks of mid-Cretaceous to Palaeocene age, and volcanic rocks ranging from basalt to dacite, have been dredged from this structure (Fox et al., 1971; Nagle, 1972) which appears to represent an extinct volcanic arc. To the east of the Lesser Antilles lies the Barbados Ridge, a thick pile of deformed Eocene to Miocene sediments, overlain by limestones.

The volcanism of the Lesser Antilles is believed to be related to the presence of a destructive plate margin to the east of the arc. The trench topography at the northern end of the arc is progressively obscured southwards by the sediments of the Barbados Ridge, but convincing evidence for the presence of a plate margin comes from the high seismicity of a zone dipping westwards beneath the arc, the top of which has been estimated to lie at depths of 100-120 km beneath the younger arc (Tomblin, 1975). The exact form of this seismic zone is not yet well constrained. The rate of subduction along the destructive

Figure 1.1.1 Map of the Lesser Antilles island arc.

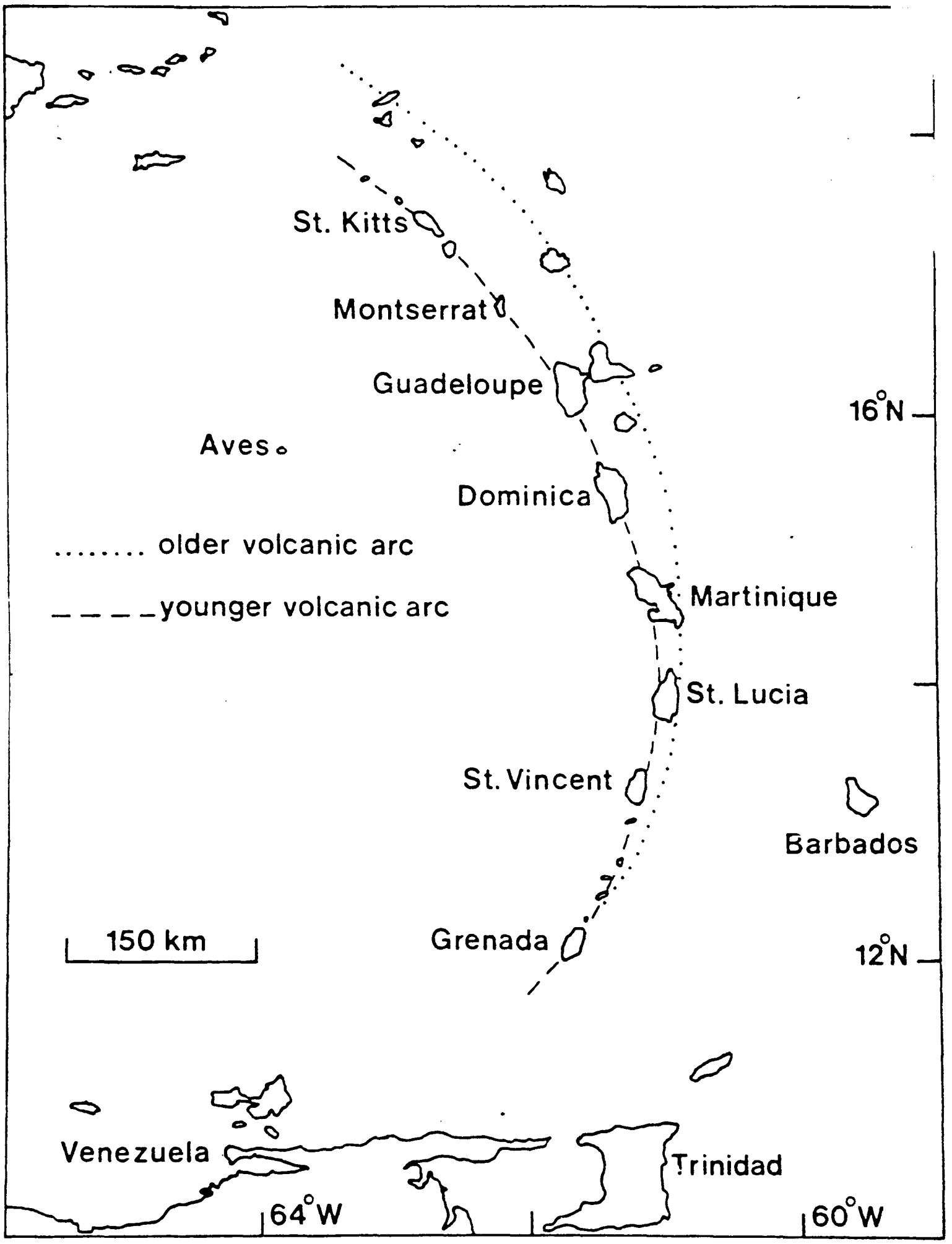

margin is not known precisely but has been estimated, by Molnar and Sykes (1969) and Westbrook (1975), at 0.5 cm per year. The margin is bounded to both north and south by complex transform fault systems (Molnar and Sykes, 1969).

Extensive research into the volcanic rocks of the younger arc has been carried out in British universities. Baker (1963), Lewis (1964), Tomblin (1964), Rea (1970), Arculus (1973), and Wills (1974) studied the geology and petrology of many of the major islands and main volcanic centres. Important contributions to the petrological knowledge of the arc have also been made by other workers, notably Gunn et al. (1974) and Rowley (1978). A regional study of the chemistry of the younger volcanics has been carried out by Brown et al. (1977), and isotopic studies have been published by Hedge and Lewis (1971), Donnelly et al. (1971), Pushkar et al. (1973), and Hawkesworth et al. (1979).

A good summary of the regional geology and petrology is to be found in Tomblin (1975).

1.2 Geology of Grenada

The volcanic geology and petrology of Grenada were studied extensively by Arculus (1973), and only a few summary details are given here. The Miocene to Recent volcanic rocks (Briden et al., 1979) are underlain by the tectonically disturbed Tufton Hall Formation (Martin-Kaye, 1969). This comprises a sequence of Eocene to Miocene, well-bedded calcareous shales, siltstones, and sandstones, with volcanoclastic horizons becoming more prominent in strata of lower Oligocene age. Minerals of volcanic origin, particularly amphiboles, sector- and oscillatory-zoned clinopyroxenes and oscillatory-zoned plagioclases, were noted in these horizons by Arculus (1973) and indicate that the pre-Miocene volcanism in Grenada was similar in character to that of

the Miocene to Recent period. Some marine limestones are also present in the basement to the volcanics.

The volcanic rocks of Grenada were assigned by Arculus (1973) to a number of eruptive centres (Figure 1.2.1), the ages of which have been estimated by K-Ar dating (Briden et al., 1979) and by the degree of their dissection (Arculus, 1973). Rock types range from a variety of basalts to andesites and dacites. Lava flows, domes, and pyroclastic rocks are present; rapid erosion of the latter was responsible for most of the abundant reworked material which forms much of the surface outcrop. Exposure is poor, and the high topographic relief combines with this to prevent close stratigraphic control of the volcanics being established. The reworked volcanics contain cumulus plutonic blocks similar to those of the Soufriere, St. Vincent (Wager, 1962; Lewis, 1973) and of other islands (Wills, 1974).

The most recent volcanic activity in Grenada has produced a series of scoria cones and explosion craters. No eruptions have been recorded in historic times but the submarine volcano Kick 'em-Jenny, 8 km north of Grenada, has erupted several times this century (Sigurdsson and Shepherd, 1974).

1.3 Aims of study

The younger volcanic centres of the Lesser Antilles are notable for the occurrence of cumulus plutonic blocks (Lewis, 1973; Wills, 1974), which are believed to represent the products of magmatic crystallisation at depth. The large amounts of published chemical and mineralogical data from previous studies of many of the volcanic centres provided an excellent opportunity to study possible fractionation relationships between these cumulates and their associated extrusive rocks. Of particular interest are the fractionation mechanisms responsible for the

Figure 1.2.1

(from Arculus, 1976)

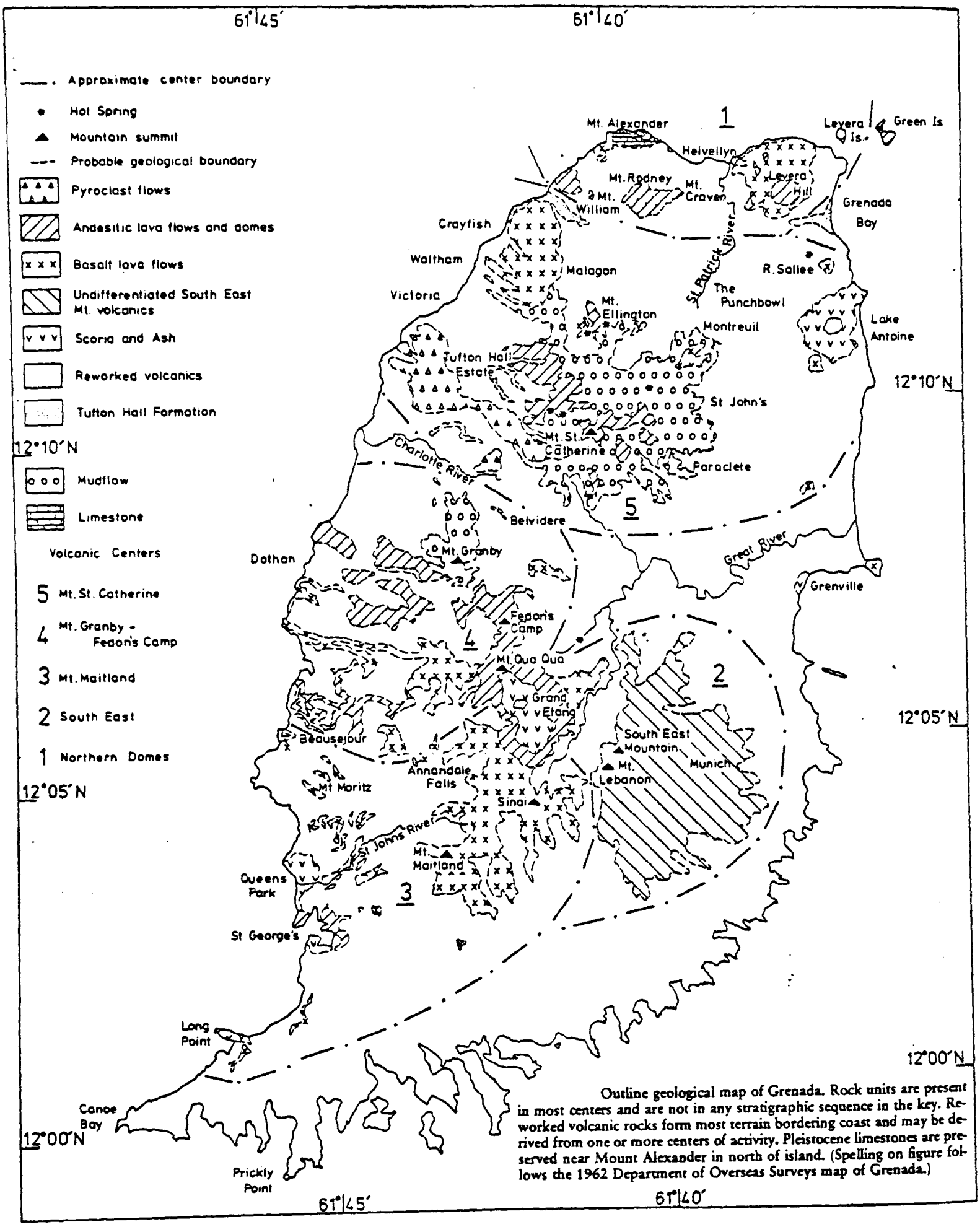

Outline geological map of Grenada. Rock units are present in most centers and are not in any stratigraphic sequence in the key. Reworked volcanic rocks form most terrain bordering coast and may be derived from one or more centers of activity. Pleistocene limestones are preserved near Mount Alexander in north of island. (Spelling on figure follows the 1962 Department of Overseas Surveys map of Grenada.)

Volcanic centres decrease in age from 1 to 5.

chemical variation of the extrusive rocks, and the physical conditions of crystallisation of the cumulates, especially the influences of pressure and volatile components. It was intended to use experimental hydrous melting studies of extrusive rocks to reproduce the phase-relations deduced from study of the cumulate blocks. Estimated conditions of crystallisation could then be compared with the results of thermodynamic analysis of equilibria involving the cumulate phases. Microprobe analyses of the experimentally-produced liquidus phases could be used to model the chemical evolution of the extrusive rock suites from different centres in the arc.

Grenada provided a particularly interesting starting point for such a study because of the unusual occurrence of undersaturated basic lavas, which appear to be genetically related to typical calc-alkaline andesites and dacites (Sigurdsson et al., 1973; Arculus, 1973). This relationship involves a transition from nepheline-normative to hypersthene-normative basaltic compositions (Cawthorn et al., 1973; Arculus, 1976).

Unfortunately, re-analysis of some of the powdered samples studied by Arculus (1973), which were to be used as starting materials for experimental work, revealed serious discrepancies between the major element analyses and those in Arculus' study. Examples are shown in Figure 1.3.1. The scope of the project therefore had to be modified, since the chemical data on which the modelling of fractionation was to be based were clearly unreliable. The revised aims of the study were therefore:

(1) to revise and reinterpret the geochemistry of the extrusive rocks

(2) to study the petrology, mineral chemistry, and conditions of crystallisation of the cumulate blocks

(3) to investigate the relationships between the cumulate blocks and the extrusive rocks, using chemical and experimental petrological

Figure 1.3.1 Comparisons of X.R.F. analyses of major elements.

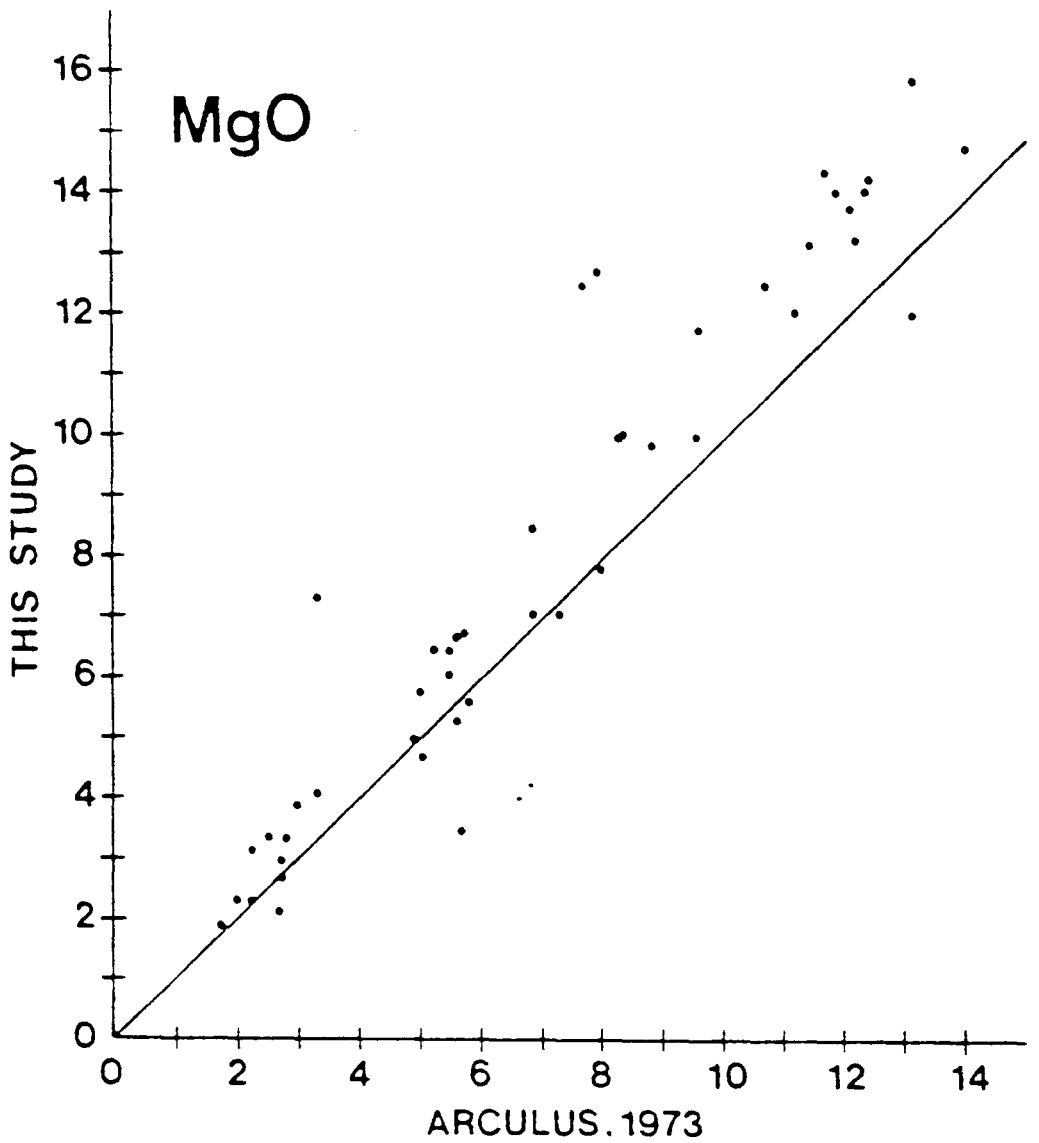

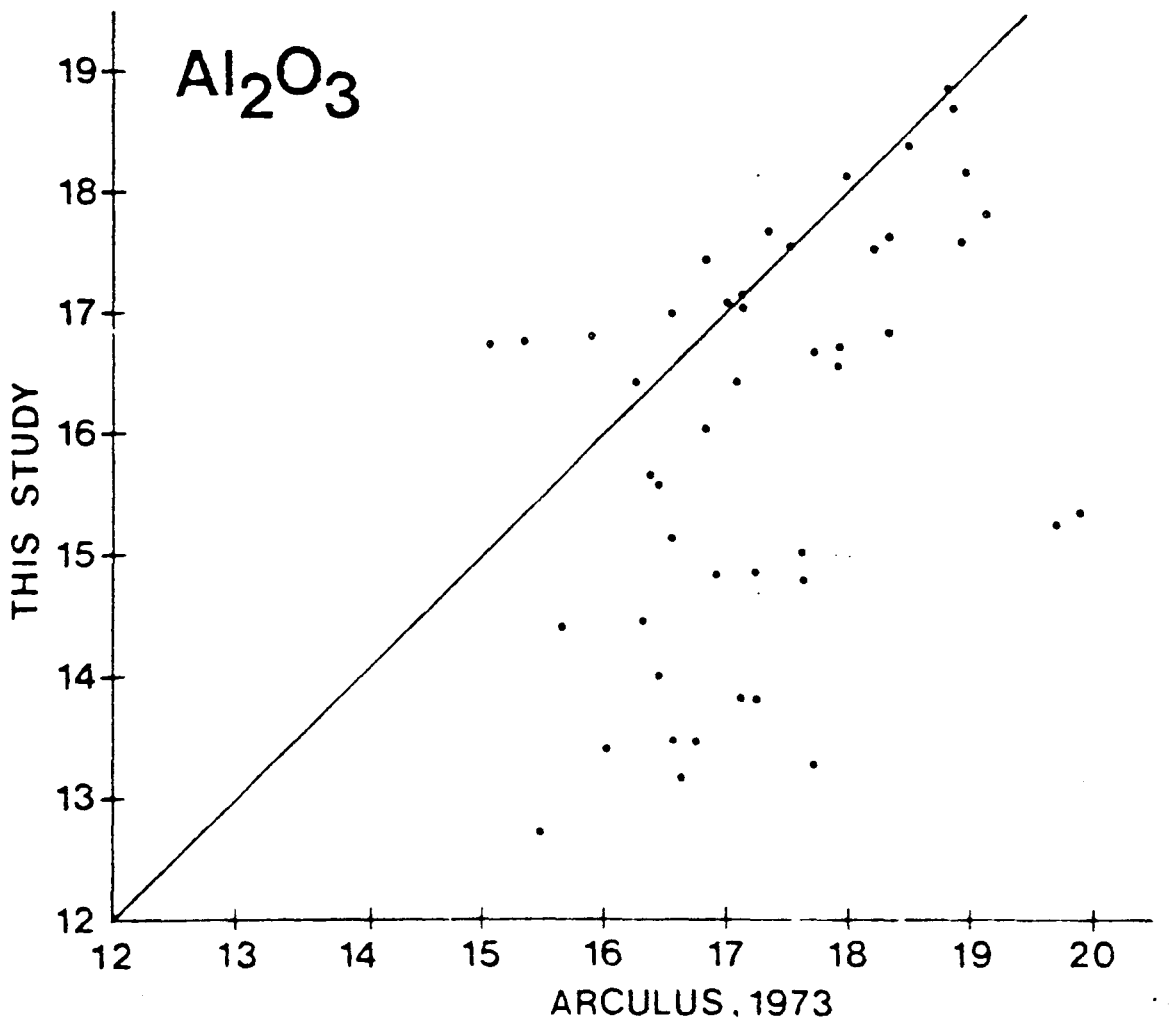

data, and

(4) to formulate an integrated model for the genesis of the Grenada igneous rock suite.

1.4 Extrusive rocks : sampling and classification

Over one hundred cumulate blocks, together with some extrusive rock samples, were collected from Grenada by the writer in February and March 1978. A small collection of cumulates was also made from the nearby Grenadine island of Carriacou, whose geology has been described by Jackson (1970). Additionally, a few samples of Grenada cumulates from the collection at the Seismic Research Unit, University of the West Indies, Trinidad, were studied. Spinel peridotite nodules, discovered by the writer in a recent basalt scoria cone on Grenada, were also sampled.

The revision of the chemistry of the extrusive rocks has been based largely on analyses of splits of the powders prepared by Arculus. These were supplemented by powders prepared by the writer from a few of Arculus' original rock samples, twelve samples collected by the writer (prefixed 6) and six of the Grenada rocks analysed by Tomblin (1968) (prefixed X). The samples were therefore largely selected on the basis of their availability. This deficiency is compensated for by the availability of Nd and Sr isotopic data, and isotope dilution rare earth element data, on many of Arculus' samples, allowing maximum correlation of these with the accurate chemical data obtained in this study. Regrettably, the great majority of the rock samples from Arculus' collection were no longer available, preventing full correlation between the data sets. Thin sections of many of the samples studied here are, however, present in the University of Durham collection.

The samples analysed in this study cover all the eruptive centres

(Figure 1.2.1) except the Northern Domes. They are, therefore, unlikely to be directly related genetically, but no significant chemical differences between samples from different centres are apparent from the data collected. A list of the samples used in this study, and their locations, is to be found in Appendix D.

The discrepancies between the major element data sets of Arculus (1973) and this study are, as can be seen from Figure 1.3.1, serious. In view of the precision and accuracy estimated for the analyses in this study (Appendix B), most of which were obtained using the same powders as Arculus, it seems likely that the X.R.F. method used by him is responsible. He analysed major elements using pressed powder discs, and employed an iterative computer procedure to make mass absorption corrections to the data. The poor results produced may be largely a reflection on this method. The accuracy and precision of Arculus' trace element data are also comparatively poor, the discrepancies between the data sets suggesting that, in a few cases, this may have been compounded by misidentification of samples. Since Brown et al. (1977) used the same X.R.F. method in their study, the accuracy of their data must be in doubt, although the differences between islands described by them are supported by other data and are believed to be real.

A wide range of extrusive rock types is present in Grenada (Arculus, 1973, 1976). For simplification purposes, the following, silica-based, chemical classification is used in this thesis for the extrusive rocks:

< 52% SiO_2	basalt
52 - 56% SiO_2	basaltic andesite
56 - 62% SiO_2	andesite
> 62% SiO_2	dacite

No rocks with greater than 65% silica are believed to be present in the Grenada suite.

The classification of Grenada volcanic rocks is discussed further in Chapter 2.

A list of the abbreviations and symbols used in this thesis is given in Table 1.4.1.

TABLE 1.4.1

List of abbreviations and symbols used

a_i^a	activity of component i in phase a
am, amph	amphibole
An	anorthite
C_i^a	concentration of component/element i in phase a
CMS	$CaO-MgO-SiO_2$
CMAS	$CaO-MgO-Al_2O_3-SiO_2$
cpx	clinopyroxene
D_i	distribution coefficient for element i
En	enstatite
f_i^a	fugacity of component i in phase a
f^o_i	fugacity of component i in standard state
FeO*	total iron expressed as FeO
FGC	fluid generating compound
Fo	forsterite
gl	glass
GN	guanidine nitrate
$H_{soln,T}$	heat of solution at temperature of T (^oK)
ΔH	enthalpy change
Hy	hypersthene
HM	haematite-magnetite
HREE	heavy rare earth elements
ID	isotope dilution
INAA	instrumental neutron activation analysis
K	equilibrium constant
K_D	distribution coefficient
LILE	large ion lithophile elements
liq	liquid

ln	natural logarithm
log	logarithm (base 10)
LOI	loss on ignition
LREE	light rare earth elements
Mg-value	100 $Mg^{2+}/(Mg^{2+} + Fe^{2+})$
MORB	mid-ocean ridge basalt
MSS	monosulphide solid solution
mt	magnetite
Ne	nepheline
NNO	nickel-nickel oxide
OAD	oxalic acid dihydrate
ol	olivine
opx	orthopyroxene
P	pressure
P^{o}	pressure at standard state
pl,plag	plagioclase
R	gas constant (1.987 cal deg^{-1})
REE	rare earth elements
S_T	entropy at temperature T (^{o}K)
ΔS	entropy change
sp	spinel (sensu lato)
S.U.R.R.C.	Scottish Universities Research and Reactor Centre
T	temperature
TiO_2CR	TiO_2 analysis on pressed powder pellet (Cr-anode)
TiO_2W	TiO_2 analysis on pressed powder pellet (W-anode)
U.W.I.	University of the West Indies
V	volume
$\bar{V}_i^a$	partial molar volume of component i in phase a
ΔV	volume change

X_i^a	mole fraction of component i in phase a
X.R.F.	X-ray fluorescence spectrometry
Z.A.F.	atomic number, absorption, and fluorescence
μ_i^a	chemical potential of component i in phase a
$\mu^o{}_i$	chemical potential of component i in standard state.

CHAPTER 2

EXTRUSIVE ROCKS

2.1 Introduction

The discovery of serious discrepancies between chemical data obtained on Grenada lavas by the writer at Edinburgh and by Arculus (1973) at Durham has, as previously explained, necessitated a reappraisal of the petrology of the extrusive rocks. Unfortunately, only a limited number of the samples analysed by Arculus were obtainable, so that twelve samples collected during the 1978 field season and six samples from the U.W.I. collection were also analysed. The work in this study has been concentrated on the basic rocks, and therefore the proportion of basic compositions in the data should not be regarded as representative. However, as noted by Brown et al. (1977) basic compositions are more common in Grenada than in other islands in the Lesser Antilles.

Although several earlier workers had described features of the petrology of Grenada lavas, the accounts of Sigurdsson et al. (1973) and Arculus and Curran (1972) were the first to list substantial analytical data and attempt an interpretation of the petrogenesis. These workers pointed out the wide range of basaltic compositions present and the undersaturated nature of some of them. A particular feature of the extrusive rock chemistry is the transition from nepheline- to hypersthene-normative magmas displayed in the basaltic rocks. Sigurdsson et al. (1973), in particular, suggested that the most undersaturated compositions might be produced by fractionation of orthopyroxene from a slightly Ne-normative alkali picrite magma, with the alkaline and subalkaline basalts evolving from the same parent by olivine and calcic clinopyroxene fractionation. They discounted, on the basis of major element chemistry, amphibole fractionation as the

mechanism for driving magma compositions from Ne- to Hy-normative. In contrast, Cawthorn et al. (1973a) argued that experimental evidence supported amphibole fractionation. However, Arculus (1973, 1976) concluded that the chemical evidence ruled out substantial amphibole fractionation from basanitoid and alkali picrite magmas.

Arculus (1973, 1976) proposed a model wherein the major element chemical variation within the basalts was produced by fractionation of variable proportions of the observed phenocrystal olivine, clinopyroxene, and spinel, with the spinel removed enabling magma compositions to cross the low-pressure thermal divide close to the normative Di-Fo-An plane of Yoder and Tilley (1962). Amphibole was restricted to basaltic andesites and more evolved lavas in this model, and was therefore thought to be related only to the origin of the andesites and dacites. This model represents a refinement of the general amphibole fractionation hypothesis of Cawthorn et al. (1973a).

Arculus (1973) pointed out that the large range of trace element abundances in the basic magmas could not be wholly a result of crystal fractionation processes, and proposed that the variation resulted partly from different degrees of melting of an upper mantle peridotite source. This melting was modelled by Shimizu and Arculus (1975) and Minster and Allegre (1978) using REE analyses. These models are re-evaluated below in the light of the improved analytical data.

2.2 Classification

The nomenclature of igneous rocks still poses problems for the petrologist. In view of the petrographical diversity which can result from differing conditions and rates of crystallisation of a magma, there is much to commend classification of basaltic rocks in terms of

their major element chemistry. The classification of Grenada lavas is already highly confused. Sigurdsson et al. (1973) based their classification on the normative compositions of the magmas, while Arculus (1973, 1976) used this scheme alongside a silica-based basalt-andesite-dacite classification. Arculus also divided the rocks of each eruptive centre into two series, based on the abundances of trace elements, particularly Sr, which he termed 'low-Sr' and 'high-Sr' series and he noted that, in general, the high-Sr rocks were petrographically distinguishable by their highly porphyritic textures. A textural classification of the basaltic rocks has subsequently been used by Arculus (1978) and Hawkesworth et al. (1979b) with little reference to earlier schemes.

While there are advantages in each of these schemes, the chemical data on which some are based are unreliable, and the rocks have been reclassified, largely on the basis of major element chemistry (MgO and CaO) but with some reference to trace elements. Representatives of all the basalt types defined on normative composition by Arculus (1973) are still present, but two basaltic groups have been distinguished, characterised by high MgO/CaO and low MgO/CaO. These groups become indistinguishable at MgO contents close to 4 wt.% (equivalent to approximately 56% SiO_2) and therefore include basaltic andesites. Rocks with less than 4% MgO are classified separately. The high MgO/CaO (M-series) rocks are generally microphyric in texture, while the low MgO/CaO (C-series) rocks are strongly porphyritic. A summary of the characteristics of these series is presented in Table 2.2.1.

2.3 Petrography

Previous workers have fully described the petrography of the Grenada lavas, and only a few additional features are noted here.

Table 2.2.1

Characteristic features of the M-series and C-series basaltic rocks

	M-series	C-series
Phenocryst phases	olivine, cpx, Cr-Al spinel	olivine, cpx, plagioclase, Ti-magnetite
Texture	predominantly microphyric, often glassy	always strongly porphyritic; often large clinopyroxene phenocrysts
Phenocryst mode	generally olivine > cpx	cpx always > olivine
CaO/MgO	low	high
FeO*/MgO	low	high
Ni,Cr	high	low
Sr	low	high
Relationship to other classifications	includes all alkali picrites and basanitoids; includes most Ne-normative compositions; approximates to 'microphyric' type and 'low-Sr' series	restricted to alkaline and subalkaline basalt types; includes 'ankaramitic' type and approximates to 'high-Sr' series

Microphyric basaltic rocks are dominated by the presence of abundant olivine microphenocrysts. Further examination of these lavas showed that many of the olivines exhibit skeletal growth habits. Examples are illustrated in Plate 2.1. Under the classification of Donaldson (1976) they are hopper, or branching (linked parallel growth) types, and reflect rapid cooling of a magma close to its liquidus temperature, probably under near-surface conditions.

The microphyric rocks also contain clinopyroxene microphenocrysts. However, in some cases, these show irregular habits and strong sector zoning and are interpreted here as large quench crystals. These are distinguished from sector- and oscillatory-zoned clinopyroxene microphenocrysts in other microphyric basalts, which are interpreted as equilibrium primocrysts. It is notable that olivines with well-developed skeletal habits are only found in lavas lacking the clinopyroxene primocrysts, supporting the interpretation that these magmas were close to their liquidus temperatures on eruption.

An examination of the basaltic lavas was made to determine evidence for the order of crystallisation of the phenocryst phases. All the basalts show evidence for crystallisation of olivine and spinel, followed by clinopyroxene, and then by plagioclase feldspar. Plagioclase is not a phenocryst phase in basalts of the M-series and clinopyroxene may also be absent, as described above. The significance of these features is described with reference to the experimental melting studies in Chapter 5.

2.4 Mineral Chemistry

Selected basaltic lavas were studied by electron microprobe. Analytical details are given in Appendix A, with data in Table A3.

Plate 2.1

Hopper olivines in microphyric M-series basalts

2.4.1 Olivine (Table A3.1)

Olivine compositions in the microphyric M-series basalts range from Fo_{91} to Fo_{79} (Figure 2.4.1). The crystals are often normally zoned, and core compositions are always more magnesian than Fo_{83}, with NiO contents of 0.2-0.3 wt.%. The precision of energy dispersive analyses of Ni at this concentration is, however, poor. Olivines from the porphyritic C-series basalts cover a wide range from Fo_{86} to Fo_{57} but most lie in the range Fo_{81} to Fo_{72}. The presence of an olivine of Fo_{86} (analysis 15) in sample 6264 is interesting in that, assuming an exchange FeO/MgO K_D of 0.3 (Roeder and Emslie, 1970), this is more magnesian than the equilibrium composition of Fo_{79} for this magma. This suggests that either mixing of magmas of variable FeO/MgO is taking place at depth or, more likely, that some of the olivines in the lava originally crystallised in a parent liquid of lower FeO/MgO and have failed to equilibrate during subsequent fractionation.

2.4.2 Clinopyroxene (Table A3.2)

Calcic clinopyroxene compositions in the lavas are plotted in Figure 2.4.1. The strong zoning of the microphyric basalt clinopyroxenes is reflected in a general increase in Al and Ti from core to rim with increasing Fe/Mg. This is believed to result from rapid quench crystallisation of the clinopyroxenes resulting in Al and Ti contents in excess of their equilibrium levels, since Al and Ti are unable to diffuse away from the growing crystal-liquid interface sufficiently quickly.

The porphyritic basalts contain large sector- and oscillatory-zoned phenocrysts whose origin has been discussed by Arculus (1973), and is attributed to disequilibrium crystallisation prior to the eruption of the magma, analogous to the mechanism proposed by Bottinga et al. (1966) and Sibley et al. (1976) for oscillatory-zoned

Figure 2.4.1 Compositions of olivines and clinopyroxenes in basaltic Grenada lavas.

circles: M-series basalts

squares: C-series basalts

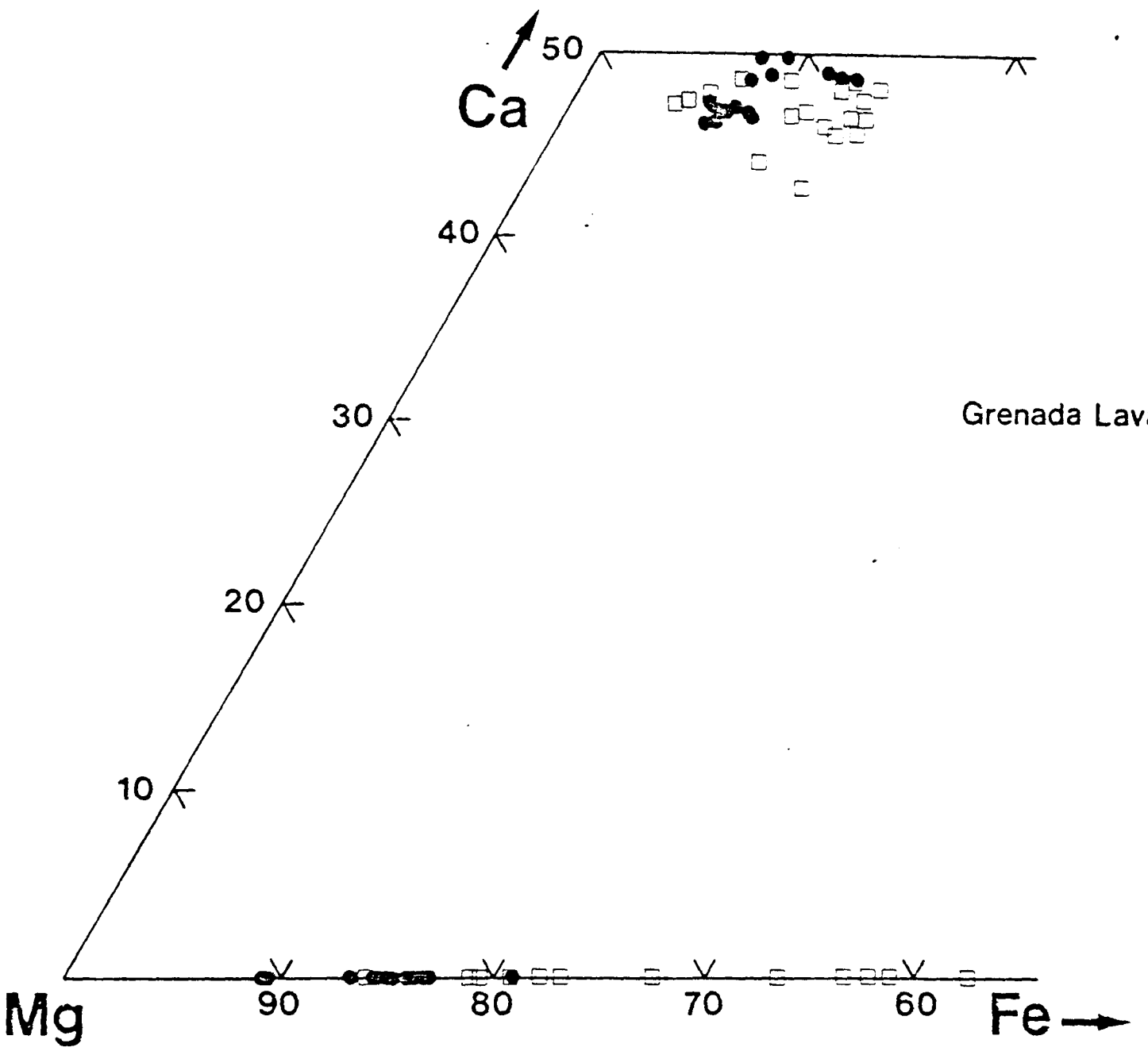

plagioclase feldspars. However an additional feature of the chemistry of these complex pyroxenes is that occasional large phenocrysts have paler coloured cores with very high Mg-values of 88-90 (analyses 17, 19, 20, 22). The frequent occurrence of these paler magnesian cores indicates that they are unlikely to be xenocrysts accidentally incorporated into the magma. Evidence from coexisting phases in peridotites shows the value of the olivine-clinopyroxene FeO/MgO exchange K_D to be close to unity, so that these compositions provide important evidence of more primitive (i.e. lower FeO/MgO) parents to the porphyritic C-series basalts. Similar features are present in the basaltic andesite phenocrysts of the 1979 eruption of Soufriere, St. Vincent (Graham and Thirlwall, in prep.).

2.4.3 Plagioclase (Table A3.3)

Analyses of plagioclase feldspar phenocrysts in C-series basalts cover the range An_{91} - An_{64}, with the most calcic compositions representing the unzoned cores of phenocrysts. The oscillatory-zoned rims are extremely variable in composition, reflecting the disequilibrium crystallisation conditions of their formation. Plagioclase phenocrysts are absent from the microphyric basalts, where groundmass crystals are of bytownite composition.

2.4.4 Oxides (Table A3.4)

The oxide phase in Grenada lavas is always a spinel. No separate rhombohedral oxide has been reported. However, an extremely wide range of spinel compositions is present in the basaltic rocks (Arculus, 1974), presumably reflecting variations in both host magma chemistry and crystallisation conditions.

2.5 Major Element Chemistry

Sixty-five lava samples were analysed for ten major elements by

X.R.F. methods. Analytical details are summarised in Appendix B and a full description of the methods used is to be found in Thirlwall (1979). Data are presented in Table B9 and summarised in Figure 2.5.1.

The most striking feature of the chemistry is the wide range of MgO contents, which makes MgO variation diagrams useful for qualitative assessment of the controls on fractionation. The basic rocks appear to be divisible into two groups on the basis of SiO_2, CaO, Fe_2O_3, and Na_2O with MgO and, to a lesser extent on TiO_2 and K_2O. The M-series lavas (higher MgO/CaO) and C-series (lower MgO/CaO) are largely defined on the basis of this separation. In an attempt to test whether this compositional distinction was the result of sampling, the last six samples analysed were selected on the basis of petrographic characteristics suggesting that their compositions might be transitional between the two groups, but they fell into the series already defined, and the gap is therefore believed to be real. The small number of analyses of M-series rocks in the 4-7% MgO range makes it possible that the two groups are not distinguishable in their major element chemistry in this range. A summary of the characteristics of the two groups was presented in Table 2.2.1, and their chemical features are discussed below.

2.5.1 M-series

The large number of picritic (>10% MgO) magmas in this group have a tendency to be scattered rather than to lie on simple mineral control lines. This is particularly noticeable in the elements Ti, K, and P which have the lowest crystal-liquid distribution coefficients for the phenocryst phases. This pattern cannot be explained by fractional crystallisation of the phenocryst phases. However, no simple linear trend is evident in the more compatible elements such as CaO, SiO_2, and MgO and instead a spread of data with a general trend is normally evident. Calcium variation suggests a main olivine-clinopyroxene

Figure 2.5.1(a) Major element variation in extrusive rocks

Key: circles: M-series; squares: C-series; triangles: evolved lavas

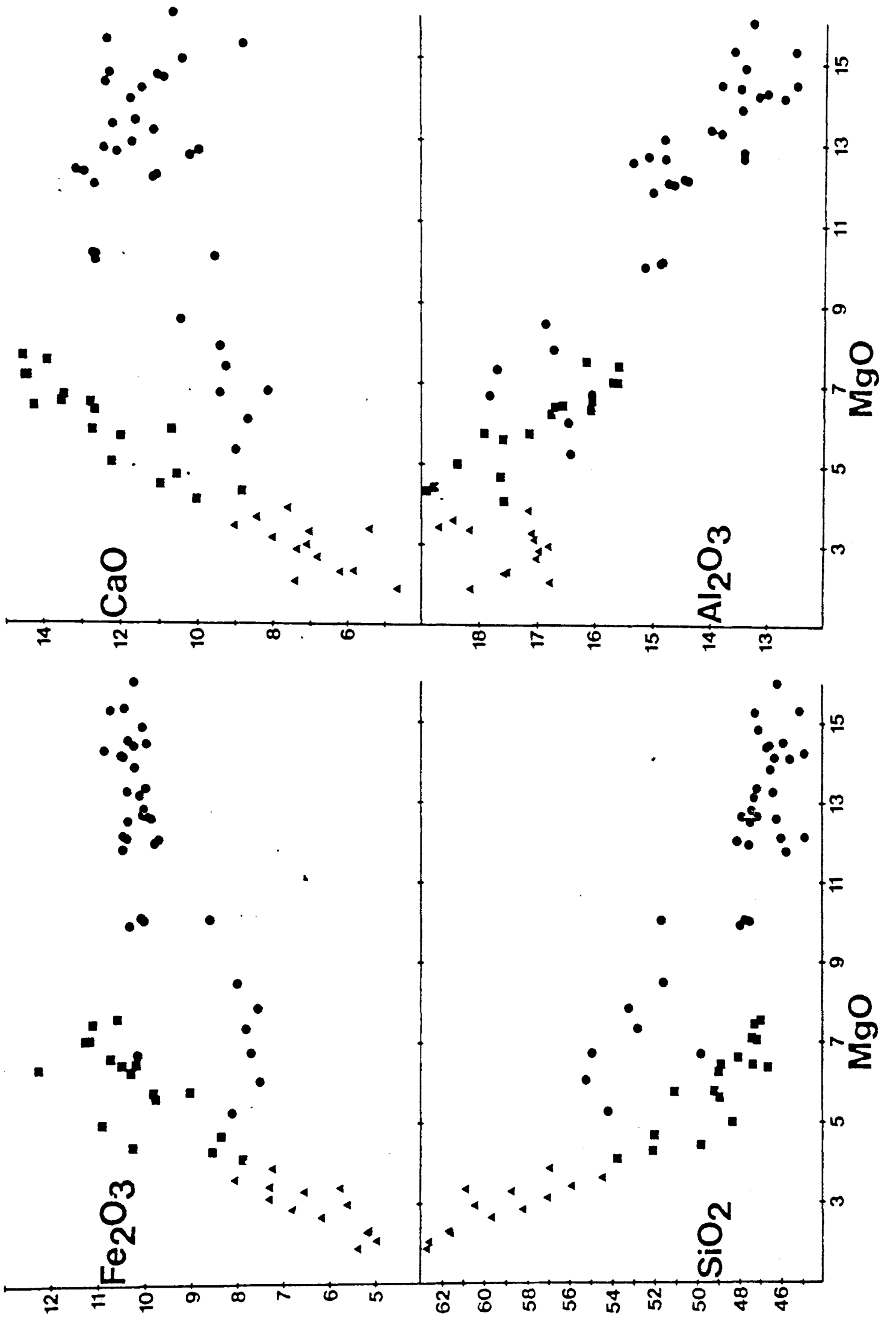

Figure 2.5.1(b) Major element variation in extrusive rocks

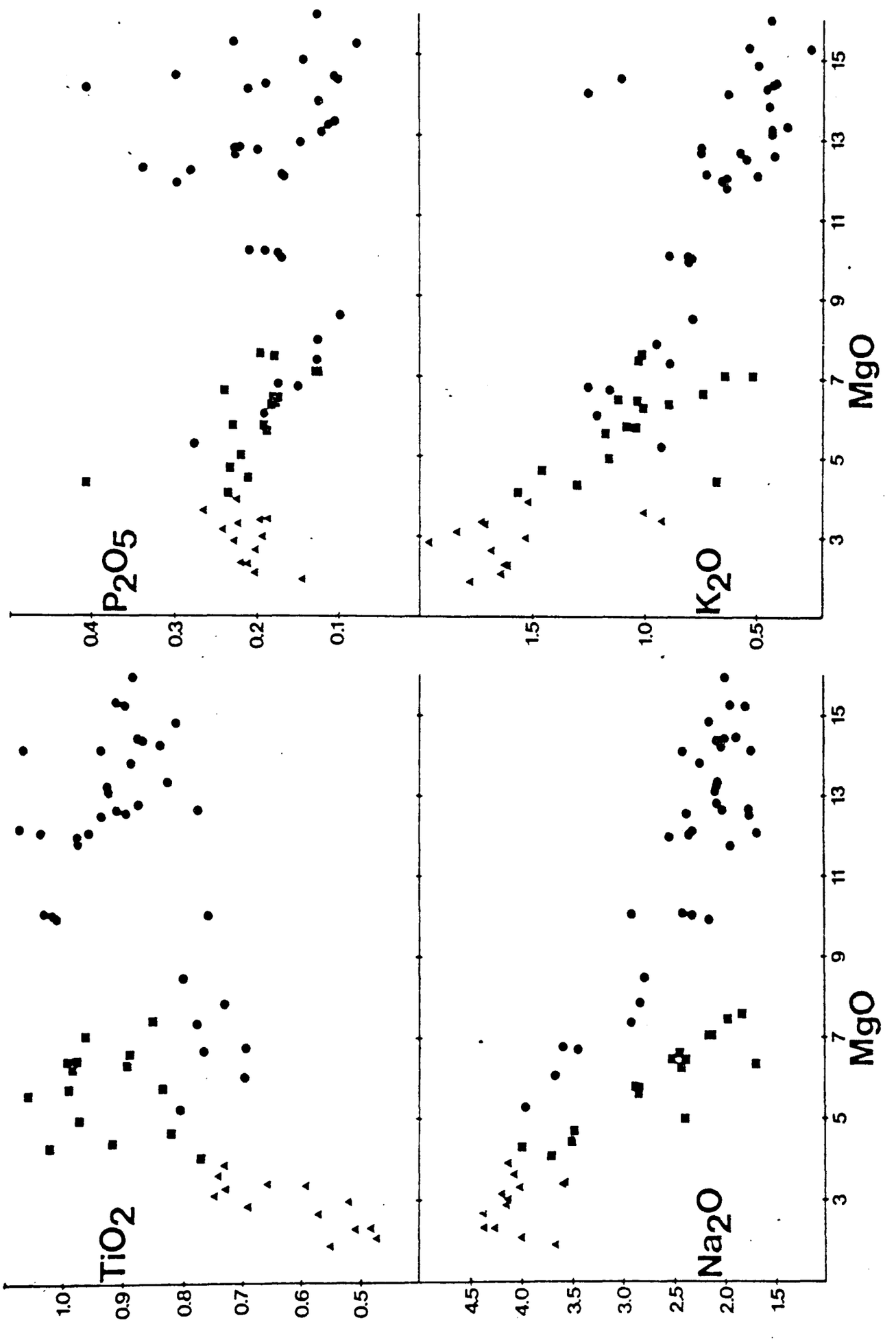

control giving rise to decreasing CaO with MgO, and a spread across this main trend related to olivine fractionation (Figure 2.5.2). This model of variable proportions of olivine and clinopyroxene fractionation, perhaps representing more than one fractionation episode, can explain the major element patterns in the M-series.

2.5.2 C-series

Major element patterns in this series are generally more tightly grouped than in the M-series although again there is considerable scatter, particularly in Ti, K, and P. The presence of large, oscillatory-zoned clinopyroxene phenocrysts in this series provides a mechanism for additional scatter in Ti, since disequilibrium fractionation may be taking place. The CaO/MgO variation diagram indicates strong control of compositions by phenocryst clinopyroxene and plagioclase, but the proportion of feldspar is limited by the increase in Al_2O_3 with decreasing MgO. Chemical variation controlled largely by calcic clinopyroxene is therefore a likely model for this series.

2.5.3 Cumulus Enrichment

Consideration of the possibility of some differential crystal enrichment process in these magmas is critical to the interpretation of the chemical variation within and between the two basic series. The bifurcating appearance of the major element patterns would be easily explained by accumulation of the large clinopyroxene and subordinate plagioclase phenocrysts from magmas of around 4% MgO, to form the C-series. Recent re-examinations of the theoretical feasibility of gravity settling of crystals in magmas (e.g. Campbell 1978, McBirney and Noyes 1979) suggest that simple gravity settling of crystals is difficult to achieve, especially in melts whose structures are sufficiently polymerised for them to crystallise plagioclase, although other differentiation processes could operate. However, the

Figure 2.5.2 M-series fractionation controls

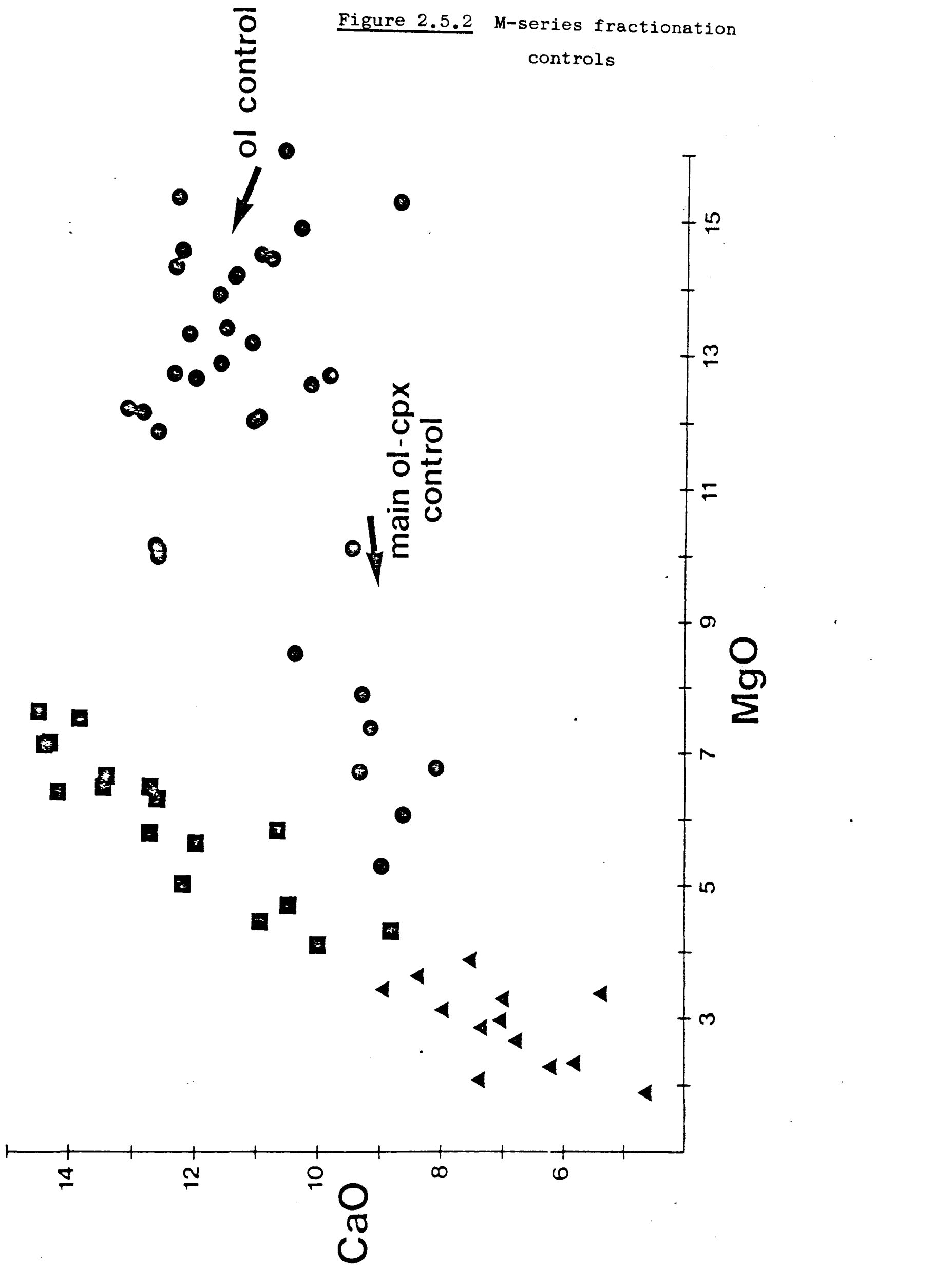

occurrence of amphibole phenocrysts in the more evolved (basaltic andesite) members of the C-series is conclusive evidence against a cumulus enrichment model. Amphibole and clinopyroxene crystals have similar densities and habits and any mechamism effective in concentrating clinopyroxene, such as flow differentiation, would also be expected to concentrate amphibole. The alkali variation argues against amphibole accumulation, while amphibole is absent from the more primitive members of this series.

Evidence against cumulus enrichment processes in the M-series comes from the generally small size of the phenocrysts and the evidence for late and rapid olivine growth. Although the possible scattering of the variation trends by olivine fractionation could be attributed to some olivine accumulation at low pressure, isotopic evidence discussed in Chapter 6 argues against this possibility.

2.5.4 Evolved Lavas

Compositions containing less than 4% MgO appear to be chemically and petrographically related to both the C-series and M-series, but their precise relationships to these lavas are not distinguishable in the major element chemistry. They have therefore been termed "evolved". This series corresponds to magmas with greater than approximately 56% SiO_2 and they are therefore essentially andesites and dacites. Qualitative interpretation of their chemical variation is difficult because of the large number of phenocryst phases (olivine, orthopyroxene, clinopyroxene, amphibole, plagioclase, and titanomagnetite), and the scatter in compositions of their possible parent magmas. However substantial plagioclase control seems necessary to explain the Al_2O_3 variation, while lack of iron enrichment and TiO_2 depletion requires amphibole and/or magnetite fractionation. The variation of K_2O is too scattered to confirm the amphibole control, while rapid silica increase precludes substantial involvement of orthopyroxene.

2.6 Major Element Fractionation Models

Quantitative crystal fractionation models, based on least squares mixing calculations of whole rock and phenocryst compositions are superior to simple oxide variation diagrams in considering the covariation of all major elements. Models of fractional crystallisation derived from these calculations may be tested subsequently by employing trace element data and estimates of crystal-liquid distribution coefficients. This type of numerical approach has been successfully applied to several lava suites (e.g. Zielinski and Frey, 1970; Leeman et al., 1976; Baker et al., 1977), but numerical models of calc-alkaline suites have been relatively unsuccessful, as discussed by Gill (1978).

Least-squares models for Grenada lavas have been formulated from the major element analyses and microprobe analyses of phenocrysts in the parent compositions using a modification of the program described by Wright and Doherty (1970). The sum of squares of residuals, Σr^2, provides a measure of the precision of the fit but it must be noted that increasing the number of variables will generally improve the fit, so that a relatively large Σr^2 may not be unsatisfactory if only one phenocryst is used. Some subjective judgement is inevitably involved. The size of the fractionation steps is a compromise since large steps will not account for the change in the compositions of phenocryst phases, while small steps will tend to lead to errors in the model parameters. Models were first produced involving all phenocrysts, and phases whose proportions were not significantly large were successively removed provided the fit was not seriously worsened. The steps chosen were also limited by the availability of microprobe data from Arculus (1973) and the present study. The models produced are summarised in Table 2.6.1.

Models (1) and (2) describe the possible fractionation trend between lava 468 - a possible parental composition with the highest

Table 2.6.1

Major element fractionation models in basic rocks

Model	Parent	Daughter	F	X_{ol}	X_{cpx}	X_{plag}	X_{sp}	X_{amph}	$\sum r^2$
1.	468	266	.8884	.1116	-	-	-	-	4.554
2.	468	286	.8796	.1204	-	-	-	-	1.623
3.	468	319	.5988	.1443	.2099	-	.0470	-	0.149
4.	468	265	.5244	.1803	.2483	-	.0470	-	0.911
5.	468	398	.4705	.1815	.2900	-	.0580	-	0.255
6.	468	313D	.4798	.2009	.2661	-	.0533	-	0.060
7.	398	307	.8911	.0504	.0503	-	.0083	-	0.443
8.	468	6104	.7920	.2080	-	-	-	-	2.973
9.	468	6264	.7747	.2253	-	-	-	-	1.931
10.	6104	6073	.4865	.0211	.2771	.1721	.0432	-	0.580
11.	6104	337	.3487	.0291	.2973	.2593	.0656	-	0.302
12.	6073	381	.5814	.0436	.0880	.2440	.0430	-	0.768
13.	337	381	.7670	-	.0667	.1049	.0126	.0488	0.100

MgO content and lowest FeO*/MgO of the analysed samples - and magmas which appear, from the MgO variation diagram to lie close to an olivine fractionation trend. Although the fit of these models is not particularly good, only one phase is involved and therefore, considering the scatter in the data, these models are not unreasonable.

Models (3) to (6) describe the main fractionation trend within the M-series involving olivine, clinopyroxene, and spinel. Although these are the only phenocryst phases, no satisfactory fit could be obtained using their analysed compositions, particularly because the analysed phenocrysts are not sufficiently rich in Al. The possibility therefore arises that the fractionation process occurred at high pressures, and that the derivative liquids were erupted carrying no trace of the phenocrysts involved, either as a result of their removal or of the magma becoming superheated during ascent. Support for the latter interpretation comes from the olivine textures described in section 2.3.

Arculus (1979), in a study of spinel compositions in Grenada basalts, reported a Cr-free aluminous spinel and aluminous clinopyroxene included together in olivine. Such a textural relationship is unusual in the microphyric lavas. He interpreted the spinel as either a high-pressure phenocryst preserved in olivine, or a xenocryst captured by the host magma. There is much evidence to suggest that spinels with low Cr/(Cr + Al) can precipitate from a Cr-rich magma under certain conditions although insufficient thermodynamic and experimental data exist to determine whether this is a result of high total pressure. An alternative possibility is that chromium exists in the divalent state under some conditions. Whatever the explanation, the textural evidence suggests a high-pressure origin for these compositions, providing an aluminous assemblage whose fractionation explains satisfactorily the major element variation within the M-series, despite the poor constraints on the compositions of the fractionated phases.

The origin of andesite 307 from an M-series parent is supported by trace element, isotopic, and petrographical evidence. This rock contains olivine, orthopyroxene, clinopyroxene, plagioclase, amphibole, and titanomagnetite phenocrysts but does not have the coarsely porphyritic texture of most C-series magmas. Model (7) demonstrates a possible origin of this lava from microphyric basalt 398 by fractionation of phenocrysts in this composition. However, the relative proportions of phases in this model are similar to those in models (3)-(6) so that a high-pressure origin for this composition could not be excluded. It is also possible, since 307 contains amphibole, that this mineral is significant in its origin. However, none of the analysed M-series samples contain phenocryst amphibole so that this possibility will be discussed with reference to the cumulate blocks in Chapter 3.

Models (8) and (9) investigate the relationship between the potential M-series parent 468 and two of the most primitive members of the C-series. Considering that olivine is the only phenocryst phase involved, and that it will change composition during fractionation, these models are not inconsistent with a hypothesis in which the C-series basalts originate by around 20% of olivine fractionation from a picritic parent similar to that for the M-series. These models cannot be significantly improved by inclusion of another phase.

Models (10) to (13) describe the fractionation trends in the C-series, using 6104 as representative of the primitive members of the series. Models producing 337 and 6073 show that an increasing proportion of plagioclase is involved in the fractionation, as evident from the trend of the CaO-MgO variation diagram. Model (12), relating 6073 to an andesite composition, shows a fit not entirely satisfactory considering the large number of phases involved and the limited degree of fractionation. Phenocryst amphibole occurs in sample 337, and in the

slightly more primitive 6177, so that this phase must be considered in the evolution of the more differentiated members of the C-series. Model (13) uses the data on 337 and its phenocrysts to produce an andesite with a very good fit, which is not improved by inclusion of olivine or orthopyroxene.

In view of the abundance of cumulus plutonic blocks containing assemblages found as phenocrysts in the evolved rocks, and the evidence for some amphibole involvement at this stage of fractionation, models for the evolved lavas will be discussed in Chapter 3.

2.7 Trace Element Chemistry

Fifty-eight samples were of sufficient size to be analysed for trace elements by X.R.F. Analytical details are summarised in Appendix B and described in detail by Thirlwall (1979). Data are presented in Table B9 and summarised in Figure 2.7.1.

Trace element concentrations in Figure 2.7.1 have been plotted against MgO contents to facilitate comparison of major and trace element behaviour especially in the light of the proposed fractional crystallisation models. Since a large amount of data are presented, a general discussion of these will be followed by a more rigorous treatment of selected elements and elemental ratios.

2.7.1 General trace element features of the basaltic lavas

Ni and Cr concentrations are very high in the picritic basalts compared with the more evolved basalts of the C-series. The variation of these elements within the M-series implies substantial fractionation of olivine and a Cr-bearing phase, such as clinopyroxene or spinel, while the greater Ni and Cr contents of M-series rocks with comparable MgO contents to the C-series is consistent with some clinopyroxene fractionation within the M-series but olivine and minor Cr-spinel fractionation

Figure 2.7.1(a) Trace element variation in extrusive rocks (symbols as Figure 2.5.1)

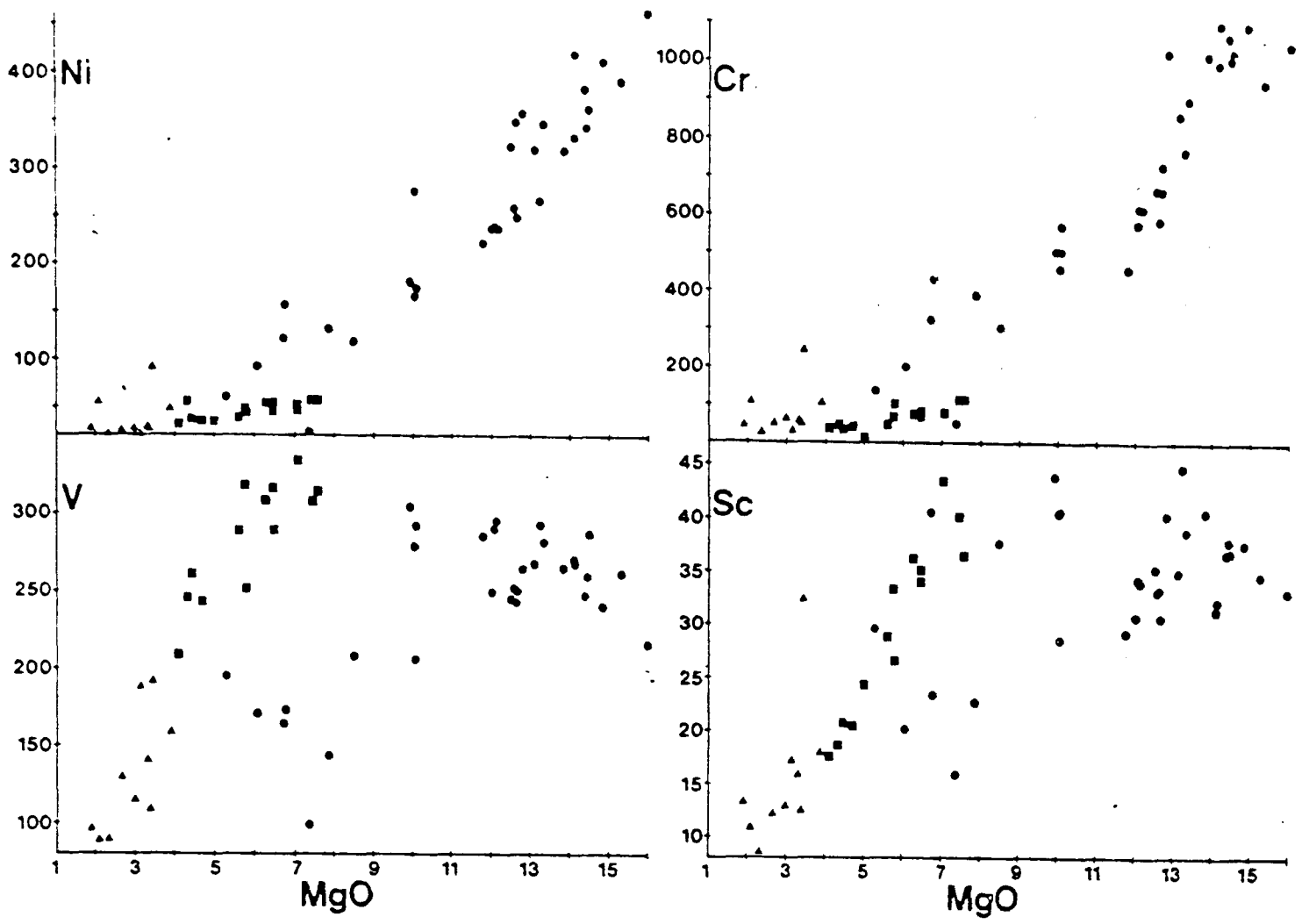

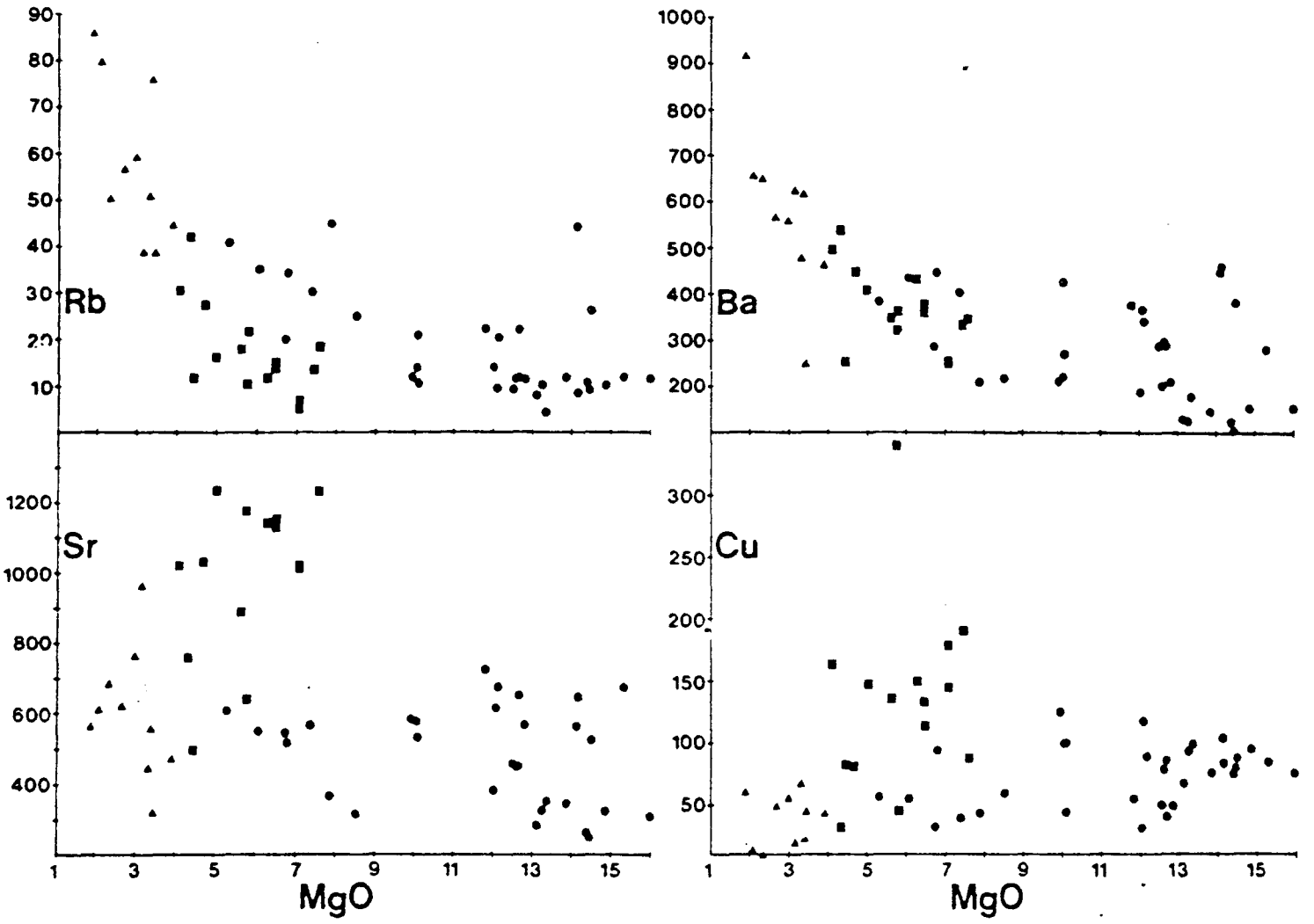

Figure 2.7.1(b) Trace element variation in extrusive rocks

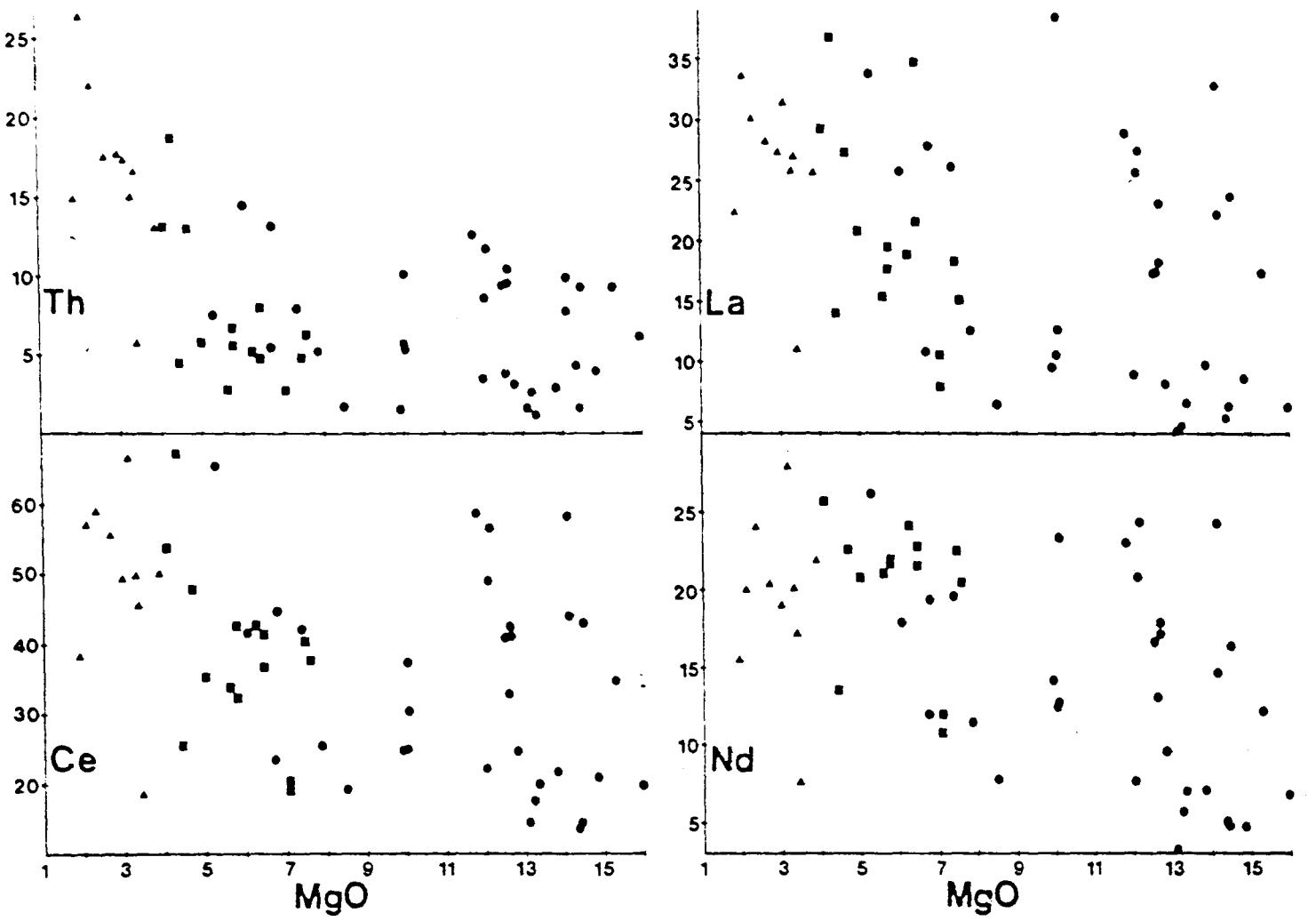

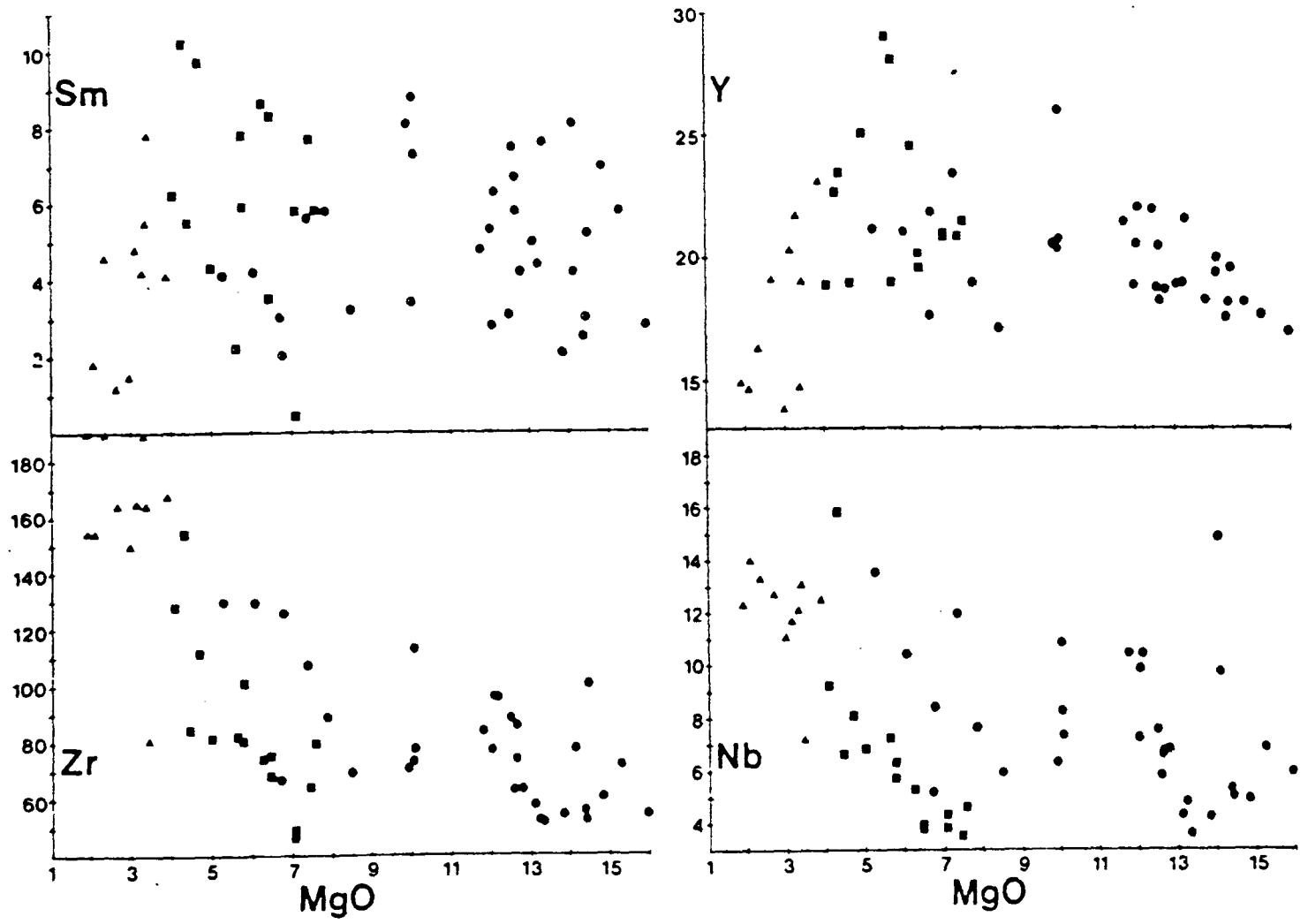

to produce the C-series. Vanadium and scandium variation patterns are similar. V is principally affected by spinel/titanomagnetite and Sc by clinopyroxene fractionation. The effects of differing proportions of olivine, clinopyroxene, and spinel fractionation in the M-series are clearly demonstrated, while clinopyroxene and titanomagnetite fractionation seem to be important in the C-series evolution. Copper shows irregular variation, as does Zn (not figured), which may be the result of control by minor sulphide phases.

Large ion lithophile elements (LILE) are very scattered in the M-series, often by as much as a factor of 4. Particularly striking are the LREE (La, Ce, Nd). These data are in accord with the isotope dilution REE data of Shimizu and Arculus (1975). The high field-strength elements Y, Zr, and Nb also show some scatter in the M-series, particularly Nb.

In the C-series LILE are again scattered, although not as seriously as in the M-series. A notable feature is the very high Sr content. Despite the scatter, the concentrations of LILE and high field-strength elements are, with the exception of Sr, compatible with the model wherein the C-series basalts are related by olivine fractionation to a high-MgO parent, but the data require this parent to lie at the lower end of the scatter in concentrations in the M-series. Fractional crystallisation is not able to explain the large variations in trace element concentrations at similar major element compositions which is a feature of both series, as concluded by Arculus (1973). However an important point to note is that the process responsible for the M-series scatter has not been followed by olivine fractionation to produce the C-series, as this would have led to an even greater scatter in the C-series derivatives. Therefore either:

(i) the scatter in the incompatible elements results from a

process occurring after that responsible for the major element variation, or

(2) the M-series and C-series have a similar origin but have been affected by different processes or differently affected by the same process, or

(3) the M-series and C-series do not have a similar origin.

2.7.2 General trace element features of the evolved lavas

Interpretation of the trace element chemistry of the evolved lavas is difficult using Figure 2.7.1 since MgO is a poor fractionation index in rocks which must, because of their alumina variation, be fractionating plagioclase. Ni and Cr concentrations are generally low, which is typical of andesitic lavas (Taylor et al., 1969). Rb, Ba, and Th behave incompatibly within this series, while LREE remain essentially constant. This suggests a small amount of fractionation of the phenocryst apatite seen in basaltic andesites and more evolved lavas. Strong Y depletion suggests that another Y-bearing phase, probably amphibole, is fractionating while Sr concentrations are rather scattered, perhaps a result of the parentage of this group by both M- and C-series lavas. However, trace elements do not provide conclusive evidence of the relationship of the evolved lavas to the basic series.

2.8 Process Identification

The compositions of magmas erupted are the product of several processes, including the essential melting of source rocks and possible partial crystallisation of the primary melt prior to eruption. Increased interest in recent years in the significance of trace elements in magmas has led to a better understanding of the effects of different processes on their concentrations. Numerical models of trace element behaviour can be used to predict the abundance patterns produced by

the processes or, conversely, the patterns may be used to help identify the processes which have operated in a particular suite. These applications of trace element data have been mathematically described by many authors, particularly Allegre and co-workers (Allegre et al., 1977; Minster et al., 1977; Allegre and Minster, 1978) in a series of papers applying rigorous numerical and statistical methods. Unfortunately the sophistication of the models now appears to be such that the limiting factors are a lack of essential partitioning data and of a real understanding of the processes of differentiation.

The main processes which may be operative on the Grenada lava suite are partial melting, fractional crystallisation, and mixing or contamination. These will produce different effects on elements with different chemical behaviour. Patterns showing these effects are illustrated in Figure 2.8.1.

(a) Elements with high D values (e.g. Ni, Cr) vary drastically in concentration during fractional crystallisation but their concentrations are relatively insensitive to the degree of melting, especially at low degrees of melting. At high degrees of melting, changes in source mineralogy may change D values but consideration of both Ni and Cr should show this effect, as it should also show preferential accumulation of a phase rich in Ni or Cr.

A log Ni - log Cr plot for Grenada lavas (Figure 2.8.2) shows the importance of fractional crystallisation in the evolution of Grenada magmas.

(b) Elements of low D have been termed hygromagmatophile or 'H' elements by Treuil (1973), Allegre and co-workers. Their bulk D values for common mineral assemblages approximate to zero. Therefore their concentration in fractional crystallisation is inversely proportional to the degree of crystallisation or melting. Abundance variation during melting will be

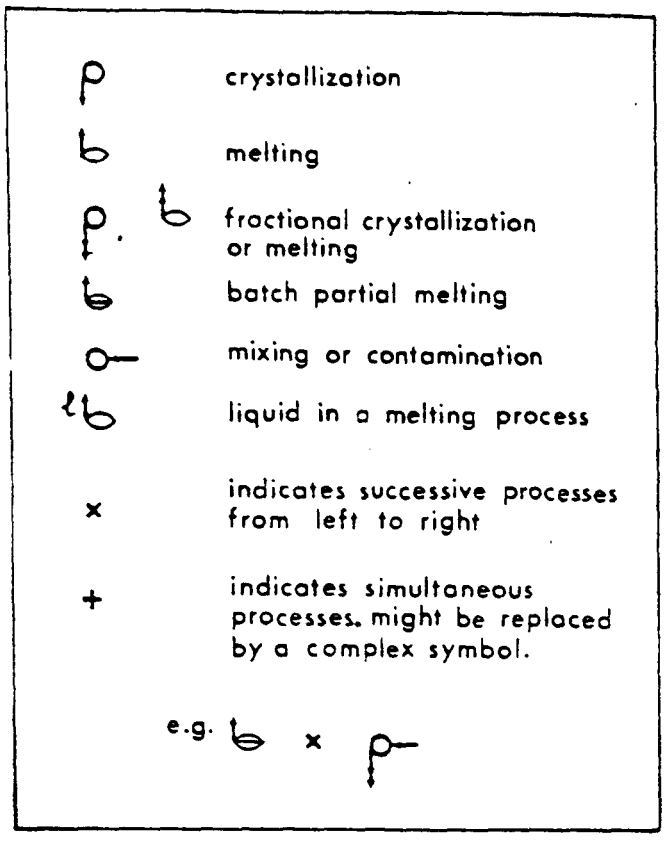

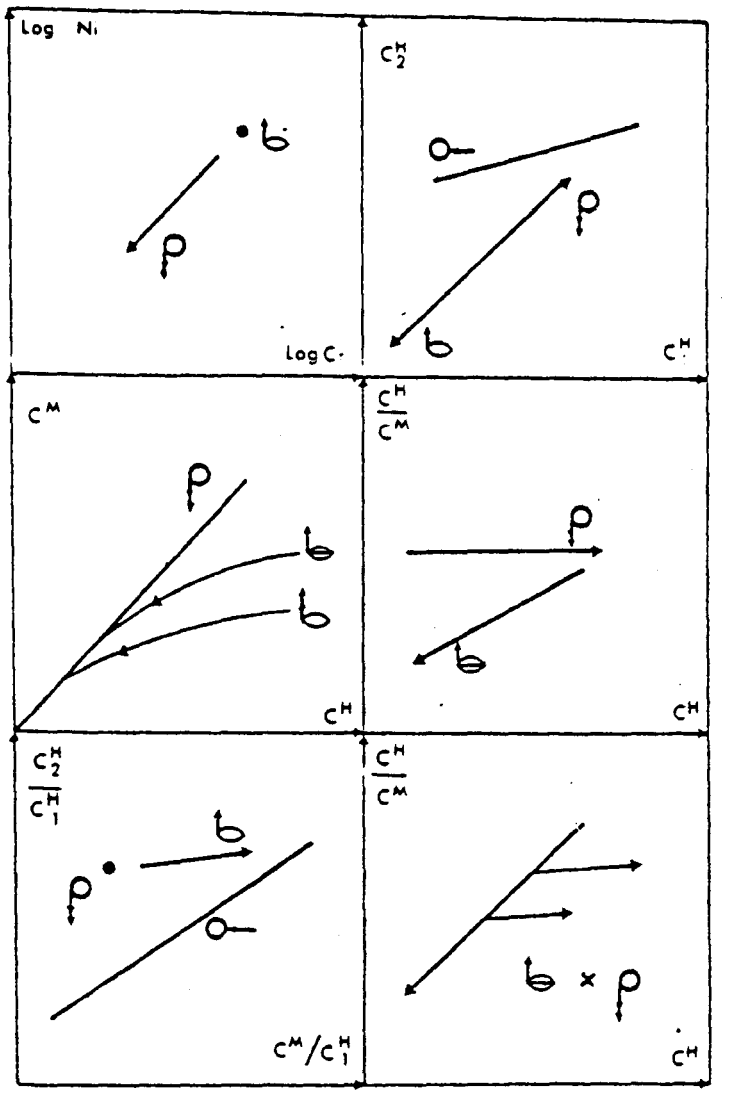

Figure 2.8.1

The qualitative behaviour of trace elements in igneous processes.

C^H represents the concentration of an 'H' element

C^M represents the concentration of an intermediate element

A dot signifies that the point does not move in the diagram for different degrees of evolution of the process.

Diagrams from Minster and Allegre (1978)

Figure 2.8.2

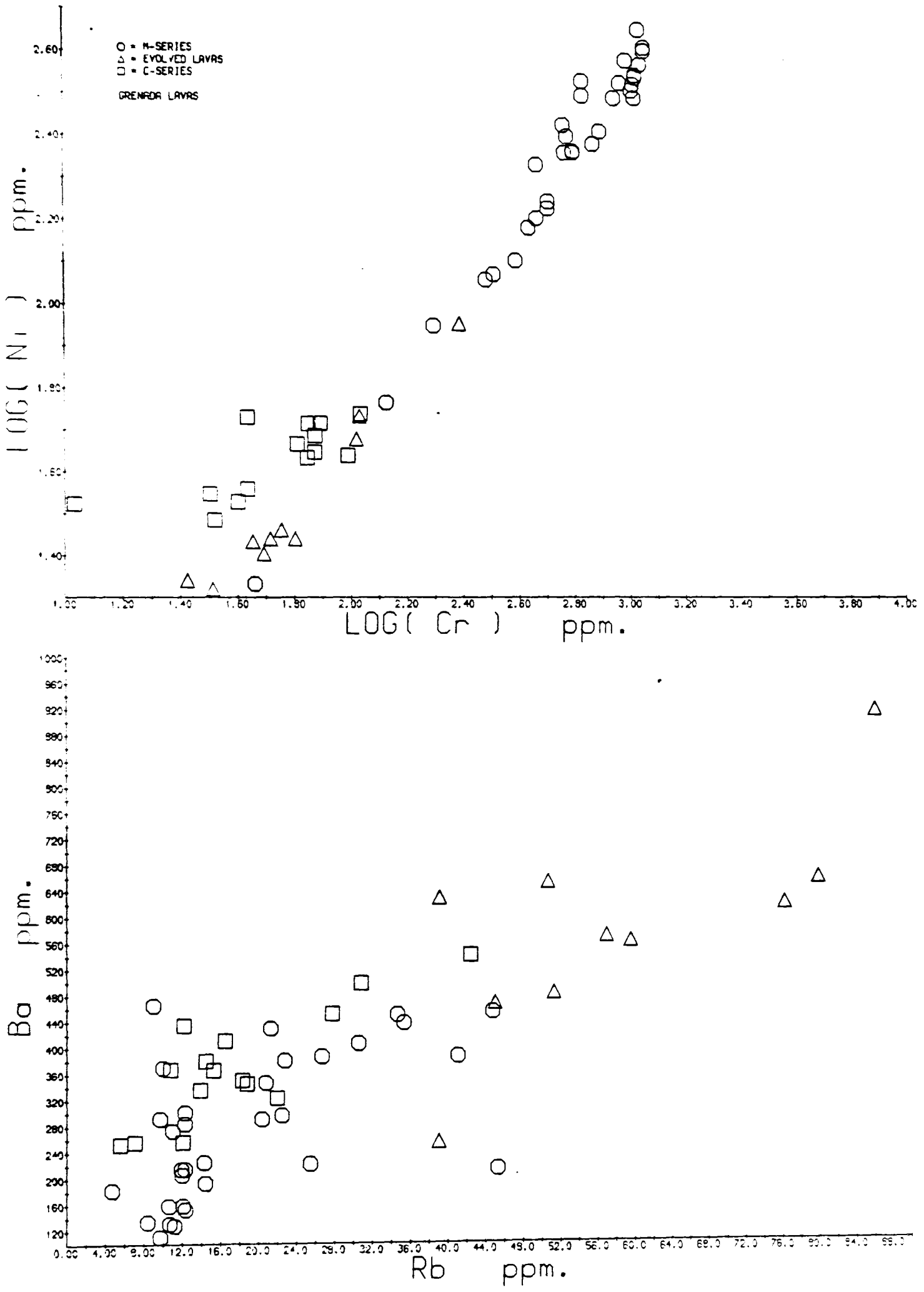
O = M-SERIES
Δ = EVOLVED LAVAS
□ = C-SERIES
GRENADA LAVAS
LOG(Ni) ppm.
LOG(Cr) ppm.
Ba ppm.
Rb ppm.

greatest at low degrees of melting, and greatly in excess of that during fractional crystallisation. The ratio of two H elements should be constant during either melting or crystallisation processes, so that variation in the ratio indicates the presence of more than one source, or contamination.

Ba-Rb, Th-Rb, and Nb-Rb diagrams (Figures 2.8.2 and 2.8.3) should therefore show a straight line relationship in both series, as these elements are H elements in assemblages involving olivine, clinopyroxene, spinel and calcic plagioclase. However the plots show large scatter in both series, although the C-series scatter is generally less than that in the M-series. It should be noted that the H-element ratios are not, on average, different in the two series. LREE show even more scatter but do not appear to behave as H elements in the evolved magmas, as previously noted. Possible explanations for this scatter are:

(i) disequilibrium melting

(ii) a chemically heterogeneous source.

(c) Elements with intermediate D are termed intermediate or M elements. Because the bulk D value for an M element is comparable with the degree of melting, the ratio of M to H elements will be variable during melting, especially at low degrees of melting. However the ratio will be little changed during fractional crystallisation. HREE are normally M elements so that variable LREE enrichment is more easily produced by melting than by fractional crystallisation.

C^H/C^M vs C^H diagrams can therefore be used to distinguish partial melting from fractional crystallisation effects. Y has ionic charge and radius similar to the heavy rare earth Ho and Drake and Weill (1975) found that D values for Y resembled those for HREE, although closest to Lu. Yttrium is therefore a good analogue for HREE and is more easily analysed.

Figure 2.8.3

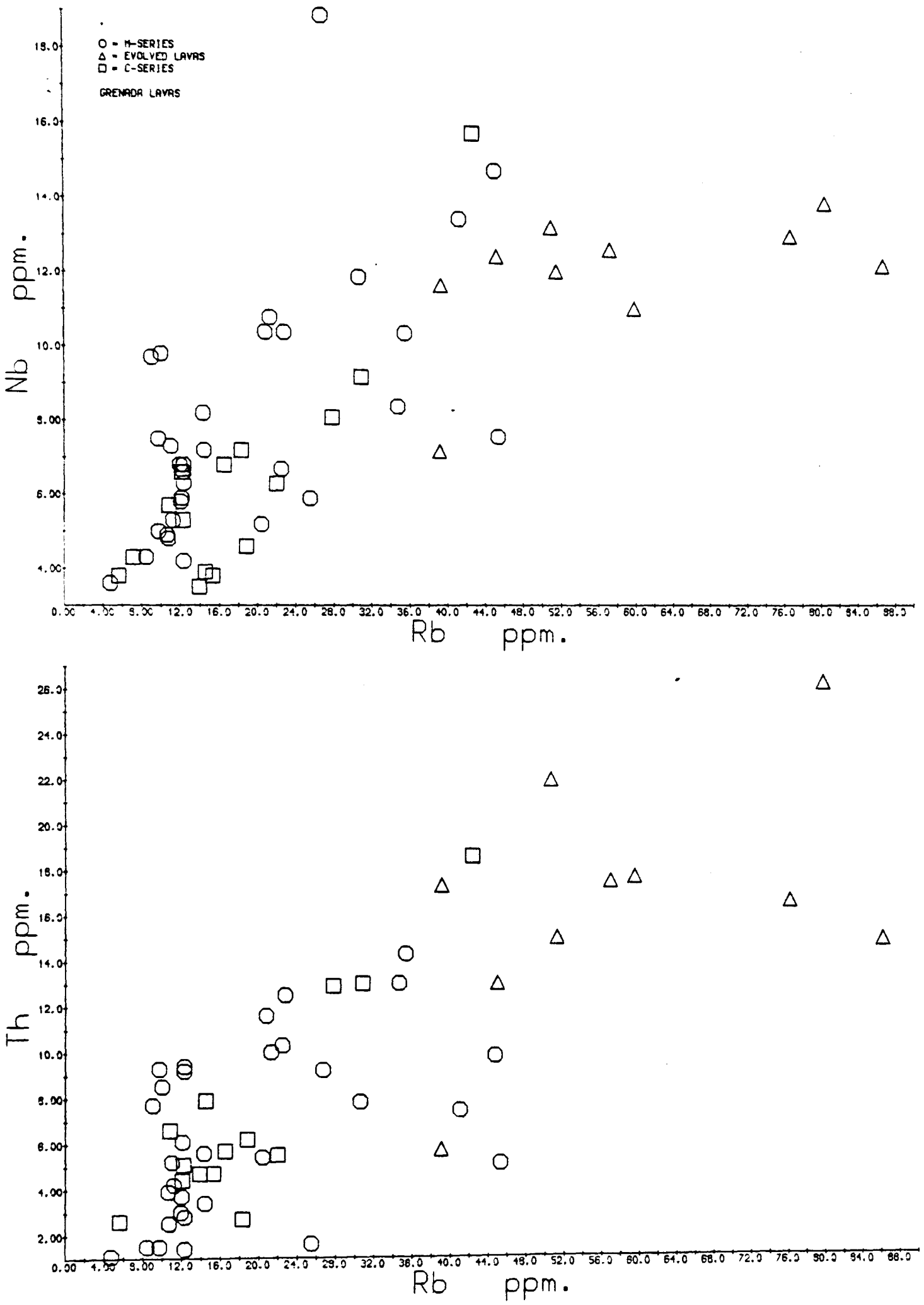
O = M-SERIES
Δ = EVOLVED LAVAS
□ = C-SERIES
GRENADA LAVAS
Nb ppm.
Th ppm.
Rb ppm.
Rb ppm.

The Ce/Y vs Ce diagram in Figure 2.8.4 shows a strong positive correlation, indicative of a melting process, while the generally high Ce/Y of the evolved lavas indicates that Y is more compatible than Ce during subsequent crystallisation. Minster and Allegre (1978) used Th as an H element to model the REE and the Th/Ce vs. Th diagram in Figure 2.8.4 again shows a pattern consistent with melting followed by fractional crystallisation, although Th analytical precision is not high.

The contrasting behaviour of M and H elements in melting is also demonstrated in C^{H_2}/C^{H_1} vs. C^{M}/C^{H_1} diagrams, where normalisation to another H element should lead to no significant variation on the diagram during fractional crystallisation. Examination of such plots in Figure 2.8.5 shows that, while the evolved lavas show little variation, their basaltic precursors are very scattered, although some scatter due to lack of Th precision is to be expected. This is again not consistent with a simple equilibrium partial melting plus fractional crystallisation model.

It is clear that the substantial fractional crystallisation complicates the interpretation of the trace element patterns, so consideration of the most primitive M-series magmas (>11% MgO), within which a large variation in trace elements is found, might be expected to present a clearer picture of the process(es) operating. Within this group, the major element variation precludes more than approximately 10% fractional crystallisation, which will not greatly affect incompatible element abundances. The REE models of Minster and Allegre (1978) and Shimizu and Arculus (1975) interpret the trace element variation as a product of batch partial melting of a garnet lherzolite source, the degree of melting varying from approximately 4 to 17%. These models appear to explain the REE data well, and the degree of LREE enrichment, which is an index of melting in the models, should therefore correlate positively

Figure 2.8.4

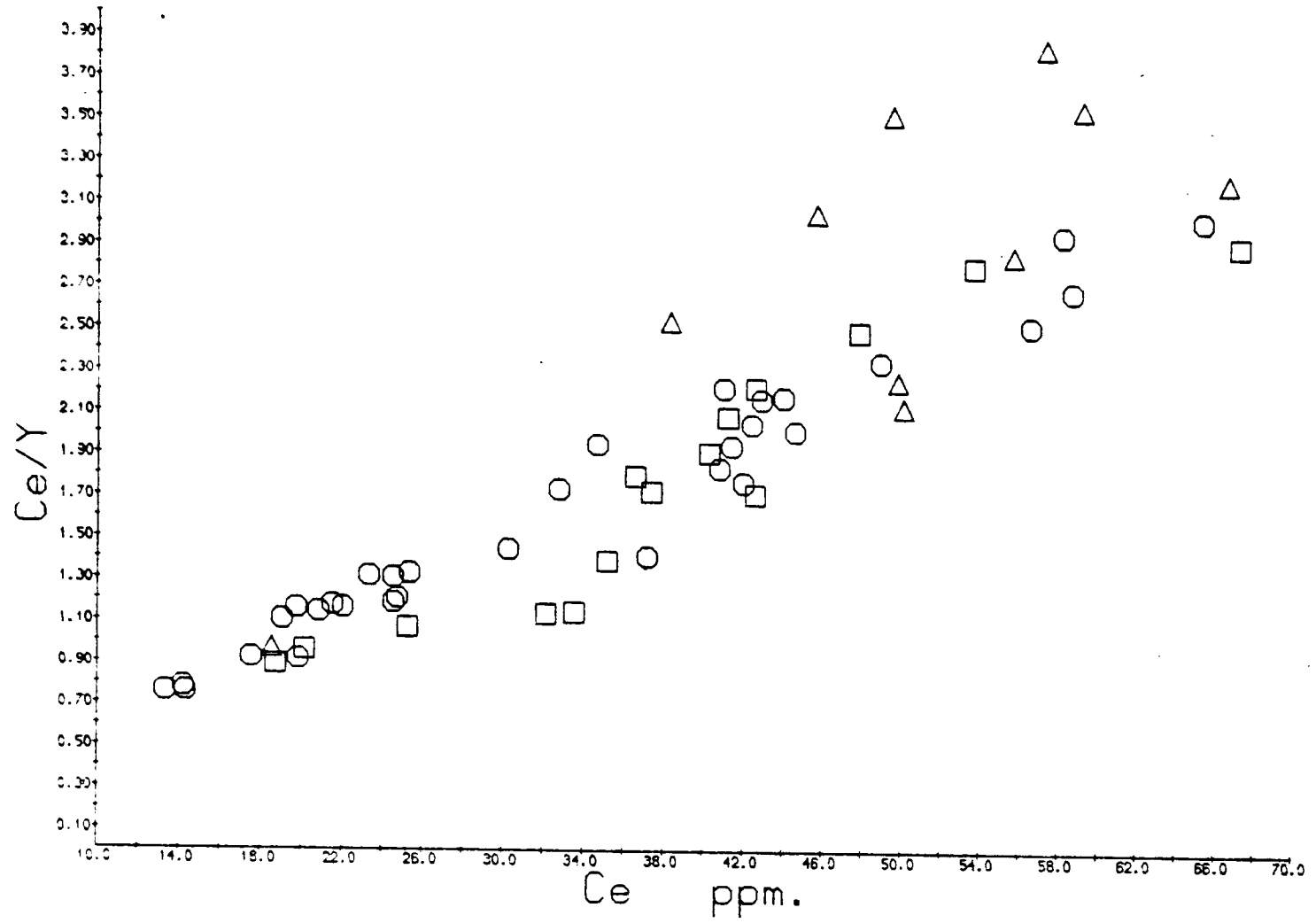
Ce/Y
3.90
3.70
3.50
3.30
3.10
2.90
2.70
2.50
2.30
2.10
1.90
1.70
1.50
1.30
1.10
0.90
0.70
0.50
0.30
0.10
10.0
14.0
18.0
22.0
26.0
30.0
34.0
38.0
42.0
46.0
50.0
54.0
58.0
62.0
66.0
70.0
Ce ppm.

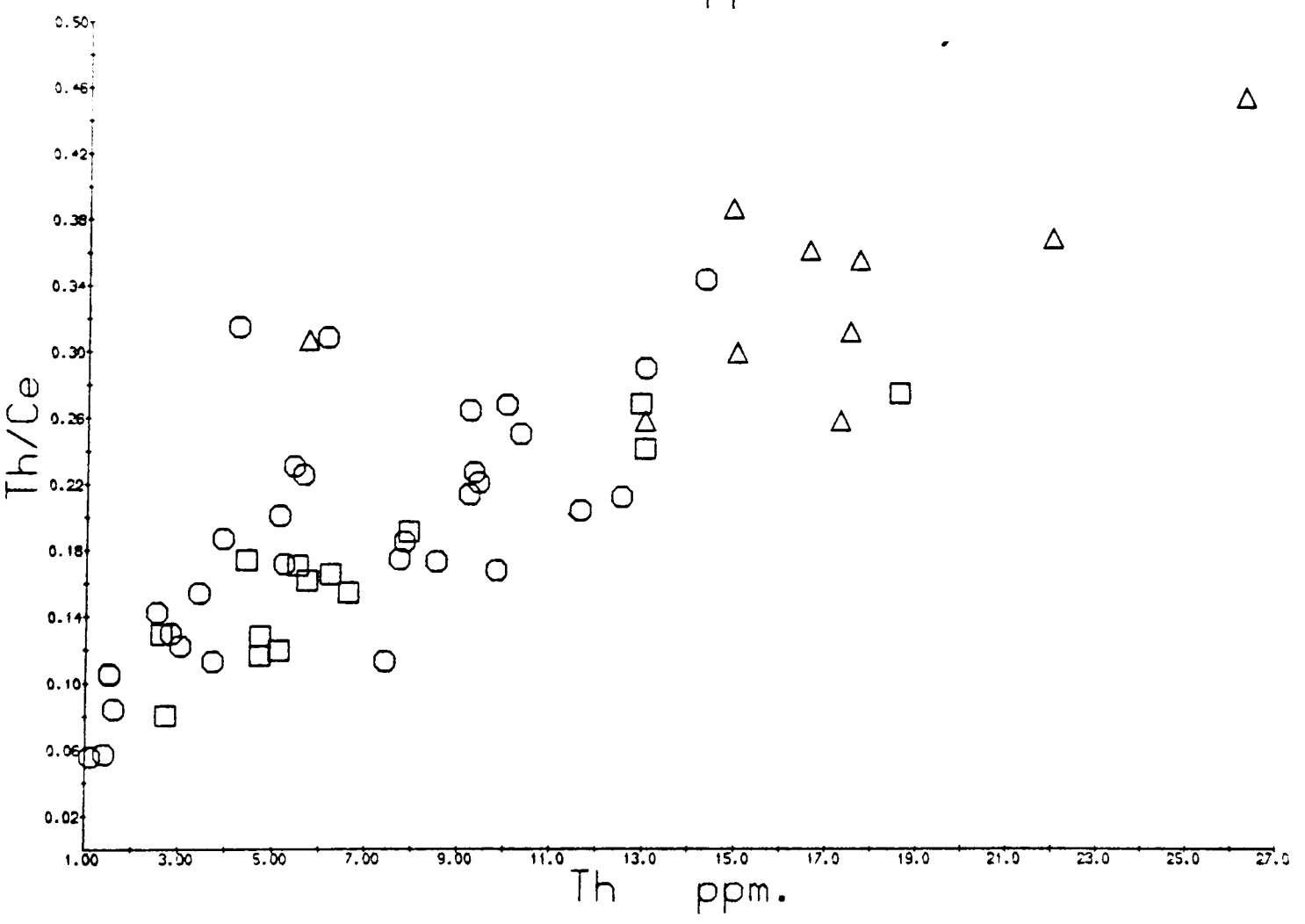
Th/Ce
0.50
0.46
0.42
0.38
0.34
0.30
0.26
0.22
0.18
0.14
0.10
0.06
0.02
1.00
3.00
5.00
7.00
9.00
11.0
13.0
15.0
17.0
19.0
21.0
23.0
25.0
27.0
Th ppm.

Figure 2.8.5

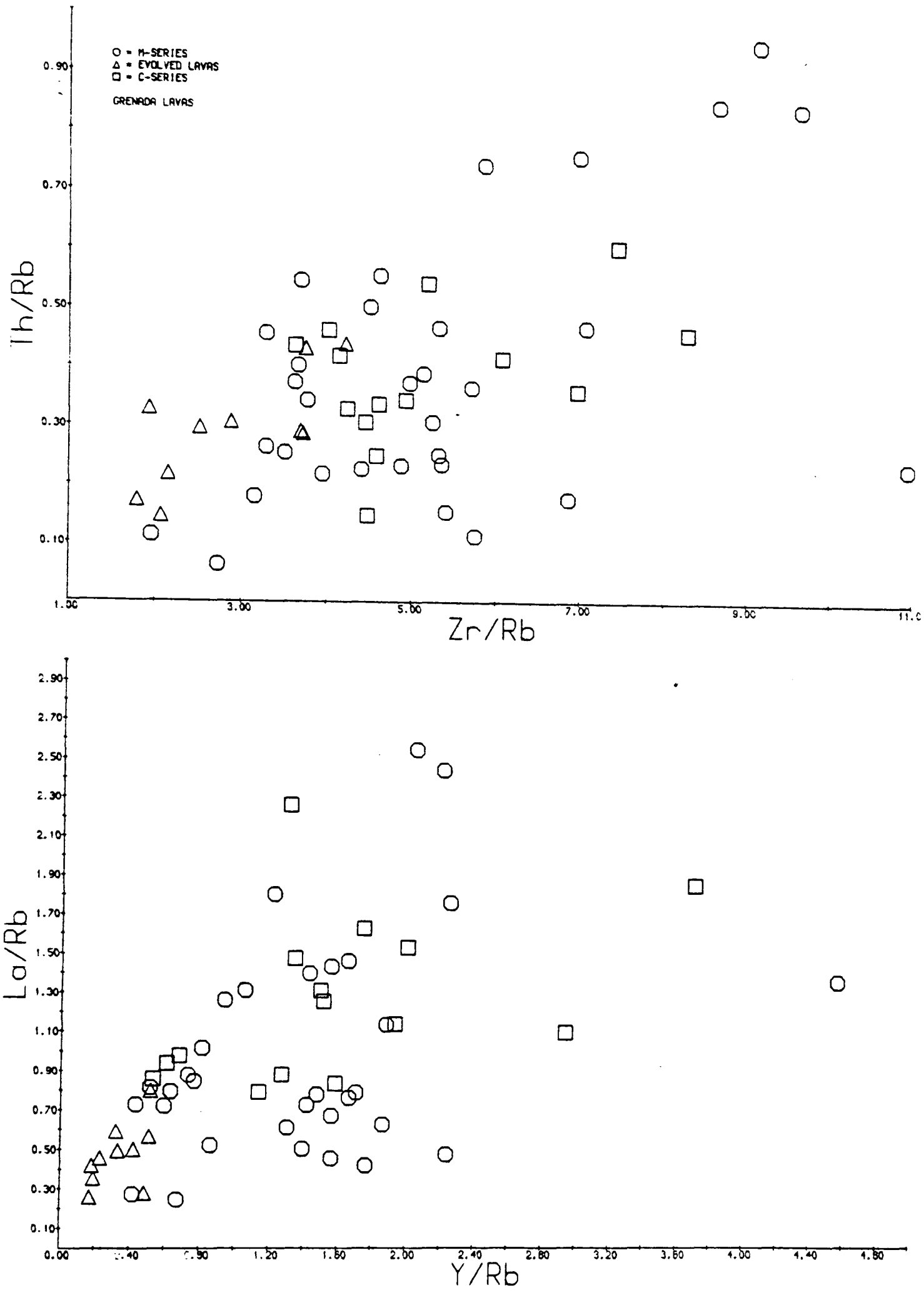
O = M-SERIES
Δ = EVOLVED LAVAS
□ = C-SERIES
GRENADA LAVAS
Th/Rb
0.90
0.70
0.50
0.30
0.10
1.00
3.00
5.00
7.00
9.00
11.0
Zr/Rb
La/Rb
2.90
2.70
2.50
2.30
2.10
1.90
1.70
1.50
1.30
1.10
0.90
0.70
0.50
0.30
0.10
0.00
1.20
1.60
2.00
2.40
2.80
3.20
3.60
4.00
4.40
4.80
Y/Rb

with concentrations of H and M elements. Plots of such elements against LREE enrichment (Figures 2.8.6, 2.8.7) show positive correlations but they are still scattered. Minster and Allegre (1978) found, however, that three of the lavas which they studied did not show particularly good agreement with their preferred model, and the increased data here confirm these discrepancies.

It was shown in section 2.6 that the major element variation in this primitive group is approximately consistent with that which would be produced by olivine crystallisation. Plots of Fe/Mg, Ni, and CaO/MgO, all of which are indices of olivine fractionation against Ce/Y (Figures 2.8.7 and 2.8.8) show rough correlations which would be expected but do not distinguish fractional crystallisation from partial melting. However the scatter on these plots is not consistent with simple partial melting. The plot of Sr against Ce/Y (Figure 2.8.7) shows a reasonable positive correlation, as do plots of other 'H' and 'M' elements.

Although these data are approximately consistent with differing degrees of partial melting followed by fractional crystallisation, they require some other mechanism to produce the observed scatter. Good positive correlations such as the Ce/Y vs. Ce diagram could be produced by mixing with a LREE enriched component with high incompatible element concentrations, whose ratios of incompatible elements were different. Variable amounts of contamination could produce the scatter on the diagrams in Figure 2.8.5. The variation of Ni and Cr is most easily produced by fractionation and suggests the effect of any mixing/contamination on compatible element concentrations would be small. This would also be expected of the major elements, with the exception of K, Ti, P (Figure 2.5.1). If the major element variation is thus due essentially to fractional crystallisation, the variation of LREE enrichment with

Figure 2.8.6 Covariation of 'H' elements with LREE enrichment in the most primitive M-series compositions

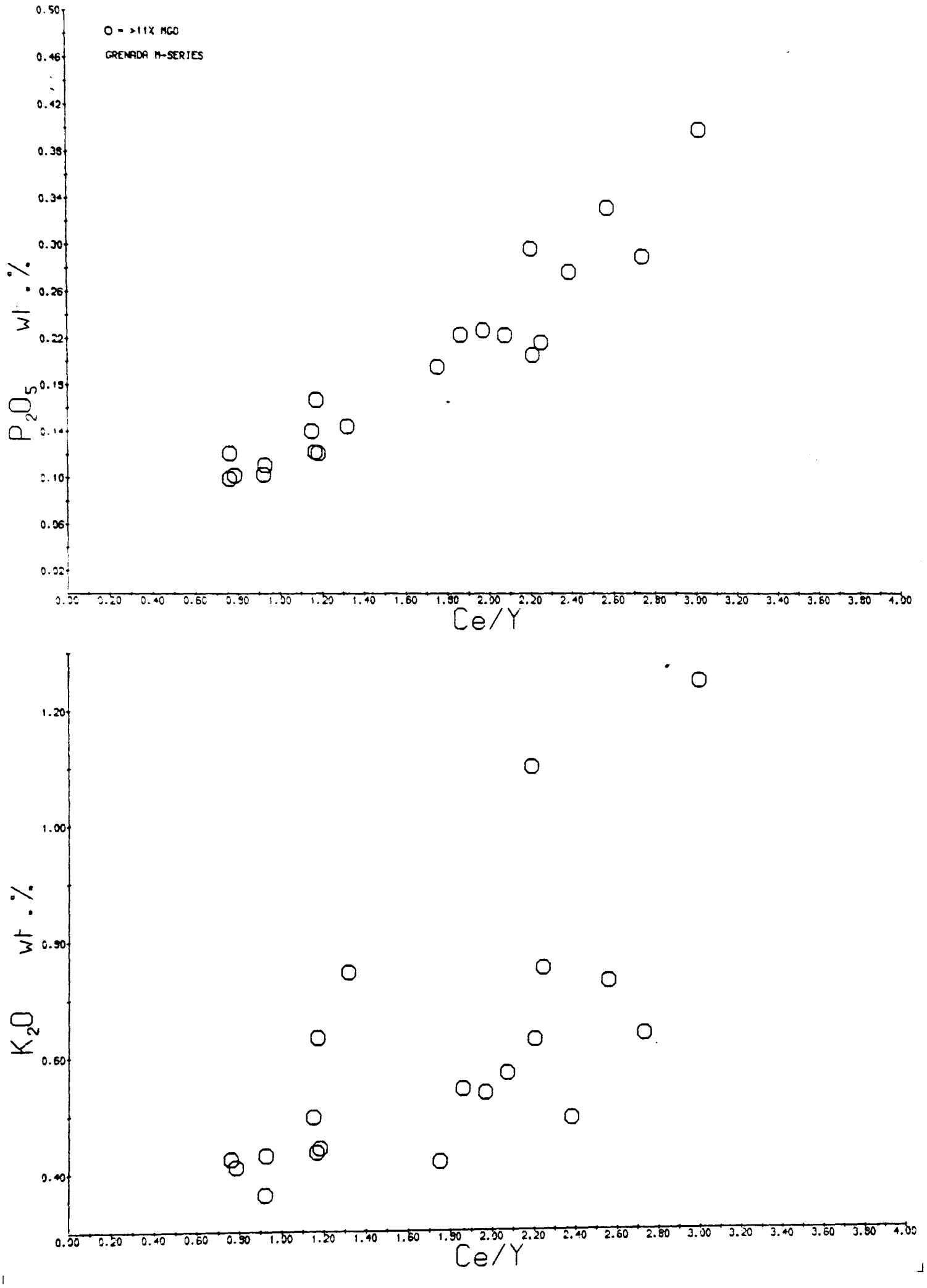

Figure 2.8.7 Covariation of Sr and Ni with LREE enrichment in the most primitive M-series compositions

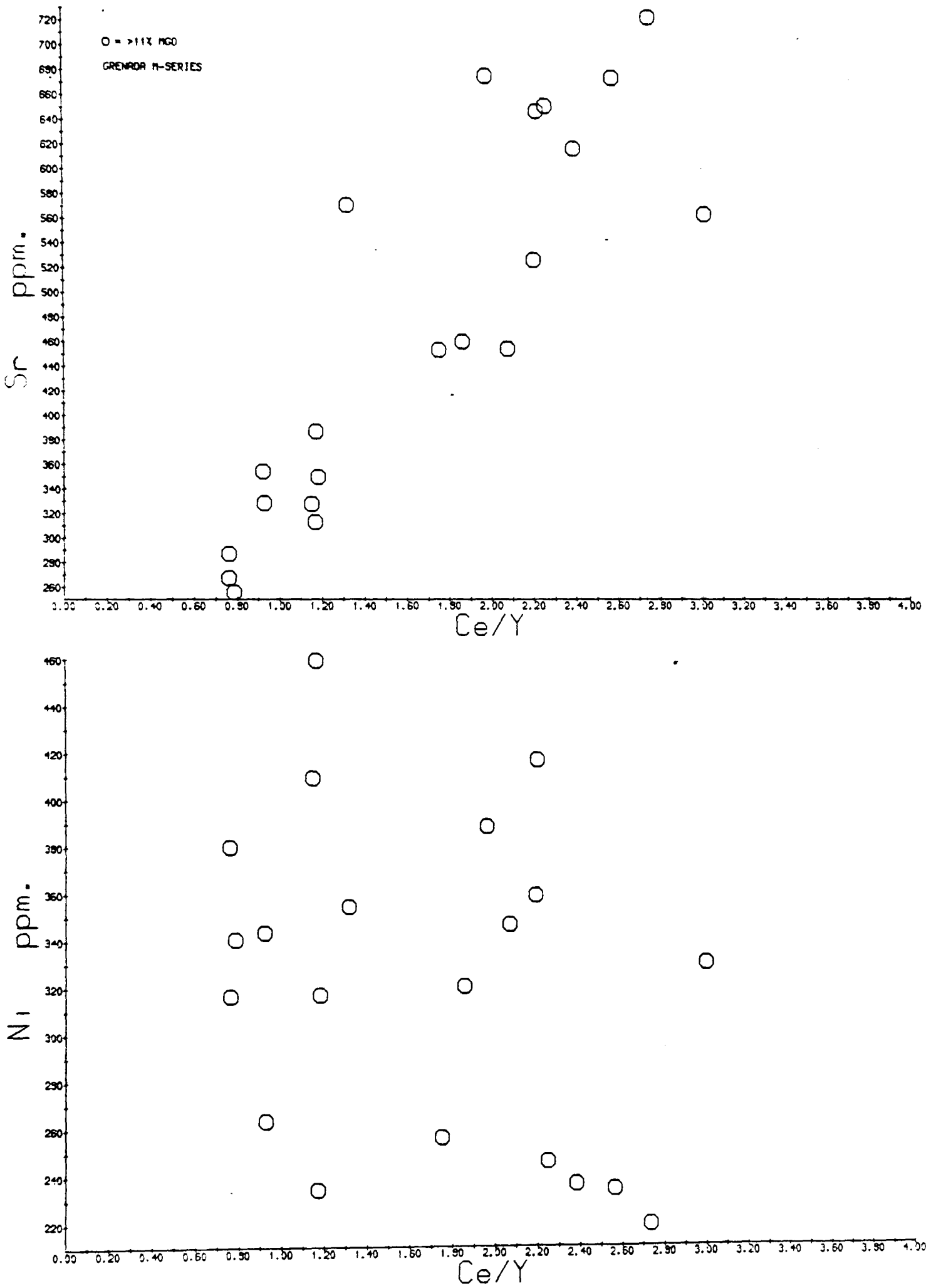

Figure 2.8.8 Covariation of major elements with LREE enrichment in the most primitive M-series compositions

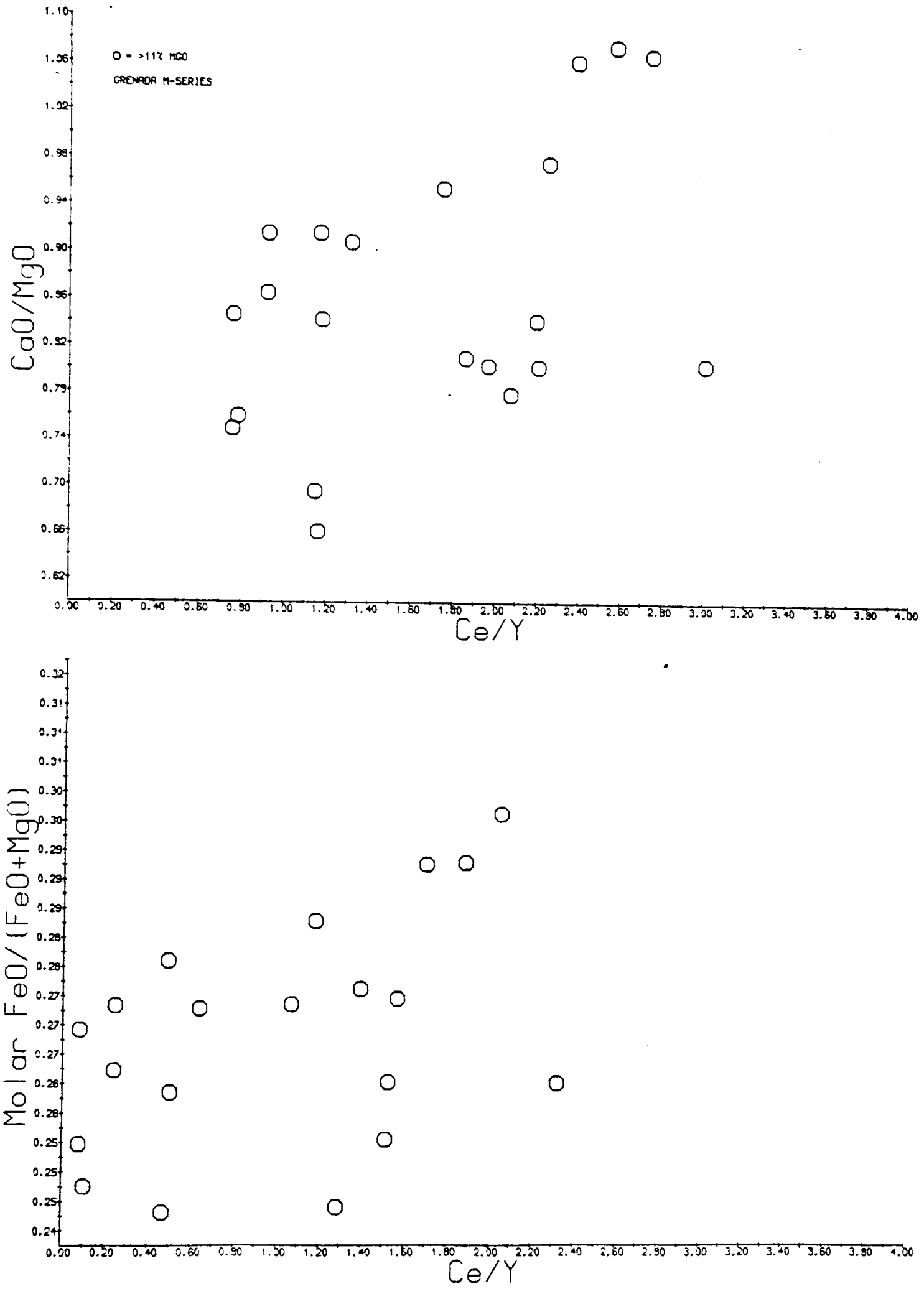

CaO/MgO suggests some sort of correlation between the amount of contamination and the amount of olivine crystallisation.

It is therefore concluded that:

(1) Much of the variation in trace element chemistry is the result of fractional crystallisation processes

(2) Partial melting followed by fractional crystallisation cannot explain the variation in H element ratios

(3) Mixing or contamination may produce trace element patterns similar to those produced by variable partial melting. If mixing is taking place, variable partial melting is not excluded but is not required

(4) If mixing has taken place, it may show some correlation with the degree of olivine fractionation in the primitive magmas.

These conclusions will be discussed further in Chapter 6 in the light of isotopic data.

2.9 Fractional Crystallisation - Qualitative Interpretation

The superimposed effects of fractional crystallisation on considerable trace element variation in the parent magmas will lead to very scattered trace element patterns in the more evolved lavas. Nevertheless, it may be possible to place constraints on the fractionating assemblages by careful analysis of the data. Qualitative interpretation is limited here to a few elements. Pearce and Norry (1979) have presented a thorough treatment of the behaviour of the high field-strength elements Ti, Zr, Nb, and Y in fractionation processes. As these elements are resistant to alteration and are commonly analysed, the data base for their study is particularly sound, and these elements were therefore selected for consideration in the Grenada suite. Figures 2.9.1 and 2.9.2 show the behaviour of Ti, Y, and Nb against Zr,

Figure 2.9.1 Trace element fractionation trends, after method of Pearce and Norry (1979). Symbols as Figure 2.8.5

Vectors represent 20% fractionation of minerals.

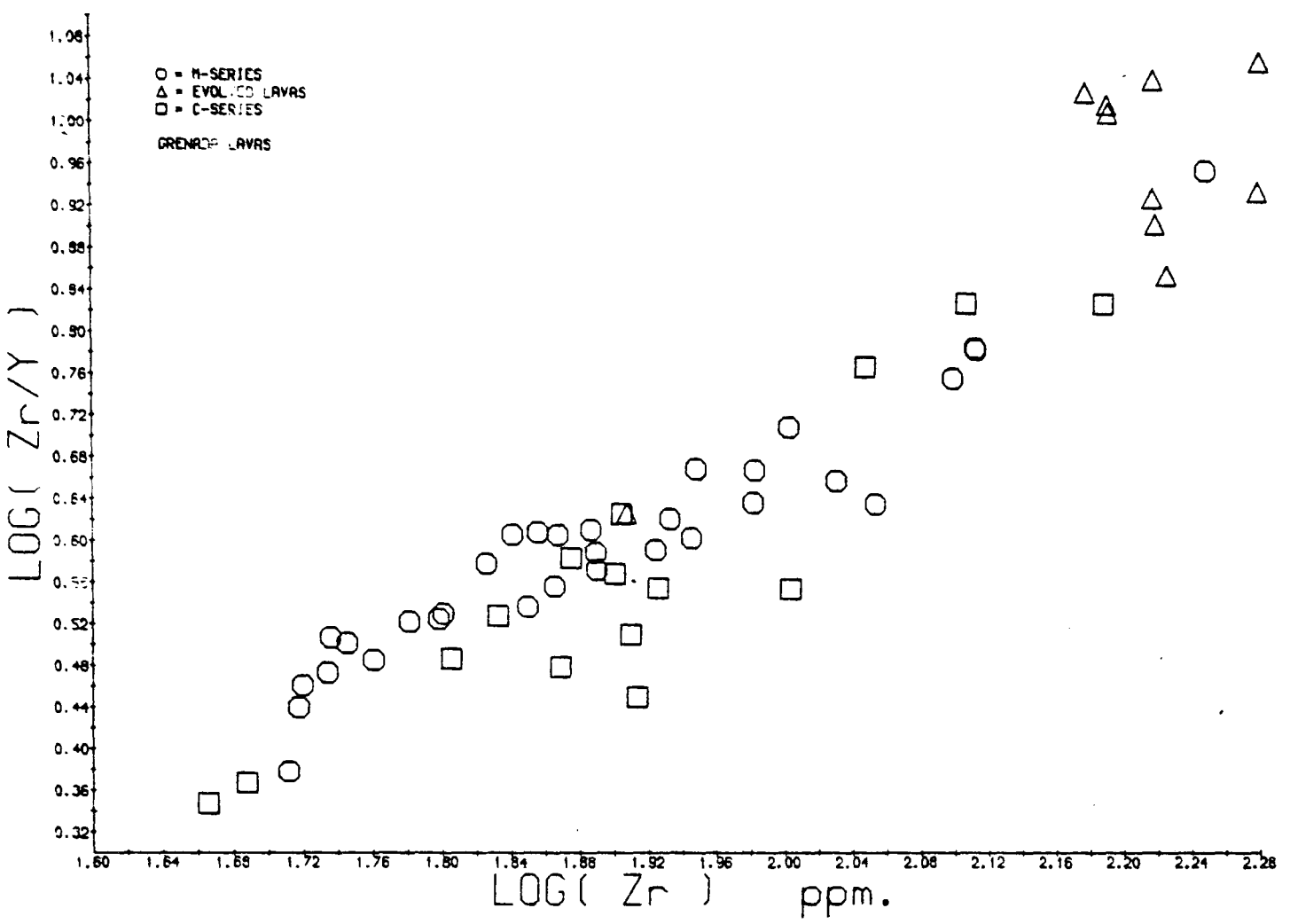

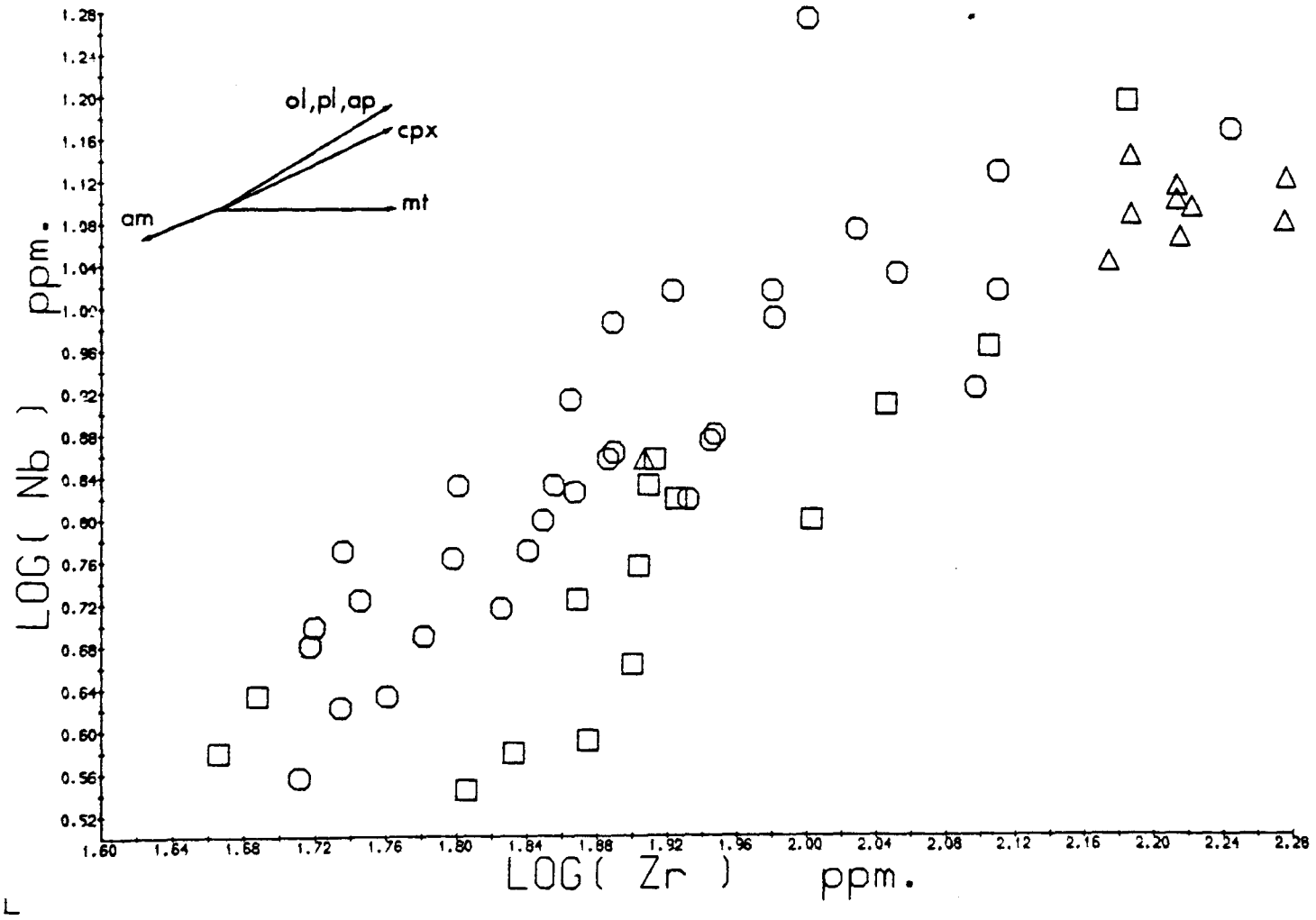

Figure 2.9.2 Trace element fractionation trends, after method of Pearce and Norry (1979). Symbols as Figure 2.8.5 Vectors represent 20% fractionation of minerals.

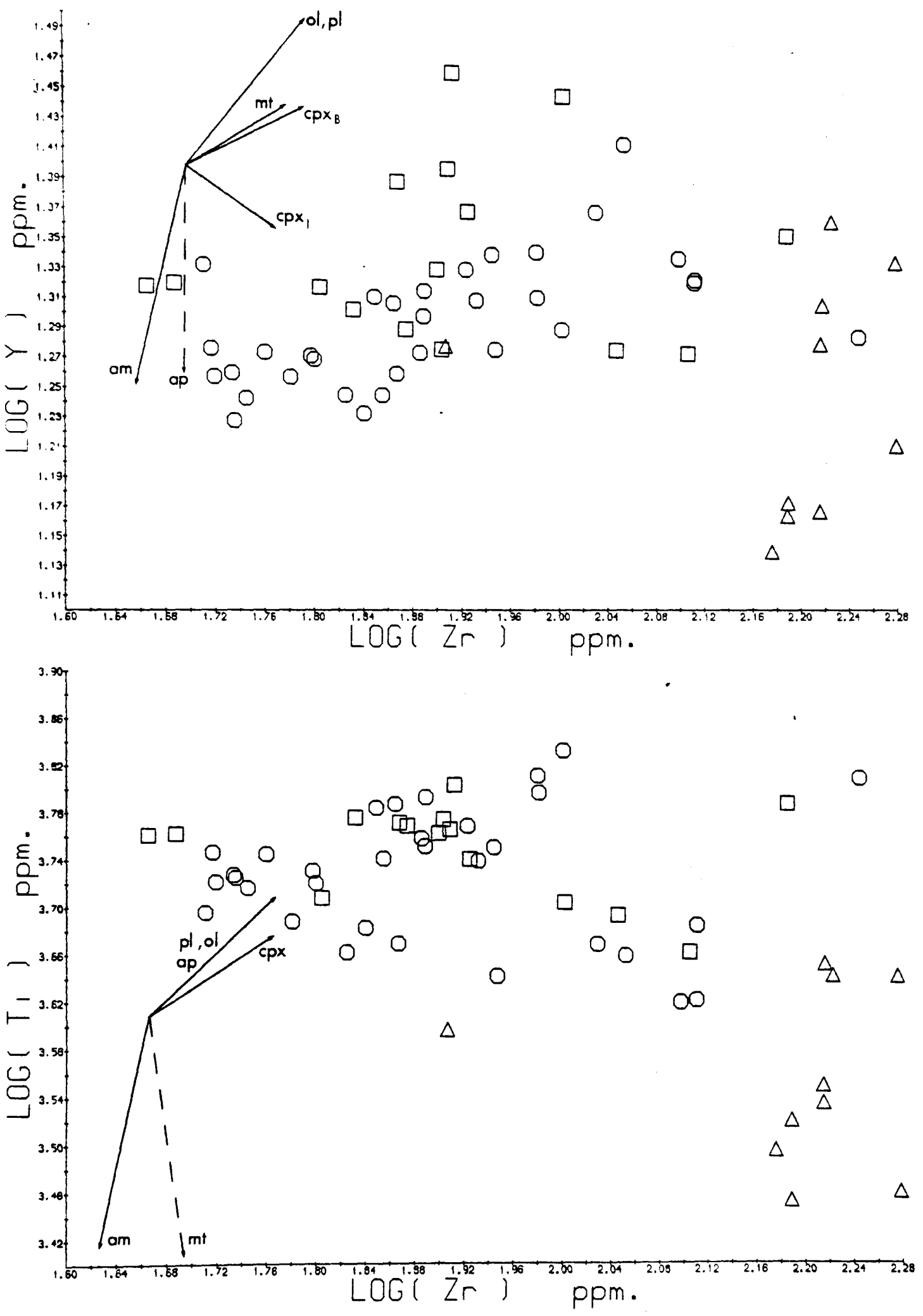

which, although not the most incompatible of trace elements, is the best index of fractionation of this group. Also shown are theoretical fractionation vectors for 20% crystallisation of various mineral phases. The Zr/Y vs. Zr diagram shows that both basaltic series have the low Zr/Y and Zr contents typical of volcanic arc basalts.

The Y-Zr diagram shows a trend within the M series consistent with olivine and clinopyroxene fractionation, while the slightly flatter C-series trend suggests a higher proportion of clinopyroxene. In the evolved lavas, the constant Zr and depleted Y could only be produced by apatite or amphibole fractionation.

The TiO_2 vs. Zr diagram suffers from the scatter on Ti in the basic lavas but some spinel phase appears necessary to explain the roughly constant TiO_2 during fractionation of both basic series. The evolved rocks show depletion in Ti consistent with fractionation of magnetite and/or amphibole.

The Nb-Zr diagram shows similar trends in the two basic series, produced by olivine and clinopyroxene or olivine, clinopyroxene, and plagioclase fractionation. The evolved lavas show a very restricted range of Nb and Zr, which indicates a substantial proportion of amphibole in the fractionated assemblage.

Ti-Y-Nb-Zr variation is therefore consistent with a model wherein the M-series evolves by fractional crystallisation dominated by olivine and clinopyroxene, and the C-series by removal of olivine, clinopyroxene, and plagioclase. Amphibole and magnetite are important phases in the fractionation of the evolved lavas, while minor apatite may also be involved.

2.10 Quantitative Trace Element Fractionation Models

The trace element concentrations may be used, along with published

distribution coefficients, to test the various major element models produced in section 2.6. Trace element models were calculated for the perfect (Rayleigh) fractional crystallisation case. This is likely to be slightly unrealistic as strongly porphyritic magmas are clearly not undergoing perfect fractional crystallisation. Also, for reasons previously stated, the magmas being considered are not directly related, and there are possible effects of disequilibrium partitioning of trace elements because of kinetic factors (Albarede and Bottinga, 1972). These factors will compound the problems caused by scatter in the trace element abundances in the primitive magmas, and it is therefore to be expected that agreement between modelled and observed trace element abundances will not be precise.

Trace element partitioning data were compiled from: Allegre et al., (1977); Arth (1976); Baker et al. (1977); Beswick and Carmichael (1978); Drake and Weill (1975); Elthon and Ridley (1979); Gill (1978); Hart and Brooks (1974); Leeman (1973); Leeman et al. (1978); Minster and Allegre (1978); Pearce and Norry (1979); Philpotts and Schnetzler (1970); Schnetzler and Philpotts (1970), and Shimizu (1974). Data for many elements are scarce and those considered most reliable are: Ni, Sc, Rb, Zr, Nb, Ba, Th, Ce, Y. Of these, the Th analytical precision is poor. Data are presented in Table 2.10.1 and selected models in Table 2.10.2.

Ni partitioning is relatively well studied, although the applicability of synthetic system experimental data to natural magmas and to high pressures is questionable (Elthon and Ridley, 1979). However, models tend to predict substantially lower Ni than is observed. Although other processes have been shown to be involved in model (2), this feature needs to be explained in the other models. A possible factor is kinetic disequilibrium which, in a large and fairly rapidly cooling magma body, would result in apparent D values substantially less than

Table 2.10.1

Trace element distribution coefficients used in fractionation calculations

Phase	ol	cpx	plag	amph	sp	mt
Ni	***	5	.20	10	16	12
Cr	1.8	6	.04	15	600*	24
V	.2	1.1	.01	32	10	20
Sc	.35	3	.03	7.3	2	2
Sr	.003	.08	***	.13	0	0
Rb	0	.003	.03	.03	0	0
Zr	.01	$.01^{B}_{.25^{I}}$	.02	$.5^{B}_{1.4^{I}}$	0	$.1^{B}_{.2^{I}}$
Nb	.01	.2	$.01^{B}_{.025^{I}}$	$.8^{B}_{1.3^{I}}$	0	$.4^{B}_{1.0^{I}}$
Ba	0	.002	.15	.07	0	0
Th	0	0	0	0	0	0
La	0	.07	.1	.2	.04	0
Ce	.004	.15	.1	.15	.04	0
Y	.01	$.5^{B}_{1.5^{I}}$	$.03^{B}_{.06^{I}}$	$1.0^{B}_{2.5^{I}}$	.04	$.2^{B}_{.5^{I}}$

*** D_{Ni} and D_{Sr} are both strong functions of T/composition

D_{Ni} estimated from data compilation of Elthon and Ridley (1979)

D_{Sr} estimated from data of Drake and Weill (1975)

* D^{sp}_{Cr} likely to be highly variable but insufficient data exist

B,I D values in basic and intermediate lavas compiled by Pearce and Norry (1979)

Table 2.10.2

Trace element fractionation models

Model	Ni	Cr	V	Sc	Sr	Rb	Zr	Nb	Ba	Th	La	Ce	Y
2. 468-286													
measured	219	454	286	29	727	23	84	10.4	380	12.5	29	59	21
predicted	172	939	240	36	356	14	62	6.7	180	6.9	6.9	22	19
3. 468-319													
measured	273	565	206	29	537	21	113	10.8	429	10.0	38	37	26
predicted	21	235	144	21	513	20	90	9.3	265	10.2	10	32	25
5. 468-398													
measured	155	427	173	23	523	35	125	8.4	450	13.0	28	45	22
predicted	5	108	119	16	645	26	115	11.5	336	13.0	13	39	29
7. 398-307													
measured	48	105	160	18	479	45	168	12.5	467	13.0	26	50	23
predicted	68	135	165	21	584	39	141	9.3	505	14.6	31	49	24
8. 468-6104													
measured	55	108	308	40	1396	14	64	3.5	336	4.7	18	40	21
predicted	31	864	261	38	395	15	69	7.4	200	7.7	8	25	21
11. 6104-337													
measured	31	33	208	18	1022	31	128	9.2	498	13.0	29	54	19
predicted	4	2	63	21	487	39	165	8.4	903	13.5	48	103	35
13. 337-381													
measured	21	33	189	17	966	39	165	11.7	629	17.3	31	66	20
predicted	13	8	33	15	668	40	150	10.8	636	17.0	37	68	19

the equilibrium values for elements of high D (Albarede and Bottinga, 1972). For chromium, the D value will be strongly dependent on factors controlling spinel compositions, such as pressure, oxygen fugacity and melt composition, so that little can be deduced from models for this element. Similar difficulties apply to vanadium. However, derivation of the C-series from a parent similar to that for the M-series would require fractionation of a small proportion of Cr-spinel along with olivine.

Sc data provide a reasonable fit, particularly in the C-series where they confirm the importance of clinopyroxene fractionation. Sr models in the M-series are subject to the large scatter in the primitive magmas, while the C-series D values, dominated by plagioclase, appear to be too large. The experimental data of Drake and Weill (1975) and Korringa and Noble (1971) do not agree well, and uncertainty over the D values may explain much of the discrepancy. Other incompatible elements also suffer from the scatter in the primitive magmas of the M-series, although Y models are reasonable. In the C-series most of these elements fit well, except LREE.

In conclusion, there are too many uncertainties in the partitioning data and its modelling to test rigorously the major element fractionation models. However, the following conclusions can be reached:

(1) The trace element models are not incompatible with major element fractionation models in the M-series, although some additional mechanism is required to provide the variation in the most primitive magmas.

(2) Models deriving the C-series from an M-series parent similar to 468 do not, in general, provide a good fit for the alkaline earths Ba and Sr.

(3) Models of fractional crystallisation in the C-series provide a reasonable fit to the trace element data, and indicate that amphibole is a fractionating phase in the origin of andesites from this series.

2.11 Conclusions

(a) Two petrographically and chemically distinct groups of basalts occur.

(b) The magnesian basalts (M-series) appear to have fractionated at high pressures and to have reached the surface close to or above their liquidus temperatures.

(c) Apart from this high-pressure mechanism, the major element chemistry is consistent with fractional crystallisation of phenocryst phases.

(d) The more evolved, porphyritic basalts (C-series) show evidence of derivation from a more primitive parent.

(e) Cumulus enrichment has not been an important factor in producing the major element chemistry.

(f) Wide variations in the abundances of trace elements in the M-series cannot be the result of simple fractional crystallisation. Variation in the ratios of H elements requires that some mixing process, rather than partial melting, was responsible. A similar process has affected the C-series parents but to a lesser extent.

(g) This trace element variability makes rigorous trace element modelling very difficult.

(h) The behaviour of high field-strength elements shows that amphibole fractionation, accompanied by small amounts of apatite, is important in basaltic andesites and more evolved rocks.

CHAPTER 3

CUMULATE BLOCKS

Cumulus plutonic blocks occur on all the major islands of the late Miocene to Recent volcanic arc in the Lesser Antilles. They were first described in detail by Lacroix (1904) who studied the abundant blocks in the products of the 1902 eruption of Soufriere, St. Vincent. Petrological studies of other islands have also recorded the occurrence of cumulates, especially those of Lewis (1964, 1973) who studied the St. Vincent blocks in considerable detail, and Wills (1974) who studied a selection of blocks from most of the islands, describing their mineralogical and textural variation and discussing their origin in terms of crystal accumulation in subvolcanic magma chambers. Further work on Wills' samples has been carried out by R. J. Arculus (Arculus and Wills, in prep.).

3.1 Occurrence and general features

In Grenada the plutonic blocks occur largely in reworked volcanics. By comparison with the St. Vincent samples, they are believed to have been erupted mainly in pyroclast flows, although a few may have originated in fall deposits. These deposits are rapidly eroded by tropical rainfall, as in St. Vincent in 1902 and 1979, and the blocks are easily collected in fluvially-reworked material or as loose boulders in the present river beds, where they range up to 25 cm. in size. Little information can therefore be derived from their occurrence, although they are believed to be present in all the Grenada eruptive centres. An important point to note is that the sampling of reworked pyroclastics will be biased towards those assemblages which are most resistant to abrasion and fracturing during transport. In St. Vincent many of the 1902 and 1979 blocks, especially the olivine-anorthite types which are believed

to have crystallised at the highest temperatures (Lewis, 1973), are very friable. It is therefore possible that some types of cumulate are under-represented or even absent from the Grenada sample. No inference is therefore drawn from the distribution of sample types.

Where remains of the host magma are preserved in contact with the blocks, the magma is an amphibole-bearing basaltic andesite or andesite, normally with a glassy, vesicular groundmass, and is therefore similar to the host scoria of the St. Vincent blocks although the presence of abundant amphibole in Grenada is distinctive.

Intercrystalline scoria is frequently present in Grenada blocks, where it is microcrystalline to glassy but, by inference from studies of the blocks from the 1979 eruption in St. Vincent (Graham and Thirlwall, in prep.), is not thought to represent equilibrium liquid. There is, of course, no reason why the andesitic lava occasionally found in contact with the blocks should represent the magma from which they crystallised, as it is probable that the basaltic magmas rarely produced pyroclast flows and the blocks may be accidental rather than cognate xenoliths. Direct observation or analysis of the magma in equilibrium with the blocks is therefore not possible.

The Grenada blocks are very heterogeneous in hand specimen appearance. They show most of the features described by Lewis (1973) in the St. Vincent blocks, and variation in grain size within and between blocks, modal proportions of the phases, and textural relationships produces a wide range of structures. Where blocks are layered, boundaries between adjacent layers are sharp and layers may be defined by modal or grain size variations. However a patchy appearance, rather than continuous layering, is often evident, and this is chiefly due to variable habit and proportion of amphibole, which may be form very large crystals (>5 cm.) and sometimes shows a well-developed harrisitic

texture. No rhythmic layering of the type found in many layered basic intrusions is evident and, if present in the original cumulate body, must have been on a greater scale than that of the sampled fragments. The blocks are generally fresh apart from common iddingsitisation of olivine and minor oxidation of magnetite-rich spinel, and are composed of olivine, clinopyroxene, amphibole, plagioclase, and spinel with orthopyroxene and apatite occasionally seen in thin section. They are distinctive from those of islands to the north of the Grenadines in including examples free from plagioclase. Texturally, the blocks are dominantly adcumulates, with occasional heteradcumulates, crescumulates and mesocumulates, while orthopyroxene-bearing samples are transitional from adcumulates to orthocumulates.

3.2 Cumulus processes

Wager (1962), Lewis (1964, 1973) and Wills (1974) interpreted the cumulate blocks of the Lesser Antilles largely as products of crystal settling in subvolcanic magma bodies with volumes, suggested by pyroclastic eruptions, of up to a few cubic kilometres. However recent workers (e.g. Campbell, 1978; McBirney and Noyes, 1979) have challenged the prevalent view of the origin of cumulates by gravitational settling of crystals. They have pointed out the theoretical difficulty of settling crystals with low, or even negative, density contrasts in a non-Newtonian magma. McBirney and Noyes (1979) suggest that this process is especially difficult in melts whose structure is sufficiently polymerised for them to be in equilibrium with plagioclase. Although the Grenada magmas may have had lower yield stresses due to the presence of water, the temperatures of the magmas are lower (Chapter 5) than those considered by McBirney and Noyes (1979) and the results of their calculations may therefore be applicable to the Grenada magmas. These authors

have also challenged the evidence for crystal settling in the Skaergaard intrusion, for long regarded as a prime example of the process. In particular they considered the textures of the cumulates and the macroscopic layering features to be more consistent with a model of *in situ* crystallisation at the margins of the intrusion.

Although macroscopic variation in the Grenada cumulates is obscured by their sampling as isolated blocks, it is believed that the textures support an *in situ* crystallisation model. This textural evidence includes the harrisitic amphiboles, igneous lamination, and inclusion patterns in cumulus amphibole and is discussed with reference to individual cumulate types.

3.3 Classification

In view of the recent challenges to conventional crystal settling hypotheses, the use of the widely accepted cumulate nomenclature of Wager *et al.* (1960) is open to criticism. However, this classification is still useful in describing textural variations, even though these may now be interpreted in terms of nucleation and growth rather than rates of crystal settling and equilibration with the parental magma, and is so widely used that it is worth retaining. The use of cumulate nomenclature in this study does not have genetic connotations.

The Grenada blocks may be classified, either in terms of their cumulus phases, or in terms of their mineral assemblages. The first is a textural classification reflecting order and rate of nucleation, rate of growth, and rate of equilibration with liquid. On the other hand, a mineralogical classification has advantages in that it simply represents the coexisting mineral phases. This is especially so since the minerals are usually unzoned and may constitute equilibrium assemblages. This assumption in classification is discussed in section 3.6. A mineralogical classification is therefore adopted in this study (Table 3.3.1).

Table 3.3.1

Classification of Grenada Cumulates

type	mineral assemblage	variants
A	ol + cpx + amph	amph.-free
B	ol + cpx + amph + pl	amph.-free
C	ol + cpx + amph + pl + opx	
D	cpx + amph + pl	amph.-free
E	cpx + amph + pl + opx	
F	amph + pl	
G	amph	

All assemblages include a spinel phase

3.4 Petrography

With the exception of relict oscillatory zoning in clinopyroxene, the minerals within the cumulate blocks show very little zoning in thin section. The general petrographic features of each group are summarised below and interpreted in terms of order of crystallisation. Examples are figured in Plates 3.1 to 3.7.

3.4.1 Type A assemblages

The type A blocks are adcumulates, heteradcumulates, or mesocumulates. There is a complete textural gradation between the adcumulates and heteradcumulates corresponding to variation in the habit of amphibole between extremes of subhedral to euhedral cumulus and large, anhedral poikilitic. Grain size is highly variable within and between samples, but no size grading is present. The generally small and subhedral olivines are always at least partially iddingsitised and are often included in clinopyroxene or amphibole, although they also occur as separate cumulus grains. The clinopyroxene shows occasional relict zoning and is only rarely replaced by amphibole, indicating that there is normally no reaction relationship between these phases and the equilibrium liquid. In all samples amphibole forms the largest grains and includes all the other phases. It is therefore interpreted as the latest silicate phase to crystallise. Cumulus amphiboles often contain many small and widely spaced inclusions, which indicates that the included phases were suspended in liquid rather than accumulated in a self-supporting framework when included by the later amphibole.

Spinel occurs, although never abundantly, in all examples and may be included in all the silicate phases. As a consequence of its small size, it is easily included by the silicates during adcumulus growth, and its place in the crystallisation sequence is difficult to determine. On balance, the textural evidence suggests continuous crystallisation

Plate 3.1 (a)

Type A adcumulate 6067, comprising colourless, slightly altered olivine, pale green calcic clinopyroxene and olive-green amphibole, with intercrystalline scoria. Small spinels are occasionally included in the silicates. Field of view 14mm. Plane polarised light.

Plate 3.1 (b)

Type B heteradcumulate 6052, showing large poikilitic amphiboles including iddingsitised olivine, clinopyroxene, and occasional plagioclase. Transitional to type A. Crossed polars; f.o.v. 14mm.

Plate 3.2 (a)

Type B adcumulate 6107, with amphibole enclosing olivine and clinopyroxene. Some reaction of clinopyroxene with amphibole is evident. The texture suggests crystallisation of amphibole before plagioclase. Plane polarised light; f.o.v. 20mm.

Plate 3.2 (b)

Amphibole-poor type B cumulate 6066. Relict oscillatory zoning is present in the clinopyroxenes in the centre of the field of view. Olivine is dark red due to iddingsitisation, while plagioclase clearly crystallised before amphibole. Plane polarised light; f.o.v. 14mm.

Plate 3.3 (a)

Type B adcumulate 6051 containing some intercrystalline scoria. Clinopyroxene shows only slight reaction, while the texture does not clearly define the relative stability of plagioclase and amphibole. Plane polarised light; f.o.v. 14mm.

Plate 3.3 (b)

Composite nodule 6099. The lower part comprises a plagioclase-free type A assemblage, separated from the overlying plagioclase-bearing and amphibole-free type D assemblage by a pyroxene-rich band. The chemistry of the minerals in the type A layer indicate equilibration with the type D assemblage (see text). Plane polarised light; f.o.v. 20mm.

Plate 3.4

Type C orthocumulates 6168 (top) and 6121 (bottom) showing abundant large poikilitic amphiboles including olivine, clinopyroxene, spinel and plagioclase. Orthopyroxene occurs as small, colourless grains at the margins of the amphiboles. Sample 6168 (top) shows a weak igneous lamination in plagioclase, suggesting crystallisation *in situ*. Plane polarised light; f.o.v. 14mm.

Plate 3.5

Type D adcumulates X28150C (top) and 6092 (bottom). These assemblages are the most common among those sectioned, and show wide variation in grain size and texture. Sample 6092 (bottom) shows the elongate amphibole habit common in andesitic extrusive rocks from Grenada. Plane polarised light; f.o.v. 14mm.

Plate 3.6 (a)

Amphibole-free type D cumulate 6096. Weak relict zoning can be seen in the clinopyroxene, while the relatively large spinels are typical of type D assemblages. The absence of amphibole is rare in Grenada cumulates, and may reflect crystallisation of a relatively dry magma. Plane polarised light; f.o.v. 14mm.

Plate 3.6 (b)

Amphibole-plagioclase type F mesocumulate 6136. The mineral assemblage indicates derivation of this assemblage from an andesitic magma. The intercumulus liquid contains ortho- and clinopyroxene and apatite. Plane polarised light; f.o.v. 14mm.

Plate 3.7

Banded, amphibole-free type D adcumulate 6222. The banded appearance results from modal variation of plagioclase and clinopyroxene and from the igneous lamination in the plagioclase-rich layer. Crossed polars; f.o.v. 20mm.

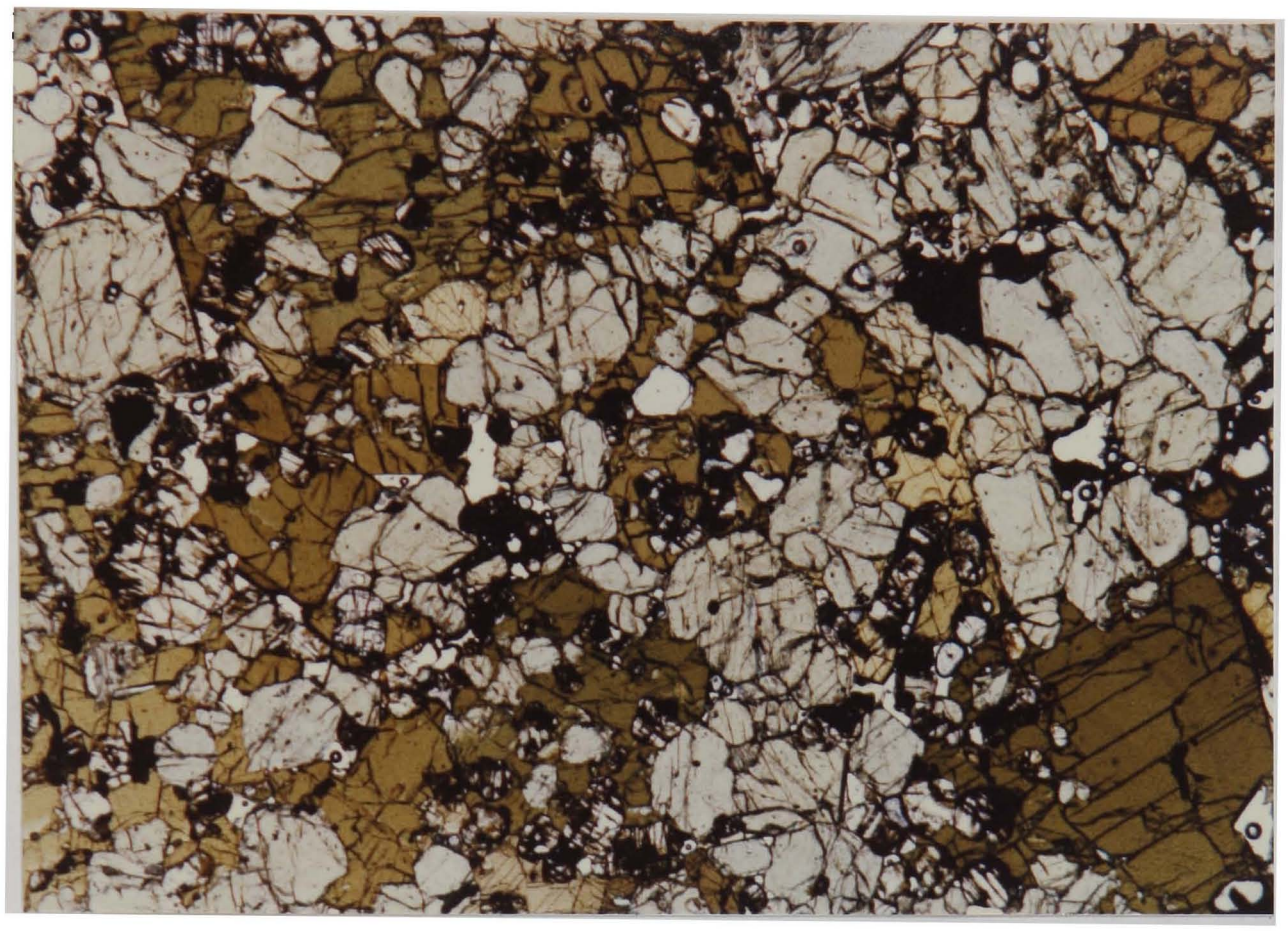

(a)

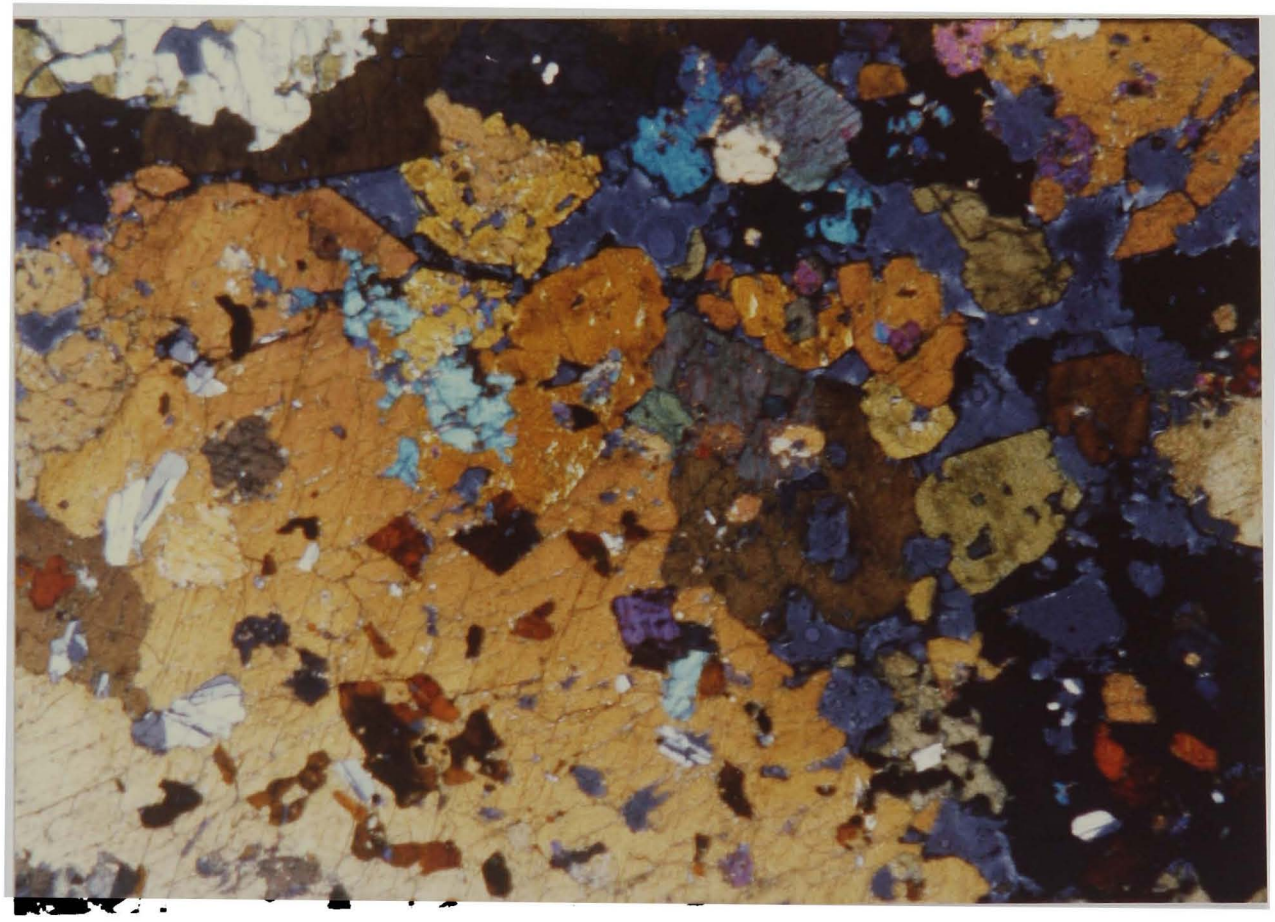

(b)

Plate 3.1

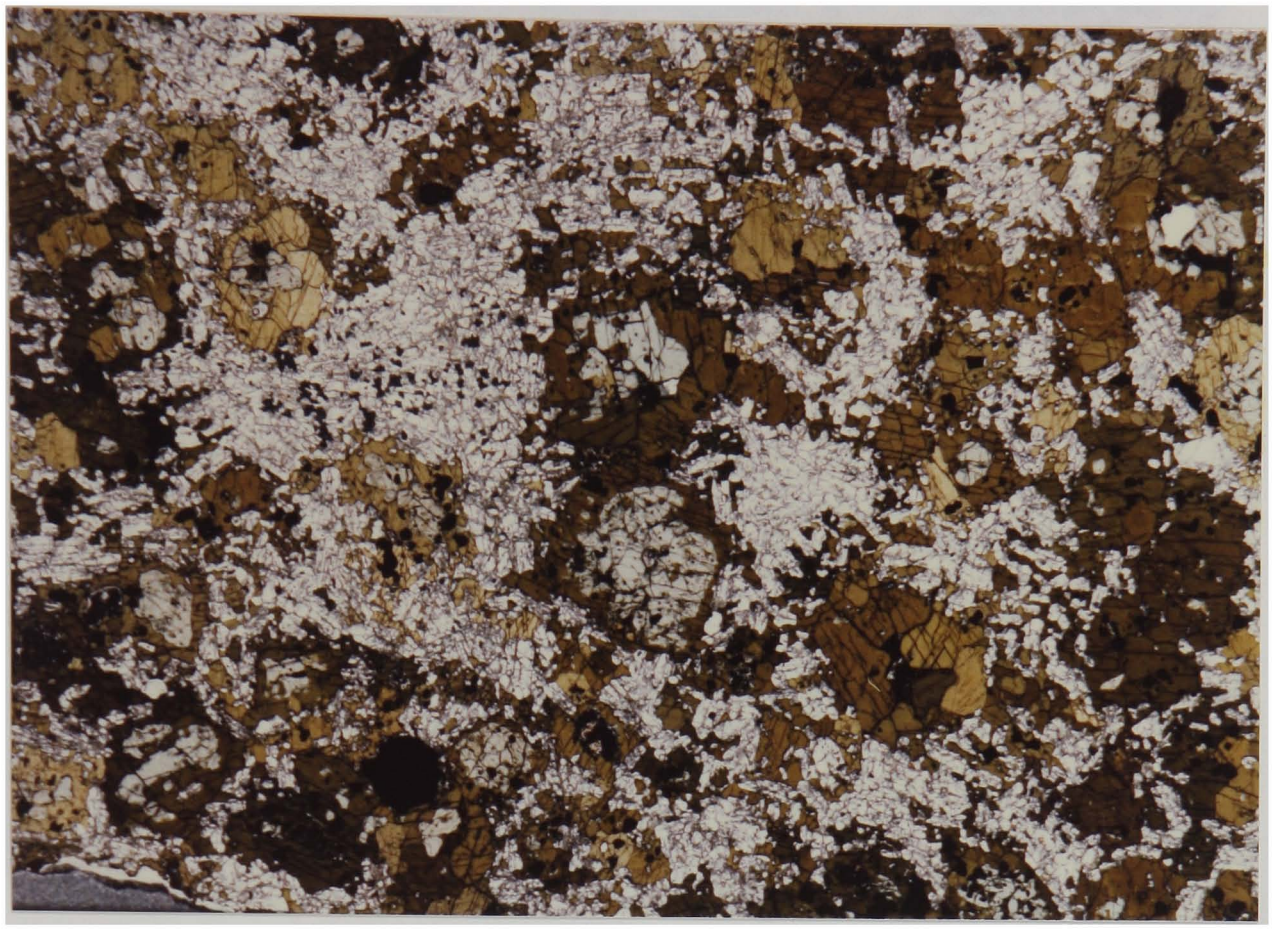

(a)

(b)

Plate 3.2

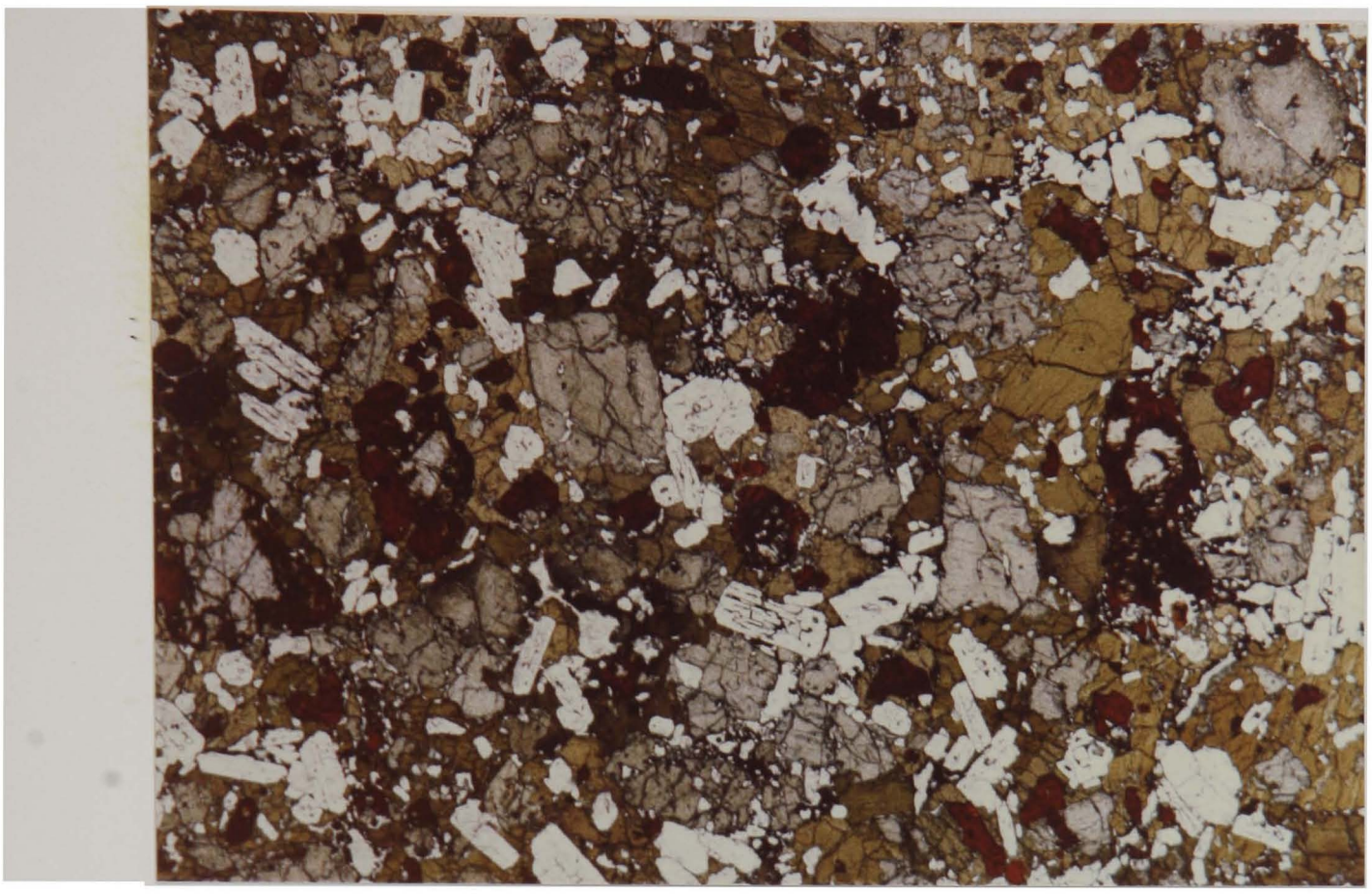

(a)

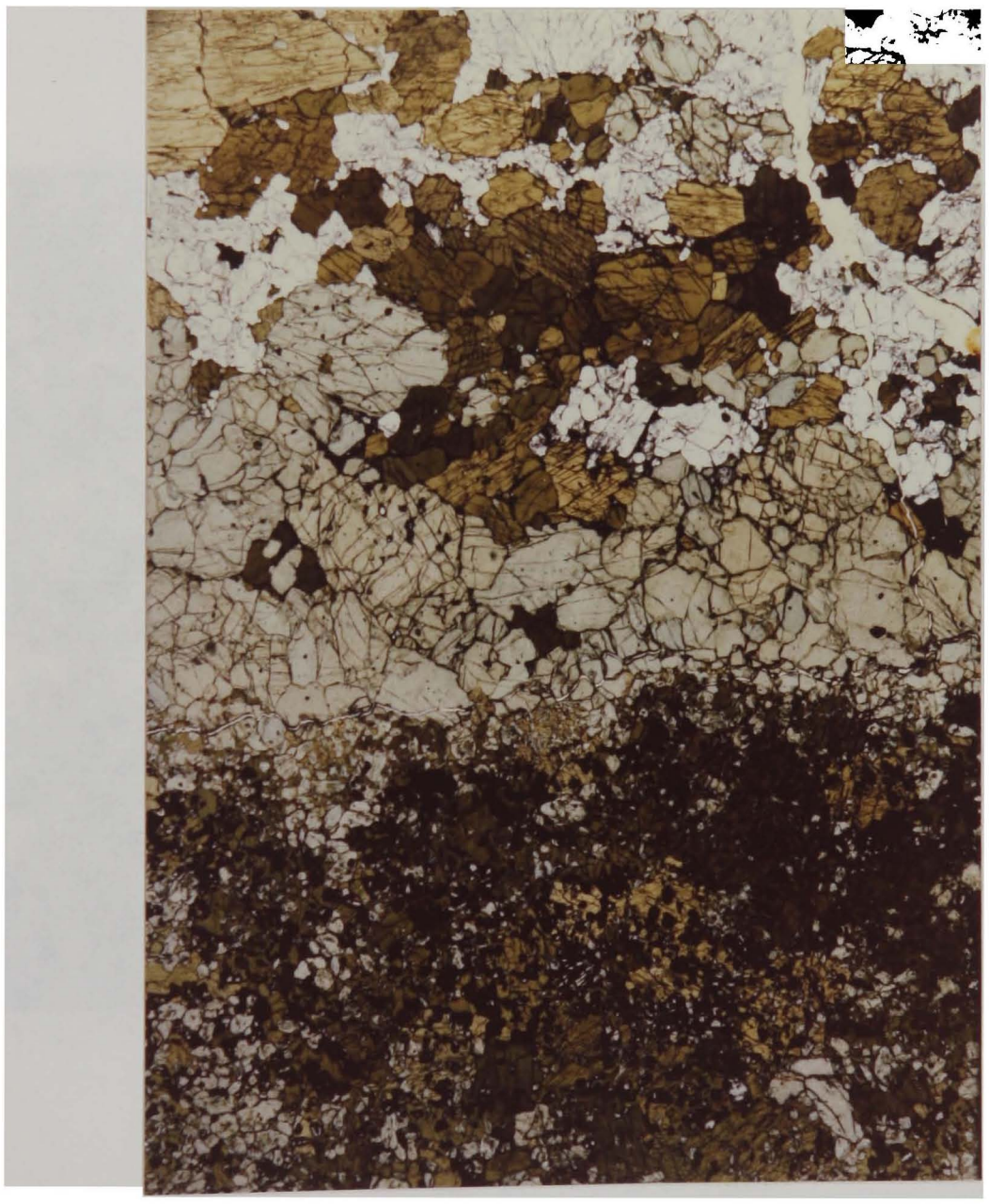

(b)

Plate 3.3

(a)

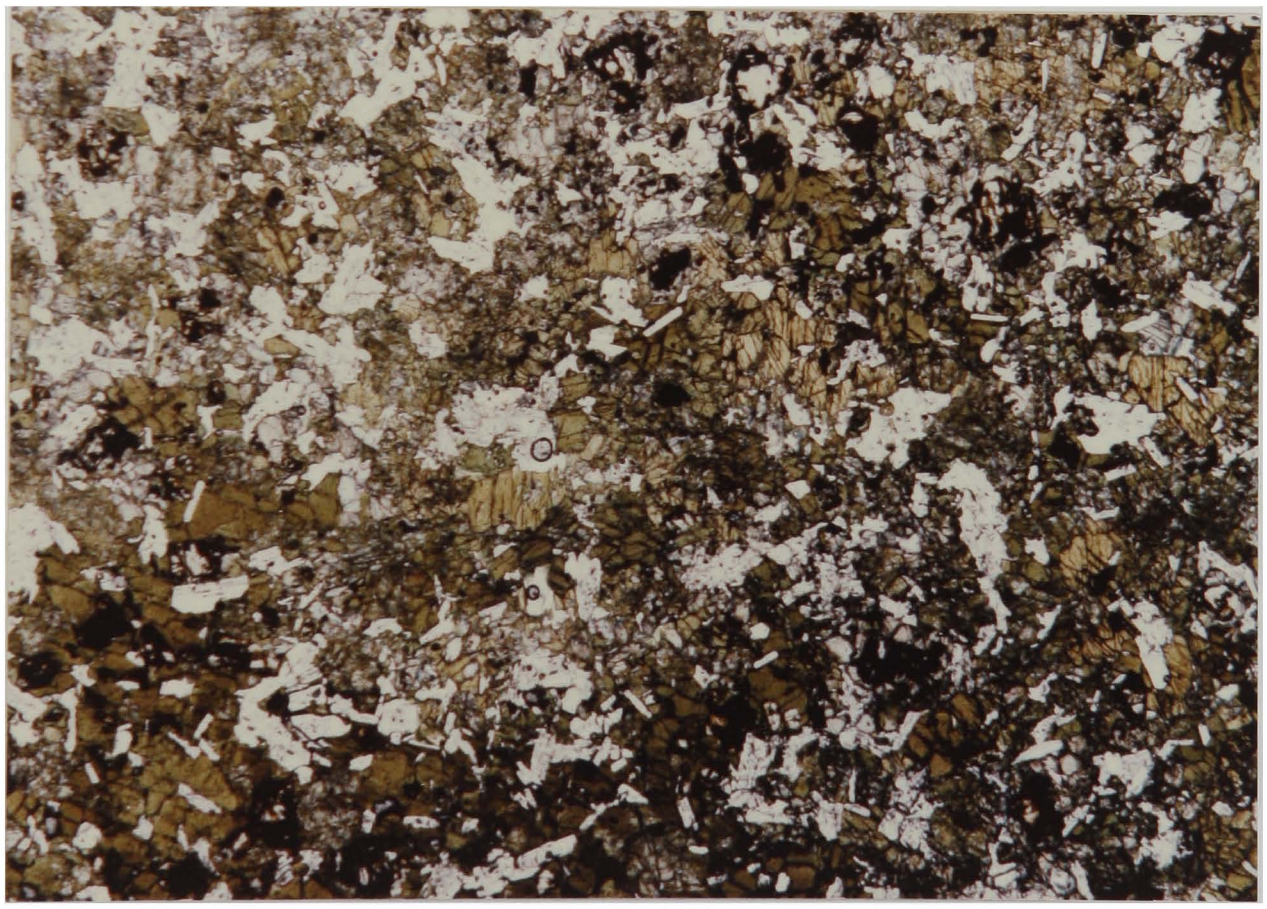

(b)

Plate 3.4

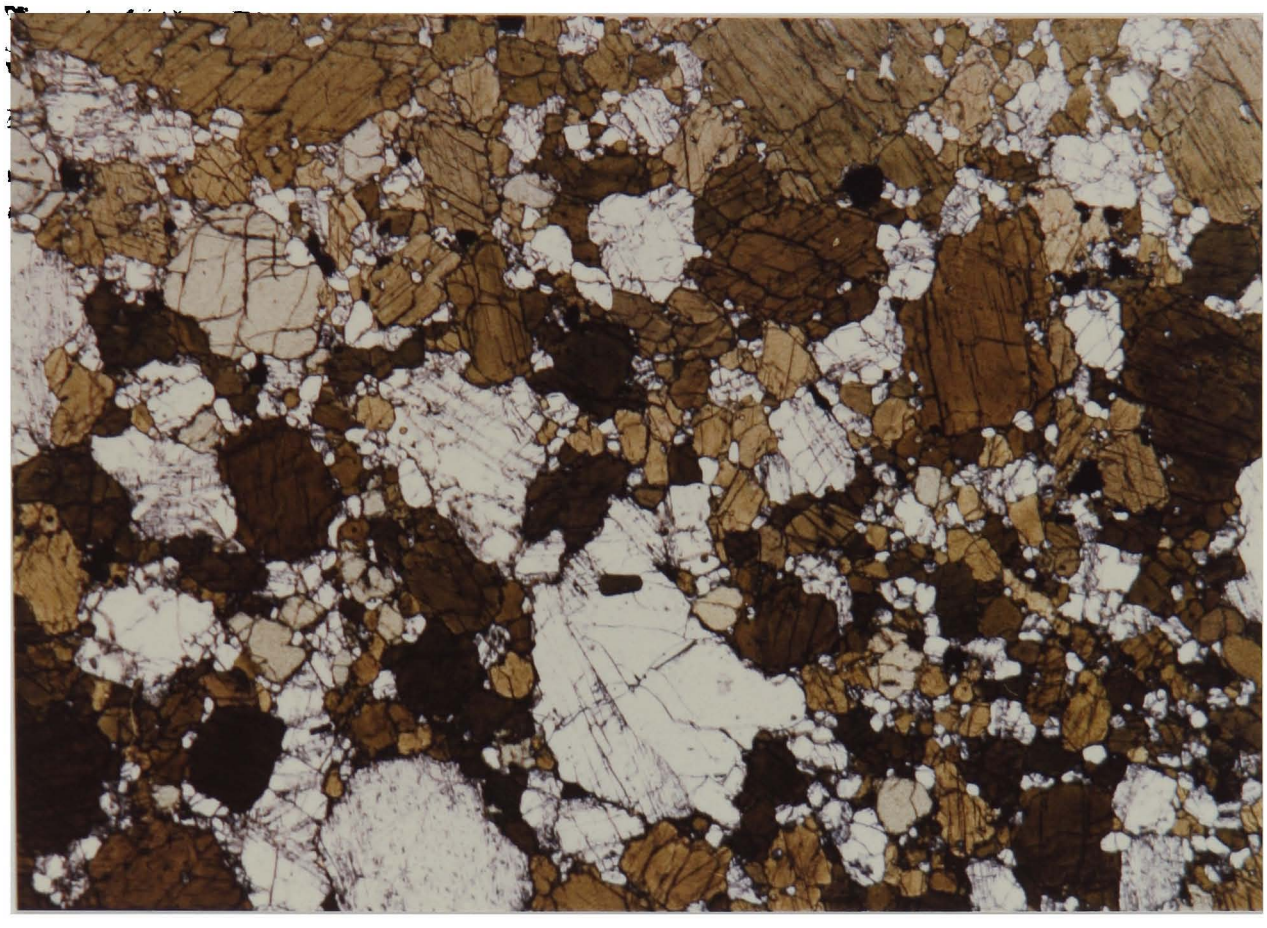

(a)

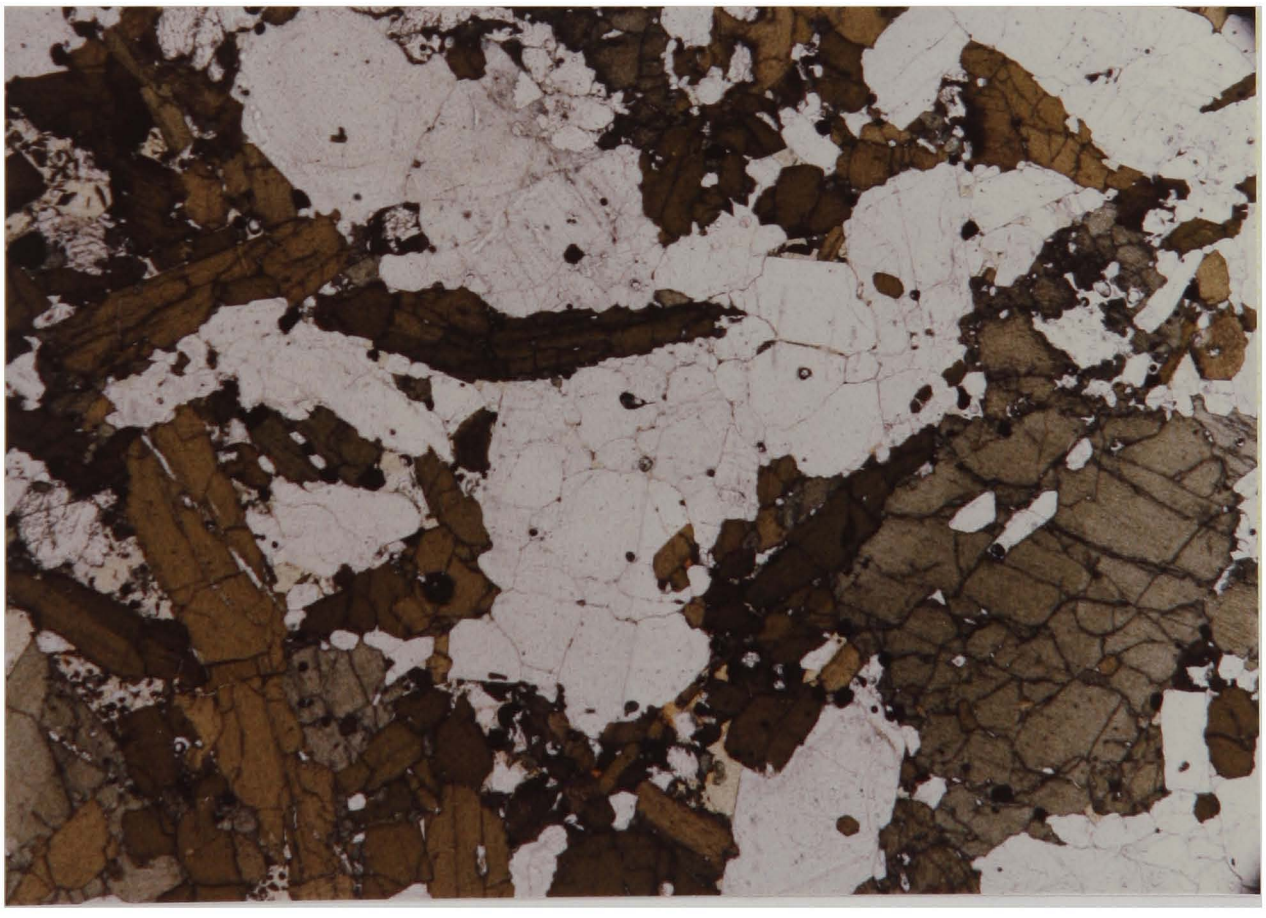

(b)

Plate 3.5

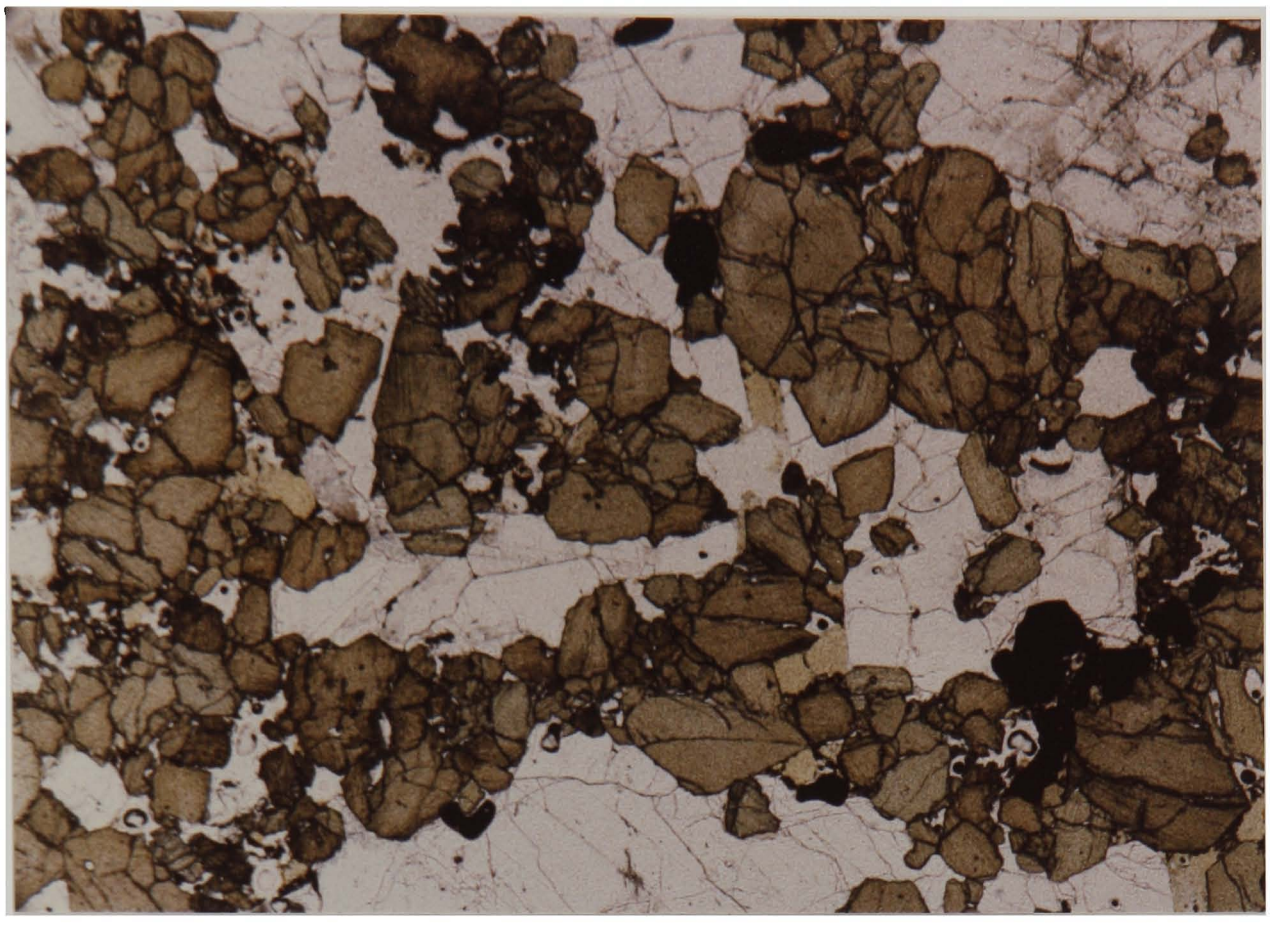

(a)

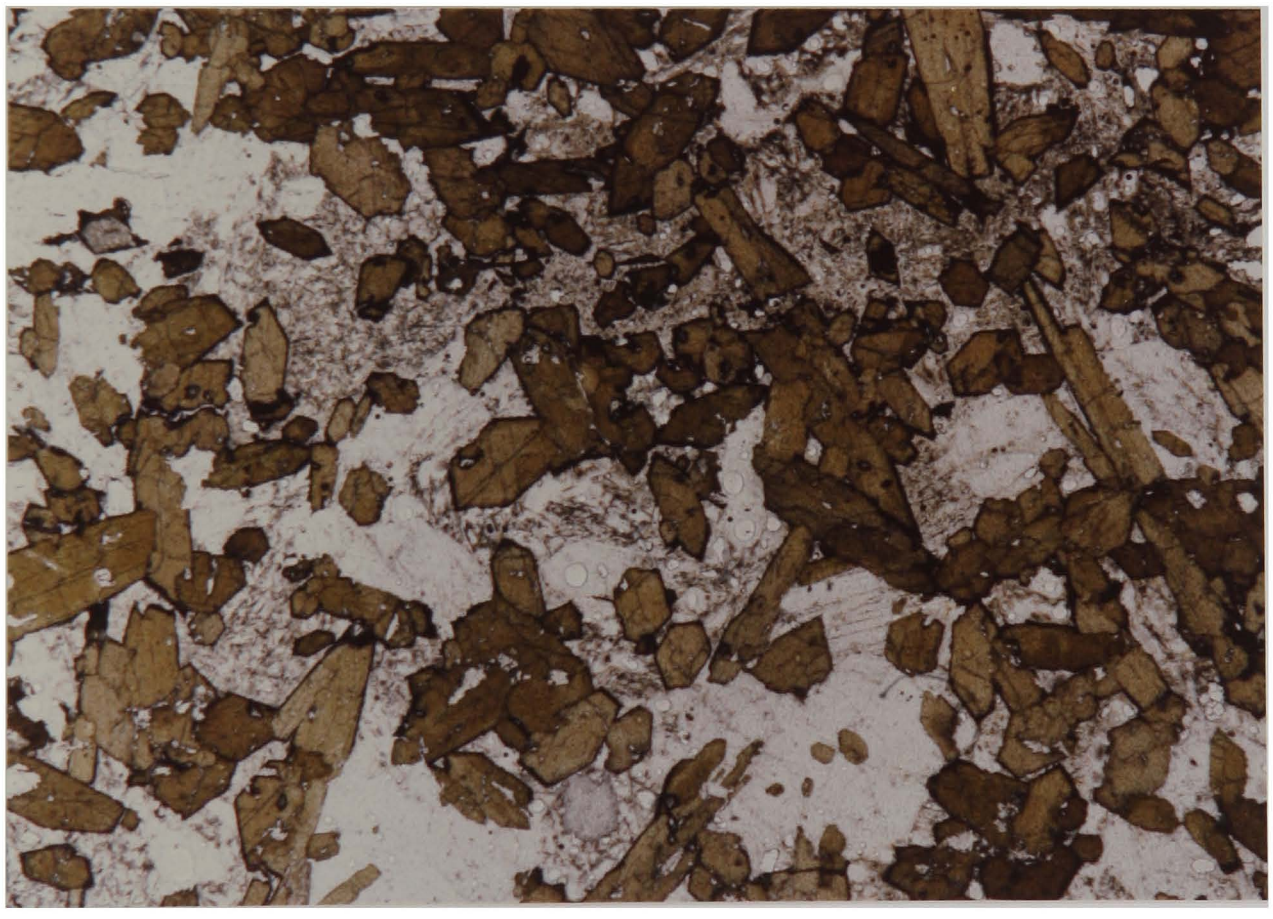

(b)

Plate 3.6

Plate 3.7

of spinel with the silicates, perhaps with an increase in abundance at the later stages. In a few samples transitional to type B, plagioclase is included as small euhedral grains in cumulus amphibole. This evidence indicates that plagioclase already existed in the magma when amphibole nucleated under some conditions. One sample, on amphibole-free mesocumulate, contains abundant skeletal (linked parallel growth) olivines and appears to have crystallised from an M-series parent. Although this one sample may not be significant, others containing amphibole have olivines with elongate habits not found in the C-series lavas examined.

3.4.2 Type B assemblages

The type B plutonics are normally adcumulates, although a few heteradcumulates are present. Grain size variations are similar to type A, but the type B blocks frequently show modal layering, primarily a result of variable proportions of plagioclase. The feldspar may show an igneous lamination parallel to the modal layering and, in one sample, a weak lamination is present in small feldspars included in amphibole, suggesting *in situ* growth. Olivine is often irregular in shape and may show slight reaction with later amphibole, while clinopyroxene shows more extensive replacement by this mineral than in type A rocks, particularly where the amphibole has crystallised late. However in some samples, where amphibole occurs as subhedral cumulus grains, there is no replacement of clinopyroxene. As in type A assemblages, cumulus amphiboles are often rich in inclusions whose uniform distribution supports a model of *in situ* growth of the amphibole, since no distinct adcumulus growth rims are observed.

The textural features in the type B blocks suggest a crystallisation sequence of olivine and clinopyroxene followed by amphibole or plagioclase. The relative stabilities of these two phases are variable,

while spinel probably crystallises throughout the sequence, becoming increasingly abundant.

3.4.3 Type C assemblages

These cumulates have a distinctive appearance in thin section. Although variable in grain size, all contain abundant poikilitic amphibole including olivine, clinopyroxene, plagioclase, and spinel. Extensive reaction of clinopyroxene is often evident. At the margins of the amphiboles orthopyroxene is found associated with plagioclase. This texture suggests that the orthopyroxene crystallised, along with some feldspar and amphibole, from liquid trapped by either the rapid *in situ* growth of the amphiboles or by their rapid accumulation. This liquid would become very rich in silica as amphibole, and probably some calcic plagioclase, grew and would therefore crystallise orthopyroxene. Consequently, orthopyroxene may never have been in equilibrium with the earlier crystallising phases and their host magma. Inasmuch as these assemblages show evidence of crystallisation of trapped intercumulus liquid, they are transitional to orthocumulates although the amphibole texture might lead them to be termed heteradcumulates.

3.4.4 Type D assemblages

Blocks of this type are the most common among the samples sectioned. Modal abundances are variable and, together with grain size variation, lead to a banded appearance in many samples. No size grading has been observed but igneous lamination is found in both plagioclase and amphibole. The blocks are mostly adcumulates, with occasional heteradcumulates, and extensive adcumulus growth of amphibole and plagioclase is often evident. Clinopyroxene is generally less abundant than in type B assemblages and is often extensively replaced by amphibole. While some samples show clear evidence of crystallisation of amphibole after plagioclase, textures of others are ambiguous in this respect and one

heteradcumulate contains euhedral to subhedral amphiboles included in large poikilitic plagioclase grains. The spinel occurs as subhedral to anhedral grains, often relatively large, and shows evidence of adcumulus growth. These blocks are notable for the occurrence of spinel as a distinct cumulus phase, although this is probably a result of the early, cumulus habit of the amphibole, which tends to be more elongate than in the type A, B, and C blocks. Several amphibole-free adcumulates occur in this group, indicating variable crystallisation conditions and/or parental melts.

The textures and mineral assemblages of the type D rocks, together with the elongate amphibole habit, are consistent with an origin from a more evolved magma which was no longer in equilibrium with olivine and which was capable of crystallising substantial proportions of amphibole. Comparison with the phenocryst assemblages of the extrusive rocks would indicate that the type D cumulates equilibrated with an andesitic magma.

3.4.5 Type E assemblages

Only one example of this type has been found in Grenada. It is essentially a variant of type C from which olivine is absent, and is texturally indistinguishable from type C assemblages. It is therefore interpreted as an orthocumulate in which amphibole grew from a magma which was no longer in equilibrium with olivine.

3.4.6 Type F assemblages

A few pyroxene-free, amphibole-plagioclase-spinel assemblages are present in Grenada. These blocks typically contain elongate amphiboles which may show an igneous lamination, and frequently include small spinels. In view of the evidence for increasing replacement of clinopyroxene by amphibole in the more evolved liquids, both in the cumulates and in the phenocryst assemblages of the lavas, these blocks are interpreted

as the products of crystallisation of relatively evolved liquids.

3.4.7 Type G assemblages

A small number of cumulate blocks contain only amphibole. These are mostly mesocumulates but one adcumulate has also been found. Small spinels are sometimes found included in the amphiboles. The habit of the amphiboles is generally more similar to that found in olivine-bearing cumulates than to the more elongate amphiboles in type D and F assemblages.

3.4.8 Summary

The cumulus plutonic blocks of Grenada are very variable in both grain size and texture. It is considered unlikely that the cumulus phases in the blocks accumulated by gravitational settling, and the textural evidence is consistent with formation by *in situ* crystallisation at the margins of subvolcanic magma bodies. The textures of the blocks show that the relative stabilities of plagioclase and amphibole were variable, while the mineral assemblages suggest derivation from a variety of basaltic and andesitic magmas. It is not possible, on the basis of petrography alone, to relate the blocks to either of the basic lava series described in Chapter 2. These relationships are discussed further in section 3.7.

3.5 Mineral Chemistry

Twenty-eight cumulate blocks were analysed by electron microprobe. Both energy- and wavelength-dispersive methods were used, details of which are given in Appendix A. There were two main objectives in the probe study. Evidence was sought firstly for the order of crystallisation of the phases, and secondly, for the relationship between the extrusive rocks and the cumulates.

3.5.1 Olivine (Table A4.1)

Olivine analyses are presented in Figure 3.5.1. There is very little variation in olivine composition within individual specimens while, in three of the type B samples, this mineral is completely altered. The number of analyses is therefore restricted but is sufficient to show that:

(a) The type A cumulates have significantly more magnesian olivine than the plagioclase-bearing type B.

(b) The most magnesian olivines could not have been in equilibrium with the high-MgO lavas of the M-series, using the data of Roeder and Emslie (1970).

(c) The range of type C olivine compositions covers that shown by types A and B together.

Nickel data from olivines analysed by wavelength-dispersive methods are presented in Figure 3.5.2, along with calculated analytical precision and detection limit. Average NiO contents for type A and B cumulates are 0.145 and 0.120% respectively, equivalent to 1140 and 945 ppm Ni. These values can be used in nickel distribution expressions (Leeman, 1974; Arndt, 1977; Hart and Davis, 1978) to estimate the nickel contents of the equilibrium liquids (Table 3.5.1). The results show that, even allowing for slightly higher temperatures than 1100°C, which seem unlikely according to the evidence presented in section 3.6 and in Chapter 5, the liquids with which these olivines were in equilibrium could not have contained more than 100 ppm Ni. While C-series lavas contain less than 70 ppm Ni, most M-series lavas contain more than 100 ppm. If the cumulates are not products of perfect fractional crystallisation, re-equilibration of olivine with liquid would increase this limit, but this effect would not be large. Therefore, only the C-series magmas and the more evolved members of the M-series have the chemistry and phenocryst

Figure 3.5.1

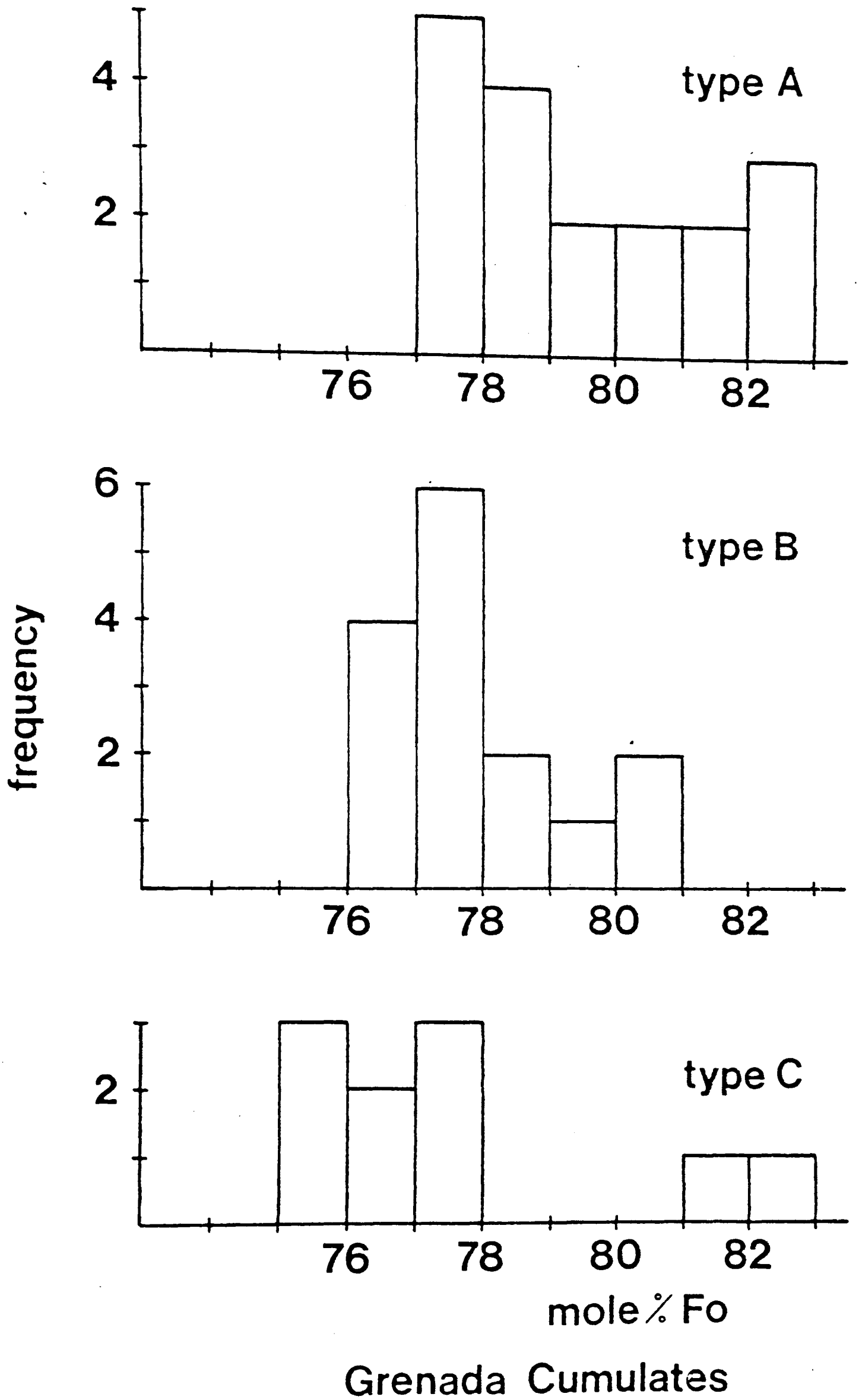

Grenada Cumulates

Figure 3.5.2 Nickel contents of olivines.

triangles = type A
circles = type B
squares = type C

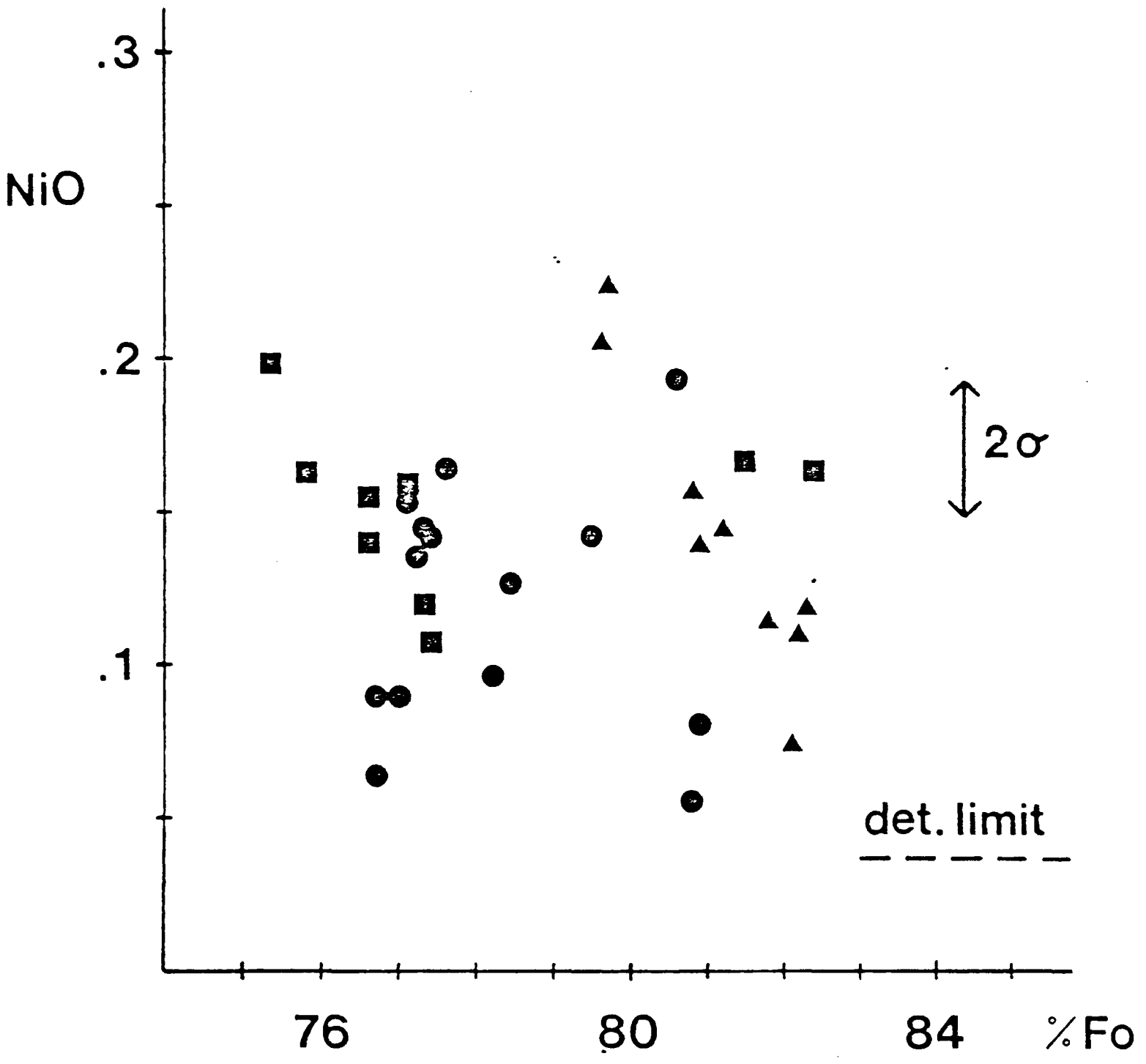

Table 3.5.1

Ni distribution in type A and B cumulates

Data	T	D	Ni_{liq} (type A)	Ni_{liq} (type B)
Leeman (1974)	1000°C	63.9	19 ppm	15 ppm
	1100°C	30.1	38 ppm	31 ppm
Arndt (1977)	1000°C	30.1	38 ppm	31 ppm
	1100°C	16.6	69 ppm	57 ppm
Hart & Davis (1978)	1000°C	60.6	19 ppm	16 ppm
	1100°C	29.9	38 ppm	32 ppm

Data sources

Leeman (1974) $\ln D = 13160/T - 6.18$

Arndt (1977) $\ln D = 10430/T - 4.79$

Hart and Davis (1978) $\ln D = 12345/T - 5.593$

Table 3.5.2

Sr distribution in type B cumulates

T	D	Sr_{liq} (minimum)	Sr_{liq} (maximum)
1000°C	6.48	91 ppm	274 ppm
1100°C	3.86	153 ppm	460 ppm

Data source

Drake and Weill (1975) $\ln D = 9050/T - 5.24$

phase relations consistent with being in equilibrium with the cumulate assemblages containing olivine.

3.5.2 Pyroxene (Table A4.2)

Analyses of pyroxenes are projected into the (Ca, Fe, Mg)SiO_3 system in Figure 3.5.3. Very little zoning is present except in some clinopyroxenes with relict oscillatory zones. In general, type A clinopyroxenes have higher Mg-values than those from types B and D, while type C and E clinopyroxenes cover a wider compositional range than the A type. Considerable variation is also found in the Mg-values of C and E type orthopyroxenes. Calculation of site occupancies for Al and Ti in clinopyroxene (Figure 3.5.4) shows the broad positive correlation of Al and Ti required for charge balance in pyroxenes low in Al^{VI} and Fe^{3+}. Zoning in Al and Ti is irregular where it occurs, as found in the phenocryst clinopyroxenes. The variation of Al and Ti suggests that the orthopyroxene-bearing samples equilibrated with a liquid in which alumina activity was low, which is consistent with petrographic evidence that adcumulus growth of plagioclase took place in trapped liquid in these rocks. By contrast, many of the type A clinopyroxenes have the highest Al and Ti contents, reflecting equilibration at high temperatures with liquids of high alumina activity. However, the clinopyroxenes in the type A layer of the composite nodule 6099 have low Al and Ti contents, suggesting that they have equilibrated with the adjacent, type D assemblage layer. The Al and Ti variation is therefore a product of variation in temperature and melt composition but, although jadeite contents are low, some pressure variation cannot be excluded.

3.5.3 Plagioclase (Table A4.3)

Plagioclase compositions are presented in Figure 3.5.5. The considerable variation within each group is believed to result from adcumulus growth of plagioclase into trapped liquid. Occasional examples of

Figure 3.5.3 Pyroxene compositions.

triangles = type A

circles = types B and D

squares = types C and E

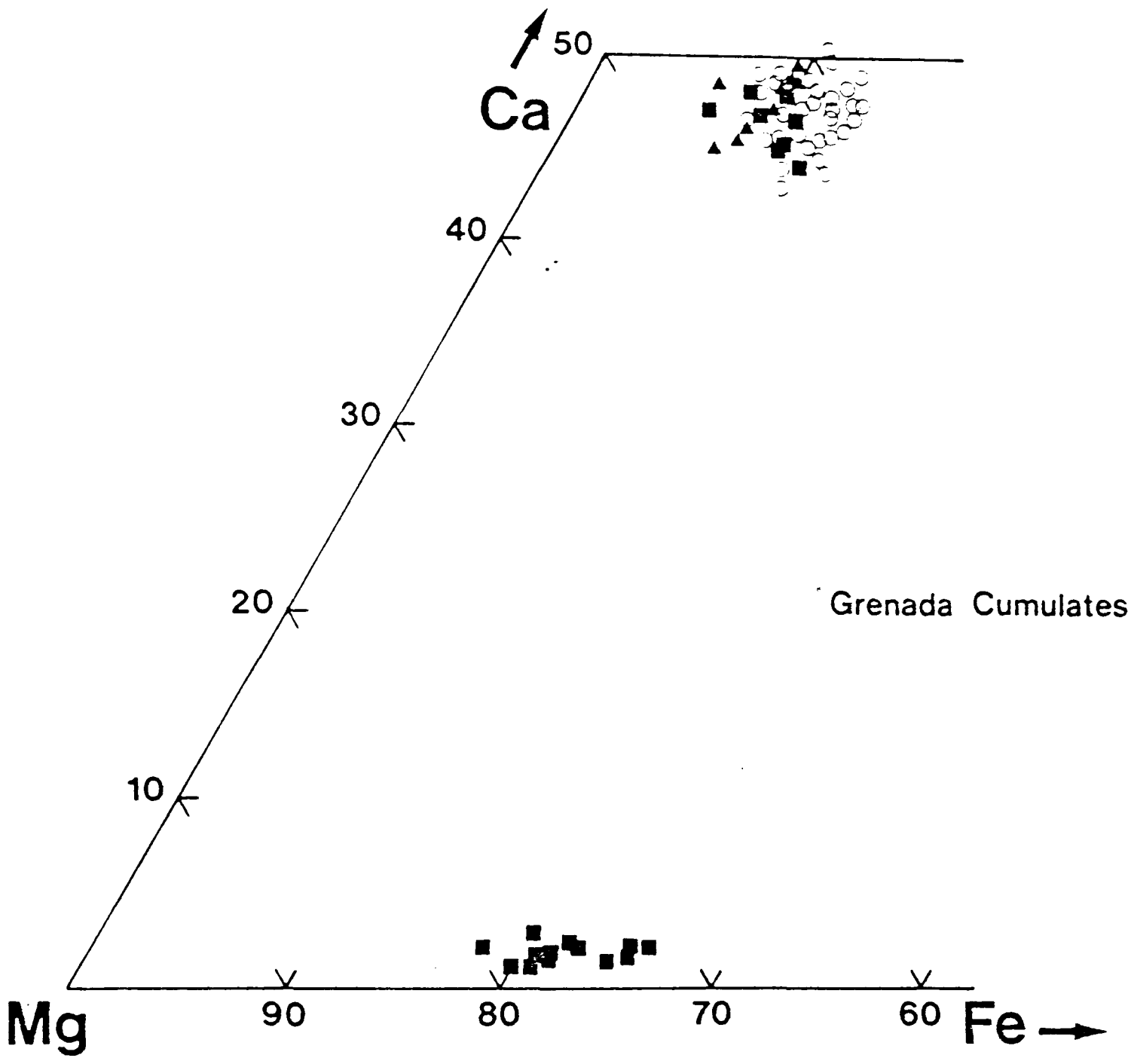

Figure 3.5.4

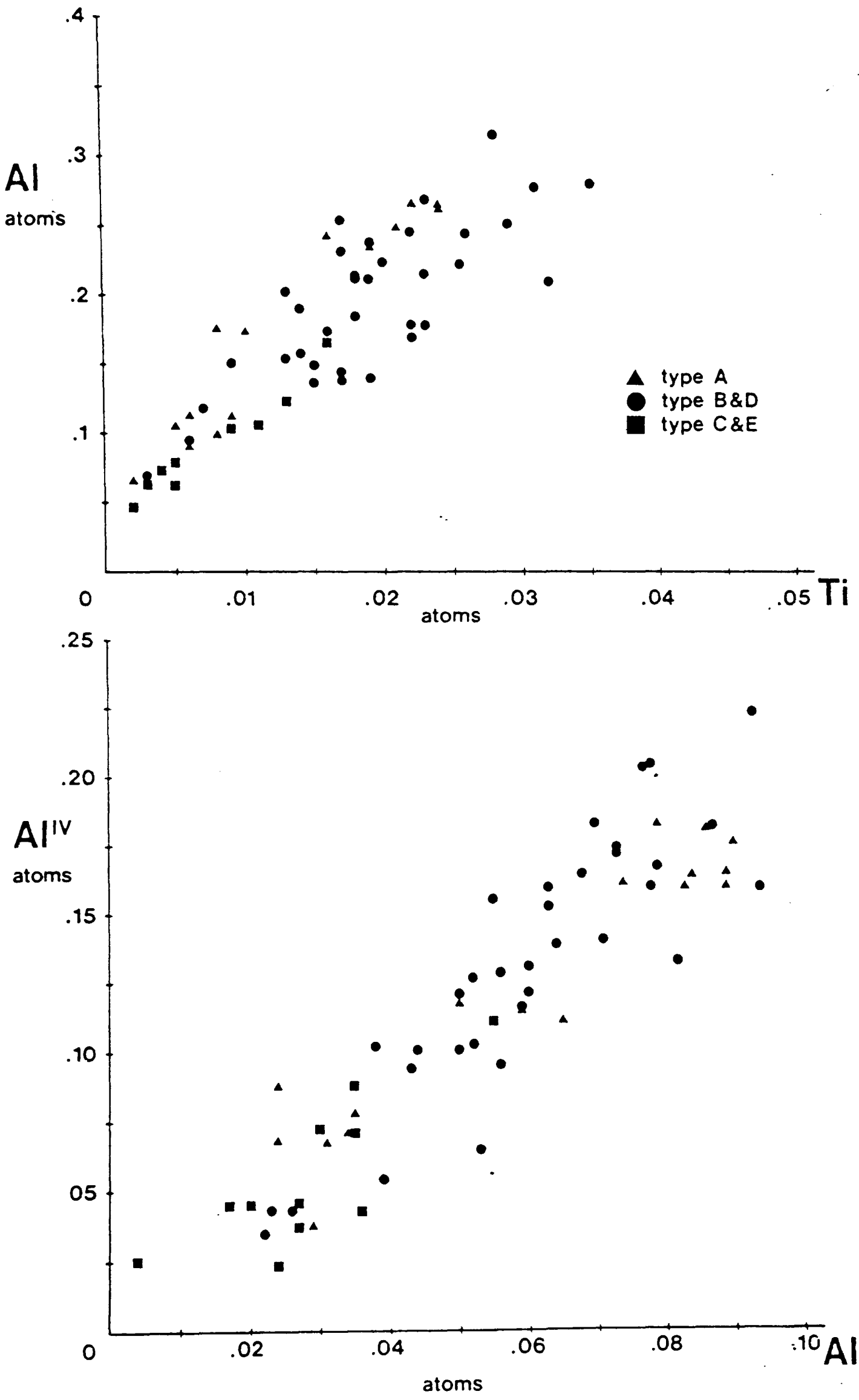
.4
.3
Al
atoms
.2
.1
0
.01
.02
.03
.04
.05
Ti
atoms
type A
type B&D
type C&E
.25
.20
Al^{IV}
atoms
.15
.10
05
0
.02
.04
.06
.08
.10
Al^{VI}
atoms

this are seen in types B and D but again it is the orthopyroxene-bearing samples which show the greatest variation. This evidence, together with the olivine and pyroxene compositions, supports an origin for the orthopyroxenes in liquid whose composition has been strongly modified from that of the parent by adcumulus growth. A further feature of the plagioclase compositions is the more calcic nature of the plagioclase in the olivine-free type D rocks than in the olivine-bearing type B. Assuming that the highest temperature assemblages are those containing olivine, this indicates an increase in the anorthite content of the feldspars during fractionation.

Since a distinguishing feature of the two basic magma series is their strontium content, it might be expected that the Sr content of the cumulate feldspars could be used to investigate the relationships between the extrusive and cumulate rocks. Strontium was analysed in some rocks by wavelength-dispersive methods using extended counting times to increase precision, and results are shown in Figure 3.5.6. Compositions of type B feldspars with anorthite contents greater than An_{80} show a clear trend towards lower strontium at higher anorthite contents. This might be predicted if the most calcic feldspars crystallised at the highest temperatures since experimental evidence (Korringa and Noble, 1971; Drake and Weill, 1975) suggests that this would lead to lowest values for the Sr distribution coefficient. However, this effect would be offset by the decrease in strontium in the magmas with plagioclase fractionation and, in view of the previous suggestion of an increase in anorthite content of feldspars during fractionation, this hypothesis cannot be confirmed.

Distribution coefficients measured by Drake and Weill (1975) were used to calculate the Sr content of melts in equilibrium with type B assemblages (Table 3.5.2), using temperatures of 1000° and $1100^{\circ}C$.

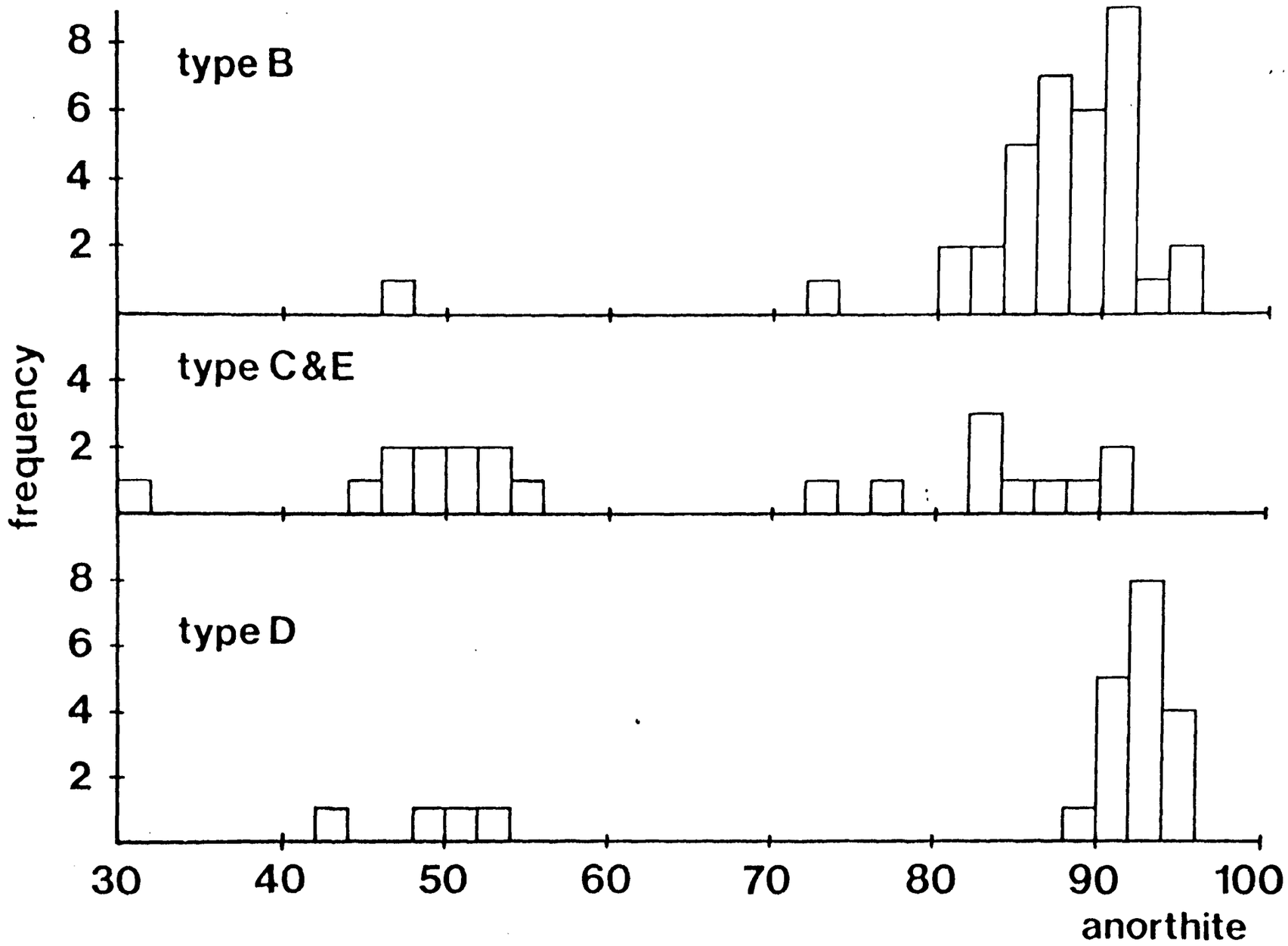
type B
type C&E
type D
frequency
8
6
4
2
4
2
8
6
4
2
30
40
50
60
70
80
90
100
anorthite
Grenada Cumulates

Figure 3.5.5

Figure 3.5.6

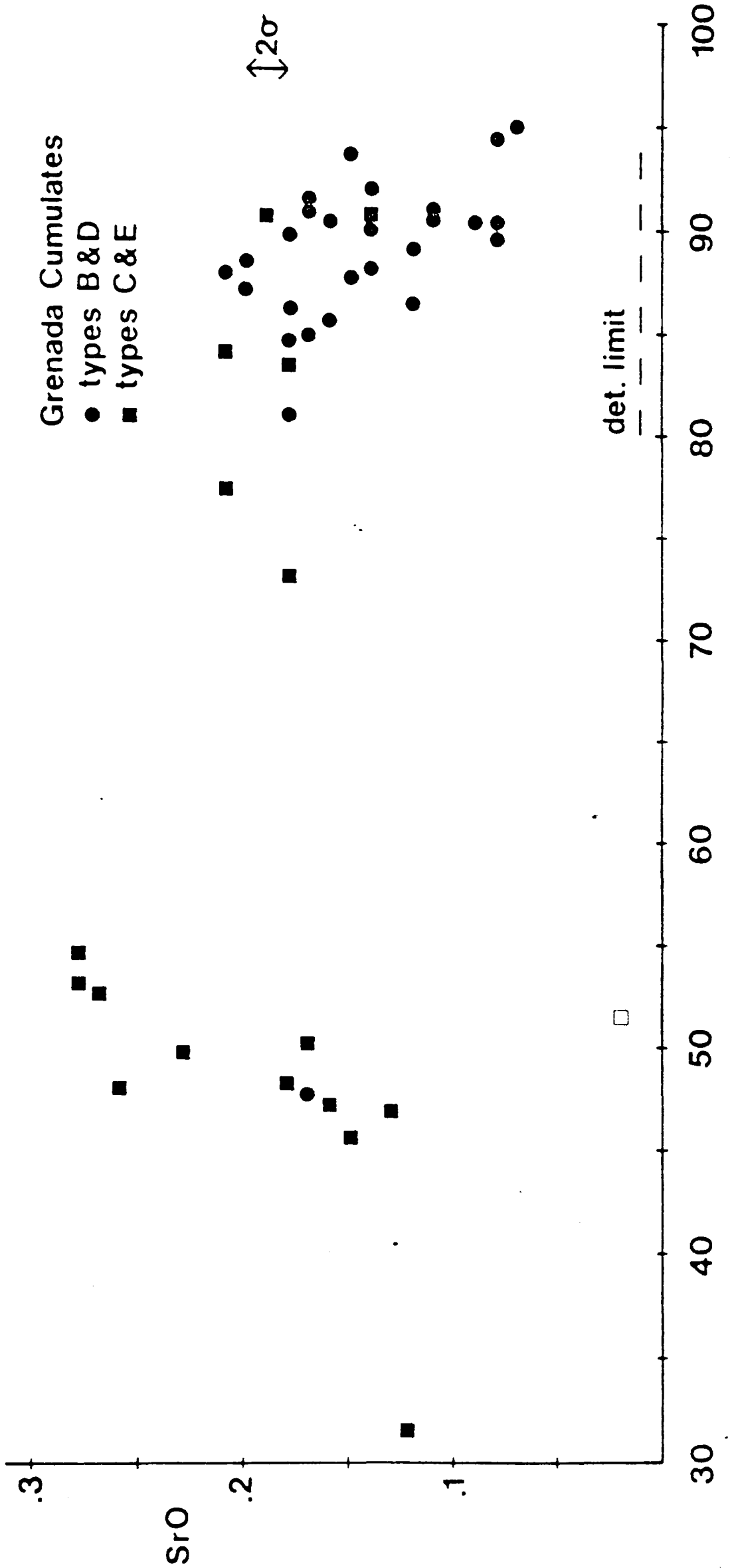
Grenada Cumulates
● types B&D
■ types C&E
↕2σ
det. limit
mole % Ar
100
90
80
70
60
50
40
30
SrO
.3
.2
.1

Minimum and maximum Sr contents in feldspars are 0.07 and 0.21% respectively, equivalent to 590 and 1775 ppm. Reference to Figure 2.7.1 shows that the calculated Sr contents indicate an origin of these cumulates from the M-series or the evolved magmas. However it must be noted that the M-series does not, until its latest stages, show phenocryst plagioclase and, more importantly, that the data of Drake and Weill (1975) could be inapplicable, having been obtained in synthetic systems under dry conditions. Water has a strong effect on plagioclase-liquid equilibrium (Yoder, 1969; Burnham, 1979) and may therefore be expected to affect the distribution coefficient for strontium.

3.5.4 Amphibole (Table A4.4)

Wavelength-dispersive analyses of amphiboles were recalculated on the basis of a ferric iron content equal to the average of wet-chemically analysed cumulate amphiboles from the Lesser Antilles (Wills, 1974). This compilation gives a value of 100 $Fe_2O_3/(FeO + Fe_2O_3)$ of 38.0 weight %. Site occupancies were calculated on a 23 oxygen basis by the method of Leake (1978). The majority of amphiboles in the Grenada cumulates, according to the classification of Leake (1978) are magnesiohastingsites, but some are sufficiently low in FeO/MgO and therefore in Fe^{3+}/Al^{VI} at fixed oxidation ratio, to be pargasites. These are mostly type A amphiboles. Two compositions have sufficiently low Al^{VI} and total alkalis to be tschermakites. Both are type E amphiboles, which may represent crystallisation in trapped liquid at lowest temperatures. Halogen contents of the amphiboles are low.

Helz (1973), in a study of amphibole compositions in the melting interval of water-saturated basalts, showed that, at constant pressure, the chemistry of amphibole was essentially described by edenite and tschermakite substitutions. Structural control appeared to produce strong positive correlations between alkalis on A sites and tetrahedral

aluminium, and between (Al^{VI} + 2Ti) and tetrahedral aluminium. The Grenada data, plotted in Figure 3.5.7 show similar correlations and the slope of the alkali vs. tetrahedral aluminium plot indicates that the temperature-dependent edenite and tschermakite substitutions are coupled in the ratio 1:2. This coupling explains the lack of a strong correlation between octahedral and tetrahedral aluminium.

The plots show that three of the type A amphiboles have much lower Al and total alkalis than the remainder of this group. These are the compositions from the composite nodule 6099, again reflecting equilibrium with the adjacent type D assemblage. The range of compositions from type C and E assemblages is again very large. The amphibole data therefore support a decrease in crystallisation temperature from type A to type B and type D. The wide range of type C and E compositions supports an interpretation of these assemblages as products of adcumulus growth into trapped liquid, with equilibration of the phases down to lower temperatures. Although less precise, data from energy-dispersive analyses are consistent with these conclusions.

3.5.5 Spinel (Table A4.5)

Wavelength-dispersive spinel analyses are plotted in Figures 3.5.8 and 3.5.9. These represent projections of compositions onto faces of a modified Johnson spinel prism (Haggerty, 1976) and therefore neglect the titanium content of the spinels. Compositions from type A cumulates have generally higher Al/(Cr + Al + Fe^{3+}) and higher Mg-values than those from assemblage types B and D, although the compositions from nodule 6099 are again exceptional. Type B and D spinels are rich in Fe^{3+}, while type C and E spinels again show large chemical variation. The plot of trivalent cations shows lower Al contents in type C and E spinels than in type A and, although the number of data points is not large, this is considered to be a real difference which probably reflects decreasing

Figure 3.5.7 Symbols as Figure 3.5.4

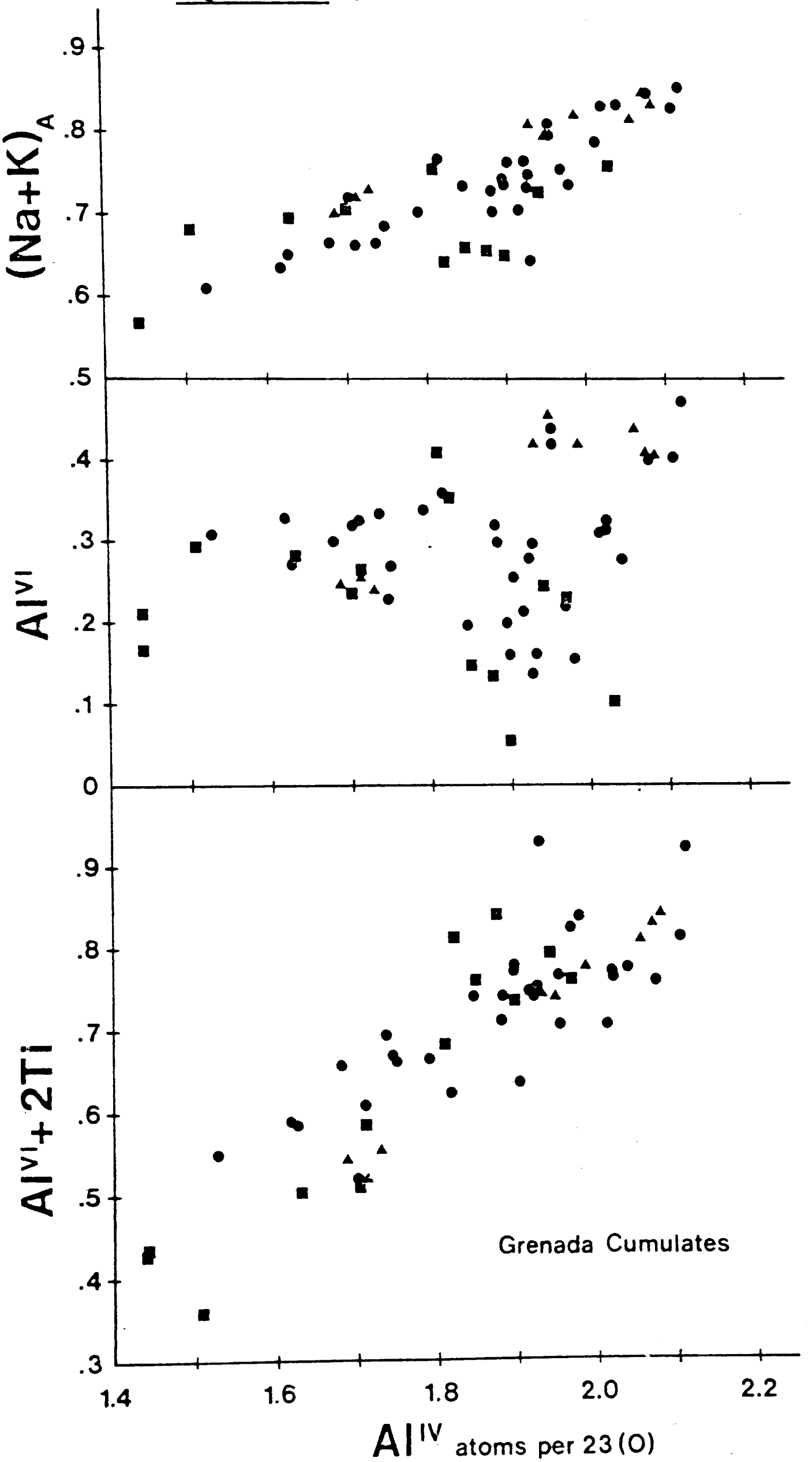

Figure 3.5.8

Symbols as Figure 3.5.4

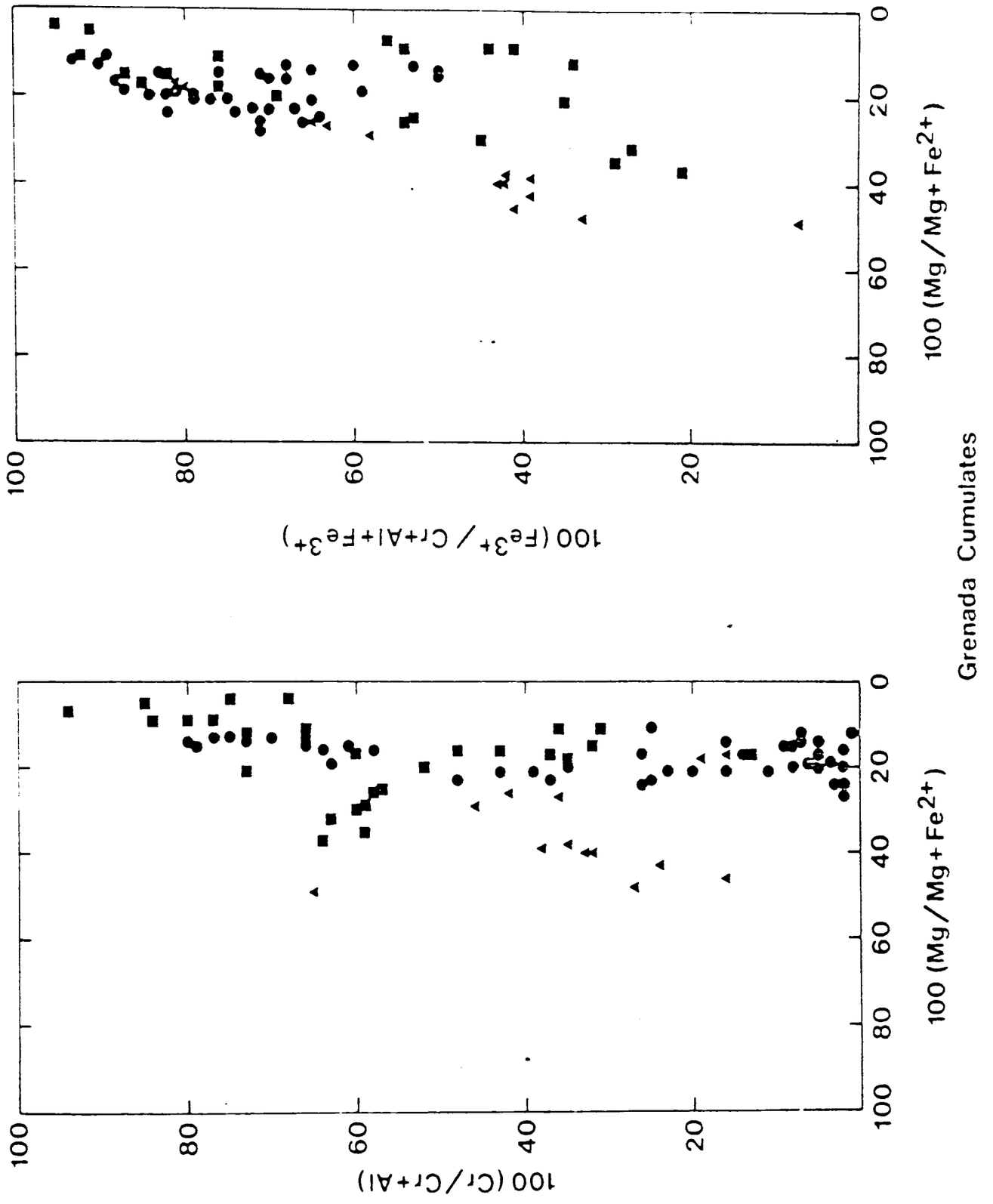

Figure 3.5.9

Symbols as Figure 3.5.4

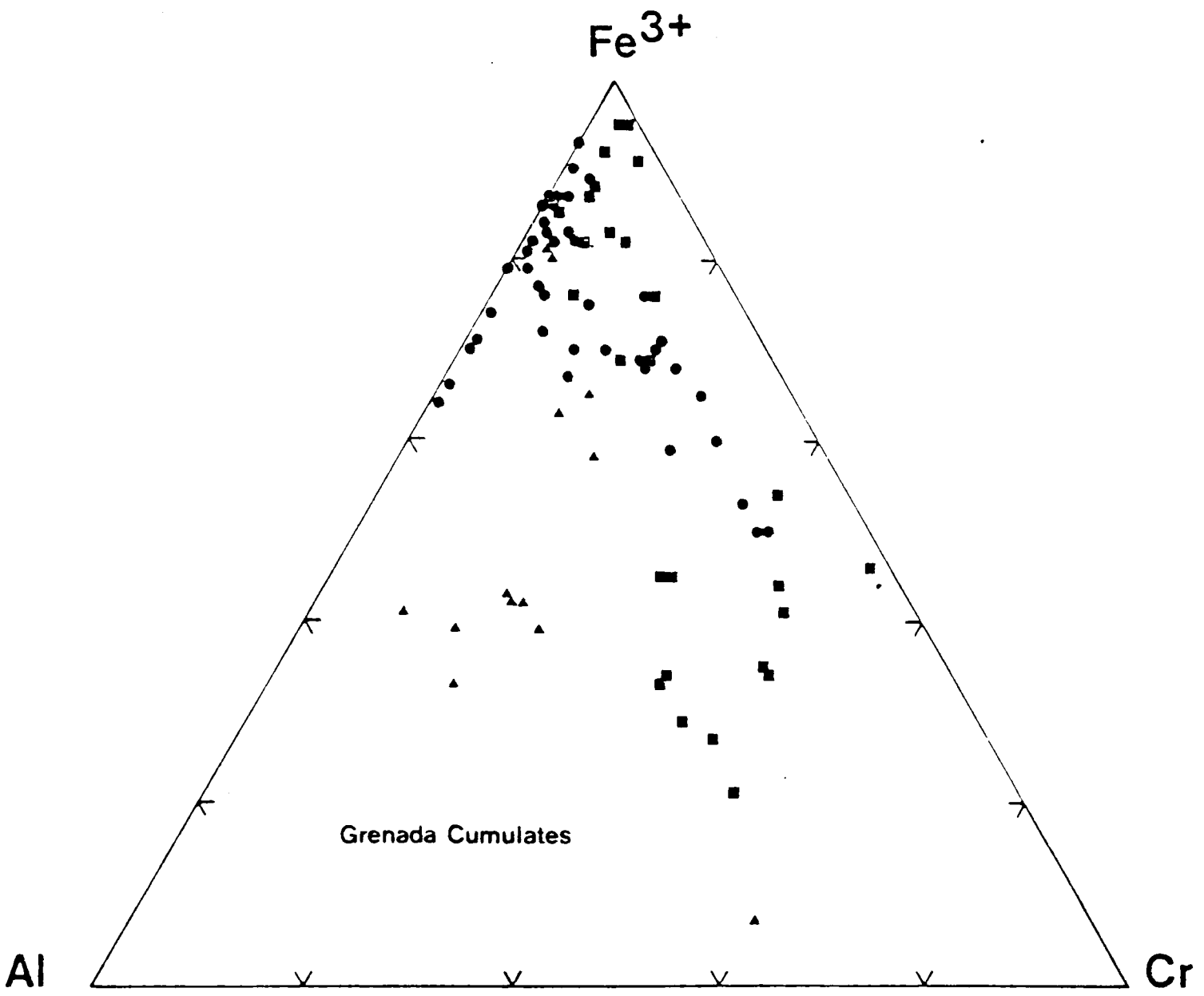

alumina activity in the trapped melt of the orthopyroxene-bearing assemblages. This conclusion is supported by the sympathetic variation in plagioclase compositions in these rocks.

Comparison of the cumulate spinel compositions with those described from Grenada basalts by Arculus (1974) is difficult because no information is given in that study relating spinel composition to host basalt type. However, the cumulate spinels have generally lower Mg-values than the lava examples, and do not include any compositions rich in alumina. It can therefore be suggested that the cumulate spinels equilibrated with liquids more evolved than the majority of Grenada basalts. Although the Cr and Al contents of most C-series oxide phenocrysts are low, occasional compositions are sufficiently rich in these elements to make C-series basalts possible parents to the cumulate spinels. Conversely, the chromium contents of many of the M-series oxide phenocrysts are greatly in excess of those found in the cumulate spinels. Therefore, although not conclusive, the data again point to equilibration with melts similar to the C-series or the more evolved members of the M-series.

3.6 Physical conditions of crystallisation

Although Wager (1962) attempted an interpretation of the conditions necessary for crystallisation of the cumulate assemblages of Soufriere, St. Vincent, Lewis (1973) carried out the first major investigation of equilibration conditions. Lewis deduced from experimental data that the coexistence of magnesian olivine with anorthite, and the presence of amphibole, required a pressure of crystallisation in the range 1-8 kilobars, while suggesting that the partial pressure of water was unlikely to have equalled total pressure.

Wills (1974) came to similar conclusions regarding the pressure of

crystallisation, suggesting that the late appearance of amphibole in lava suites in the Lesser Antilles, together with the lack of basaltic pyroclast flows, indicated that the magmas coexisting with the cumulate assemblages were not close to water saturation. Wills suggested that the compositions of coexisting olivine and calcic plagioclase might be good indicators of water activity. On this basis he concluded that the more magnesian olivine coexisting with a given plagioclase composition in the southern islands of the arc might reflect lower water activity, promoting a higher temperature crystallisation environment, but was unable to quantify this argument.

The rapid growth of interest in the application of thermodynamics to mineral equilibria has provided new methods by which the P-T-$f_{volatiles}$ conditions of cumulate equilibration can be investigated. It is important to determine which, if any, of the assemblages represent equilibrium and which, if any, of the thermodynamic methods provide accurate answers. As previously discussed, the textures of the adcumulates from Grenada, and the very limited chemical zoning of their constituent phases, are consistent with equilibrium assumptions. However, the orthopyroxene-bearing assemblages have textures suggesting substantial reaction between trapped intercumulus melt and crystals, and are therefore at least transitional from adcumulates to orthocumulates. It may not be realistic to treat these rocks as equilibrium mineral assemblages.

The coexistence of olivine with calcic plagioclase in many of the Grenada cumulate blocks requires, on the basis of Kushiro and Yoder's (1966) data for the anorthite-forsterite reaction, pressures of equilibration of less than about 8 kilobars (as for Soufriere). It might be expected that the depths of crystallisation of the blocks would be variable. There is no evidence, however, to suggest that the blocks lacking this diagnostic assemblage crystallised at significantly higher

pressures. The presence of amphibole requires pressures of crystallisation in excess of about 1 kilobar and moderate water activity. The low halogen contents of the amphiboles indicate that water is likely to have been the dominant volatile species influencing amphibole stability. Its activity was probably variable since the textural evidence indicates variable relative stabilities of amphibole and calcic plagioclase. The experiments of Holloway and Burnham (1972) show that crystallisation of amphibole before plagioclase is to be expected at high water activities. The low-pressure thermal stability of amphibole is determined by its dehydration and melting reactions. Consideration of the water activities at the crossing of these reaction curves in the P-T space by Burnham (1979) led him to conclude that the minimum water content of a melt in equilibrium with water would be close to 3 weight percent. This estimate constrains the minimum water activity at which the Grenada cumulates crystallised as a function of pressure.

Powell (1978) applied thermodynamic methods to the mineral composition data of Wills (1974) to estimate P, T, and $f_{volatiles}$ for selected cumulates from the Lesser Antilles. From the results of these calculations, she suggested a northward increase in the depth of crystallisation, generally low water activities, and high oxygen activities. However, there are some serious uncertainties in the methods used in her study, some of which have also been pointed out by Arculus and Wills (in prep.)

3.6.1 Pressure estimates

Powell (1978) used the equilibrium:

$$2Mg_2SiO_4 + CaAl_2Si_2O_8 = Mg_2Si_2O_6 + CaMgSi_2O_6 + MgAl_2O_4$$

olivine anorthite opx cpx spinel

to estimate pressure. This is the reaction describing the plagioclase lherzolite/spinel lherzolite boundary in the CMAS system. As in all

thermodynamic treatments, there are two main sources of uncertainty in this method. Firstly there are the uncertainties in the basic thermodynamic data for the pure end-members involved, which may lead to significant uncertainties in the enthalpy, entropy and volume changes of a reaction unless it has been calibrated experimentally. Secondly, the pure end-member data must be extrapolated to the more complex natural system, requiring a knowledge of the solution chemistry of the phases. It is here that serious uncertainties may become involved. While olivine and plagioclase probably approximate to ideal solutions in this case (Williams, 1972; Orville, 1972), the pyroxene and spinel solid solutions are more complex. Although uncertainties still exist, numerous workers have studied the solution chemistry of pyroxenes (e.g. Wood and Banno, 1973; Newton et al., 1977; Herzberg, 1978; Wood, 1979). In contrast, there are very few data on the complex $(Mg, Fe)^{2+}(Cr, Al, Fe^{3+}, Ti)$ spinels, except in some simple systems free of ferric iron (Muller and Kleppa, 1973; Charlu et al., 1975). Serious problems arise in treating spinels not only because of their complex chemistry but also because of their structures. Different end-member spinels have different structures so that the site occupancies in compositionally complex spinels are almost wholly unknown even when good chemical analyses are available. It seems likely that short-range ordering effects are an important factor.

Since the alumina contents of spinels in the Lesser Antilles cumulates are low, Powell (1978) chose to treat them as dilute solutions, applying an arbitrary Henry's Law constant of 1.5 and assuming that complete coupling of Mg^{2+} and Al^{3+} took place, such that $a^{spinel}_{MgAl_2O_4} = 1.5 \times X^{spinel}_{MgAl_2O_4}$. However, since there is no evidence to support this model, it is regarded as unjustifiable.

As previously described, spinels in the Grenada cumulates have a very wide compositional range, and there may be substantial variation

within a single block. Some compositions may not, therefore, reflect equilibrium. A further problem in applying this barometer to the Grenada blocks is that no orthopyroxene-bearing examples were found by Arculus (1973, 1978) and Wills (1974). The equilibrium is thus not strictly applicable, since one phase is missing. Powell (1978) attempted to overcome this difficulty by calculating the activity of enstatite in the clinopyroxene, using a regular solution model. This approach involved the choice of a fixed value for the interaction parameter of the regular solution, close to that derived by R. Powell (1978) from experimental data at 30 kilobars, mostly in the system CMS. This represents a considerable extrapolation of the data. M. Powell (1978) suggested that the expression for the activity of enstatite in clinopyroxene would be:

$$RT\ln\left(a^{cpx}_{MgSiO_3}\right)^2 = RT\ln X^{M1}_{Mg} \cdot X^{M2}_{Mg} + AX^{M2}_{Ca}(1 - X^{M2}_{Mg})$$

where A is the interaction parameter for Ca-Mg on the M2 site. Therefore the increasing diopside content (hence increasing X^{M2}_{Ca} and decreasing X^{M2}_{Mg}) from north to south of the clinopyroxenes from the plutonic blocks in the arc results in a large change in the last term of this expression, and a large change in the equilibrium constant for the reaction, which involves the square of the $a^{cpx}_{MgSiO_3}$ term. The increasing pressures of crystallisation from south to north determined by Powell (1978) are therefore largely spurious, being a function of the method employed. An additional error comes from the use by Powell (1978) of thermodynamic data for orthoenstatite when a clinopyroxene structure was being considered. These shortcomings in the method employed by Powell (1978) are fully described by Arculus and Wills (in prep.). It is therefore concluded that the pressures calculated by Powell are unreliable, and consequently, since they are dependent on these results, so are the estimates of water and oxygen activities.

A possible equilibrium for barometry which avoids spinel solution models is:

$$CaAl_2Si_2O_8 + Mg_2SiO_4 = Mg_2Si_2O_6 + CaAl_2SiO_6 \quad (1)$$

anorthite olivine opx cpx

which is a combination of the reactions:

$$CaAl_2Si_2O_8 = CaAl_2SiO_6 + SiO_2 \quad (2)$$

and

$$Mg_2SiO_4 + SiO_2 = Mg_2Si_2O_6 \quad (3)$$

Reaction (2) was studied by Wood (1978) and its slope in P-T space can be used to derive a value for the entropy change of the reaction, since

$$\frac{dP}{dT} = \frac{\Delta S}{\Delta V} = 10 \text{ bar } {}^{o}K^{-1}$$

The volume change of this reaction was calculated from molar volume data given by Robie and Waldbaum (1968) and Charlu et al. (1978) (Table 3.6.1).

The calculated entropy change of reaction (2) can be used, together with entropy data for reaction (3) (Danckwerth and Newton, 1978; Newton, 1978), to calculate the entropy change of reaction (1). The enthalpy change of reaction (1) can be calculated from the heat of solution data of Charlu et al. (1975), Newton et al. (1977) and Charlu et al. (1978), and the volume change from molar volume data. All the values used are listed in Table 3.6.1, together with the data sources. It should be noted that errors introduced by considering a standard state at 970°K and applying entropy data from 1000°K, together with molar volume data from 298°K will be very small, and are neglected.

$$\Delta S_1 = \Delta S_2 + \Delta S_3 = -3.48 - 1.61 - 5.09 \text{ cal } {}^{o}K^{-1}$$

$$\Delta H_1 = 2990 \text{ cal, and } \Delta V_1 = -.4357 \text{ cal bar}^{-1}$$

Therefore, assuming that $\Delta C_p = 0$ (reasonable for a standard state at 970°K), and that ΔV is constant,

Table 3.6.1

Thermodynamic data used in calculations

phase	$\Delta H_{soln,970}$ (kcal mole^{-1})	S_{1000} (cal $^{o}K^{-1}$)	V (cm^3 mole^{-1})
$CaAl_2SiO_6$	11.55 ± .23	**	63.61
$Mg_2Si_2O_6$	17.56 ± .26	92.42	62.70
Mg_2SiO_4	16.11 ± .24	66.23	43.67
SiO_2	-1.23 ± .07	27.80	22.69
$CaAl_2Si_2O_8$	15.99 ± .37	**	100.87

** derived from experimental data of Wood (1978)

Data sources

Robie and Waldbaum (1968)
Charlu et al. (1975)
Newton et al. (1977)
Newton (1978)
Danckwerth and Newton (1978)
Charlu et al. (1978)

Solution models used in calculations

phase	model	reference
olivine	$(X_{Mg})^2$	Williams (1972)
orthopyroxene	$X_{Mg}^{M1}.X_{Mg}^{M2}$	Wood and Banno (1973)
clinopyroxene	$X_{Al}^{M1}.X_{Ca}^{M2}$	Herzberg (1978)
plagioclase	X_{Ca}	Orville (1972)

$-RT\ln K = 2990 + 5.09\,T - .4357(P-1)$ at equilibrium where P is in bars, T in ^{o}K and

$$K = \frac{a_{En}^{opx} \cdot a_{CaTs}^{cpx}}{a_{Fo}^{ol} \cdot a_{An}^{plag}}$$

The solution models used in the application of this equation are given in Table 3.6.1. Application of this barometer is limited to the orthopyroxene-bearing assemblages, although unfortunately these are the very assemblages in which the assumption of equilibrium is most in doubt. The equilibrium constants and pressures have been calculated for three of these assemblages using microprobe data from Table A4, and are listed in Table 3.6.2.

This barometer has the disadvantage of producing results which, because of the very low CaTs activity, are strongly dependent on the ln K term, and significant errors are thus introduced by errors, or variations, in phase compositions. Plagioclase compositions within these assemblages are variable, as are the alumina contents of the clinopyroxenes. Evidence from some cumulates, where oscillatory-zoned clinopyroxenes are present, shows that aluminium diffusion is very slow. Additionally, the low CaTs activities are liable to significant analytical error, even though only wavelength-dispersive analyses have been used. Therefore, although this barometer is theoretically promising, it is not readily applicable to the Grenada assemblages, and the pressures calculated, while low, are believed to be very approximate.

3.6.2 Temperature estimates

Estimates of crystallisation temperatures can be made using the equilibrium:

$$\underset{\text{orthopyroxene}}{Mg_2Si_2O_6} = \underset{\text{clinopyroxene}}{Mg_2Si_2O_6}$$

Table 3.6.2

Pressure calculations for Grenada cumulates

$$CaAl_2Si_2O_8 + Mg_2SiO_4 = CaAl_2SiO_6 + Mg_2Si_2O_6$$
anorthite forsterite CaTs enstatite

$-RT\ln K = 2990 + 5.09T - 0.4357P$ (P in bars; T in ^{o}K)

rock	phase	analysis no.	a_i
6167	olivine	16	0.579
	plagioclase	27	0.729
	clinopyroxene	35	0.023
	orthopyroxene	33	0.603
6095	olivine	23	0.557
	plagioclase	29	0.906
	clinopyroxene	42	0.025
	orthopyroxene	43	0.535
X28406	olivine	42	0.658
	plagioclase	83	0.482
	clinopyroxene	102	0.033
	orthopyroxene	103	0.618

rock	lnK	pressure (kbar)
6167	-3.42	1.9 at 1000°C
6095	-3.63	0.6 at 1000°C
X28406	-2.74	5.8 at 1000°C

calibrated by experiments on the diopside-enstatite solvus in simple systems, but are again only applicable to the problematical orthopyroxene-bearing cumulates. Wells (1977) updated the calibration of this thermometer by Wood and Banno (1973) and estimated an accuracy of ±70°C in results within the range 785° to 1500°C. Because the solvus is steep, and therefore insensitive to temperature, at temperatures below 1000°C, inaccuracies are greatest in this range. Temperatures calculated for the three rocks already used, and rock 6135, an olivine-free assemblage, are listed in Table 3.6.3. The presence of some ferric iron, which can be inferred from the wet-chemical data of Lewis (1973), will increase these values slightly. Different pairs of pyroxenes in each rock give a spread of values, but always well within the accuracy quoted and average temperatures are therefore close to 950°C. In view of this result, it is surprising that Powell (1978) chose temperatures of 1100°-1200°C on which to base her calculations.

Although these values are estimates of equilibration temperatures, it is possible that they are less than the temperatures of cumulate crystallisation. There is no evidence in the pyroxenes of re-equilibration of the assemblages during cooling, such as exsolution and experimental data (Chapter 5) confirm that these are not unreasonable crystallisation temperatures. The lack of exsolution in the oxides supports this view, indicating rapid cooling. Together with the frequent presence of interstitial scoria and glass, this suggests that the blocks were usually at magmatic temperatures on eruption and could therefore be essentially cognate cumulates.

3.6.3 Oxygen activity estimates

Powell (1978) used the equilibrium

$$3Mg_2SiO_4 + 3Fe_2SiO_4 + O_2 = 6MgSiO_3 + 2Fe_3O_4$$

olivine olivine fluid cpx spinel

Table 3.6.3

Temperature calculations for Grenada cumulates

rock	analysis nos.	temperature (^{o}C)
6167	33 and 35	988
6095	42 and 43	907
X28406	102 and 103	898
6135	61 and 62	963

Temperatures calculated according to the calibration of Wells (1977), assuming all iron as Fe^{2+}.

to estimate the oxygen fugacity during crystallisation of the cumulates. This method is subject to the problems of treating the activities of $MgSiO_3$ in clinopyroxene and of magnetite in complex spinels (section 3.6.1), and is believed to be unreliable. A more promising equilibrium, applicable to orthopyroxene-bearing assemblages, is

$$\underset{\text{opx}}{3FeSiO_3} + \underset{\text{spinel}}{Fe_3O_4} = \underset{\text{olivine}}{3Fe_2SiO_4} + \underset{\text{melt}}{\tfrac{1}{2}O_2}$$

but there is a lack of reliable thermodynamic data and the results would anyway be dependent on total pressure which is not accurately known.

The absence of coexisting oxides in the Grenada cumulates prevents $T - a_{O_2}$ determinations using the data of Buddington and Lindsley (1964). Comparison with the results from St. Kitts cumulates obtained by Wills (1974) suggests values of f_{O_2} slightly above those of the NNO buffer curve, but these need not be applicable to Grenada.

3.6.4 Water activity estimates

An equilibrium involving tremolite and aluminous spinel was used by Powell (1978) to estimate the activity of water in Grenada cumulates.

$$\underset{\text{amphibole}}{Ca_2Mg_5Si_8O_{22}(OH)_2} + 0.5\ \underset{\text{cpx}}{CaMgSi_2O_6} + 2.5\ \underset{\text{spinel}}{MgAl_2O_4} =$$

$$2.5\ \underset{\text{plagioclase}}{CaAl_2Si_2O_8} + 4\ \underset{\text{olivine}}{Mg_2SiO_4} + \underset{\text{melt}}{H_2O}$$

The amphibole and spinel solution models used by Powell are considered unsatisfactory. Amphibole presents a problem in that the Grenada compositions are far from tremolite and the thermodynamics of amphibole solid solutions are virtually unknown. Arculus and Wills (in prep.) have suggested the use of pargasite as the amphibole end-member, since some thermodynamic data for this composition are available, but considerable extrapolation is still required. Use of a solution model involving ideal mixing on each site in the amphibole structure is clearly

unrealistic in view of the evidence for coupled substitutions in the Grenada amphibole chemistry, and results in very low pargasite activities in amphiboles which are clearly close to pargasite in composition. So few amphibole data are available that little confidence can be placed in results obtained from these equilibria.

3.6.5 Summary

In conclusion, it is evident that thermodynamic data are still too few, and the knowledge of the solution chemistry of many phases too incomplete for confidence to be placed in the estimates of crystallisation conditions obtained by Powell (1978). Calculations from coexisting pyroxene compositions indicate temperatures of crystallisation below 1000°C, and pressures calculated from orthopyroxene-bearing assemblages are variable, but not close to the upper stability limit of coexisting olivine and calcic plagioclase at around 8 kilobars (Kushiro and Yoder, 1966). The stability of amphibole requires a minimum water content for the melt, and oxygen activities may have been high. Hopefully thermodynamic data and solution models will improve to allow precise estimates of crystallisation conditions to be made, as these would provide a powerful method of study of the conditions in subvolcanic magma bodies.

3.7 Fractionation models involving cumulate assemblages

Least-squares mixing calculations involving cumulate phases (Table 3.7.1) can be used to test lava-cumulate relationships, subject to the uncertainties discussed in Chapter 2. However, the nature of these relationships is dependent on genetic interpretations of the cumulate textures. The predominance of adcumulates in Grenada, and the presence of orthopyroxene-bearing orthocumulates, both argue against formation of the cumulates by perfect fractional crystallisation. However, since

the extrusive rocks are not all directly related, and the mixing calculations therefore only broadly illustrate the fractionation processes, there is little justification for using more complex numerical models involving trapped intercumulus liquid, or open-system fractionation (O'Hara, 1977), even though they may be more realistic. The simple, least squares mixing approach used in Chapter 2 is therefore retained. As previously described, amphibole and plagioclase occur more abundantly in the more evolved, olivine-free blocks, and this feature, together with the strikingly higher abundance of amphibole in the cumulates than in the lava phenocrysts, could be at least partially explained if the blocks more closely represent the products of equilibrium crystallisation than of fractional crystallisation. However, the bulk compositions of the blocks which could be obtained by mixing the mineral analyses are very different from any Grenada magma composition. The approximation to perfect fractional crystallisation used here is therefore believed to be reasonable.

3.7.1 C-series models

The fractionation models for this series described in Chapter 2 have been recalculated using average analyses of the phases in type B cumulate 6051. Models (10) and (11) fit the data well without the inclusion of amphibole, although indicating smaller degrees of fractionation than the corresponding phenocryst-based models in Table 2.6.1. The different degrees of fractionation may be the result of zoning in the phenocrysts, whose cores are closer to the cumulate grains in composition than their rims, but the differences are not large enough to be testable using the already scattered incompatible element concentrations in the lavas.

The important feature is that these models do not involve amphibole but do involve a substantial proportion of plagioclase, which is at

Table 3.7.1

Fractionation models involving cumulate assemblages

	Parent	Daughter	F	X_{ol}	X_{cpx}	X_{plag}	X_{sp}	X_{amph}	Σr^2
(10)	6104	6073	.5945	.0273	.2590	.0896	.0296	-	0.506
(11)	6104	337	.4587	.0371	.2753	.1734	.0554	-	0.141
(12)	6073	381	.5781	-	.0539	.2028	.0486	.1166	0.502
(13)	337	381	.7675	-	.0599	.1014	.0126	.0586	0.078
(14)	307	274	.7446	-	.0736	.0498	.0215	.1106	1.630
(15)	381	274	.7533	-	.1148	.0747	.0311	.0261	2.785
(7)	398	307	.8353	.0402	.0124	-	-.0120	.1241	0.121
(16)	313D	307	.8069	-.0232	.0325	-	.0030	.1809	0.309

variance with the modes of the type A, and many of the type B, blocks. It has already been inferred from the cumulate mineral chemistry that the type A and B cumulates originated at the highest temperatures, and therefore the type A assemblages cannot be related to the C-series magmas. This is consistent with the variation of yttrium in this series (Figure 2.9.2) which precludes substantial amphibole fractionation within the C-series.

Models (12) and (13) agree well with their counterparts in Table 2.6.1, although amphibole is involved in model (12) using the cumulate data. The large proportion of plagioclase and lack of olivine in these models suggests a relationship between the more evolved members of the C-series and the olivine-free type D rather than the type B cumulates.

3.7.2 M-series models

Models (7) and (16) relate two of the most evolved members of the M-series to andesite 307, described in Chapter 2. Although both models involve small amounts of fractionation, and are therefore subject to considerable error, they show small olivine and spinel proportions and large proportions of amphibole. These features are in agreement with the modes of type A cumulates, showing that these assemblages can be related to the evolved members of the M-series.

3.7.3 Models for evolved magmas

Variation within the andesitic magmas is related to the olivine-free cumulate 6136 in models (14) and (15). Both models show poor fits which are largely due to high residuals for alkalis. The proportion of amphibole involved in the extract is strongly dependent on alkalis and these models are therefore not satisfactory. Use of other magmas and cumulates did not produce models which fitted the data well. Difficulties in modelling the evolution of these magmas might be expected, given the evidence in Chapter 2 that they are derived from a

variety of parents whose concentrations of alkalis are highly variable. Correlation of the cumulates with the evolved magmas is therefore restricted to the petrographical evidence discussed in section 3.4.

3.7.4 Summary of cumulate-lava relationships.

Least-squares fractionation models relating the compositions of the extrusive rocks to the cumulate assemblages can constrain cumulate-lava relationships provided that the cumulates are essentially products of fractional crystallisation. Using additional constraints from petrography and trace element chemistry, it can be shown that the type A cumulates cannot be produced by fractionation of C-series magmas, but instead were probably produced by fractionation of the more evolved members of the M-series.

There is considerable modal variation, particularly in plagioclase and amphibole, in type B assemblages, and the almost constant FeO*/MgO of the C-series magmas prevents a clear correlation of this magma series with any of the cumulate types. Therefore, although a substantial proportion of amphibole cannot have been involved in the variation within this series, it is not possible to rule out a relationship between the C-series magmas and some type B cumulates poor in amphibole. It is therefore possible that the variable relative stability of plagioclase and amphibole in the cumulates is at least partly a result of variation in parent magma composition rather than in conditions of crystallisation. However, it may be that cumulate blocks related to C-series magmas are rare or absent. These interpretations are discussed in Chapter 5 in the light of experimental melting studies.

The type D and F cumulates crystallised from basaltic andesite and andesite magmas, but satisfactory modelling of the evolved magma variation using these cumulates is not possible using the limited data available. Type C and E cumulates originated from magmas similar to those

which produced types B and D, but the larger proportion of trapped liquid resulted in orthopyroxene crystallisation.

3.8. Conclusions

(a) Cumulate blocks from Grenada show wide variation in grain size and texture, and have been classified on the basis of their mineral assemblages.

(b) The blocks are predominantly adcumulates and heteradcumulates. Some orthocumulates are present, usually containing orthopyroxene which nucleated in the trapped intercumulus liquid.

(c) Many of the textures exhibited are more consistent with an origin by *in situ* crystallisation rather than by gravitational crystal settling.

(d) The mineral chemistry, together with the textures, suggests an order of crystallisation of olivine, clinopyroxene, amphibole or plagioclase, and orthopyroxene. A spinel probably crystallised continuously with the silicates.

(e) Orthopyroxene-bearing orthocumulates show a very wide range of mineral compositions, reflecting crystal growth in trapped intercumulus liquid and indicating that these rocks may not represent equilibrium assemblages.

(f) Mineral compositions, including trace element concentrations, preclude derivation of the cumulates by fractional crystallisation of the primitive magmas in the M-series.

(g) Thermodynamic calculations applied to the orthopyroxene-bearing assemblages are subject to interpretation of equilibrium, but indicate pressures of 0.5 to 6 kilobars and temperatures of 900 to 1000^{o}C. The precision of the pressure estimates is poor and they do not greatly reduce the bracket of 1-8 kilobars imposed

by published experimental studies. The pressure calculation of Powell (1978) is not considered to be usefully applicable to the Grenada cumulates without improved data on the solution chemistry of the mineral phases.

(h) No reliable thermodynamic estimates of oxygen or water activities can be made using published data. Variation in the relative stability of amphibole and plagioclase may be the result of variable water activity, although variable magma composition cannot be excluded.

(i) Least-squares mixing models for the evolution of the extrusive rocks employing cumulate minerals preclude an origin for the plagioclase-free cumulates from the C-series magmas and support an origin from the evolved compositions in the M-series. Some plagioclase-bearing cumulates may be derived from C-series magmas. The olivine-free assemblages probably crystallised from basaltic andesite and andesite magmas.

CHAPTER 4

PERIDOTITES

Peridotite nodules occur abundantly in microphyric basalt scoria at Grenville, on the east coast of Grenada (Figure 1.2.1). The nodules are up to 4 cm in diameter and often covered by a skin of microphyric basalt. They are pale green in colour, apart from occasional reddened olivines. The host forms one of the scoria cones believed to be among the most recent products of Grenada volcanism but is, as yet, undated. It is deeply reddened, reflecting oxidation of olivine.

Wills (1974) and Arculus (1978) described an olivine-orthopyroxene-clinopyroxene nodule from Grenville which is included in the University of the West Indies collection (no. X28148). They interpreted this rock as a heteradcumulate, the presence of magnesian orthopyroxene suggesting a high-pressure origin. A further 14 perioditites were collected by the writer in 1978 and sectioned. They are rich in olivine and subordinate orthopyroxene, and therefore essentially harzburgitic. Clinopyroxene, spinel, and accessory sulphides occur in some nodules and many specimens show evidence of interaction with the host magma.

4.1 General texture (Plates 4.1(a) and 4.2)

The abundance of olivine and orthopyroxene and scarcity of spinel and clinopyroxene is a striking feature of the nodules in thin section. Grain size is very variable, particularly in olivine, and ranges up to 10 mm. Apart from the partial oxidation of olivine, all the nodules are fresh.

Some parts of the nodules are extensively recrystallised, showing a mosaic texture (Harte, 1977), while adjacent parts contain porphyroclasts. These are dominantly orthopyroxenes, but some large olivines are also strained and may be porphyroclasts, although they are not as

Plate 4.1 (a)

General texture of peridotite nodule 6232 showing granuloblastic olivine with variable grain size and larger orthopyroxene porphyroclasts. Fine grained areas are melt patches produced by interaction with the host melt, a microphyric basalt (top right). Orthopyroxene adjacent to melt patches is embayed due to reaction with the melt. Crossed polars; field of view 20mm.

Plate 4.1 (b)

Turbid orthopyroxene porphyroclast in an olivine mosaic. The turbidity results from very fine scale exsolution, probably largely of ilmenite, but clear selvedges are present. Sample 6238 Plane polarised light; f.o.v. 2.5mm.

Plate 4.2 (a)

Spinel peridotite nodule 6237 showing trains of opaque spinel grains, possibly produced by disruption of original large spinels. Two fine grained orthopyroxene veinlets traverse the specimen perpendicular to the spinel trains. The darkened areas on the left are due to alteration of olivine. Plane polarised light; f.o.v. 23mm.

Plate 4.2 (b)

General texture of peridotite nodule 6123 showing large strained orthopyroxene porphyroclasts (one in extinction) and smaller olivines with variable grain size. Elongate inclusions are visible in the orthopyroxene at the top right. Crossed polars; f.o.v. 19mm.

Plate 4.3

Elongate olivine inclusions in strained orthopyroxene porphyroclasts from nodule 6123. The olivines, which are up to 2mm long, appear to form tabular inclusions parallel to (100) in the orthopyroxene, but are themselves variable in optical orientation. Crossed polars; f.o.v. 3mm.

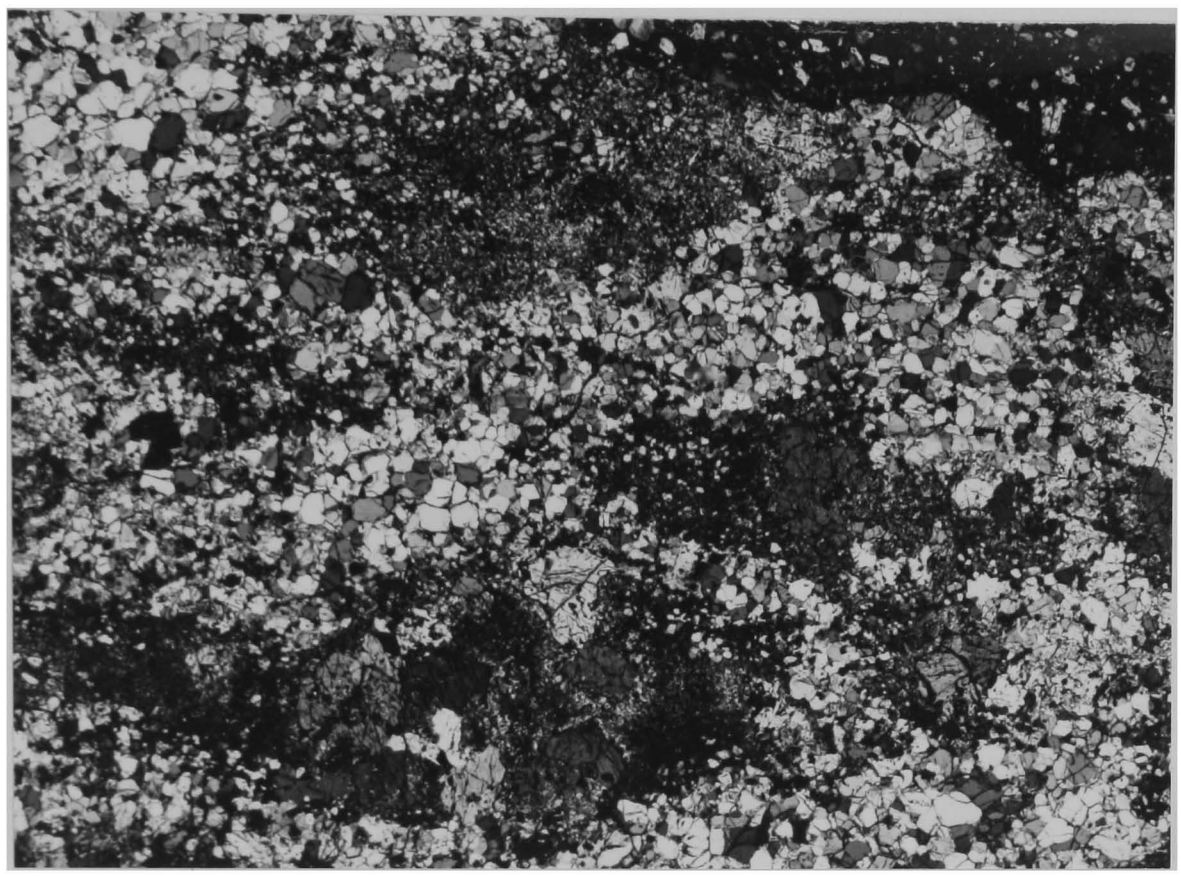

(a)

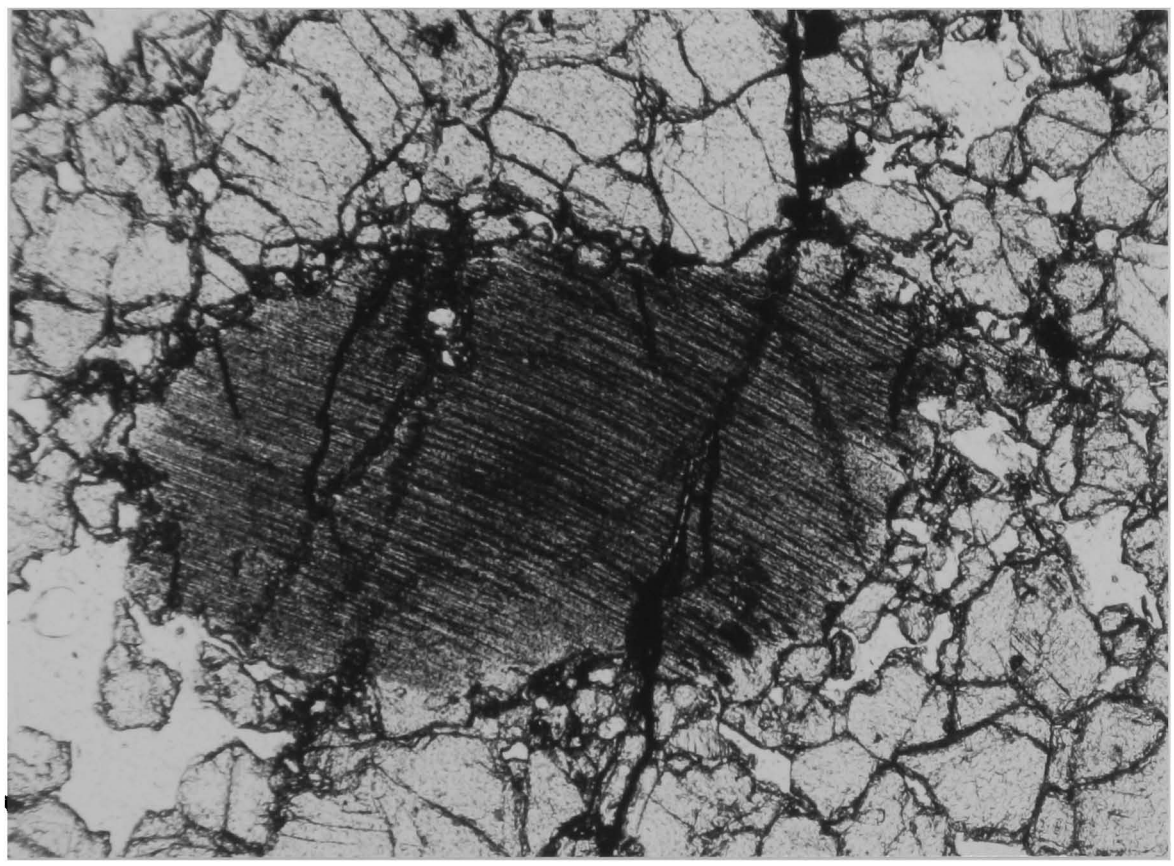

(b)

Plate 4.1

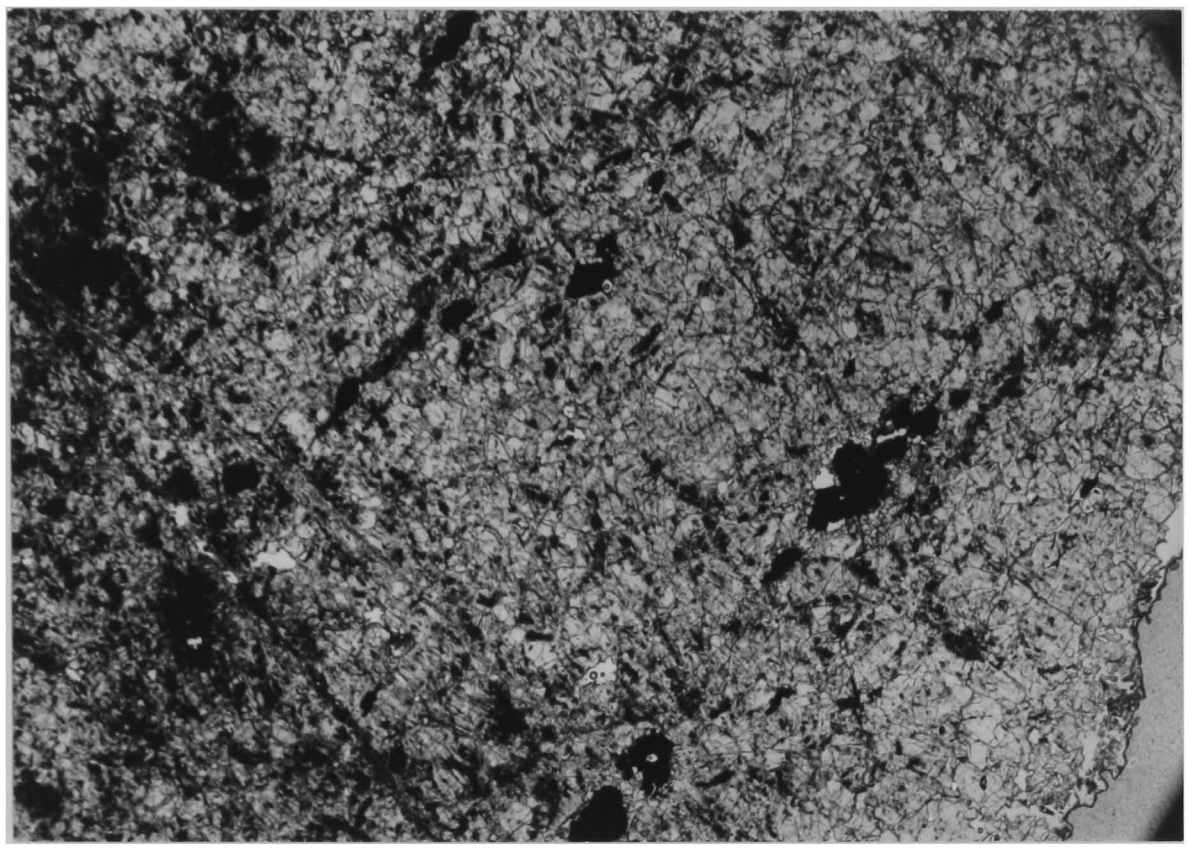

(a)

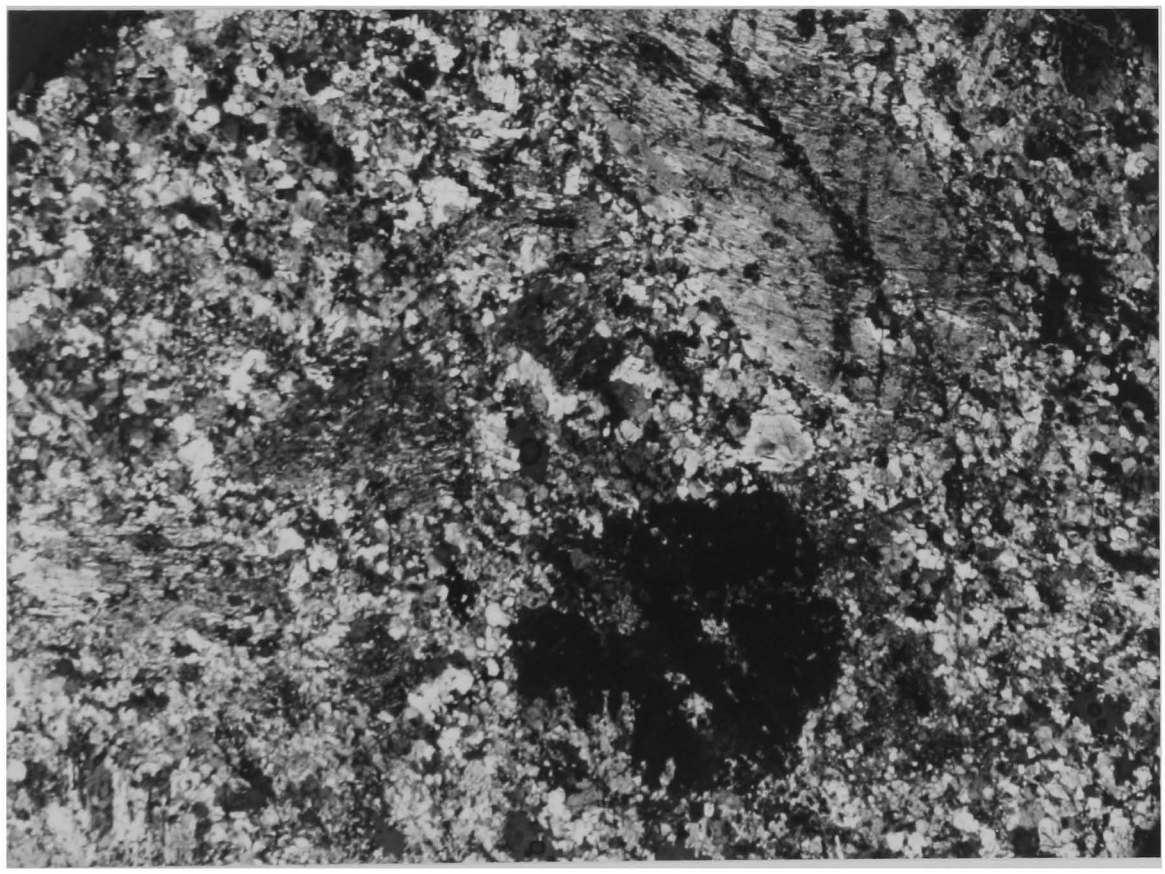

(b)

Plate 4.2

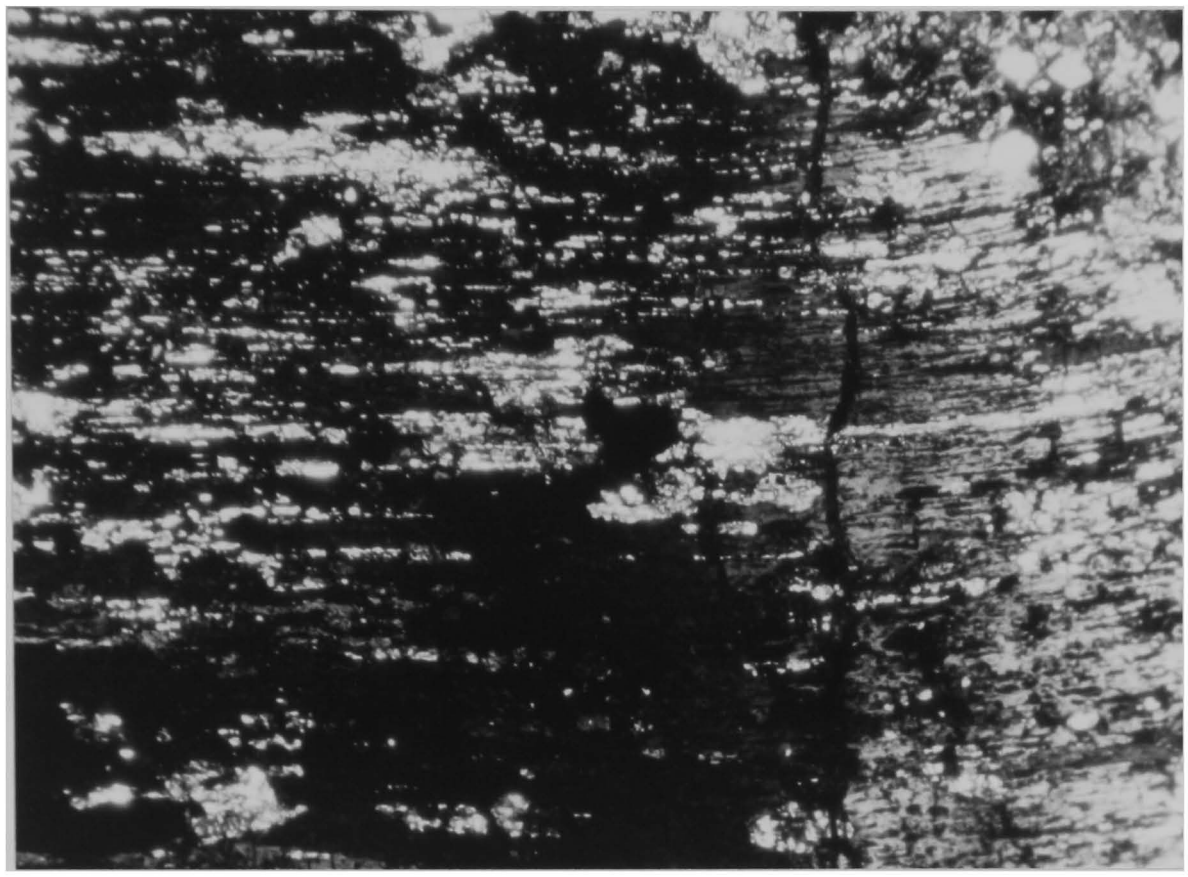

(a)

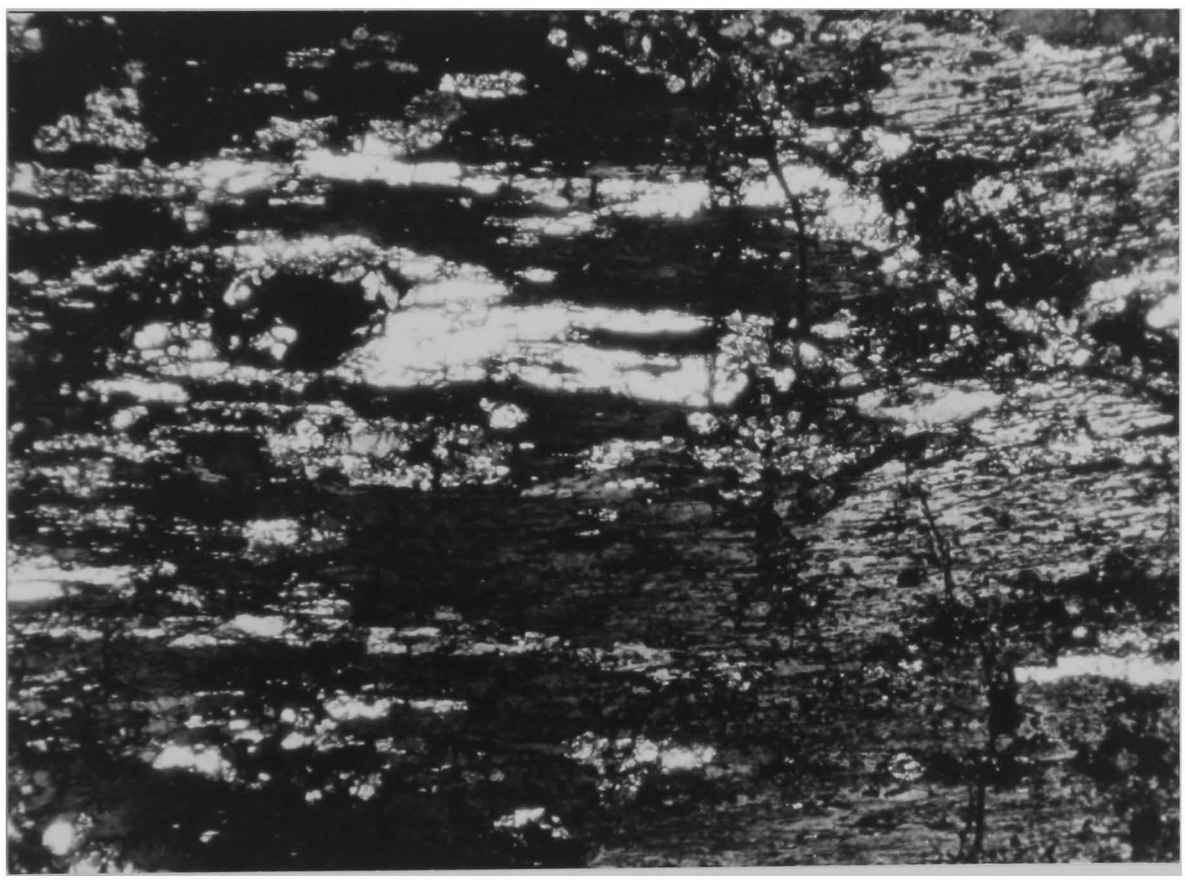

(b)

Plate 4.3

large as the orthopyroxenes. The variation in olivine grain size makes distinction of olivine porphyroclasts difficult. The nodules are mosaic porphyroclastites in the classification of Harte (1977). Fine grained, dark patches commonly occur within the nodules and, in some specimens, are continuous with the host melt. These are interpreted as melt patches produced by interaction of the nodules with the host magma. Further features of the nodule textures are discussed below with reference to the individual minerals.

4.2 Olivine

The majority of olivine grains are equant and strain-free, but very variable in grain size. The larger porphyroclasts are generally strained and show kink-banding. Alteration is also variable within and between specimens, with heavily-strained grains showing more extensive oxidation. This is believed to be due to the preferential nucleation of oxide minerals at dislocations in the olivine structure (Champness, 1970; Nitsan, 1974). In a few samples the oxidation is so intense that some olivines are almost opaque. Preferred orientation of olivine is observed in a few specimens, reflecting recrystallisation in a stress field.

4.3 Orthopyroxene

Orthopyroxene normally occurs as large porphyroclasts up to 10 mm in size although smaller, equant grains are sometimes present. The porphyroclasts are equant to tabular and are irregularly distributed in the nodules, some specimens containing areas rich in orthopyroxene. The porphyroclasts are often bent or fractured, and others show undulose extinction (Plate 4.2(b)).

While the orthopyroxenes of some specimens are essentially free of

inclusions, others have a turbid appearance, similar to that reported by Best (1974) and Harte et al. (1977) (Plate 4.1(b)). This turbidity is caused by very small brown rod- and plate-like inclusions, which are difficult to identify optically but appear to be an oxide phase, possibly ilmenite. A few very thin birefringent silicate lamellae are also present, probably of clinopyroxene. The turbidity is therefore possibly an exsolution phenomenon. It is concentrated in the centres of the grains, often leaving clear outer selvedges.

Other orthopyroxenes contain abundant silicate inclusions (Plate 4.3) which range from round to highly elongate in shape. Extreme examples are 2 mm long but less than 100 microns wide. The inclusions appear to be plate-like and parallel to (100) in the orthopyroxene. Microprobe studies showed that these inclusions are not, as expected, clinopyroxene, but olivine. The abundance of the inclusions, which can occupy up to 30% of the pyroxene, argues strongly against an origin by exsolution from the host pyroxene. An alternative possibility is that the texture formed by deformation and recrystallisation processes, involving the recrystallisation of many small olivine inclusions towards a minimum energy configuration largely controlled by the orthopyroxene structure. A similar conclusion was reached by Best (1974) in considering anhedral olivine inclusions in orthopyroxenes from spinel peridotites in the Grand Canyon. It is difficult, however, to accept that the plate-like habit of the olivines reflects a minimum energy configuration since it involves a large interfacial area with the host pyroxene.

A further alternative hypothesis is that the texture is the product of a eutectic-like intergrowth of olivine and orthopyroxene, analogous to the diopside-ilmenite and enstatite-ilmenite intergrowths found in kimberlites, which have been reproduced experimentally (Wyatt, 1977).

These growths have been shown by X-ray studies (McAllister et al., 1975; Wyatt et al., 1975) to be composed of single crystals of pyroxene and ilmenite. However, the optical orientations of the olivine inclusions in the orthopyroxene are variable in this case. This could be explained by eutectic-like growth in which the densities of nuclei of the two phases were different, or in which the direction of heat transport was a more important factor than the crystallographic orientation relationships between the phases. The exact mechanism of growth is not understood but, in view of the difficulties involved in the other hypotheses, this mode of origin is preferred.

4.4 Clinopyroxene

Excepting its widespread occurrence in the fine-grained 'melt patches', which is interpreted as a secondary feature (section 4.6) clinopyroxene occurs in only one specimen (no. 6122) which shows considerable interaction with the host magma. It is found as anhedral equant grains, sometimes including olivine or overgrowing orthopyroxene. No exsolution has been observed in the clinopyroxenes.

4.5 Spinel

A few of the nodules contain a dark brown spinel, almost opaque and carrying occasional silicate inclusions. Where sufficient grains are present, they define a fabric (Plate 4.2(a)), possibly the product of deformation of original larger spinel grains, and the grains themselves approach a lenticular shape. They could therefore be termed 'disrupted' (Harte, 1977), although an alternative origin as simple cumulate layers cannot be excluded. The margins of the spinels are often irregular, particularly adjacent to the melt patches.

4.6 Melt patches

Fine grained areas comprising olivine, clinopyroxene, and occasional plagioclase laths in an altered glassy matrix are present in all nodules. Their abundance is variable, but shows some correlation with the abundance of orthopyroxene. As already described, the orthopyroxene shows irregular margins adjacent to the melt patches, reflecting reaction with the melt. It is very rare within the patches, being present only as isolated, deeply embayed relics. The clinopyroxenes and olivines in the patches are, in contrast, subhedral in form. The abundance of clinopyroxene in the melt patches, compared with its absence elsewhere in most of the nodules, argues strongly against the patches being products of eutectic melting of the nodules, and implies the introduction of Ca from the host melt. The textures associated with the melt patches are therefore the result of reaction of the host melt, which has penetrated the nodules, reacting with their primary orthopyroxene, producing secondary olivine and clinopyroxene. This process is reflected in the chemistry of the pyroxenes, as discussed in section 4.9.

4.7 Orthopyroxene veins (Plate 4.2(a))

Veins of orthopyroxene up to 250 microns wide traverse sample 6237 parallel to the olivine fabric and perpendicular to the spinel trains. Occasional sulphide grains are present in the orthopyroxene. There are two possible origins for these essentially monomineralic veins. Firstly, they may have been formed by reaction of a silicic melt with the olivine-rich nodule forming orthopyroxene. Experimental evidence (Nicholls, 1974; Mysen and Boettcher, 1975) indicates that relatively silicic melts can be formed at high water pressures in the mantle, although the degree of silica saturation of these melts is controversial (Mysen et al., 1974). Alternatively, the veins may simply result from

passage along cracks of a magma with liquidus orthopyroxene. It is considered unlikely that this magma had an orthopyroxene composition, but rather that the veins would have a cumulate origin. There is no evidence on which to distinguish between these alternative modes of origin.

4.8 Textural interpretation

The preferred orientation of olivine, the disrupted spinels, and the lack of recognisable cumulate textures argue against an origin for the peridotites as simple cognate cumulates from the microphyric, M-series basalts. The abundance of orthopyroxene and rarity of clinopyroxene also argue against a cognate cumulate origin, since fractionation models for the M-series basalts, discussed in Chapter 2, involve substantial clinopyroxene but do not involve orthopyroxene.

The variable grain size of the nodules is believed to reflect variable deformation and recrystallisation of the peridotites, the olivine and orthopyroxene porphyroclasts representing relics of an original coarser-grained peridotite which has been deformed. The small grain size of the olivines adjacent to the orthopyroxene porphyroclasts results from concentration of strain at the margins of the larger orthopyroxenes during deformation. Recrystallisation of these olivines has produced essentially strain-free neoblasts, while the larger olivine porphyroclasts are clearly strained.

Interpretation of the spinel fabric in sample 6237 as the product of disruption of originally larger grains implies a deformation event prior to that which produced the preferred orientation of olivine in the sample, which runs perpendicular to the spinel trains. Veining by orthopyroxene in this nodule is subparallel to the olivine elongation, and is interpreted as a later feature. These is no evidence of deformation

of these veins. In summary, this specimen indicates that the peridotite body sampled by the magma had suffered a complex deformational history.

Fine grained patches reflect reaction of orthopyroxene in the peridotite nodules with the undersaturated host melt, producing olivine and clinopyroxene. There is also some evidence to suggest reaction of spinel with the melt.

4.9 Mineral chemistry

Selected peridotites were studied by electron microprobe, both wavelength- and energy-dispersive methods being used. Data are presented in Table A5, and analytical details in Appendix A.

4.9.1 Olivine (Table A.5.1)

Olivine shows a very restricted range of composition from $Fo_{88.3}$ to $Fo_{91.2}$. Melt patch olivines have average composition $Fo_{90.5}$ while others average $Fo_{89.9}$. No significant difference in composition exists between olivines in the matrix of the nodules and those included in orthopyroxene porphyroclasts. Wavelength-dispersive analyses of nickel and calcium (Table 4.9.1) show lower concentrations of Ni and higher concentrations of Ca in the melt patch olivines. These differences are interpreted as evidence of reaction of the host melt with the peridotites. An interesting feature is the slightly higher forsterite contents but lower nickel contents of the melt patch olivines compared with the primary peridotite olivines. This is explicable by partial equilibration of a host melt containing some ferric iron, with the peridotite minerals in the melt patches. The nickel contents of the secondary olivines are, however, controlled by those of the host melt and dissolved orthopyroxene, resulting in lower olivine nickel contents.

Table 4.9.1

Wavelength-dispersive analyses of nickel and calcium in peridotite nodule olivines

probe no.	mole % Fo	CaO (wt.%)	NiO (wt.%)
23210	89.7	0.00	0.41
23211*	90.6	0.10	0.30
23212*	90.8	0.11	0.25
23213	89.7	0.00	0.40
23305	89.8	0.03	0.40
23306	89.5	0.04	0.42
23307*	89.6	0.11	0.35
23308*	89.3	0.13	0.30
23601	89.7	0.01	0.54
23602*	90.7	0.09	0.39
23603*	90.9	0.10	0.36

* in melt patches

4.9.2 Orthopyroxene (Table A5.2)

Orthopyroxene compositions are plotted in a pyroxene quadrilateral in Figure 4.9.1. With the exception of those from sample 6122, the analyses are almost identical, an interesting feature being their low alumina contents. Orthopyroxenes in sample 6122 are slightly richer in iron, as are the olivines in this specimen. Vein orthopyroxenes in sample 6237 (analyses 58 and 59) are not significantly different in composition from other orthopyroxenes in this nodule.

4.9.3 Clinopyroxene (Table A5.2)

Clinopyroxene compositions plotted in Figure 4.9.1 show distinct differences between primary grains in peridotite 6122, those in melt patches, and microphenocrysts in the host magma. The primary clinopyroxenes are notably poor in alumina (average 0.68 wt.%) while those in the melt patches are always richer in this component. The variation in the alumina contents in the melt patch grains probably reflects disequilibrium crystallisation, as postulated for some extrusive rocks (Chapter 2). The compositional distinction between the clinopyroxenes in the host lava and those in the melt patches is believed to result from reaction of the invading melt with the primary orthopyroxene, producing clinopyroxenes with lower Ca and higher Al contents than those of the primary peridotite clinopyroxenes, and/or from differing temperatures of crystallisation of the two types. The limited amount of invading melt involved prevents the melt patch grains having substantially lower Mg-values than the primary orthopyroxenes which are reacting with the melt.

4.9.4 Spinel (Table A5.3)

Spinel compositions from four nodules are plotted in Figure 4.9.2, together with the spinels from Grenada lavas analysed by Arculus (1974), the field of cumulate spinels (Chapter 3) and spinels from other

Figure 4.9.1

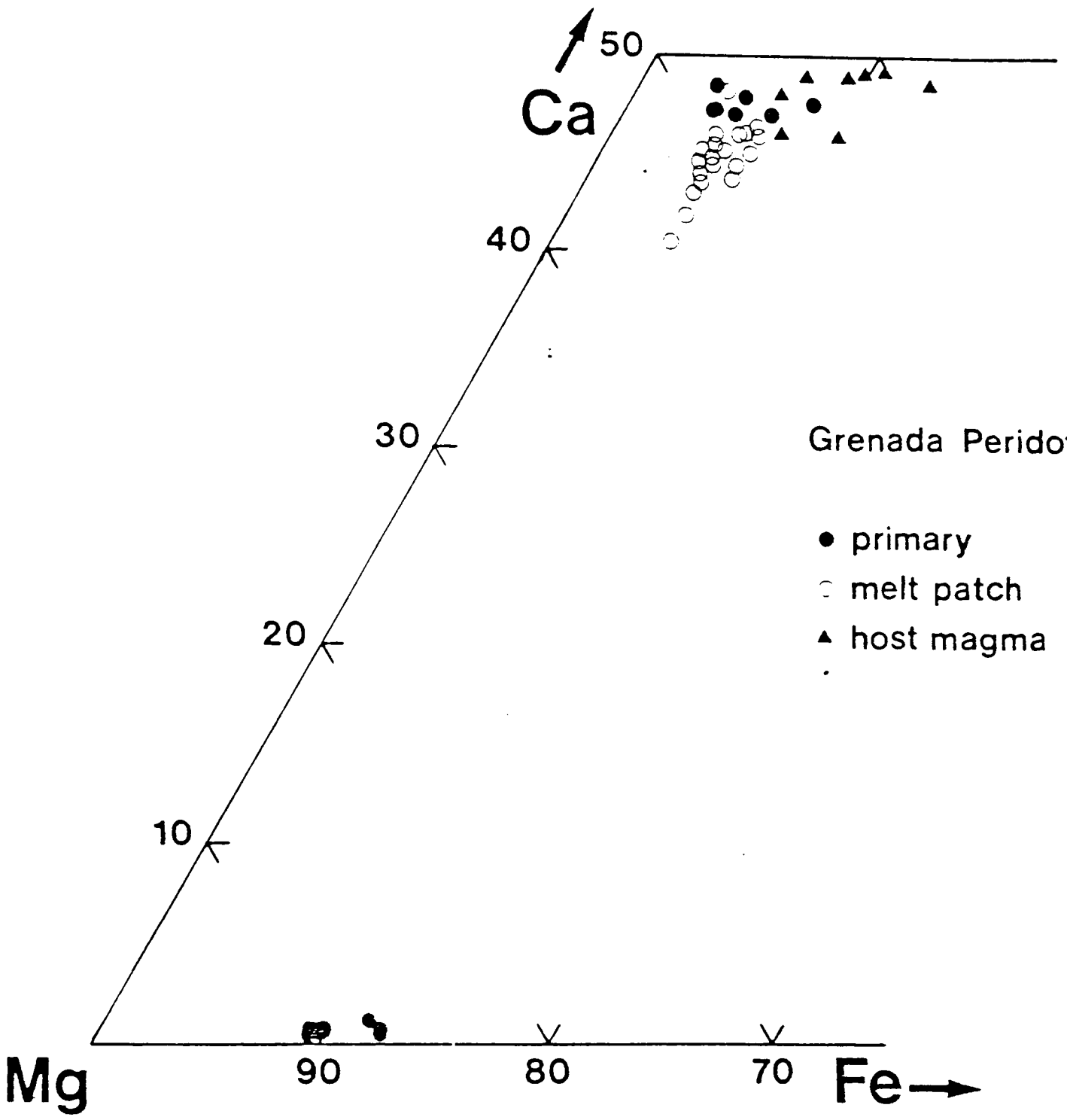
Ca
50
40
30
20
10
Mg
90
80
70
Fe
Grenada Peridotites
primary
melt patch
host magma

Figure 4.9.2

(a) comparison of peridotite spinels with those from other Grenada rocks. Lava spinels from data of Arculus (1974). Outlined field is that of cumulate spinels (Chapter 3).

(b) comparison of Grenada peridotite spinels with those from other peridotite associations, and spinels from MORB (Sigurdsson and Schilling, 1976). Field of stratiform complexes after Irvine (1965). Field of kimberlite nodules after compilation by Jackson (in prep.). Field of basalt nodules from data of: Frisch (1971), Aoki and Prinz (1974), Ross et al. (1954), Littlejohn and Greenwood (1973), Bacon and Carmichael (1974), Frey and Green (1974), Pike (1976), Donaldson (1978), Suwa et al. (1975), Varne (1977), Brousse (1968), Basu (1975), Best (1974), Frey and Prinz (1978), and B.G.J. Upton (pers. comm.). Ophiolite data from Malpas and Strong (1975), Greenbaum (1977), and Neef and Plimer (1979).

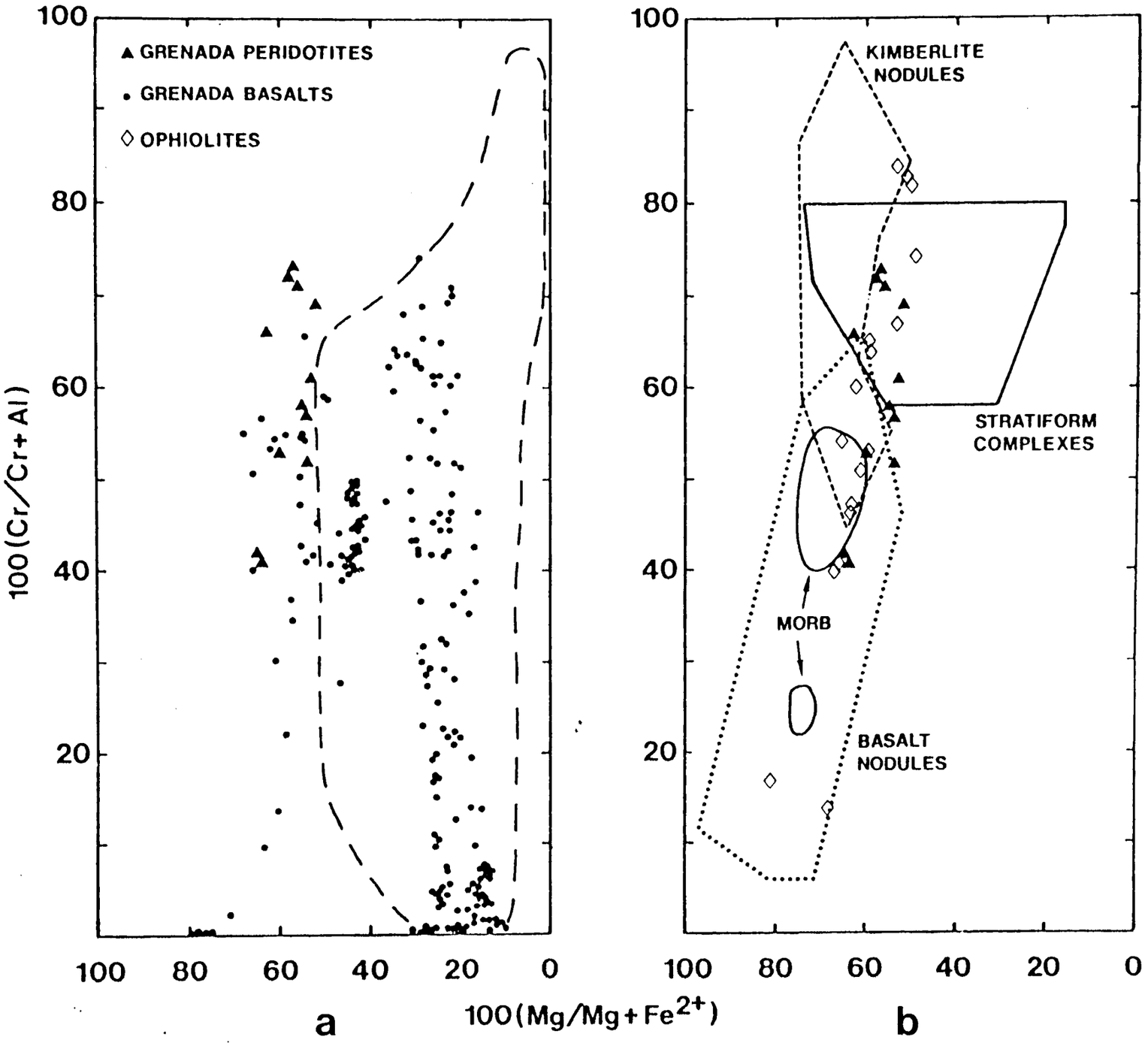
▲ GRENADA PERIDOTITES
• GRENADA BASALTS
◇ OPHIOLITES
100
80
60
40
20
100(Cr/Cr+Al)
100 80 60 40 20 0
100(Mg/Mg+Fe2+)
a
KIMBERLITE NODULES
STRATIFORM COMPLEXES
MORB
BASALT NODULES
100 80 60 40 20 0
b

peridotites and lavas. The ferric iron contents of Grenada peridotite spinels, calculated assuming stoichiometry, are low, comprising a maximum of 14% of trivalent cations. Only minor zoning of spinel grains is present. Cr/(Cr + Al) values are high, with moderate Mg-values.

The peridotite spinels are clearly different in composition from those of the cumulate blocks, particularly in their low ferric iron contents. There is some overlap with the lava spinels. Comparison with data from other peridotites shows (considering only spinels coexisting with olivine close to Fo_{90} in composition) that the Grenada spinels have Cr/(Cr + Al) ratios higher than most spinels from peridotite nodules in basalt and comparable with spinels from stratiform complexes. They are not, however, as rich in Cr as some kimberlite nodule spinels. The negative correlation of Cr/(Cr + Al) with Mg-value is similar to that shown by basalt nodule spinels, and distinct from the larger variations of Mg-value in cumulate peridotite spinels from stratiform complexes.

Peridotites containing spinels of composition closely comparable with the Grenada examples are those from the tectonite peridotites of ophiolite complexes, although the data available are limited. These peridotites are also harzburgitic in character and are believed to have been depleted by extraction of large scale partial melts at constructive plate margins (Menzies and Allen, 1974; Malpas, 1978).

4.9.5 Sulphide

Sulphide inclusions occur in silicates and spinels in several Grenada peridotites. Their small size makes optical examination difficult but many appear to be optically homogeneous. Energy-dispersive analyses (Table 4.9.2) suffer from some interference between element peaks but clearly show that the sulphides are Ni-Fe-S monosulphide solid solution (MSS). Although occasional exsolution, forming complex Ni-Fe-Cu sulphides, is present, the occurrence of optically homogeneous

Table 4.9.2

Energy-dispersive microprobe analyses of sulphides in Grenada peridotites

probe no.	12201	12202	12202A	23701
host	cpx	cpx	cpx	opx
Fe	40.89	47.55	47.36	47.65
Co	0.71	0.80	0.53	0.77
Ni	19.21	13.93	14.21	12.53
Cu	0.00	0.25	0.00	0.19
Zn	0.23	0.00	0.00	0.47
S	38.35	37.81	38.10	38.54
Total	99.39	100.34	100.20	100.15

MSS is unusual, and reflects rapid cooling from high temperatures (Craig and Scott, 1974).

4.10 Thermometry

Temperature estimates can be made from coexisting primary pyroxenes in sample 6122 (Table 4.10.1). The different calibrations of Wood and Banno (1973) and Wells (1977) result in slightly different temperatures and the small spread of results is largely a function of the slightly variable clinopyroxene compositions, to which the calculations are sensitive.

An alternative method of estimating equilibration temperatures is the olivine-spinel thermometer which has been investigated by several workers (Irvine, 1965; Evans and Frost, 1975; Roeder et al., 1979; Fabries, 1979). This thermometer can be calibrated empirically or theoretically, the latter approach being desirable but limited by the availability of reliable thermodynamic data. Fabries (1979) has reviewed the empirical calibration and application of this thermometer and demonstrated that, in natural peridotites, it tends to produce lower temperature estimates than the Wood-Banno (1973) two-pyroxene thermometer. Fabries (1979) interpreted this difference as a consequence of differing rates of diffusion and recrystallisation in different phases, suggesting that Mg and Fe diffuse faster than Ca, allowing the olivine-spinel pairs to re-equilibrate to lower temperatures during cooling than coexisting pyroxenes. The olivine-spinel temperatures for nodule 6122 (Table 4.10.1) are only slightly lower than those derived from the Wood-Banno (1973) thermometer and greater than those from the Wells (1977) calibration. This may reflect slight re-equilibration of the olivine-spinel pairs in some nodules during heating by the host magma, but insufficient data are available for a full comparison of the different

Table 4.10.1

Temperature estimates for Grenada peridotite nodules

orthopyroxene - clinopyroxene

sample	no. of pairs	temperature	
		Wood & Banno (1973)	Wells (1977)
6122	4	1004°C	914°C

olivine - spinel (Fabries, 1979)

sample	no. of pairs	temperature
6122	3	985°C
6123	2	1050°C
6233	4	896°C
6237	3	927°C

temperature estimates.

Since, as previously described, the temperatures calculated may reflect the diffusion and recrystallisation properties of the minerals, they may represent 'closure' temperatures of exchange equilibria during cooling. However, such closure temperatures may not represent any point on the cooling path of the nodules, since different equilibria are likely to 'close' for different phases at different temperatures. The estimates of equilibration temperatures for Grenada nodules may therefore have little meaning beyond an indication that the peridotites were well below magmatic temperatures when captured by the host magma, supporting the other lines of evidence against a cognate cumulate origin. The presence of MSS in the nodules indicates that the nodules cooled quickly after eruption, and therefore that the temperature estimates do not represent surface cooling.

4.11 Origin of the nodules

Several possible origins for the Grenada peridotite nodules must be considered.

(a) cumulate

Evidence has already been presented that the textures, modes, and temperatures of equilibration of the nodules argue against a cognate cumulate origin. However, this does not rule out an initial cumulate origin, with subsequent deformation and recrystallisation prior to capture by the host magma. The limited variation in mineral compositions could reflect re-equilibration during metamorphism and cannot be regarded as conclusive evidence against derivation of the nodules from a cumulate peridotite body.

(b) magma source or residual source

It is possible that the nodules represent samples of the mantle

from which the Grenada magmas were produced, or of mantle from which Grenada-type magmas have been extracted. The first possibility is considered unlikely since the nodules are clearly very depleted in fusible components such as CaO, FeO, Al_2O_3 and alkalis, a feature reflected in the chrome-rich spinel compositions. The second possibility cannot be dismissed on the available evidence although the deformational history of the nodules, as recorded in their textures, shows that they are not genetically related to their host magma. The nickel contents of the primary olivines indicate (Table 4.11.1) that they could not have been in equilibrium with any of the magmas erupted on Grenada, although the values of the distribution coefficient are uncertain, as discussed in Chapter 3. The primary olivines could, however, be in equilibrium with magmas slightly more primitive than the erupted compositions. It could be expected that the source region for the Grenada magmas would be at temperatures considerably in excess of those recorded by the nodules, so that this hypothesis of their origin is not thought to be correct.

(c) accidental inclusions

The alternative to the residual mantle source hypothesis is that the nodules are genetically unrelated to Grenada magmas. In view of their depleted composition and the similarity of the spinel compositions to those in tectonite basements of ophiolite complexes, it is tempting to suggest that the nodules represent fragments of the oceanic lithosphere upon which the Lesser Antilles arc was built. However, it is not easy to visualise complex deformation and recrystallisation of the nodules in the lithosphere under the arc, which is likely to be relatively rigid. It might be expected that the mantle closer to the subduction zone would be more likely to suffer deformation. Unfortunately there are few constraints on the depth of origin of the nodules within

Table 4.11.1

Ni distribution between primary olivines and liquid

For a Grenada picrite containing 16% MgO,

D_{Ni} = 6.9 (Hart and Davis, 1978)

or D_{Ni} = 4.8 (Elthon and Ridley, 1979)

For an average olivine C_{Ni} = 3380 ppm, therefore:

C_{Ni}^{liq} = 490 ppm (using Hart and Davis, 1978)

or C_{Ni}^{liq} = 704 ppm (using Elthon and Ridley, 1979)

The maximum Ni content of Grenada lavas is 460ppm

the interval between the surface and the top of the subducted lithosphere in which the Grenada magmas are believed to have originated. This is particularly so because the Al_2O_3-poor nature of the peridotites might preclude the presence of garnet or plagioclase at any depth within this interval. On balance, the interpretation of the nodules as accidental xenoliths genetically unrelated to Grenada magmatism is preferred.

4.12 Conclusions

(a) Spinel peridotite nodules occur in microphyric M-series basalt in Grenada. The nodules are poor in spinel and clinopyroxene and are essentially harzburgitic.

(b) These nodules are believed to represent the first reported occurrence of spinel peridotite nodules in an island arc volcanic suite.

(c) The nodules are mosaic porphyroclastites in the classification of Harte (1977).

(d) The textural features and modal abundances of the minerals argue against the nodules being cognate cumulates from the M-series magmas.

(e) The textures indicate a complex deformation and recrystallisation history for the parental peridotite body.

(f) The nodules have a depleted character, being poor in Fe, Ca, Al and alkalis.

(g) Thermometry calculations indicate that the nodules equilibrated at temperatures in the range 900° to $1050^{\circ}C$.

(h) The mineral chemistry of the nodules reflects their depleted character. In particular, the spinel compositions are more comparable with those in tectonite peridotites of ophiolite complexes

than with those in other spinel peridotite nodules in basalt.

(i) The host melt has reacted with orthopyroxene in the nodules, producing secondary olivine and clinopyroxene.

(j) The nodules probably represent accidental xenoliths of depleted peridotite captured by the magma, although an initial origin as cumulates cannot be excluded.

CHAPTER 5

EXPERIMENTAL STUDIES

Experimental petrological studies provide a means of investigating several aspects of the evolution of the Grenada rock suite. Of particular interest are the postulated role of amphibole in the transition from moderately Ne-normative to Hy-normative compositions in the M-series basalts (Cawthorn et al., 1973a), the identification of the magmas in equilibrium with the cumulate assemblages, and the constraints on the total pressure and activity of volatile components in the environment of cumulate crystallisation.

The experiments of Cawthorn et al. (1973a) have been used, along with experiments in synthetic systems (Cawthorn, 1976) to support a hypothesis of andesite genesis by fractional crystallisation of amphibole-rich assemblages from basaltic magmas (Cawthorn and O'Hara, 1976) despite the fact that the experiments of Cawthorn et al. (1973a) did not show amphibole as a near-liquidus phase in basalt under water-saturated conditions. Careful control of water activity in experiments on a range of lava compositions might be expected to provide further evidence as to the viability of this hypothesis.

As demonstrated in Chapter 2, the chemical variation of the extrusive rocks of Grenada is largely explicable in terms of fractional crystallisation of phenocryst mineral assemblages, and the abundant cumulate blocks described in Chapter 3 support this hypothesis, although the exact relationships between the extrusive rocks and the cumulate assemblages could not be defined. The cumulate assemblages demonstrate variable relative thermal stability of plagioclase and amphibole, which existing experimental data (see discussion below) can explain by variable water activity, and significant spinel crystallisation which may be influenced by oxygen activity. It may therefore be possible to use

experimentally studied phase relations to explain aspects of the chemical evolution of the extrusive rocks and place constraints on the conditions of fractionation in the subvolcanic magma bodies.

5.1 Experiment design

The principal aim of the experimental work is to study the phase relations of a series of magmas which appear, from chemical evidence, to be related largely by fractional crystallisation. If the fractional crystallisation process was a perfect one, only the primary liquidus phases in the experiments would be of interest. The strongly porphyritic nature of many of the lavas suggests, however, that perfect fractional crystallisation has not taken place, and a series of equilibrium crystallisation experiments will therefore be relevant provided that the percentage of crystals is not very large. The experiments should, nevertheless, be extrapolated to the natural magmas with caution since liquid composition paths in fractional and equilibrium crystallisation will differ, as will the nature of the reaction relationships between phases (e.g. O'Hara, 1969).

Study of the relative stability of spinel, plagioclase and amphibole requires close control of water and oxygen activities. Control of water activity can be achieved using vapour-present experiments in which the activity of water in the vapour is known. This has an advantage over vapour-absent experiments in that the presence of a vapour phase assists the equilibration of water with the melt. Phase relations involving a melt can then be studied as a function of the mole fraction of water in the vapour, which approximates to the activity at low pressures and high temperatures. Variable water content of the vapour may be produced by the use of the fluid generating compounds listed by Holloway and Reese (1974) together with water.

It was decided to attempt control of the weight fraction of water dissolved in the melt in each experiment. This is possible provided that the relationship between solubility of water and melt composition is known. Burnham (1975, 1979) has shown that P-V-T data on the albite-water system (Burnham and Davis, 1971, 1974) can be applied to more complex silicate melts given a model for the water solubility mechanism. Calculation of the effective molecular weight of a melt in terms of the molecular solubility model of Burnham (1975) allows prediction of the water solubility in a wide range of natural melt compositions at pressures up to 10 kilobars. A computer program was written to calculate the weights of rock powder, water, and fluid generating compound required for each experiment, using the results of Burnham and Davis (1974) and available water solubility data for the albite-water system. An additional program calculates the water content of the melt and oxygen fugacity in buffered experiments using the weights of the run starting materials. Listings of both programs and a more detailed description of the calculations, together with an estimate of the likely errors involved, are to be found in Appendix C.

Control of oxygen fugacity was achieved by the use of synthetic buffer assemblages in capsules surrounding the charges (Eugster and Wones, 1962). In water-undersaturated charges this double capsule technique results in an oxygen fugacity in the charge which is lower than that defined by the buffer assemblage (Whitney, 1972).

Several workers have studied the loss of iron to noble metal containers in high temperature experiments (e.g. Merrill and Wyllie, 1973; Stern and Wyllie, 1975). In view of the large losses to platinum which would be expected at the liquidus temperatures of some of the compositions studied, platinum-iron alloy sample containers (Ford, 1978) were employed in this work. Details of capsule preparation and iron exchange

studies are given in Appendix C.

Difficulties were experienced in growing crystals to a sufficient size for microprobe study from the finely ground starting materials. An attempt was therefore made to grow fewer, larger crystals by producing only a few nuclei of each phase on cooling from an all-liquid starting material. These runs were melted over a short period and then cooled rapidly (ca. 200 deg.min.$^{-1}$) to the run temperature. Two experimental methods were thus used:

(1) heating to the desired run temperature with no overshoot, so that crystals were always dissolving in the melt, and

(2) superheating to an all-liquid state and cooling rapidly to the run temperature, so that crystalline phases were required to nucleate from the melt.

The effects of the different methods on phase relations are discussed in section 5.6.

All samples were loaded as very finely crushed powders to promote reaction and minimise the persistence of relict phases. Examination of the powders showed the largest grains to be usually less than 15 microns in diameter and average grain size to be less than 5 microns. Although some variation in phase compositions was found in the simple melting runs, equilibrium is believed to have been approached sufficiently closely not to have affected the observed phase relations.

5.2 Previous work

5.2.1 Study of Cawthorn et al. (1973a)

The phase relations of five Grenada lava compositions were studied by Cawthorn et al. (1973a) under water saturated conditions at 5 kilobars (Figure 5.2.1). In all three nepheline-normative compositions olivine was the liquidus phase, closely followed by clinopyroxene,

Figure 5.2.1

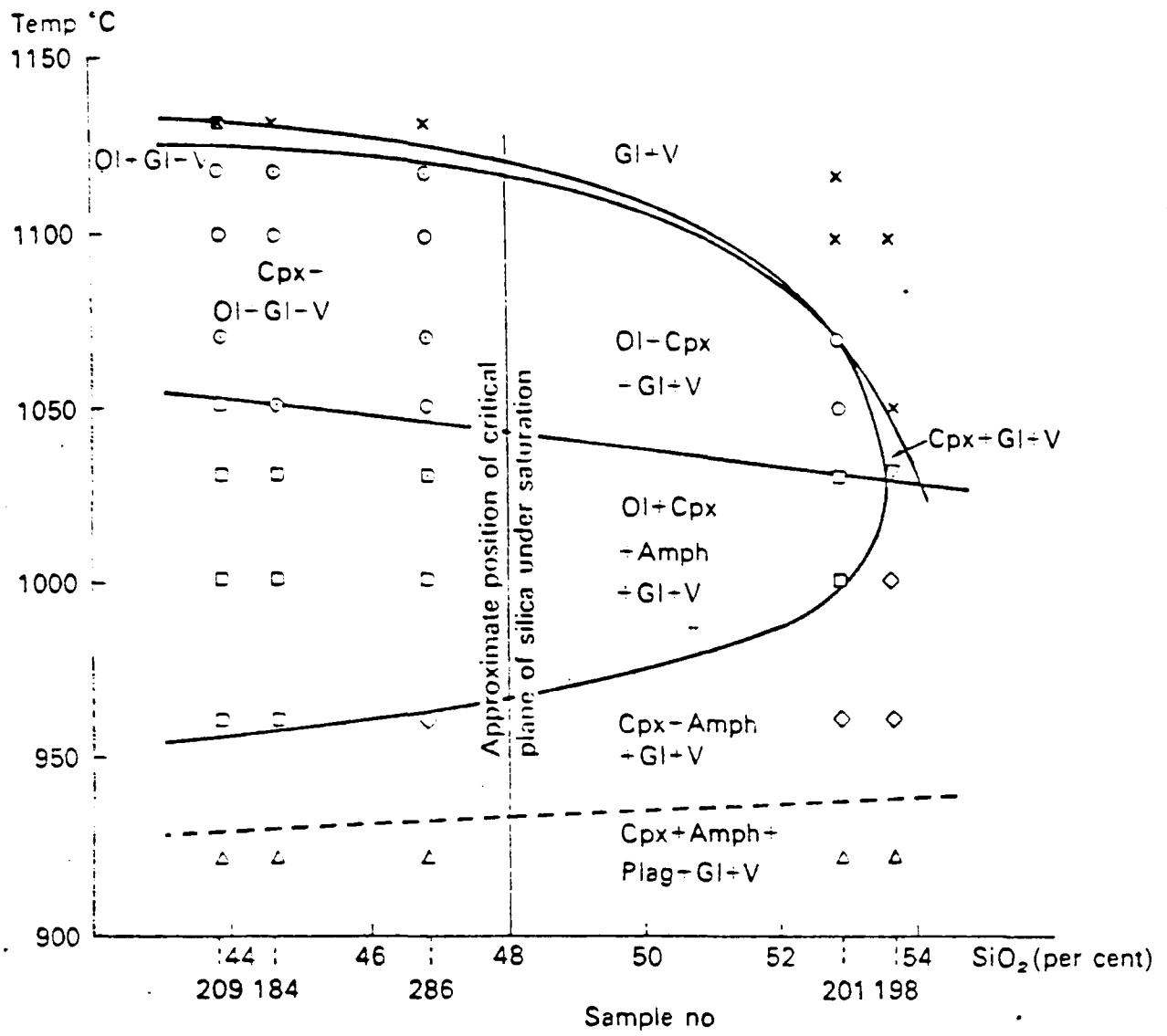

Phase relations of Grenada lavas determined by Cawthorn et al. (1973a) at 5kbar under water-saturated conditions.

while in the two hypersthene-normative compositions clinopyroxene was the liquidus phase. Amphibole was only found within 50°C of the liquidus in these hypersthene-normative compositions. Nevertheless, Cawthorn et al. (1973a) reasoned that increased pressure might bring amphibole closer to the liquidus under water-saturated conditions and its crystallisation would then drive originally undersaturated magmas through the low pressure thermal divide close to the normative Di-Fo-An plane, producing hypersthene-normative compositions. Recent work by Presnall et al. (1978) shows that this thermal divide only exists up to a pressure of approximately 4 kilobars even in sodium-bearing systems and that an undersaturated magma crystallising olivine, clinopyroxene, and spinel can become hypersthene normative. The results of Cawthorn et al. (1973a) are therefore not strongly supportive of a hypothesis in which amphibole fractionation produced hypersthene-normative magmas from undersaturated parents, the experimental data of Presnall et al. (1978) supporting the conclusion of Arculus (1973, 1976) that fractional crystallisation of olivine, clinopyroxene and spinel produced this trend.

A number of studies by other workers are relevant to the evolution of Grenada magmas. Since the experimental work in this study is designed to investigate fractional crystallisation models, which are strongly supported by the chemical data, experimental studies investigating mechanisms for genesis of primary andesitic magmas are excluded here, but discussed in Chapter 7.

5.2.2 Experimental studies of amphibole stability

As described above, Cawthorn and O'Hara (1976) have suggested that amphibole fractionation is important in the genesis of andesite from basalt. The chemical evidence from Grenada (Chapter 2) indicates that amphibole is only an important fractionating phase in magmas more evolved than basaltic andesite in this suite. Cawthorn (1976) has studied

amphibole stability as a function of melt composition, while amphibole stability has been studied as a function of water activity by Eggler (1972a), Holloway (1973), Allen and Boettcher (1978), and Ritchey and Eggler (1978), and as a function of oxygen activity by Helz (1973) and Allen et al. (1975). In general, water activity is a more important influence on amphibole stability than oxygen activity.

The experimental data show that amphibole thermal stability is increased by increased a_{H_2O} at low (<3 kilobar) pressures while, at higher pressures, a thermal stability maximum develops at intermediate water activity. This can be explained in terms of the variable water content of the host melt at different pressures and its effect on the stoichiometry of the amphibole melting reaction. This change in amphibole melting behaviour with pressure in water-undersaturated melts has been modelled theoretically by Sykes (1979).

Available data show that amphibole thermal stability is limited to temperatures less than 1075°C, even at pressures up to 20 kilobars. Amphibole is only a liquidus phase at pressures above 10 kilobars and it is questionable whether Allen and Boettcher's (1978) high pressure experiments are applicable to the more magnesian Grenada magmas. There is therefore no strong support in published experimental studies for amphibole fractionation from the more magnesian, undersaturated Grenada magmas.

5.2.3 Experimental studies of spinel stability

The Grenada cumulate assemblages and the chemistry of the extrusive rocks indicate that spinel is a significant fractionating phase in the evolution of the extrusive rocks. Osborn (1959, 1978) has postulated that fractionation of a magnetite-rich spinel is capable of explaining the characteristic lack of strong iron enrichment in calc-alkaline fractionation trends, although this hypothesis has been questioned on the

basis of both chemical (Taylor et al., 1969) and experimental (Eggler and Burnham, 1973) studies. However, experimental evidence does show increased magnetite thermal stability at increased oxygen fugacities (Hill and Roeder, 1974). Oxygen and water activities are not independent, being related through the dissociation constant of water, and the presence of more and more dissolved water will increase the oxygen fugacity in a crystallising magma (Hamilton and Anderson, 1967; Mueller, 1970).

5.2.4 Hydrous melting studies in basaltic and andesitic systems at low pressures

The results of several studies are applicable to the phase relations observed in the Grenada cumulate blocks. The importance of amphibole in hydrous basaltic systems was first demonstrated by Yoder and Tilley (1962) under water-saturated conditions. Phase relations and phase compositions in water-saturated melting were studied by Helz (1973, 1976). Similar phase relations showing increased amphibole stability and decreased plagioclase stability in the presence of water were observed in water-undersaturated melting by Holloway and Burnham (1972), Eggler (1972a, 1972b) and, more recently, by Ritchey and Eggler (1978). Eggler (1972b) and Ritchey and Eggler (1978) estimated the water contents of natural magmas by comparing orders of crystallisation in natural magmas with those in water-undersaturated melting experiments, while the application of data from the albite-water system to natural magmas (Burnham, 1979) shows that the minimum water content required for amphibole stability in halogen-free melts is close to 3 weight percent. The effect of fluorine on amphibole stability has been investigated by Holloway and Ford (1975) but the fluorine and chlorine contents of the cumulate amphiboles are low (Table A4.4) and are not believed to have been an important influence on their stability.

5.3 Experimental results

Melting experiments were carried out on five Grenada lavas whose compositions are given in Table 5.3.1. Samples 43 and 114 are microphyric picritic basalts from the M-series while 311 and 313D are more evolved members of this series. Sample 6264 is one of the more primitive C-series magmas. Although comparable chemical data are not available for most of the samples studied by Cawthorn et al. (1973a) it is nevertheless clear that 43 and 114 are similar in composition to their samples 209, 184, and 286 while 313D is similar to 201 and 198. Both 43 and 6264 are slightly nepheline-normative.

Experiments were carried out in internally-heated pressure vessels at 2 and 4 kilobars. Experimental methods are described in Appendix C and results presented in Table C1 and Figures 5.3.1 to 5.3.4. The analysis of sample 114 by Arculus (1973) suggested that this sample was substantially different in composition from sample 43. This is not the case, and the runs using 114 were left incomplete and are not figured here.

Run products were studied optically using transmitted and sometimes also reflected light. X-ray diffraction (CuKα radiation) and microprobe methods were also used. The presence of abundant quench clinopyroxene and/or amphibole in most charges often made optical identification of minerals and interpretation of diffraction traces difficult. Problems were also experienced identifying primary clinopyroxene in sample 43 in the presence of abundant olivine and quench pyroxene. Microprobe analysis provided the only solution to this problem since etching of polished mounts of charges in dilute hydrochloric acid rapidly attacked the hydrous glasses. Plagioclase proved difficult to identify optically in many charges because the small grains were surrounded by abundant quench crystals. X-ray diffraction was more reliable for plagioclase identification although the plagioclase detection limit of this method is higher

Table 5.3.1

Chemical compositions of starting materials

sample	43	114	311	313D	6264
SiO_2	46.51	47.85	51.61	54.22	48.05
Al_2O_3	13.46	15.08	16.86	16.42	16.04
Fe_2O_3*	10.25	10.05	8.03	8.15	10.77
MgO	13.83	12.63	8.48	5.28	6.61
CaO	11.66	9.86	10.39	8.98	13.44
Na_2O	2.24	1.75	2.79	3.97	2.43
K_2O	0.44	0.57	0.79	0.93	0.74
TiO_2	0.89	0.92	0.80	0.81	0.89
MnO	0.18	0.18	0.15	0.21	0.16
P_2O_5	0.12	0.23	0.10	0.28	0.24
Total	99.60	99.12	100.00	99.25	99.37

*All analyses on ignited samples with total iron as Fe_2O_3

CIPW norms (weight percent)

Q	-	-	-	1.23	-
or	2.63	3.43	4.70	5.57	4.44
ab	14.21	15.06	23.76	34.07	18.82
an	25.69	32.16	31.35	24.58	31.14
ne	2.70	-	-	-	1.11
di	25.66	12.95	16.00	15.37	28.61
hy	-	17.42	15.31	14.77	-
ol	24.34	13.98	4.96	-	10.67
mt	2.76	2.72	2.15	2.20	2.91
il	1.71	1.76	1.53	1.56	1.72
ap	0.29	0.53	0.24	0.65	0.58

norms calculated using $Fe_2O_3 / (FeO + Fe_2O_3) = 0.20$ (weight)

than that of optical work. Plagioclase is believed not to occur as a quench mineral.

5.3.1 Sample 43 (Figure 5.3.1)

Runs on sample 43 at 2 kilobars show a large (> 100°C) primary phase field of olivine and chrome spinel. As could be predicted from the starting composition, the liquidus temperature is high, in excess of 1300°C. Both clinopyroxene and plagioclase melt at temperatures close to 1150°C. Increasing water activity lowers the melting temperature of all phases. By inference from results on other samples, the plagioclase melting curve has been drawn with a steeper slope than that of clinopyroxene. A few runs at 4 kilobars show that olivine is still the primary silicate liquidus phase at this pressure.

5.3.2 Sample 311 (Figure 5.3.1)

This more evolved microphyric basalt has olivine as its primary liquidus phase, followed by plagioclase and clinopyroxene. A brown chrome spinel coexists with all silicate assemblages as in sample 43. The plagioclase melting curve shows considerably steeper slope than those of olivine and clinopyroxene, reflecting the depolymerisation of the melt structure by solution of water. Runs on this composition at high water contents were carried out using an all-liquid starting material. These crystallisation experiments failed to produce the same phase relations as melting experiments with respect to plagioclase stability. Although the data presented here represent only a partial reversal of the plagioclase stability curve, the 1075°C melting run produced only a very small amount of feldspar and the preferred phase relations in Figure 5.3.1 are believed to be correct. A few melting runs with 5 percent water were carried out using a haematite-magnetite (HM) buffer (runs 591, 601, 611). The spinel produced in these runs was opaque, in contrast to the translucent brown spinel in the NNO-

Figure 5.3.1

Phase relations of M-series basalts

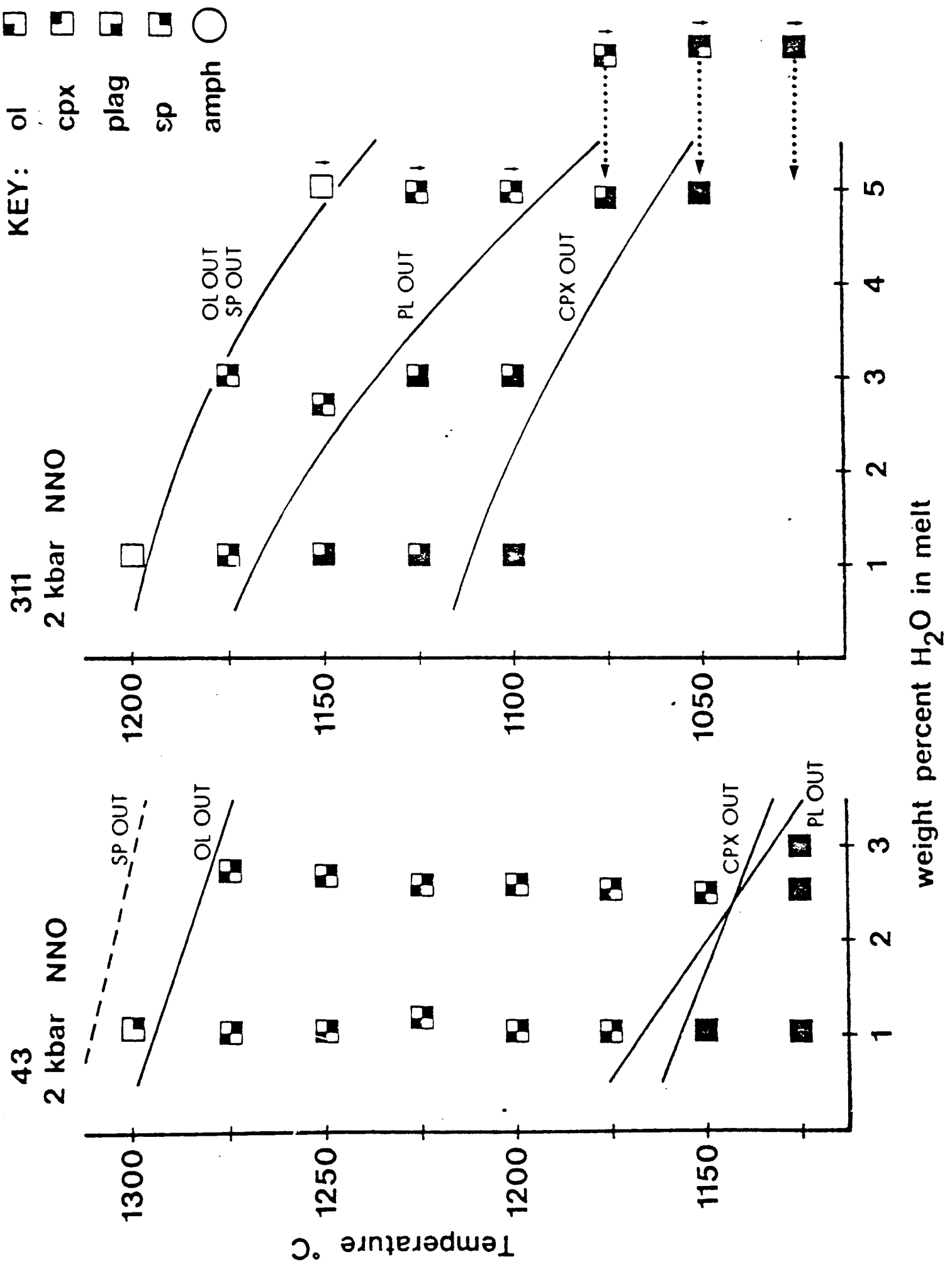

Downward-pointing arrows indicate crystallisation experiments

buffered runs, presumably reflecting an increased ferric iron content at higher oxygen fugacities.

5.3.3 Sample 6264 (Figure 5.3.2)

Runs at 2 and 4 kilobars on this C-series basalt were unbuffered. Buffer capsules included with each experiment showed that the hydrogen fugacity in water-undersaturated charges always lay between those in the NNO and HM buffer capsules, the rates of buffer exhaustion suggesting effective f_{O_2} values closer to NNO than HM. This procedure allowed much longer run times to be used.

At 2 kilobars clinopyroxene is normally the primary liquidus phase although plagioclase is equally stable in melts of low water content. Olivine melts at lower temperatures, the slope of its melting curve being similar to that of clinopyroxene but less than that of plagioclase. An opaque, magnetite-rich spinel is present at low temperatures, the flatter spinel melting curve reflecting the increased oxygen fugacity in runs of higher water contents. At 4 kilobars the thermal stability of plagioclase is increased relative to that of olivine, as predicted by studies in synthetic systems (O'Hara, 1965, 1968). Spinel stability is also decreased at 4 kilobars. Plagioclase again shows a steeper melting curve than the ferromagnesian silicates at both 2 and 4 kilobars.

5.3.4 Sample 313D (Figures 5.3.3 and 5.3.4)

The majority of data at 2 kilobars on this composition are from crystallisation experiments, which were carried out in an attempt to grow crystals large enough for microprobe analysis. Melting experiments have generally not produced the same stability field for plagioclase as crystallisation experiments. There is also a discrepancy between the data sets in spinel stabilities. These differences are discussed in section 5.6. Preferred phase relations are shown in Figure 5.3.4. Clinopyroxene is the liquidus phase, closely followed by olivine and,

Figure 5.3.2 Phase relations of C-series basalt 6264

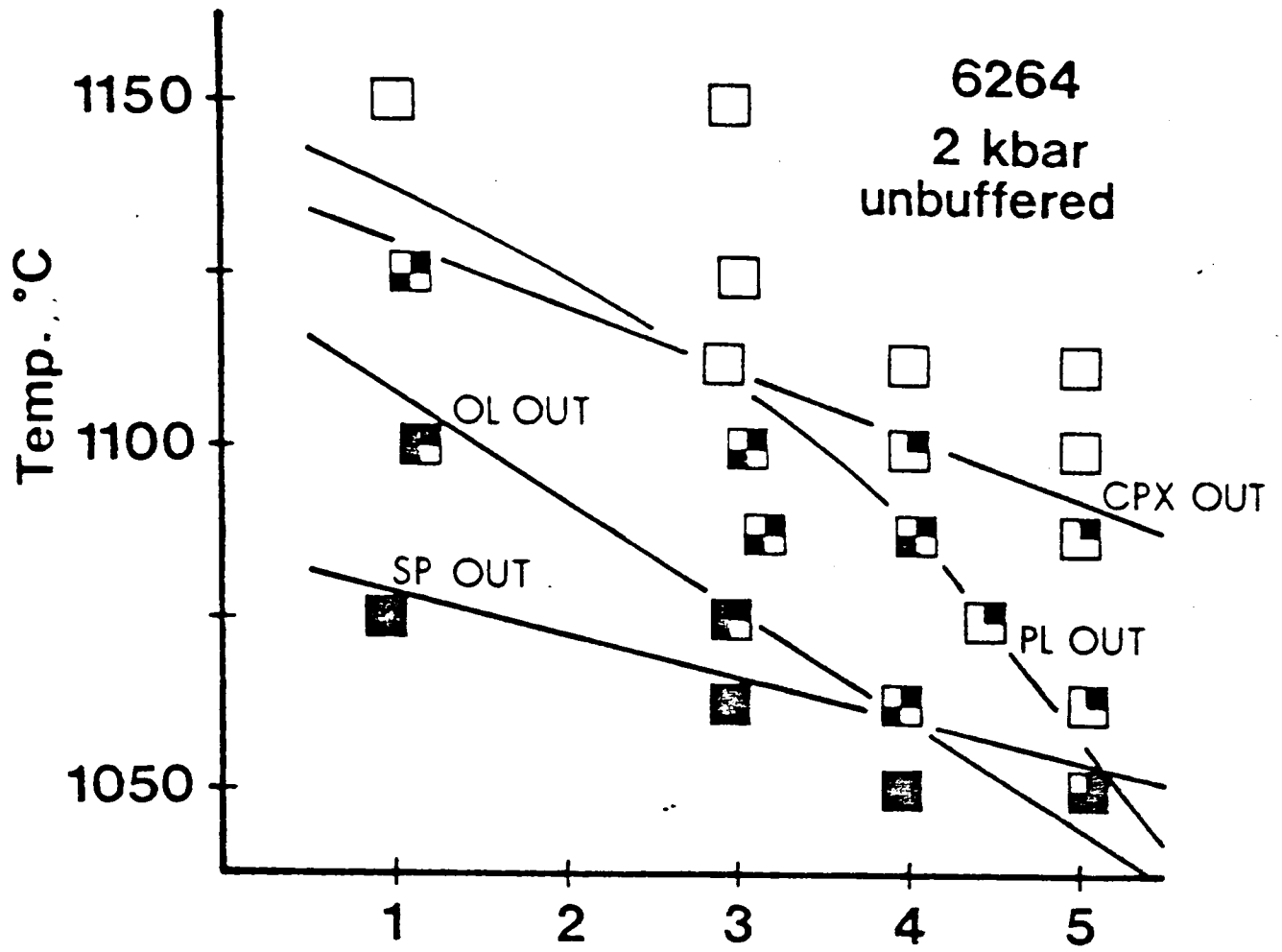

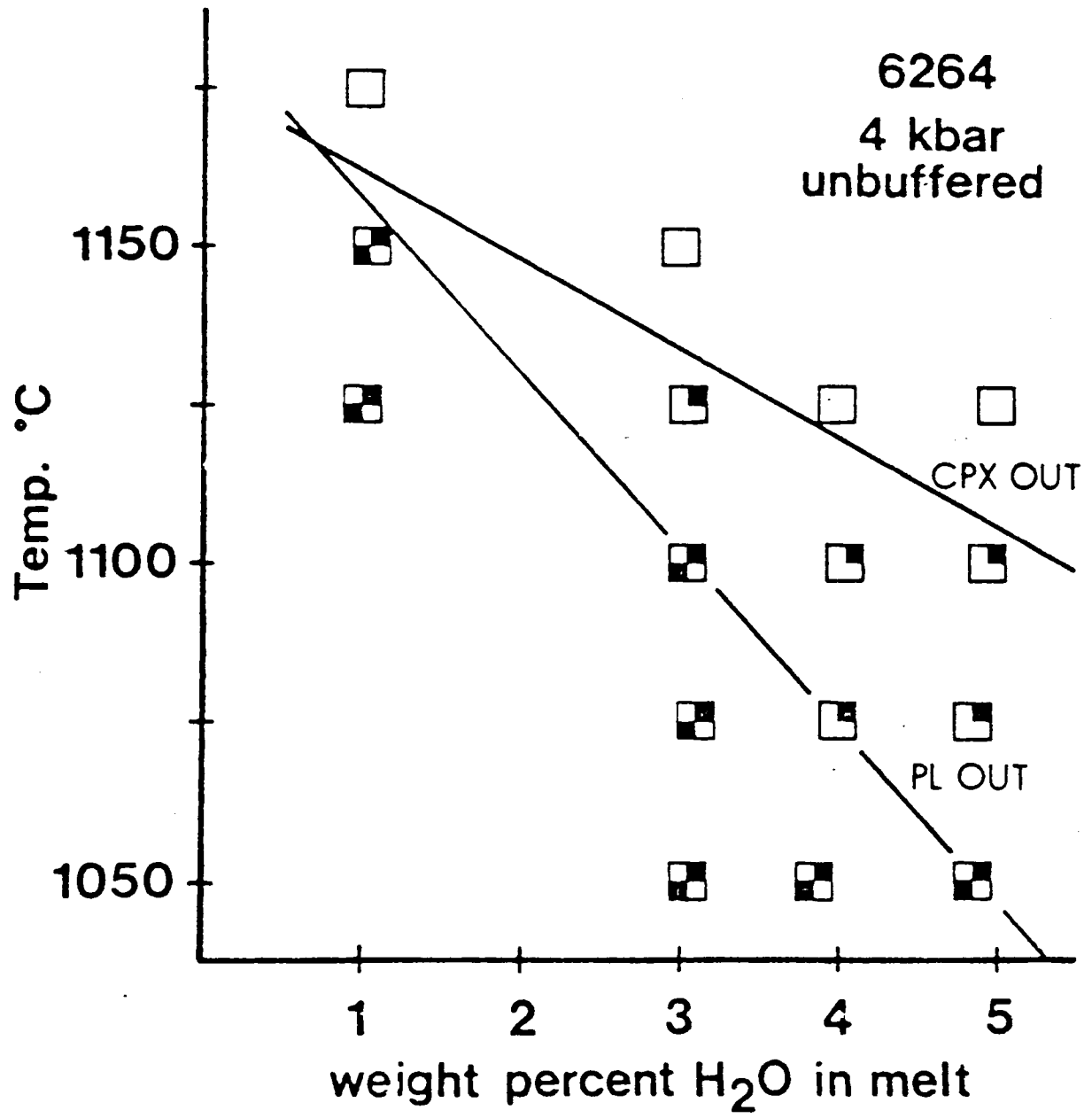

Figure 5.3.3

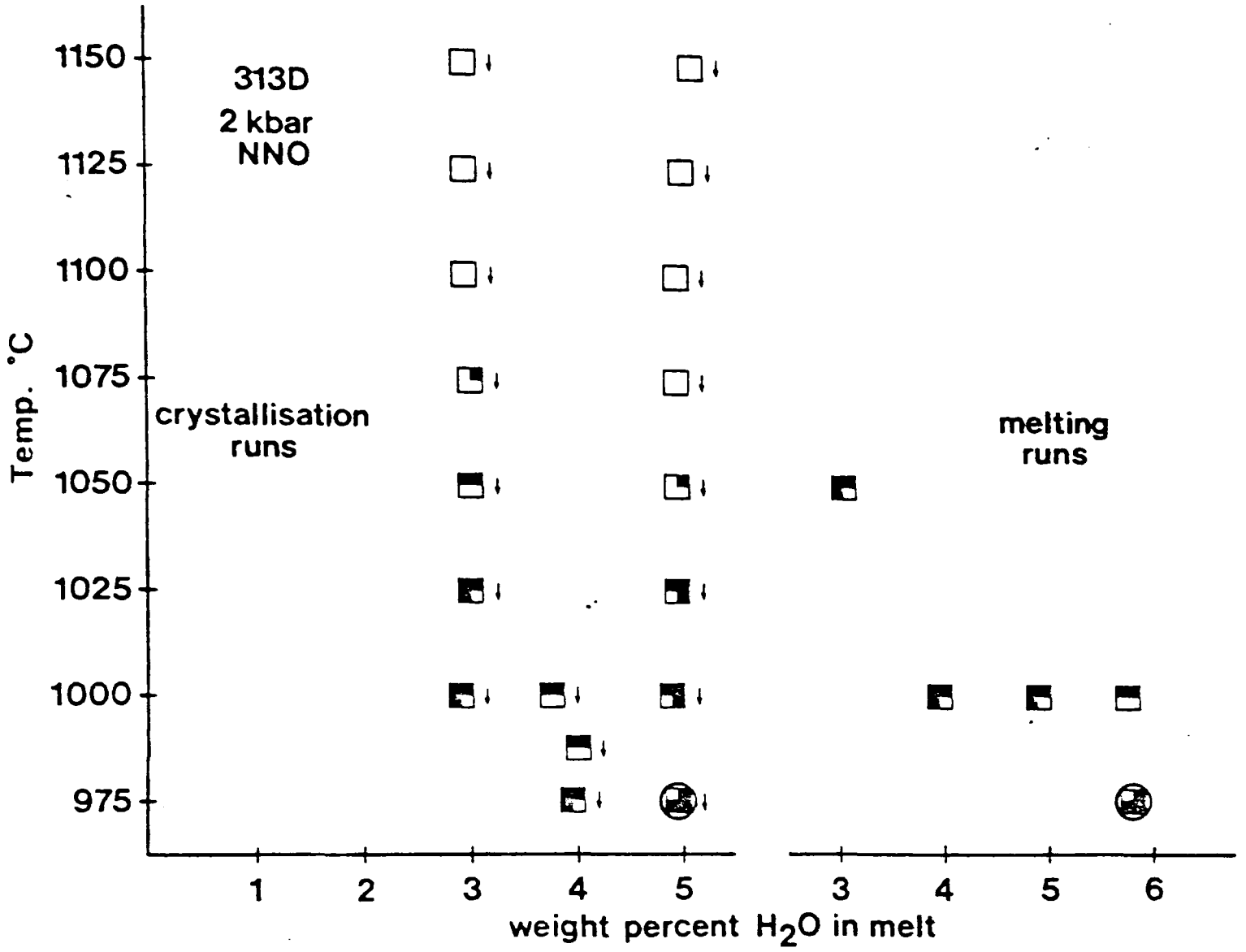

Comparison of the phase relations of basaltic andesite 313D produced in melting and crystallisation experiments.

Figure 5.3.4 Phase relations of basaltic andesite 313D at 2kbar (preferred data) and at 4kbar.
Arrows indicate crystallisation experiments.

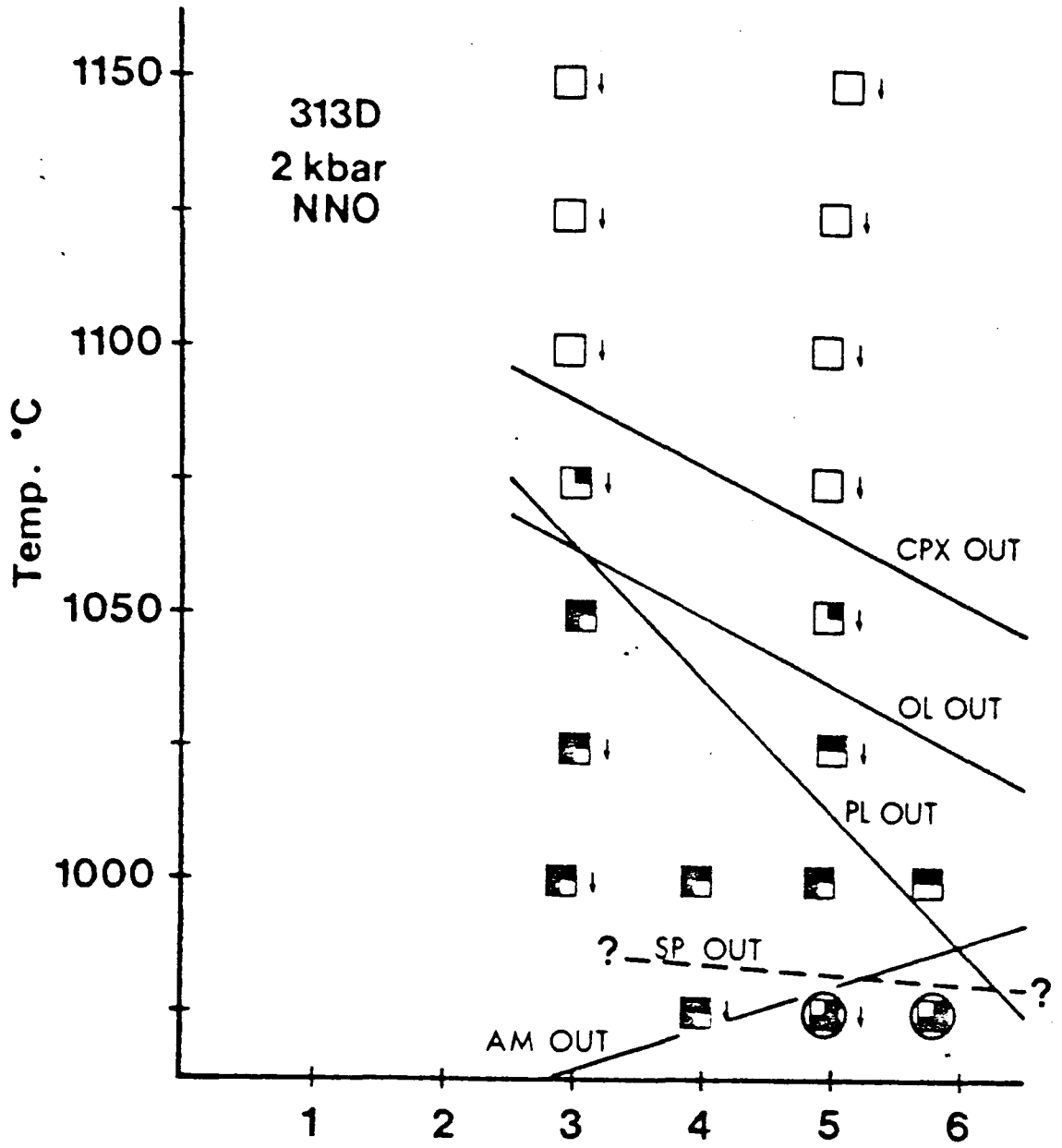

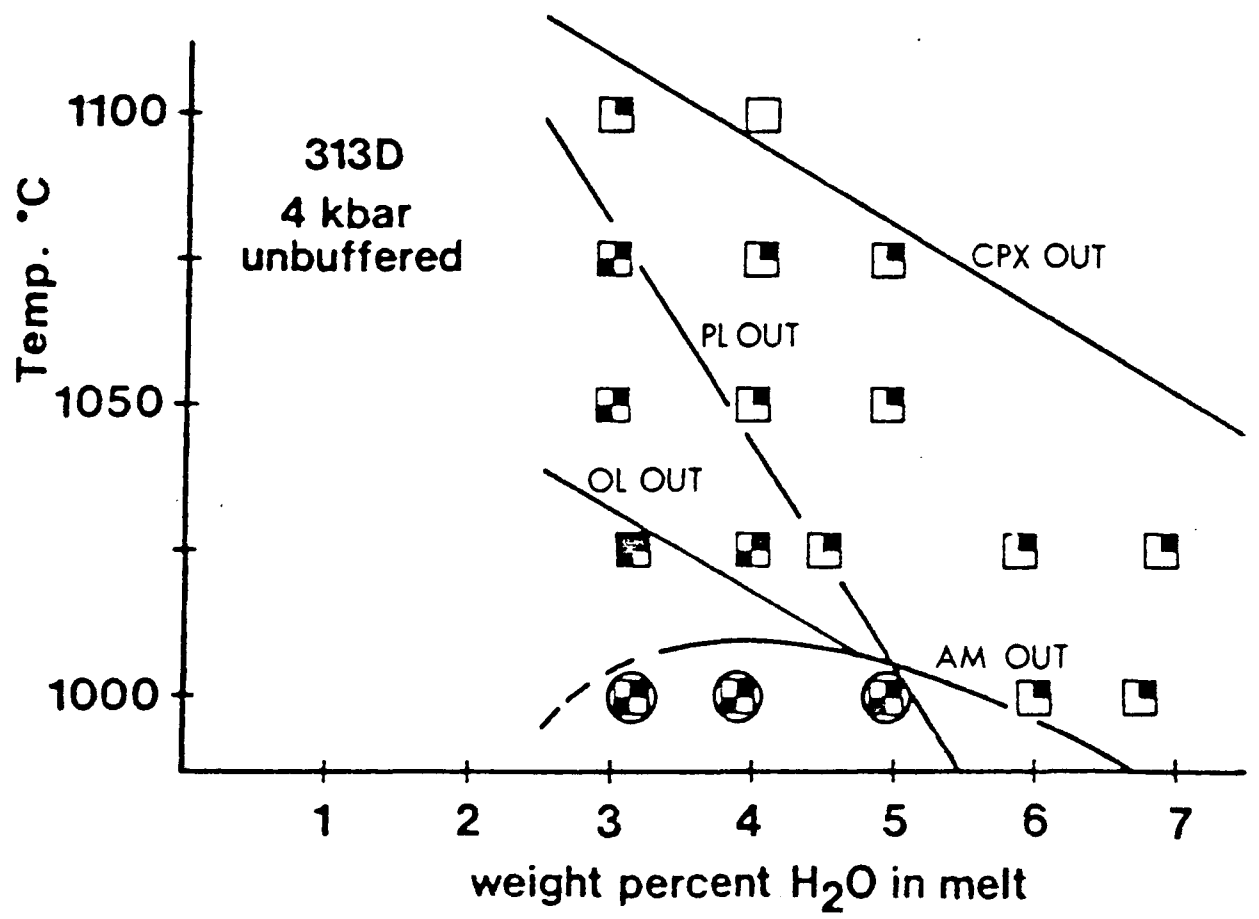

at low water activities, plagioclase. As high water activities, plagioclase stability decreases and amphibole becomes stable, although only at least 50°C below the liquidus. A reaction relationship exists between olivine and liquid once amphibole becomes stable. As in sample 6264, increased water activity stabilises spinel at low temperatures. Runs with 3 and 5 percent water at 1100°C with a HM buffer contained primary spinel, confirming a substantial increase in the stability of spinel at higher oxygen fugacities.

Owing to the difficulty experienced in reversing crystallisation experiments, all the 4 kilobar results on this composition are from melting runs, which were unbuffered to allow longer run times and were therefore at slightly higher oxygen fugacities than the 2 kilobar experiments. As observed in sample 6264, olivine stability decreased relative to clinopyroxene at the higher pressure, and plagioclase stability decreased sharply at higher water activities. Amphibole was stable at lower water contents and higher temperatures than in 2 kilobar runs, and olivine again showed a reaction relationship with liquid once amphibole crystallised. Crystallisation of amphibole before plagioclase appears to be possible at melt water contents greater than 5 weight percent (close to saturation) although the thermal stability of amphibole shows evidence of a maximum in the 3-5 weight percent region, in contrast to the results at 2 kilobars.

5.4 Interpretation of experimental results

5.4.1 Comparison of phenocryst assemblages and experimental phase relations

The picritic basalt 43 shows a large primary olivine field at low pressures, although major element chemical evidence suggests that clinopyroxene is also important in controlling the chemical variation in the

M-series basalts. This strongly suggests that the magnesian basalts are the product of a high pressure fractionation process. The probable absence of genuine clinopyroxene primocrysts from some M-series basalts, described in Chapter 2, therefore shows that these magmas often contain only low pressure phenocrysts despite the evidence that high pressure phase relations control much of the M-series chemical variation. Basalt 311 shows a less extensive olivine primary phase field but is clearly not in equilibrium with clinopyroxene at the pressures investigated.

The phase relations of C-series basalt 6264, in contrast, indicate that this lava was in equilibrium with its phenocryst phases at low pressures and therefore that the chemical variation within the C-series is a low-pressure feature. This conclusion is supported by the abundant crystallisation of clinopyroxene over a small temperature interval shown in the experimental charges. While the interval between the clinopyroxene and olivine melting curves is not large at 2 kilobars, the olivine melting curve lies below 1050°C at 4 kilobars, suggesting that 6264 would not have been in equilibrium with its phenocrysts at pressures much in excess of 2 kilobars.

The basaltic andesite 313D, at the pressures investigated, shows all of the major silicate phases within 100°C of the liquidus at high water contents, with olivine and clinopyroxene again close to each other in the crystallisation sequence. No thin section of this lava was available, but the petrography of chemically similar rocks in the suite indicates that the phenocryst assemblages of the basaltic andesites are of low pressure origin.

5.4.2 Comparison with results of Cawthorn et al. (1973a)

Sample 43 has a much larger primary phase field of olivine than reported from similar compositions at 5 kilobars by Cawthorn et al.

(1973a), even allowing for the difference in pressure between the data sets. The experiments of Kushiro (1972) on olivine-pyroxene equilibrium suggest that the higher water activity of Cawthorn et al.'s runs should if anything, have stabilised olivine relative to clinopyroxene. In addition, Arculus (1975) found that olivine was the liquidus phase in Grenada basalt 531 at pressures in excess of 15 kilobars although, according to the analyses of Arculus (1973), this composition contains less normative olivine than the samples used by Cawthorn et al. (1973a). A likely explanation for the differences in phase relations is the use of platinum containers in the study of Cawthorn et al. (1973a). Loss of iron to the platinum would increase the normative diopside content of the melt and therefore promote clinopyroxene stability.

No runs at high water activities were carried out on sample 43, so that amphibole stabilities cannot be compared with the results of Cawthorn et al. (1973a), but it is clear from the observed phase relations in both sets of experiments that amphibole is not a liquidus phase in silica-undersaturated M-series basalts and that the amphibole fractionation hypothesis of Cawthorn et al. (1973a) has little support from experimental studies.

The results on basaltic andesite 313D are comparable to those obtained on samples 201 and 198 by Cawthorn et al. (1973a), showing the increasing stabilisation of amphibole relative to other ferromagnesian silicates in the more evolved magmas and the greater thermal stability of amphibole relative to plagioclase at high water activities and total pressures.

5.5 Phase chemistry

Fragments of selected experimental charges were mounted in Araldite, polished, and analysed by electron microprobe using energy-dispersive methods described in Appendix A. Location of phases in fine-grained charges presented difficulties, especially with spinels and plagioclases, and many analyses were rejected. The abundance of quench crystals normally made analysis of glass impossible but several all-glass charges were analysed. Glasses were analysed using a defocussed beam to minimise volatilisation during analysis.

5.5.1 Olivine (Table A6.1)

Olivine compositions within individual charges normally show a range of only a few mole percent Fo, especially at near-liquidus temperatures. A few charges showed greater variation, up to 8 mole percent, which is attributed to insufficient run duration to re-equilibrate the starting compositions and/or iron exchange with the container. Although the available data indicate a decrease in forsterite content with decrease in run temperature, variable iron exchange with the container results in a scatter of compositions.

While the near-liquidus olivines in sample 43, 114, and 311 are, in general, more magnesian than those in the cumulate blocks, those produced in experiments on basaltic andesite 313D are more iron-rich than the cumulate olivines, suggesting that a basaltic andesite magma cannot be in equilibrium with olivine-bearing cumulate assemblages.

5.5.2 Clinopyroxene (Table A6.2)

The abundance of quench pyroxene makes identification of primary pyroxenes in many charges difficult. The primary grains were often located by searching for spots giving low aluminium count rates, so that the analyses may be biased towards low alumina contents. Compositions of primary clinopyroxenes showed considerable variation within single charges

especially in alumina content, which is believed to reflect difficulty in attaining equilibrium due to slow diffusion of aluminium in the clinopyroxene structure.

A large number of clinopyroxenes were analysed from runs at both 2 and 4 kilobars on samples 6264 and 313D. Alumina concentrations were averaged for each run and plotted in Figure 5.5.1. The data on sample 6264 show a large scatter with no evident correlation of alumina content with total pressure or melt water content, but a possible weak positive correlation with temperature. The scatter, attributed above to incomplete equilibration within the duration of the experiments, is slightly reduced at higher temperatures where diffusion is fastest.

In contrast to the results from sample 6264, the clinopyroxenes in charges from runs on 313D show a distinct separation of alumina contents between the 2 and 4 kilobar runs (Figure 5.5.1). Although increased pressure might be expected to increase the alumina contents of clinopyroxenes (e.g. Thompson, 1974), the reverse is the case. However, the 4 kilobar charges were produced in melting experiments while the 2 kilobar charges crystallised from a superheated liquid starting material. Rapid clinopyroxene growth as these experiments were cooled to run temperature would, by analogy with the zoned clinopyroxenes in the M-series basalts discussed in Chapter 2, trap excess aluminium in the pyroxene structure because of its slow diffusion away from the growing crystal-melt interface. The alumina contents of the 2 kilobar clinopyroxenes are therefore believed to be in excess of the equilibrium concentrations, providing evidence that crystallisation experiments do not result in a close approach to equilibrium.

5.5.3 Plagioclase (Table A6.3)

Feldspars produced in experiments on samples 43, 114 and 311 were usually too small for analysis and their compositions, where determined,

Figure 5.5.1 Alumina contents of clinopyroxenes in experimental charges. Filled symbols: 2kbar runs, open symbols: 4kbar runs.

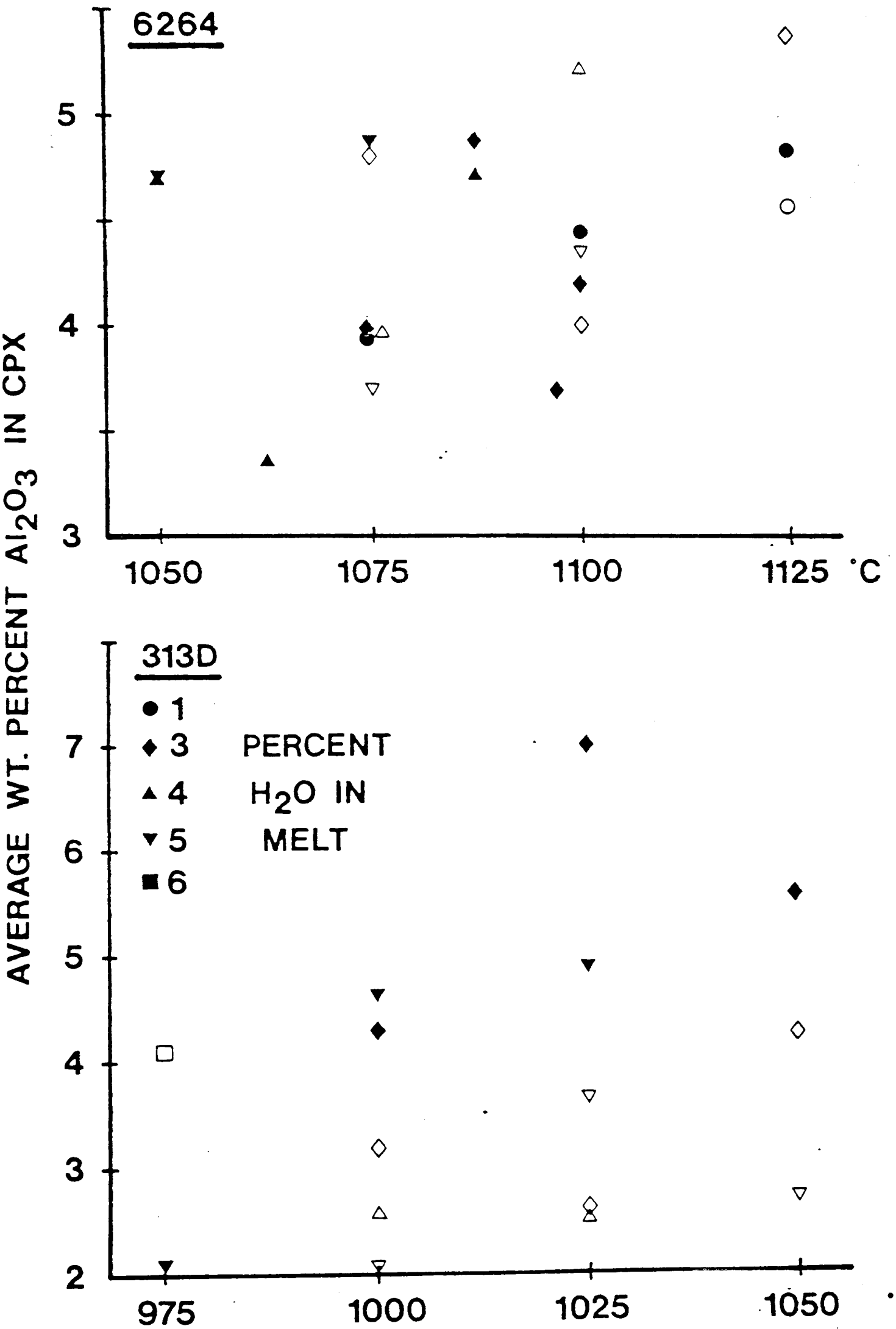

are variable, especially at low temperatures. The total range of compositions is An_{69} to An_{84} (analyses 1 to 12). Feldspars in charges produced from basaltic andesite 313D at 2 kilobars are considerably more sodic, lying in the An_{55} to An_{65} range (analyses 13 to 20) and therefore clearly different from the primary cumulate plagioclase compositions (Table A4.3). Increase of pressure to 4 kilobars did not significantly change these compositions. C-series basalt 6264 produced plagioclases in the range An_{74} to An_{89}, the more calcic examples being comparable to those found in the cumulate blocks.

Insufficient data were collected to study the variation in plagioclase composition with pressure, temperature, and water activity. In only one experiment (run 83) were sufficient analyses collected to demonstrate the effect on feldspar composition of variable water activity. In this experiment increased water activity increased the average anorthite content from $An_{50.6}$ to $An_{62.1}$, as would be expected from the results of Yoder et al. (1957) and Johannes (1978). However it is clear from the limited data collected that melt composition is at least as important in controlling the composition of crystallising plagioclase as water activity.

5.5.4 Amphibole (Table 6.4)

When recalculated to the same ferrous-ferric iron ratio as the cumulate amphiboles (100 Fe_2O/Fe_2O_3 + FeO = 38.0), the amphiboles produced in sample 313D are magnesiohastingsites at 2 kilobars and transitional between magnesiohastingsites and pargasites at 4 kilobars. Although slightly lower in Na and in Mg-value they are comparable in composition with the cumulate magnesiohastingsites and pargasites, and considerably closer to them in composition than the amphiboles produced by Cawthorn et al. (1973a). Their amphiboles were much lower in Fe and Mg and richer in Ca and Si than the natural compositions. The analyses

from this study are very limited but suggest that amphibole chemistry is not strongly pressure dependent in the 2 to 4 kilobar range. The higher titanium contents of the 4 kilobar amphiboles may result from the absence of a coexisting spinel phase at the higher pressure.

5.5.5 Spinel (Table A6.5)

The spinel phase is often too small and insufficiently abundant for analysis, and there are insufficient data to determine the extent of equilibration of the spinels in any individual experiment. The analysed spinels are similar in composition to those in the starting materials and no clear trends in their compositions are apparent. Hill and Roeder (1974) found that run times of two to four days at 1100°C were sufficient to attain equilibrium and, in view of the much shorter run times used in this study, interpretation of the analyses collected as equilibrium compositions cannot be justified.

5.5.6 Glass (Table A6.6)

Abundant quench crystals prevented analysis of glass in most charges. Where glasses were analysed, compositions usually showed little variation within each run while discrepancies between analysis totals and 100 percent were often considerably greater than the predicted water content of the original liquids. Analyses of all-glass charges showed no evidence of extensive leaching of alkalis from the melt by the vapour phase in the experiments.

The glass coexisting with amphibole at 2 kilobars (run 54) is of andesitic composition. Analyses of this glass were variable in MgO, FeO, and Al_2O_3, probably as a result of quench modification of the original melt composition (Cawthorn et al., 1973b).

5.6 Equilibrium considerations

The considerable differences between results of crystallisation and melting experiments and the variation in phase compositions indicate that at least some runs have not achieved complete equilibrium. The difficulty experienced in reversing the plagioclase melting curves in samples 311 and 313D could be a consequence of either the presence of relict plagioclase grains in melting runs, or failure to nucleate plagioclase in crystallisation runs. Gibb (1974) found that plagioclase melted rapidly above its liquidus temperature and several previous workers have found difficulty in nucleating plagioclase in molten charges in both atmospheric pressure experiments (Brown and Schairer, 1971; Gibb, 1974; Walker et al., 1976) and in water-saturated experiments at higher pressures (Lofgren, 1974).

Donaldson (1979) has carried out an extensive study of nucleation delay of olivine in cooling experiments, finding that the delay increases with decreasing degree of supercooling, cooling rate, superheat, olivine content of the melt, and increasing melt viscosity. Gibb's (1974) less thorough study of nucleation delay of plagioclase, and the cooling experiments of Walker et al. (1976) both indicate that olivine nucleates more readily than plagioclase. This is confirmed in this study, where no evidence was found for differing stabilities of olivine and clinopyroxene in the two types of experiment. A crystallisation experiment on sample 43 at 1150°C (run 45) failed to nucleate plagioclase but produced clinopyroxene. No study of possible nucleation delay of amphibole was carried out but its ready nucleation as a quench phase suggests that it is not seriously affected.

In view of the evidence for nucleation delay of plagioclase, the preferred phase relations of sample 313D at 2 kilobars are based largely on the results of melting runs. However there is also a discrepancy in

the spinel stabilities between melting and crystallisation runs, a melting run at 1000°C with approximately 6 percent water failing to produce spinel. Unfortunately there are no data to determine whether this result is due to increased iron loss to the container or nucleation effects in the crystallisation runs due to depolymerisation of the melt during superheat (Donaldson, 1979). Evidence that melt structure is affected by superheat comes from the greatly decreased abundance of quench crystals in crystallisation runs.

Crystallisation experiments produced skeletal olivines similar to those described by Donaldson (1976) and glomerocrystic clinopyroxenes which are often curved and show uneven extinction. It is clear from the analyses in Figure 5.5.1 that, even if a phase does manage to nucleate during cooling, any supercooling may lead to growth of crystals with disequilibrium compositions. This removes the principal advantage of crystallisation experiments of restricting nucleation and promoting growth of crystals to a size amenable to microprobe analysis.

5.7 Application of results to the Grenada rock suite

The most important consideration in applying the experimental data of this study and of Cawthorn et al. (1973a) is the crystallisation process responsible for generation of the cumulate blocks. As discussed in Chapter 3, it is possible that the Grenada cumulates originated by in situ equilibrium crystallisation of part of their parent magma, and therefore do not represent products of perfect fractional crystallisation. Equally, it is clear that the bulk compositions of the blocks would be very different from those of the extrusive rocks so that they are unlikely to represent products of perfect equilibrium crystallisation either. These two extreme processes require very different interpretations of the experimental phase relations.

In the fractional crystallisation case the parental magma to the cumulates should be capable of coprecipitating the cumulate phases within a small temperature interval close to the liquidus, but in equilibrium crystallisation all that is required is that the cumulate assemblage should coexist with liquid at some temperature which may be substantially below the melting temperature. Constraints imposed on the chemistry of the equilibrium liquid coexisting with the cumulates apply to the bulk magma in the former case, but only to the residual liquid after partial crystallisation in the latter.

There are considerable difficulties in producing the cumulate assemblages by fractional crystallisation. The magnesian M-series basalts 43, 114, and 311 do not crystallise amphibole close to their liquidi and have large primary olivine phase fields. The C-series basalt 6264, although capable of crystallising olivines of similar composition to those in the cumulate blocks cannot crystallise plagioclase after amphibole even when nearly water-saturated. At higher pressures olivine stability in this composition is decreased, making it difficult to produce assemblages containing substantial olivine by fractional crystallisation. The basaltic andesite 313D can crystallise amphibole before plagioclase at both 2 and 4 kilobars, but its olivine is in reaction relationship with liquid once amphibole crystallises and therefore could not coprecipitate with amphibole during fractional crystallisation. Its olivine is also more iron-rich than the olivines found in the cumulate blocks.

The absence of amphibole as a primary liquidus phase in any of the samples studied implies that substantial equilibrium crystallisation of the parental liquids must have taken place to produce the cumulate assemblages. If this is the case, M-series magmas whose primary liquidus olivines are more magnesian than the cumulate olivines could

have re-equilibrated during cooling to the amphibole crystallisation temperature, producing more iron-rich olivine compositions. Partial resorption of olivine, and perhaps also of clinopyroxene, during amphibole crystallisation would allow formation of crystal assemblages rich in both olivine and amphibole. Reaction of clinopyroxene with liquid during amphibole crystallisation was predicted by Cawthorn (1976) and is supported by the textures of some of the cumulates. The residual liquid in equilibrium with the olivine-bearing cumulates would be of basaltic andesite composition. These magmas fit the constraints imposed by olivine compositions in the cumulates (Chapter 3), and often carry amphibole phenocrysts. They are also the most primitive lavas found in contact with the cumulate blocks and are similar in composition to the glasses in equilibrium with olivine, clinopyroxene, and amphibole analysed by Cawthorn et al. (1973a).

It seems, from the above considerations, that a model for partial equilibrium crystallisation of the cumulate assemblages can more easily explain the petrographical, chemical, and experimental data than a perfect fractional crystallisation model. As discussed earlier, the bulk chemistry of the cumulate blocks indicates at least a partial fractional crystallisation model. The exact amount of equilibrium crystallisation is difficult to estimate, but modes of experimental charges in this study suggest at least 20 percent crystallisation would be needed to produce the olivine- and amphibole-bearing type A cumulates. The orthopyroxene-bearing cumulates show textures transitional between adcumulate and orthocumulate, indicating that the degree of equilibrium crystallisation was probably variable.

The partial equilibrium crystallisation model does not exclude an origin of some of the olivine-free cumulates from C-series magmas but requires the generation of the olivine-bearing cumulate types from M-series magmas.

5.8 Constraints on conditions of cumulate crystallisation

The results of this study and of Cawthorn et al. (1973a) do not give a clear indication of the depth of crystallisation of the cumulate assemblages within the constraints imposed by the maximum pressure for coexistence of olivine and calcic plagioclase (Kushiro and Yoder, 1966) of approximately 8 kilobars, and the minimum pressure required for amphibole stability of approximately one kilobar. Below this minimum pressure water is insufficiently soluble to stabilise amphibole in basaltic melts. The experimental evidence indicates that the melt water content required to crystallise amphibole before plagioclase is at least 5 to 6 weight percent. The activity represented by this water content is pressure dependent but probably lies in the range 0.5 to 1.0 within the pressure bracket. Temperature of crystallisation is limited to the stability field of amphibole, and therefore to values less than about 1050°C. Experimental evidence from this study suggests that in order to crystallise an iron-rich spinel phase, oxygen fugacities greater than those of the NNO buffer are required

5.9 Conclusions

(a) The phase relations of magnesian M-series basalts observed in this study differ from those reported by Cawthorn et al. (1973a), probably because of iron loss in the latter study.

(b) The hypothesis of generation of Hy-normative M-series magmas by amphibole fractionation from Ne-normative parents proposed by Cawthorn et al. (1973a) is not supported by this study. The experimental results of Cawthorn et al. (1973a) also provide little support for their model. Rather, the phase relations observed in the Grenada basalts, and in simple systems, support an origin for this chemical variation by fractionation

of olivine, clinopyroxene, and spinel.

(c) Magnesian M-series basalts could only have evolved by fractionation at high pressures, although they often carry only low-pressure phenocrysts.

(d) C-series basalts carry low-pressure phenocrysts and the chemical variation within this series is controlled by low-pressure fractionation.

(e) The cumulate assemblages cannot be produced by perfect fractional crystallisation of any of the Grenada basalts or basaltic andesites. Considerable equilibrium crystallisation is required to produce the phase relations observed in the cumulate blocks.

(f) Olivine-bearing cumulates formed by the partial crystallisation, under equilibrium conditions, of M-series basalts, leaving residual liquids of basaltic andesite composition.

(g) Some olivine-free cumulates may have formed by the crystallisation of C-series basalts under similar conditions.

(h) Comparison of the experimentally-produced phase relations with those of the cumulates indicates crystallisation of the cumulate assemblages at pressures between 1 and 8 kilobars and temperatures below 1050^{o}C. Oxygen fugacities were probably in excess of those defined by the NNO buffer, and the water contents of melts in equilibrium with the cumulates were, in some cases, greater than 5 to 6 weight percent.

CHAPTER 6

GENESIS OF GRENADA MAGMAS

The purpose of this chapter is to discuss the evidence for the origin of the Grenada igneous rock suite presented in the preceding chapters, together with additional data, and to formulate preferred models for the origin of Grenada magmas. The significance of the Grenada models for island arc magma genesis is discussed in Chapter 7.

6.1 Source of the parental magmas

The variation in H-element ratios described in Chapter 2 requires the sources of both M-series and C-series to be chemically heterogeneous. The large scatter in the trace element abundances in both series, but especially in the M-series, makes their interpretation difficult. Fortunately, Sr and Nd isotopic data on Grenada rocks, including many of the samples used in this study, are available.

6.1.1 Isotopic data

Hawkesworth et al. (1979b) analysed a large number of Grenada rocks for Sr isotopes and selected specimens for Nd isotopes also. The data on samples included in this study are listed in Table 6.1.1. Hawkesworth et al. (1979b) demonstrated that the two basic series are essentially distinct in both Sr and Nd isotopic compositions. Sr isotopic compositions are plotted on the CaO vs. MgO variation diagram in Figure 6.1.1. The combined major element and Sr isotopic data demonstrate that the possible olivine fractionation trend in the most primitive members of the M-series correlates with a general increase in the $^{87}Sr/^{86}Sr$ ratio, but that the C-series rocks have generally lower $^{87}Sr/^{86}Sr$ ratios. This clearly demonstrates that the C-series isotopic compositions cannot have resulted from an extension of the trend shown in the primitive M-series rocks. The two series are clearly different in origin and should therefore be considered separately in discussion of the isotopic data.

Table 6.1.1

Isotopic data for samples analysed in this study

	$^{87}Sr/^{86}Sr$	$^{143}Nd/^{144}Nd$
M-series		
43	0.70509	
262	0.70481	
265*	0.70569	
266	0.70530	0.51283
286	0.70544	0.51287
306*	0.70464	
313D	0.70538	
314	0.70527	0.51284
319	0.70498	
375*	0.70522	
376	0.70475	
413*	0.70463	
449	0.70511	
457	0.70498	
468	0.70488	
500	0.70464	0.51296
507	0.70511	
509	0.70565	0.51264
6078*	0.70493	
C-series		
109	0.70522	
225B	0.70441	0.51308
230	0.70461	
239	0.70448	0.51304
333B	0.70501	
337	0.70455	
380	0.70467	0.51297
450	0.70447	0.51306
454	0.70435	0.51306
487A	0.70456	

Table 6.1.1 (contd.)

	$^{87}Sr/^{86}Sr$	$^{143}Nd/^{144}Nd$
Evolved lavas		
214	0.70492	
274	0.70517	
310A	0.70579	0.51282
313L	0.70530	
381	0.70451	

All data from Hawkesworth et al. (1979) except for asterisked samples which were analysed at Leeds by M.F. Thirlwall (pers. comm., 1979).
All $^{87}Sr/^{86}Sr$ ratios normalised to Eimer and Amend $SrCO_3$ standard of 0.70800.
Sample 313L was not analysed for trace elements in this study.

Figure 6.1.1

$^{87}Sr/^{86}Sr$ ratios of extrusive rocks from Grenada

Symbols as Figure 2.5.1

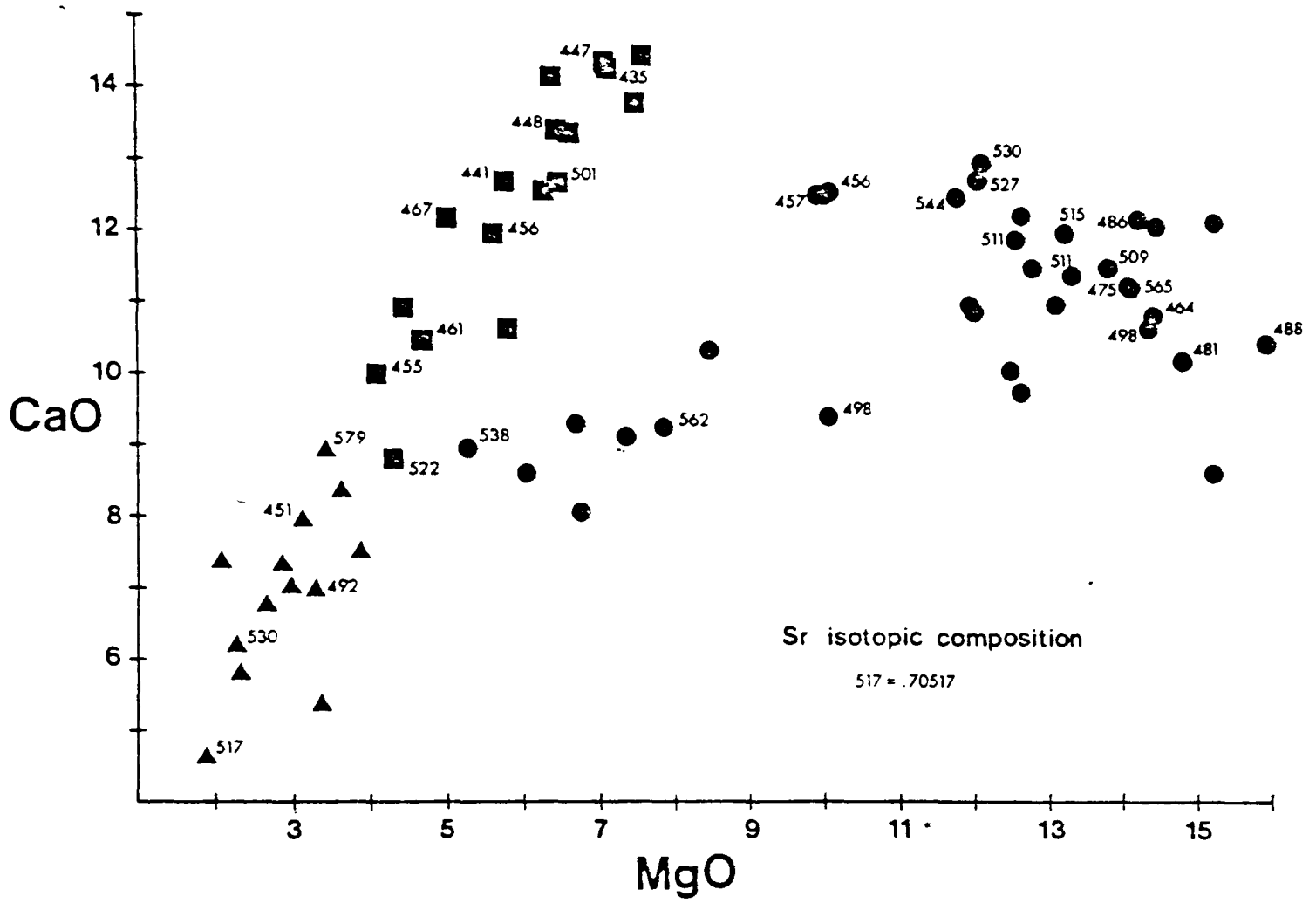

Isotopic data from Hawkesworth et al. (1979b) and this study (M.F. Thirlwall, pers. comm. 1979).

The samples 306 and 413, with approximately 10%MgO and 12.5% CaO, have isotopic and trace element characteristics transitional between those of M-series and C-series basalts.

For each series several potential sources must be considered. These are: the subducted oceanic lithosphere; possibly subducted sediments; the overlying upper mantle wedge; and the island arc crust.

6.1.2 M-series source

Thirteen of the M-series lavas with greater than 10% MgO were among those studied by Hawkesworth et al. (1979b). Their results are plotted in Figure 6.1.2.

Although a wide range of $^{143}Nd/^{144}Nd$ and $^{87}Sr/^{86}Sr$ ratios is present, there is a lack of correlation between these parameters and the Sm/Nd and Rb/Sr ratios respectively. The positive correlation of $^{143}Nd/^{144}Nd$ with Sm/Nd suggested by Hawkesworth et al. (1979b) is not supported by their data when the two basic series are considered separately. The Sr isotope data of these workers are plotted against several chemical parameters from this study in Figure 6.1.3. The extreme isotopic composition of sample 509 is evident in most of the plots, but, regardless of this sample, there is a general correlation of $^{87}Sr/^{86}Sr$ with Sr, Ce/Y, P_2O_5, TiO_2, and Fe_2O_3/MgO. The data of Hawkesworth et al. (1979b) also show a positive correlation of $^{87}Sr/^{86}Sr$ with Nd. As already stated, Figure 6.1.1 shows the correlation of $^{87}Sr/^{86}Sr$ with a possible olivine fractionation trend although sample 509 is again somewhat exceptional. It seems clear that LREE enrichment, $^{87}Sr/^{86}Sr$ ratio, major element composition, and certain trace element concentrations are in some way related within the M-series.

The high MgO, Ni, and Cr contents of the primitive M-series members are compatible with a source in the peridotitic upper mantle above the subduction zone, but not with an origin by melting of subducted oceanic crust, although a minor contribution from the subducted crust is possible. Given that the M-series magmas are essentially products of fusion of the mantle wedge above the subduction zone, then their trace element

Figure 6.1.2(a)

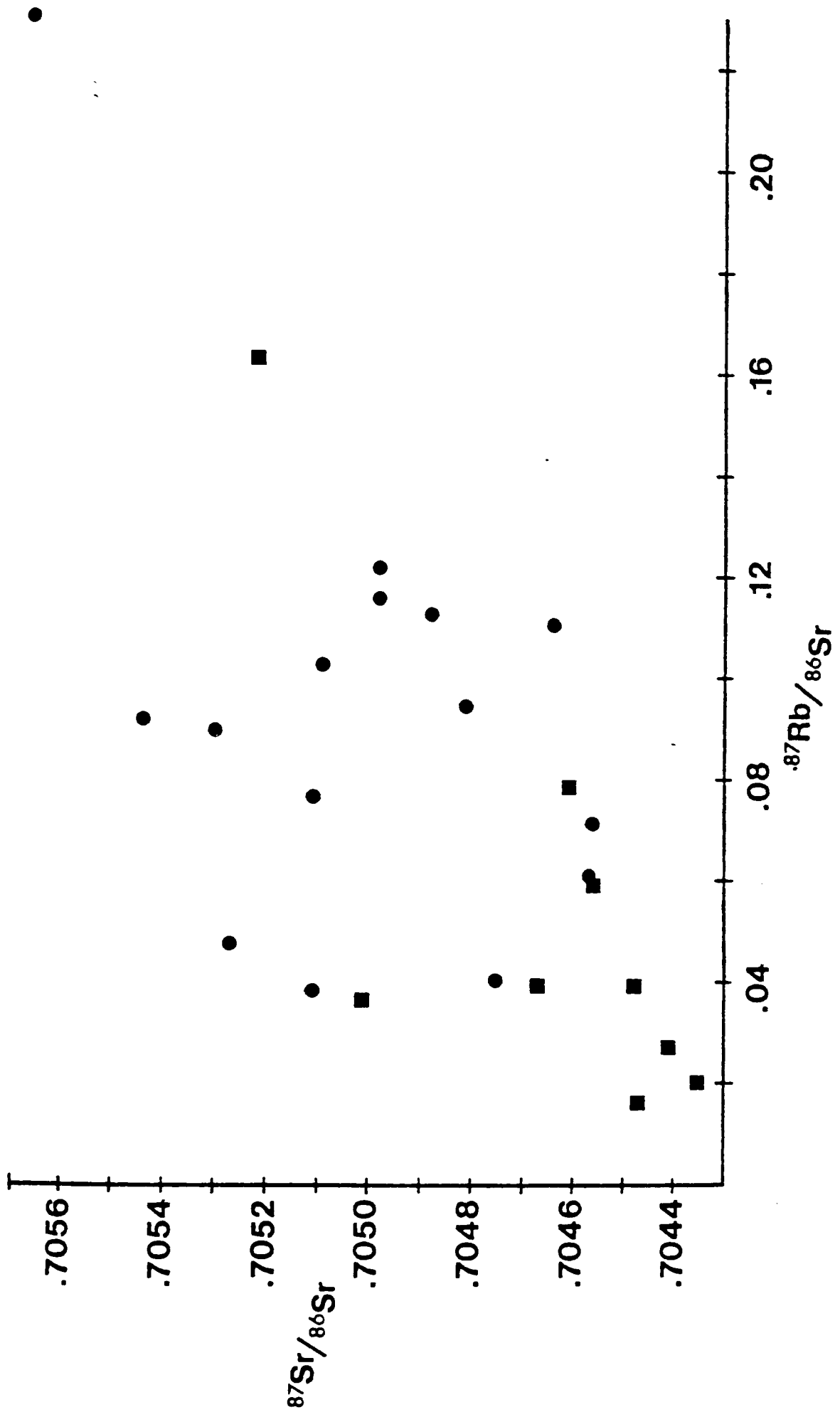

Isotopic data for M-series (>10%MgO) and C-series basalts. Rb and Sr concentrations from this study. Sr concentrations in C-series basalts may have been affected by plagioclase fractionation.

Figure 6.1.2(b)

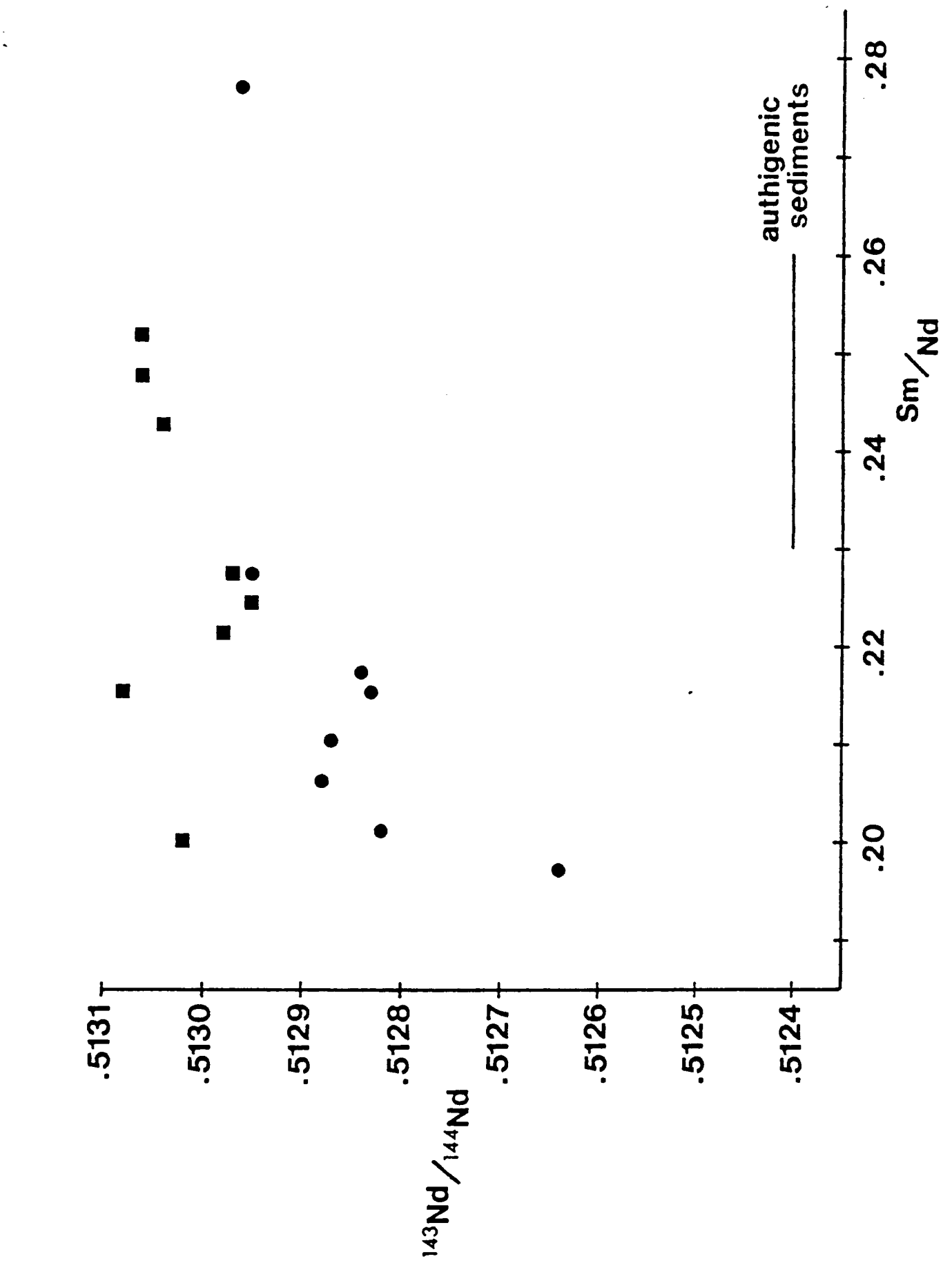

Isotopic data for M-series and C-series basalts (after Hawkesworth et al., 1979b), with possible range of authigenic sediments (see text).

Figure 6.1.3 Covariation of Sr isotopic composition with chemistry in primitive (>10%MgO) M-series basalts.

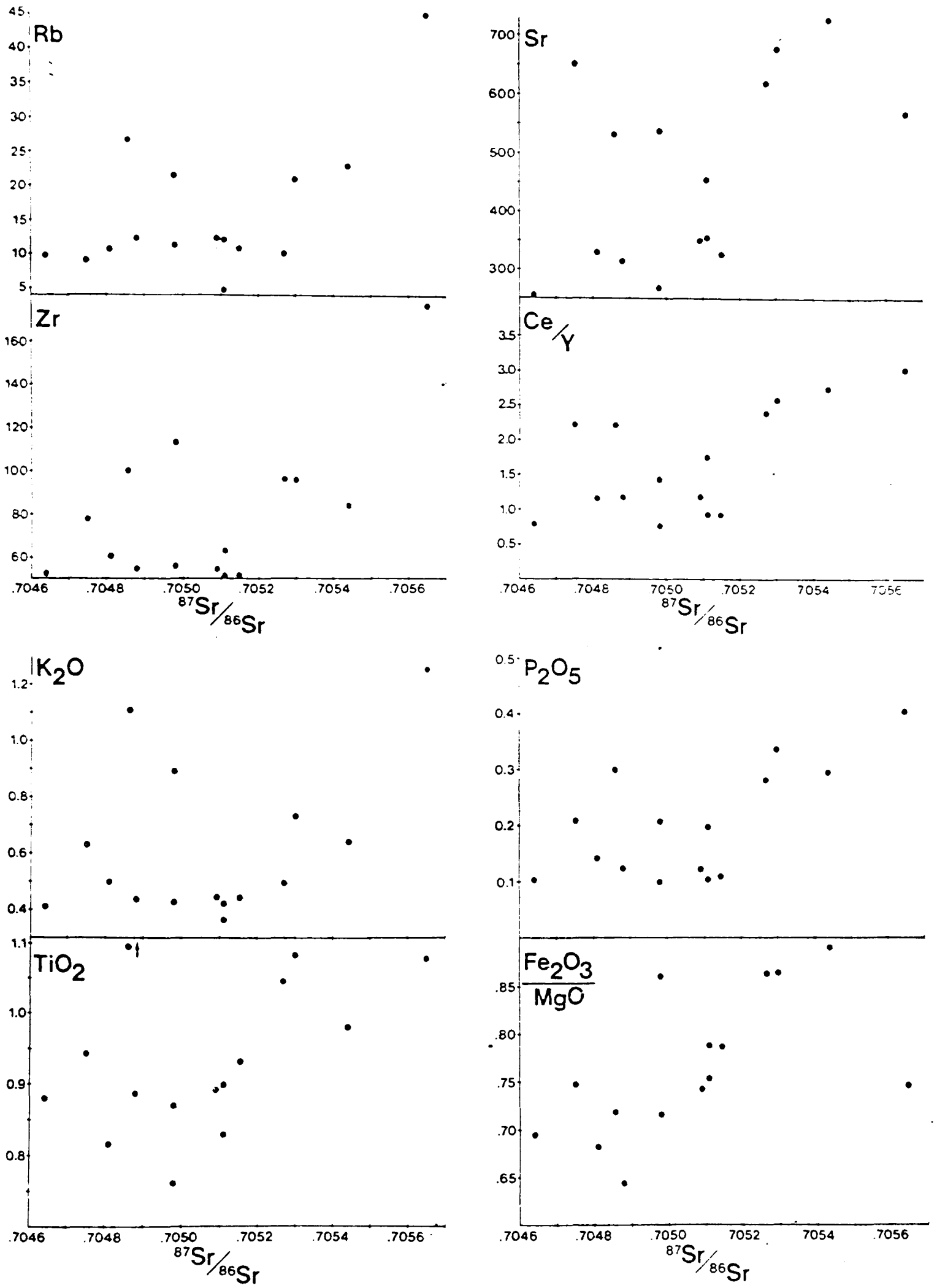

and isotopic variation may result from mixing of these melts with another source, or with its derived melt. Possible sources for this additional component are:

(1) the subducted oceanic crust, or

(2) subducted sediments, or

(3) the island arc crust.

Alternatively, the mantle wedge itself may be chemically heterogeneous, perhaps as the result of subduction processes.

The lack of petrographic evidence for high-level contamination and the near-liquid state of many of the M-series magmas on reaching the surface (Chapter 2) argue against involvement of the island arc crust in their genesis. In addition, mixing with large amounts of contaminant would be needed to explain the observed variation in LREE enrichment. This wide variation makes any direct mixing model very difficult to reconcile with the chemical evidence, since large effects on major elements and compatible trace elements would be predicted but are not observed. Therefore, in considering mixing models involving material derived from the subducted oceanic lithosphere, indirect mixing, in which this material modifies the composition of the source(s) of the M-series magmas, is implied. This type of mixing process avoids the mass balance problems of direct mixing.

Langmuir et al. (1978) have discussed how two-component mixing will affect trace element and isotope concentrations and ratios. This process should produce a hyperbolic array of points on a trace element ratio-ratio plot. Examples of two of these diagrams in Figure 6.1.4 show that this is not the case for the primitive M-series compositions, although the distribution of data points is not random. Simple mixing of two homogeneous sources has not therefore taken place.

Hawkesworth et al. (1977, 1979a, 1979b) have argued that, since

Figure 6.1.4 Incompatible element ratio-ratio plots for primitive M-series basalts.

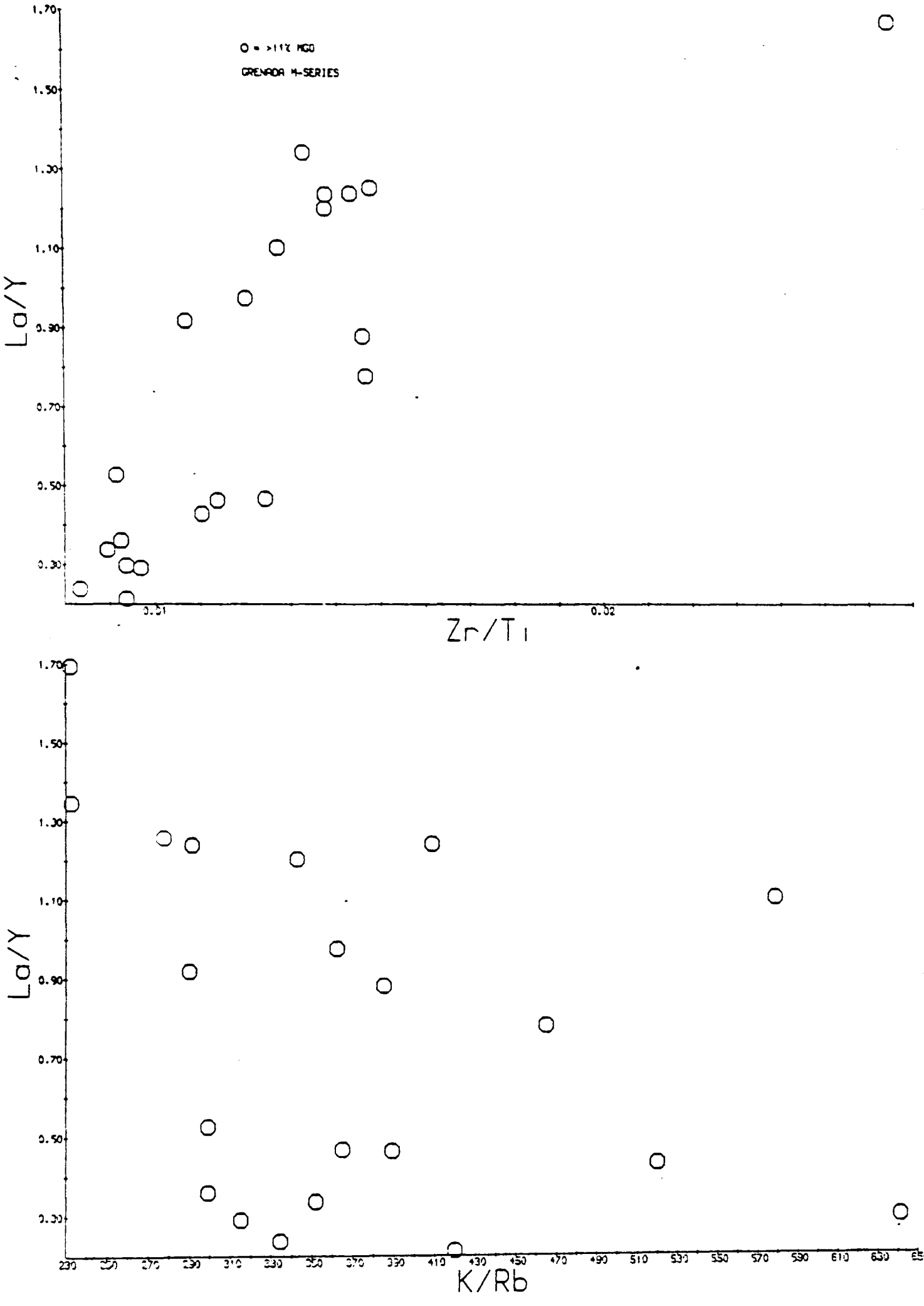

the Nd content of seawater is very low, the subducted oceanic crust cannot have had its $^{143}Nd/^{144}Nd$ ratio altered significantly by hydrothermal ocean-floor processes. Melts derived from the subducted crust would therefore have similar $^{143}Nd/^{144}Nd$ to mid-ocean ridge basalts (MORB) but probably higher $^{87}Sr/^{86}Sr$ due to hydrothermal alteration. The Grenada M-series rocks have variable $^{143}Nd/^{144}Nd$ and $^{87}Sr/^{86}Sr$ (Figure 6.1.5) but higher $^{87}Sr/^{86}Sr$ for a given $^{143}Nd/^{144}Nd$ than basalts from mid-ocean ridges and Atlantic islands (O'Nions et al. 1977). Although the Sr isotopic compositions in the M-series could reflect a contribution from subducted oceanic crust, the Nd and Sr isotopic covariation cannot be the result of such a contribution since increased contamination of the mantle source by melt derived from subducted oceanic crust would give increasing $^{87}Sr/^{86}Sr$ with increasing $^{143}Nd/^{144}Nd$, and this is not observed.

Hawkesworth et al. (1979b) pointed out that, although the trend of the Nd and Sr isotopic ratios suggests that mixing of authigenic sediments with MORB-type mantle could have taken place during subduction, the isotopic characteristics of such sediments are poorly known, and they considered that this mixing model would not produce the observed $^{143}Nd/^{144}Nd$ vs. Sm/Nd trend. Considering only the M-series data, the values of $^{143}Nd/^{144}Nd$ and Sm/Nd in authigenic sediments quoted by Hawkesworth et al. (1979b) are still inconsistent with such a model, unless partial melts derived from the sediments had substantially lower Sm/Nd ratios (Figure 6.1.2). The effect of subducted authigenic sediments on Sr isotopic compositions can also be considered in a plot of $^{87}Sr/^{86}Sr$ vs. 1/Sr (Figure 6.1.6). The primitive M-series rocks show an approximate mixing line on this plot, but this does not suggest the involvement of a component with the very high $^{87}Sr/^{86}Sr$ (0.709) of authigenic sediments, or of a mixture of these with continental sediments

Figure 6.1.5 $^{143}Nd/^{144}Nd$ vs. $^{87}Sr/^{86}Sr$ for Grenada extrusive rocks (after Hawkesworth et al., 1979b).

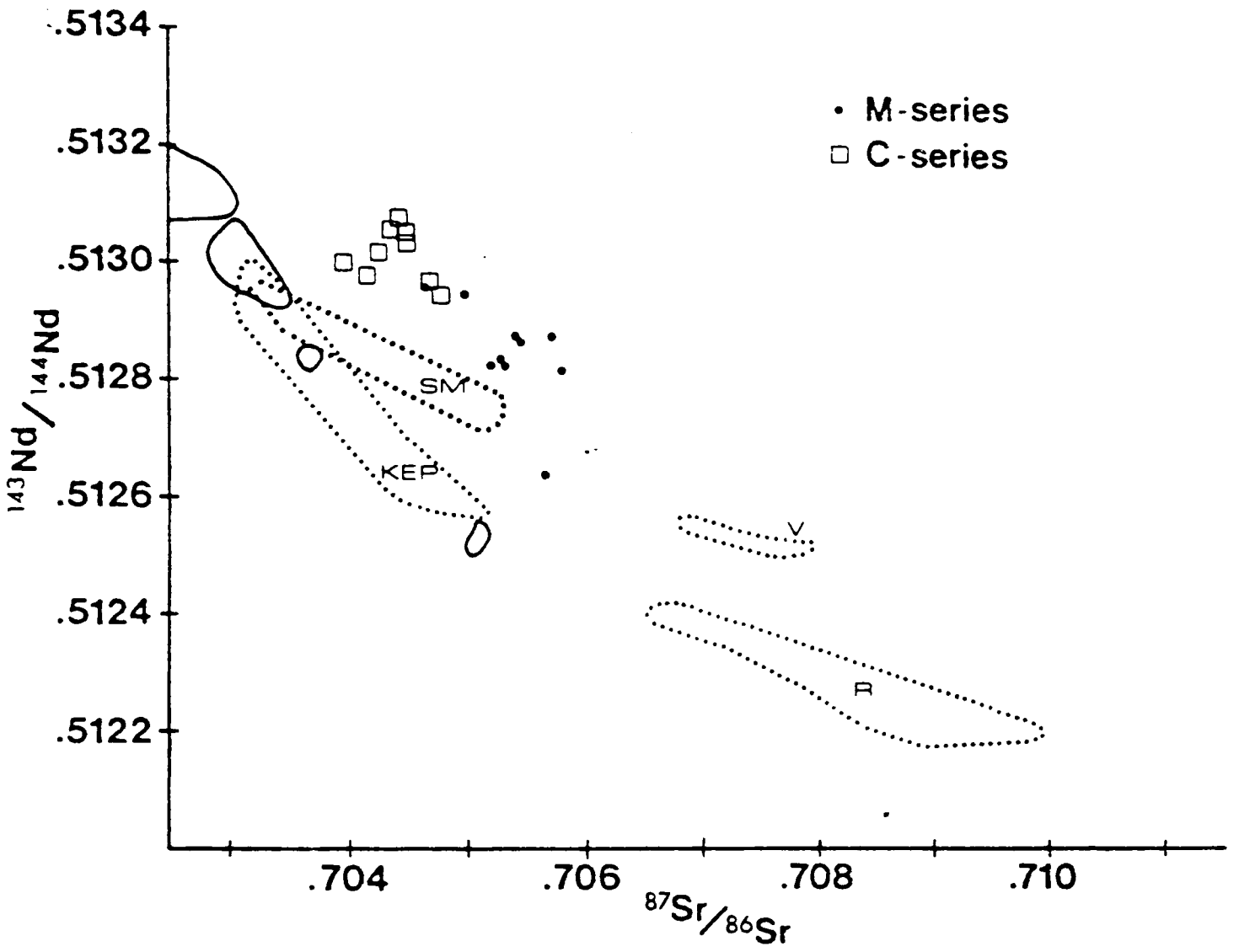

Solid outlined fields represent MORB and Atlantic islands data of O'Nions et al. (1977). Other fields after Hawkesworth et al. (1979c):

KEP = Kenya, Etna, Patagonia

SM = Sao Miguel (Azores)

R = Roccamonfina

V = Vesuvius

Figure 6.1.6 $^{87}Sr/^{86}Sr$ vs. 1/Sr for primitive M-series basalts

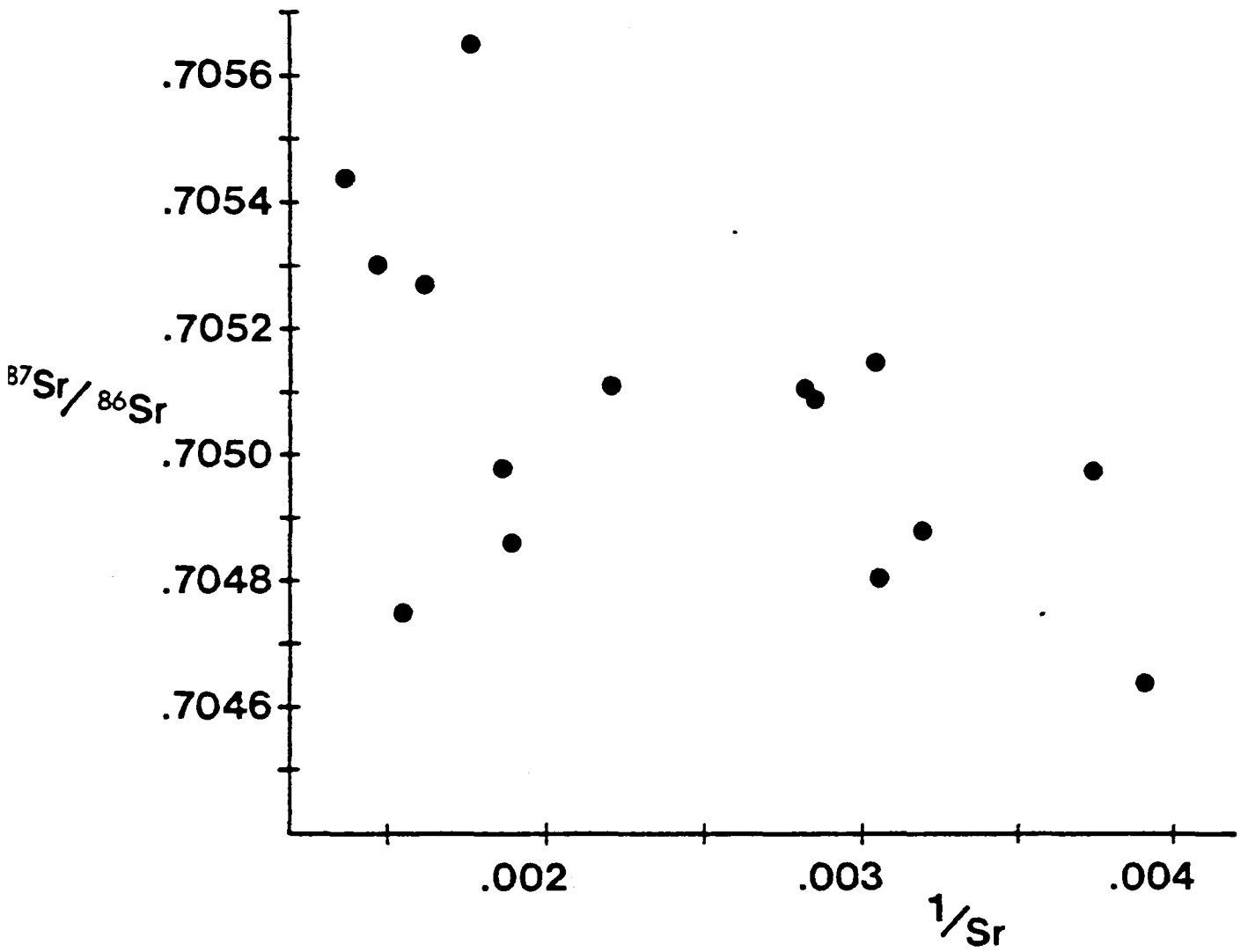

with lower Sr contents but even higher $^{87}Sr/^{86}Sr$.

Although rigorous testing of mixing models involving subducted sediment is limited by poor knowledge of the isotopic characteristics of possible sediment types, these arguments suggest that this mixing hypothesis is not easily reconciled with the available data. Hawkesworth et al. (1979b) therefore concluded that the isotope and trace element data could be explained by selective mobilisation of alkali and alkaline earth elements by hydrous fluids during dehydration of the subducted lithosphere, as proposed by Hawkesworth et al. (1979a). These fluids would then modify the composition of the overlying upper mantle wedge which the Nd isotope data require to have been already chemically heterogeneous. This model therefore considers the Nd isotope variation to reflect the pre-subduction history of the mantle wedge but the Sr isotope variation to reflect additionally subduction-related processes.

There are difficulties in explaining the correlation of major element, trace element, and Sr isotope data using this model. The correlation of increasing LREE enrichment with increasing $^{87}Sr/^{86}Sr$ could reflect source heterogeneity prior to subduction but there seems no reason why the more LREE-enriched sources should then produce magmas which differ substantially in major element composition, possibly as a result of olivine fractionation. As previously argued, a direct mixing of magma with some contaminant is unlikely to have occurred, so that a model wherein the M-series magmas mixed with some contaminant and crystallised olivine is discounted.

A possible explanation is that, if the mantle source was enriched not only in alkalis and alkaline earths, but also in LREE, P_2O_5, TiO_2 and probably other elements, by subduction processes, it would be expected to be enriched in water also. Melts subsequently produced from the

more 'contaminated' portions of the mantle wedge would then be more water-rich, at similar degrees of melting, than melts produced from less contaminated mantle. The more water-rich melts would therefore crystallise olivine more extensively during ascent before crystallising clinopyroxene (Kushiro, 1972). The negative correlation between $^{87}Sr/^{86}Sr$ and Ni (Figure 6.1.7) supports this model. Sample 509 has anomalously low $^{143}Nd/^{144}Nd$ and its source may also have had anomalously high $^{87}Sr/^{86}Sr$ prior to subduction. This model also explains the lack of close correlations between $^{87}Sr/^{86}Sr$ and Rb/Sr, and between $^{143}Nd/^{144}Nd$ and Sm/Nd, since both Rb/Sr and Sm/Nd ratios have been affected by recent processes.

An alternative possibility is that the isotopic variation is primarily the product of disequilibrium melting. The presence of minor phlogopite in the source, entering the liquid entirely at low degrees of melting might explain the variation of $^{87}Sr/^{86}Sr$ with MgO and Ni contents, and also the correlation of $^{87}Sr/^{86}Sr$ with LREE enrichment, since early melts would be relatively low in MgO and Ni and enriched in LREE. However, available estimates for the distribution coefficient of Ni between olivine and liquid (Elthon and Ridley, 1979) do not support a primary melt origin for the high $^{87}Sr/^{86}Sr$, primitive M-series magmas. It is also unlikely that the observed isotope, trace element, and major element trends could be produced by disequilibrium melting and preserved during subsequent fractional crystallisation. Perhaps the strongest evidence against a disequilibrium melting model comes from the available diffusion data, which indicate that isotopic disequilibrium between minerals cannot be maintained over a substantial time interval in the presence of a melt phase (Hofmann and Hart, 1978). This model is therefore not preferred.

Figure 6.1.7 $^{87}Sr/^{86}Sr$ vs. Ni for primitive M-series basalts (>11%MgO).

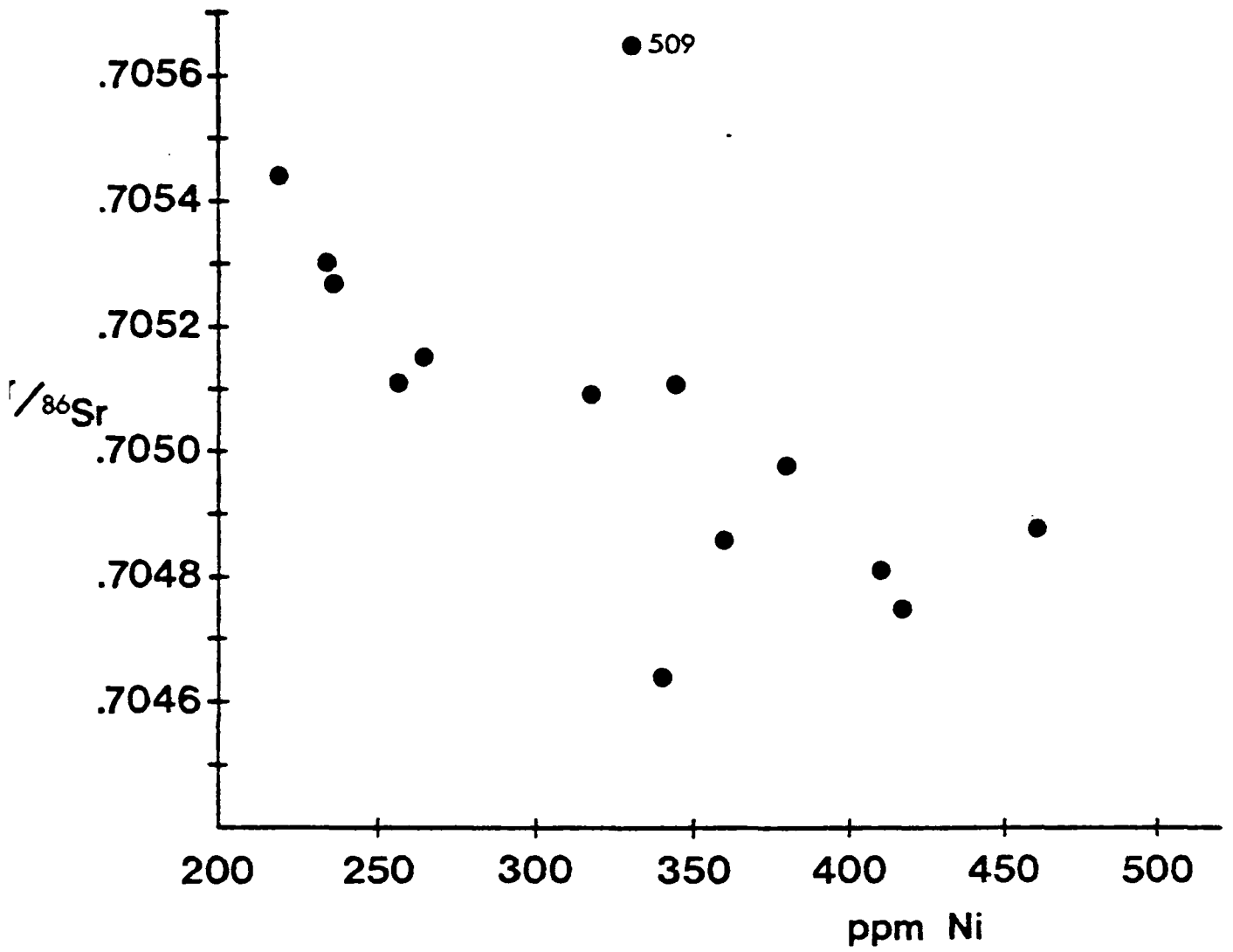

Summary of the preferred model:

(1) The mantle wedge overlying the subducted slab, with minor heterogeneity in trace element and isotopic compositions, is variably contaminated by hydrous melt or hydrous fluid derived from the underlying subducted lithosphere.

(2) The component derived from the subducted lithosphere is rich in alkalis and alkaline earth elements, LREE, radiogenic Sr, radiogenic Nd, water and probably other incompatible elements.

(3) Melting of the variably contaminated mantle produces picritic melts of variable water content, trace element chemistry and isotopic composition.

(4) Larger water contents result in increased stabilisation of olivine relative to pyroxenes on the liquidi of the picritic melts.

(5) Variable olivine fractionation is followed by olivine, clinopyroxene and spinel fractionation during magma ascent.

6.1.3 C-series source

As discussed in Chapter 2, the compositions of clinopyroxene phenocryst cores in C-series rocks suggests that magmas of this series had more primitive parents from which they were derived by fractional crystallisation. The major and trace element contents of C-series rocks are, in general, not inconsistent with these parents being similar in chemistry to the less 'contaminated' M-series magmas. The concentrations of Sr and Ba are however, not consistent with this simple relationship.

Isotopic data (Figure 6.1.5) show that both the Sr and Nd isotopic compositions of the C-series rocks are similar to those of the least 'contaminated' M-series parents, although tending to be slightly lower in $^{87}Sr/^{86}Sr$ and higher in $^{143}Nd/^{144}Nd$. The higher Sr contents of the

C-series magmas therefore cannot be the result of addition of a slab-derived Sr component similar to that envisaged in the preferred model for the M-series, since such a process would result in very high $^{87}Sr/^{86}Sr$ in the C-series rocks. Either the sources for the two series were affected by different components derived from the slab, or the very high Sr content of the C-series rocks simply reflects a source rich in Sr. Such a source would be less sensitive to addition of a slab-derived component rich in radiogenic Sr than the low-Sr source for the M-series magmas. Nd isotopic compositions confirm that the same slab-derived component cannot have affected both the M-series and C-series sources. It therefore seems unjustifiable to assume that these sources both lay on the MORB-Atlantic islands trend of Sr and Nd isotopic compositions prior to subduction.

Ratio-ratio plots of C-series trace element concentrations (Figure 6.1.8) show considerable scatter, and do not define simple mixing hyperbolae, as is also the case in the M-series (Figure 6.1.4). The range of trace element contents in the C-series rocks is almost as great as that in the M-series, and the sources of both clearly show considerable chemical heterogeneity. The wide range of Sm/Nd ratios and limited variation in $^{143}Nd/^{144}Nd$ (Figure 6.1.2) indicate that this heterogeneity was produced by recent processes.

There are two possible models for the C-series source, either:

(a) variable contributions to an originally homogeneous mantle source from the subducted lithosphere produce the isotopic and trace element variability of the magmas later produced, or

(b) at least some of the variation in the C-series reflects heterogeneity in the source mantle prior to subduction.

Hawkesworth et al. (1979b) pointed out a negative correlation between $^{87}Sr/^{86}Sr$ and Sr content in the C-series rocks. This is not

Figure 6.1.8 Incompatible element ratio-ratio plots for primitive C-series basalts.

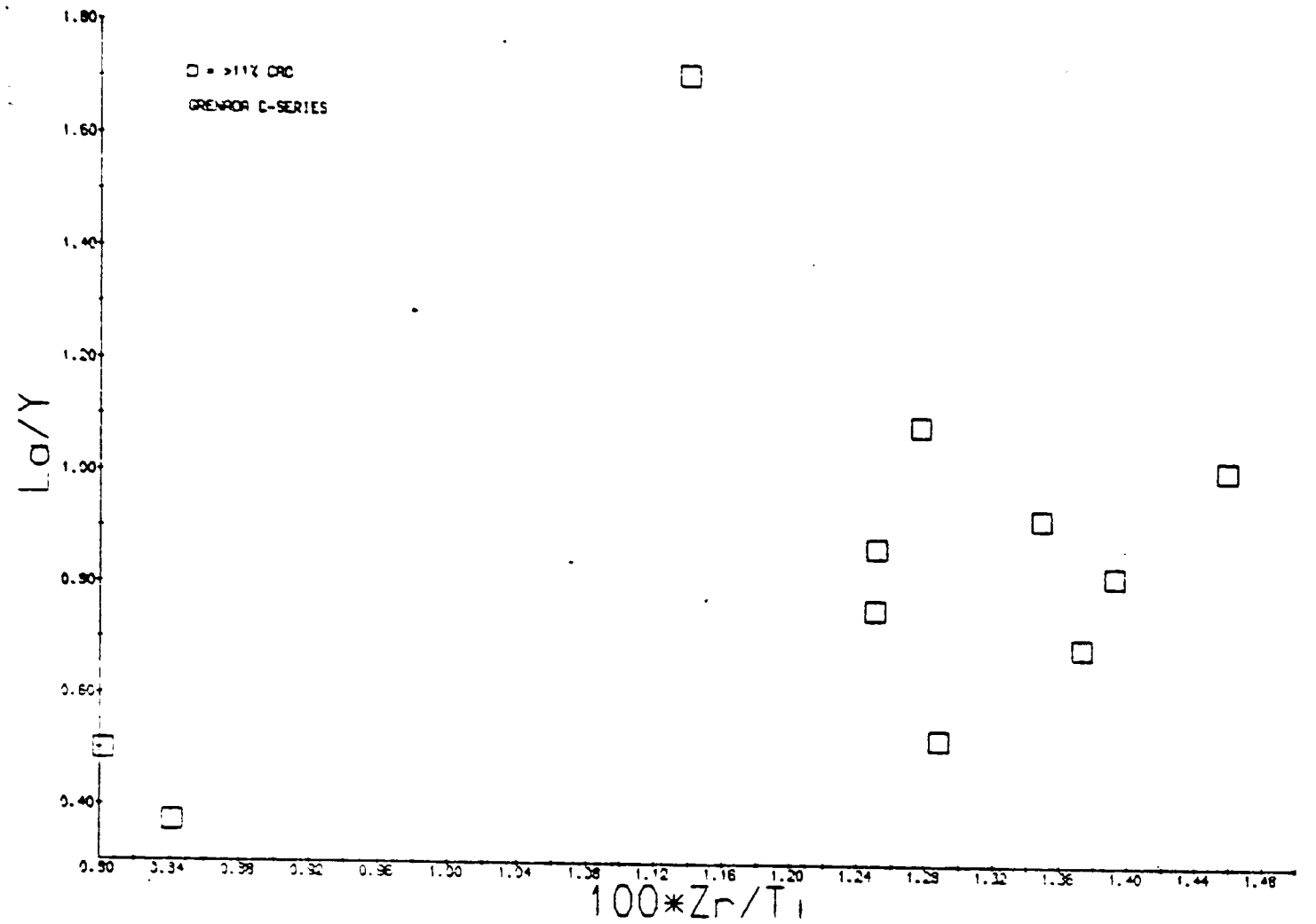

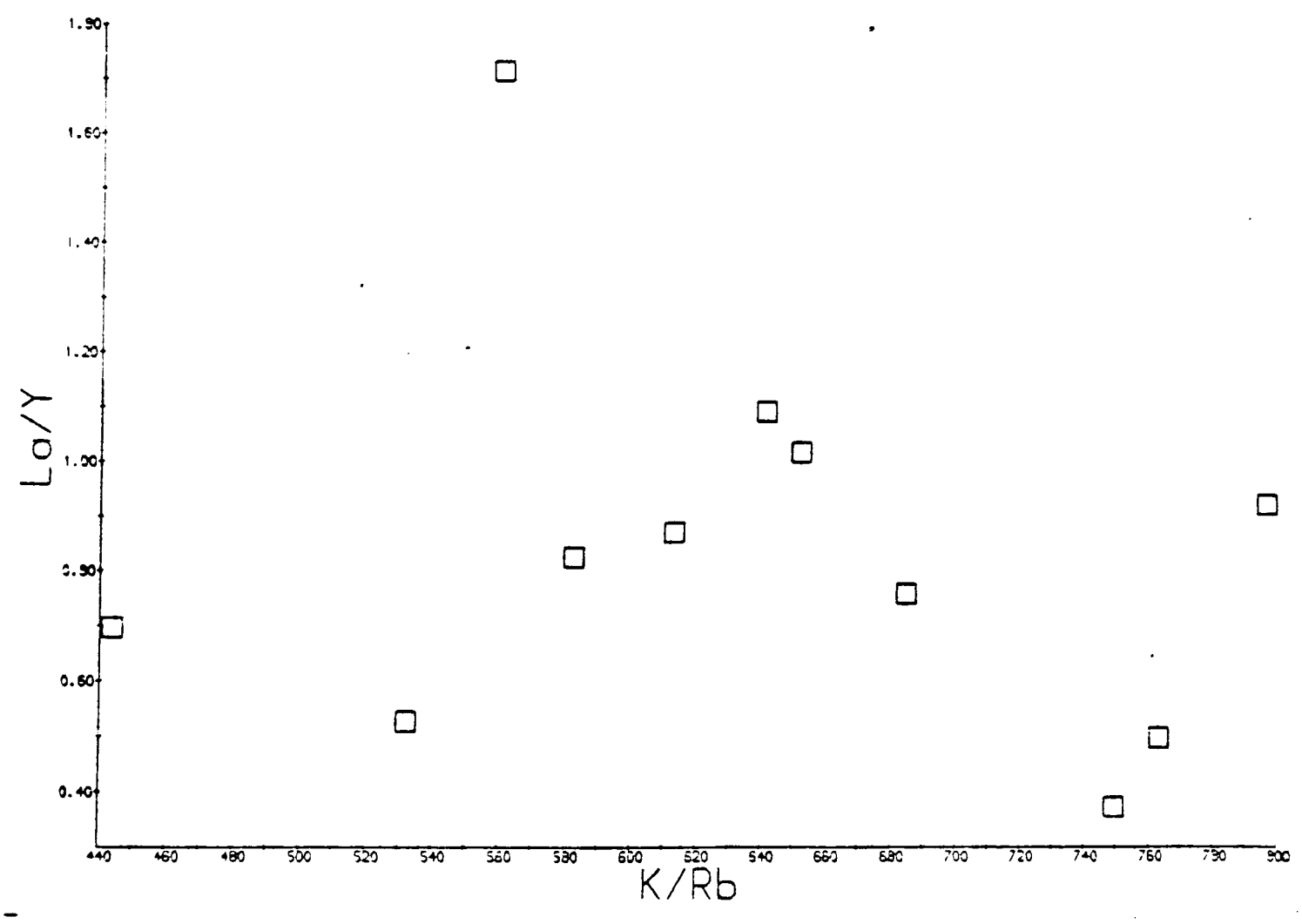

the trend to be expected from mixing with a sedimentary component with high Sr and $^{87}Sr/^{86}Sr$, whether at high levels or above the subducted lithosphere. The negative correlation is more easily reconciled with the addition of similar amounts of a slab-derived, high $^{87}Sr/^{86}Sr$ component to a mantle with variable Sr content than with the addition of variable amounts of a low $^{87}Sr/^{86}Sr$ component to a mantle of uniform Sr content. This is because the generally higher $^{87}Sr/^{86}Sr$ of island arc volcanics, at a given $^{143}Nd/^{144}Nd$, is thought to reflect addition of a high $^{87}Sr/^{86}Sr$ component to their source from the subducted lithosphere (Hawkesworth et al., 1977; DePaulo and Wasserburg, 1977). Additional support for model (b) comes from the observation that the Sr concentrations of C-series rocks are much greater than those of the most primitive lavas found on other islands of the active Lesser Antilles volcanic arc. Assuming that these lavas are also linked to subduction processes, this indicates that the source of the Grenada C-series was anomalously rich in strontium. Model (b) is therefore preferred.

Figure 6.1.9 shows a possible correlation between $^{87}Sr/^{86}Sr$ and LREE enrichment in the C-series, which could result from addition of LREE to the mantle wedge during subduction. The limited Nd isotopic variation in the C-series indicates that any slab-derived component must have had similar Nd isotopic composition to the mantle wedge, and that a different component from that involved in the genesis of the M-series was involved.

6.1.4 Relationships between the basic Grenada rock series

M-series and C-series magmas are closely related in space and time in Grenada (Arculus, 1976) at least in the Mount Maitland - Mount Moritz, Mount Granby - Fedon's Camp, and Mount St. Catherine centres. The more evolved members of both series contain amphibole, and both series appear to be parental to andesites. It is also possible that the parent magmas

Figure 6.1.9 LREE enrichment vs. $^{87}Sr/^{86}Sr$ for C-series basalts.

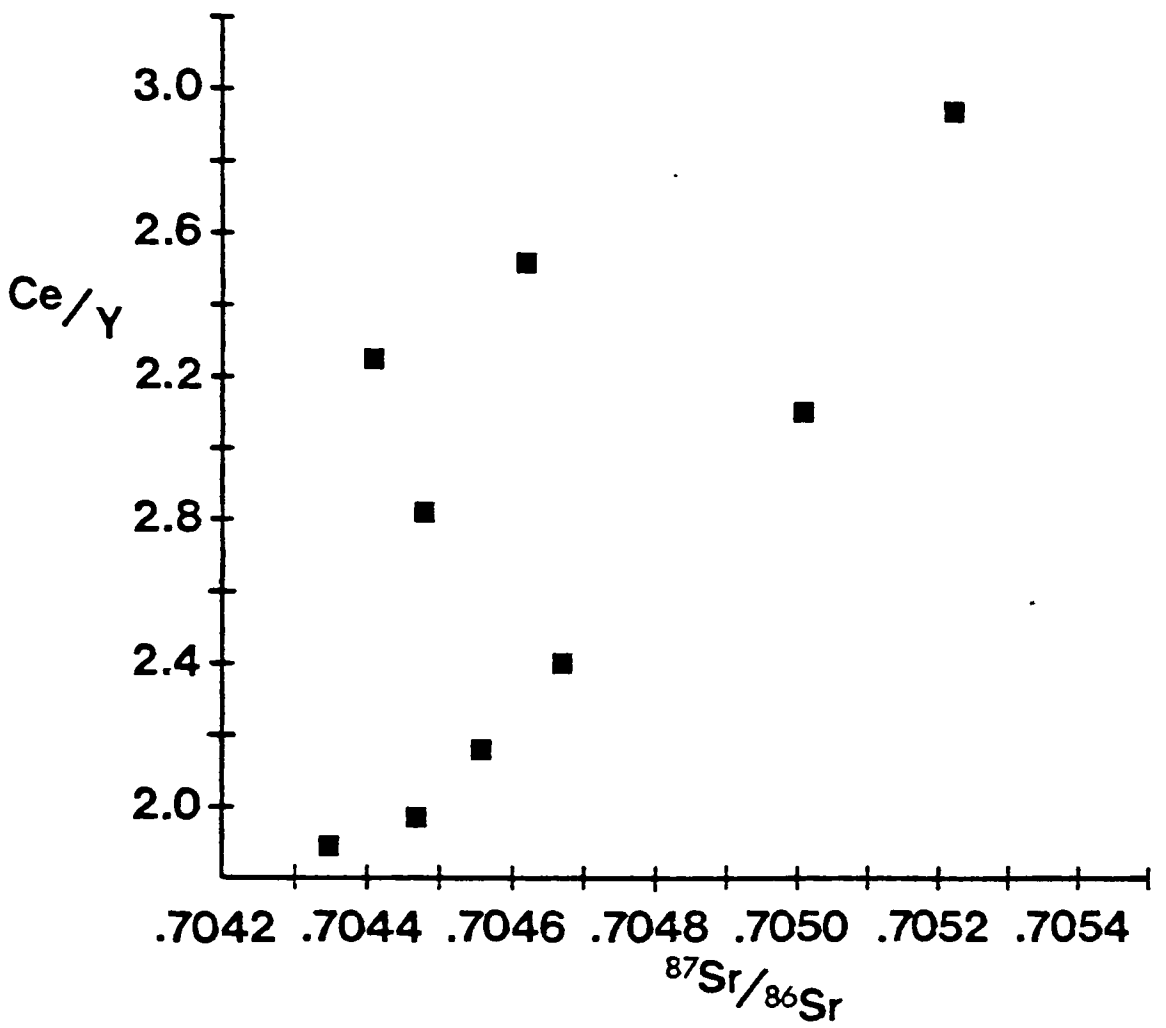

to both series were similar in major element composition, although distinct in certain isotope ratios and trace element concentrations.

The close spatial and temporal relationship of the two series suggests that they were generated at similar depths, presumably superjacent to the Benioff Zone, which is thought to lie at approximately 100 km. beneath Grenada (Tomblin, 1975). The hydrous nature of the magmas in both series strongly suggests some involvement of the subducted lithosphere in their genesis, although the postulated major element compositions of the parent magmas require a mantle peridotite source. The combined chemical and isotopic data in the previous sections have been interpreted as indicating that the sources of the two magma series have been affected by different components derived from the subducted lithosphere, but probably also differed in chemistry prior to subduction. A possible explanation of the difference in slab-derived components is that the C-series source includes a contribution from subducted oceanic crust while the M-series source also includes a contribution from subducted sediments. As previously discussed, the isotopic evidence does not confirm the involvement of sediment in the genesis of M-series magmas, but rigorous interpretation of the data is limited by a lack of knowledge of the isotopic and trace element characteristics of sediments and by the scatter of the data. A study of the isotopic composition of lead in Grenada rocks might help to clarify the preferred models.

In the same way that the preferred model for the origin of the M-series magmas involves an effect of source chemistry on subsequent fractionation processes, the absence of the postulated parents to the C-series from the Grenada rock suite may be a consequence of the effect on their source of a slab-derived component. A relatively high water content in the C-series parents might promote substantial crystallisation

during ascent in addition to stabilising olivine as the dominant fractionating phase. However, little is known of the effect of volatiles on the ascent and crystallisation of complex silicate melts.

6.2 Do some M-series compositions represent primary magmas?

The preferred model for the origin of the M-series implies that the samples with the highest MgO contents have undergone the minimum fractionation of olivine subsequent to their genesis as partial melts of peridotite. These magmas have high Mg values and may therefore be unmodified or 'primary' melt compositions. The olivine-liquid distribution coefficients for Mg and Fe of Roeder and Emslie (1970) may be applied to test this possibility using the method of Hanson and Langmuir (1978).

Figure 6.2.1 shows the molar MgO and FeO contents of some estimates of the composition of the upper mantle, and the field of permissible primary melt compositions in equilibrium with olivine, contoured for temperature, for one of these estimated compositions. The estimate chosen is the average composition of a group of sheared garnet lherzolite nodules from kimberlite analysed by Nixon and Boyd (1973), although the sheared nature of the nodules is not regarded as significant for their chemical composition. Choice of any of the other source compositions will simply move the position of the melt field slightly. Also shown is a melt field calculated using partition coefficients extracted from the data of Bickle et al. (1977) on experimental charges run at 30 kilobars. The position of the melt field is clearly strongly dependent on pressure, but few data are available for a rigorous treatment of this dependence.

It has been assumed that all iron in the primitive M-series magmas was in the ferrous state under the conditions of melting. This is a

Figure 6.2.1

Molar MgO vs. FeO for primitive Grenada M-series basalts, after method of Hanson and Langmuir (1978).

Triangles are estimates of source mantle composition:

O = average garnet lherzolite in kimberlite (O'Hara et al., (1975)

SL = average spinel lherzolite (Maaloe and Aoki, 1977)

K = mantle composition derived from the chemistry of ultramafic lavas (Bickle et al., 1976)

P = 'pyrolite' (Ringwood, 1966)

1611 = garnet lherzolite 1611 (Nixon and Boyd, 1973)

Chosen source is the average of six sheared garnet lherzolites from Nixon and Boyd (1973).

Isotherms in degrees C.

See text for further description.

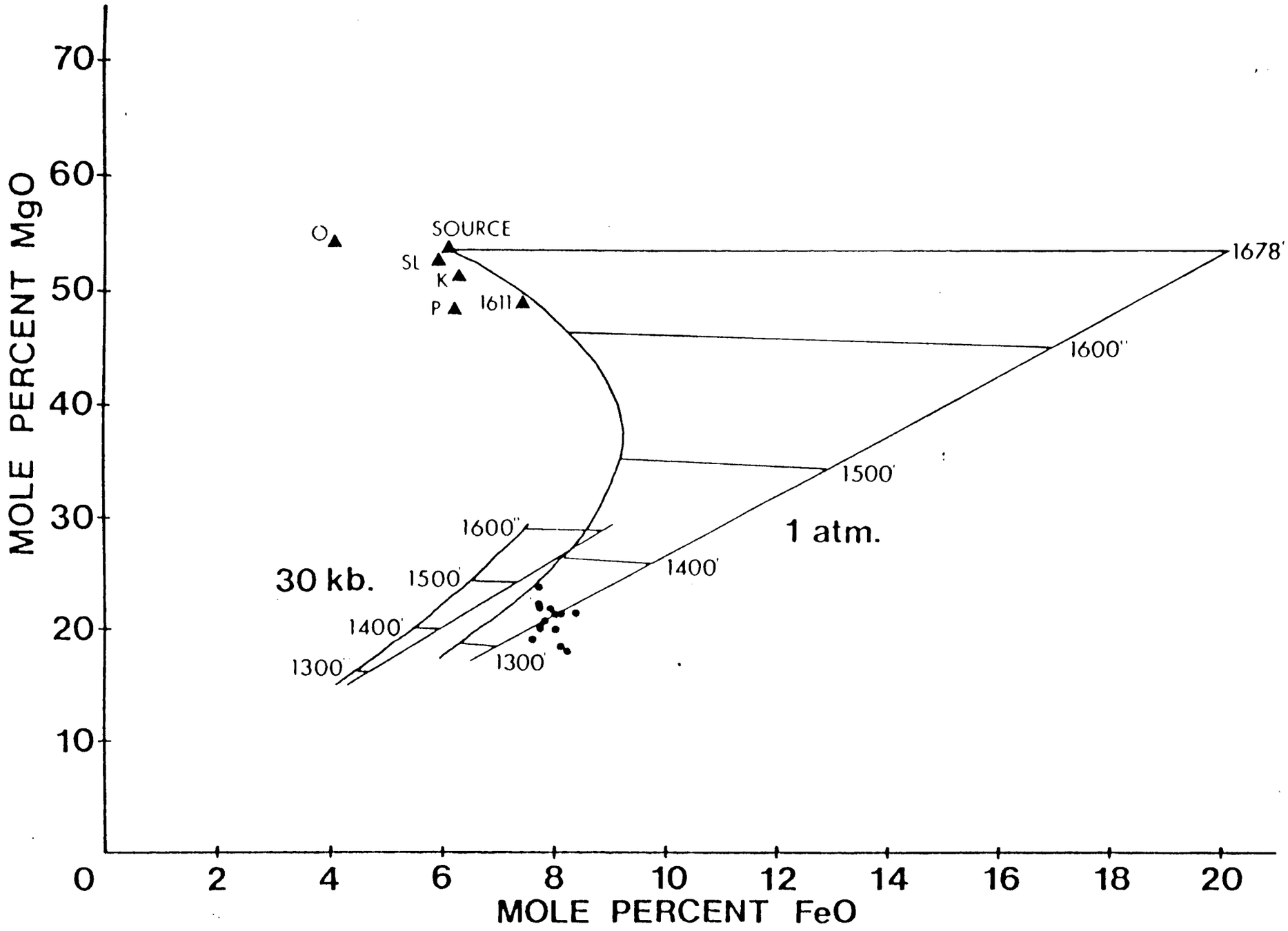
MOLE PERCENT MgO
70
60
50
40
30
20
10
0
2
4
6
8
10
12
14
16
18
20
MOLE PERCENT FeO
O
SOURCE
SL
K
P
1611
1678'
1600''
1500'
1400'
1600''
1500'
1400'
1300'
1300'
30 kb.
1 atm.

reasonable approximation since the Fe_2O_3/FeO ratio of peridotite nodules in kimberlite is very low. If a small amount of the iron is ferric, the M-series compositions will lie towards lower FeO contents than their plotted positions. The melts which have fractionated least olivine lie in the primary melt field at 1 atmosphere, and sample 468, with close to 16% MgO lies close to the maximum degree of melting at temperatures close to 1360°C of approximately 19%. However, even this composition cannot be a primary melt at pressures close to 30 kilobars. Nevertheless, it can be concluded that the available data do not preclude some of the Grenada M-series compositions representing primary magmas. This conclusion is supported by the experimental results of Arculus (1975) which showed olivine as the primary liquidus phase in an M-series composition containing only about 11% MgO at pressures in excess of 15 kilobars.

6.3 Evolution of M-series magmas

The major element fractionation models discussed in Chapter 2 indicate that, after variable amounts of initial olivine fractionation, the M-series magmas crystallised olivine, clinopyroxene, and spinel. The phase relations reported by Arculus (1975) and in Chapter 5 show that this fractionation scheme must have operated at high pressures, probably in excess of 15 kilobars. The more Ne-normative M-series magmas are, in general, higher in CaO/MgO, $^{87}Sr/^{86}Sr$ and LREE, and lower in Ni which suggests that magmas originally only slightly undersaturated in silica became more so as a result of removal of olivine. Subsequent fractionation of olivine, aluminous clinopyroxene, and aluminous spinel drove the compositions of the magmas back through the low-pressure thermal divide Di-An-Fo into the hypersthene-normative field.

Experimental evidence from Cawthorn et al. (1973a) and this study

shows that the amphibole-bearing, plagioclase-free assemblages in the Grenada cumulates must have formed from M-series magmas at relatively low pressures, and that substantial equilibrium crystallisation is required to generate the observed phase relations. Therefore, the magmas in equilibrium with the cumulate assemblages must have contained a considerable proportion of crystals, yet most of the M-series rocks examined are microphyric in texture. A further problem arises from the fact that the trace element chemistry of the M-series, discussed in Chapter 2, does not suggest that amphibole was an important fractionating phase, yet the plagioclase-free cumulates are rich in amphibole.

Sigurdsson and Shepherd (1974) reported analyses of dredge samples from the Kick 'em Jenny submarine volcano north of Grenada, which has been active several times this century. These samples included porphyritic, amphibole-bearing scoria whose composition is given in Table 6.3.1. Both the major and trace element compositions of this sample show its affinity to Grenada M-series rocks, although it differs texturally from typical M-series samples. It is possible that the inconsistencies in cumulate-lava relationships in the M-series result because some M-series magmas beneath Grenada are phenocryst-rich, like the Kick 'em Jenny scoria. Because of the lower temperatures and therefore higher viscosities of such phenocryst-rich magmas they might be only rarely erupted in comparison with the almost totally liquid M-series magmas described in Chapter 2. The higher viscosity of the phenocryst-rich melts could be expected to promote slow ascent, with crystal accumulation on the walls of conduits, or in small chambers, producing the cumulate assemblages. The residual magmas from such crystal accumulation would be basaltic andesites rich in water and carrying all of the cumulate phases as phenocrysts. The high water content would result in explosive eruptions, sampling the wall rocks of the magma bodies,

Table 6.3.1

Chemical composition of scoria from Kick'em-Jenny submarine volcano

SiO_2	46.42
Al_2O_3	19.57
Fe_2O_3	9.28
MgO	9.86
CaO	10.43
Na_2O	2.23
K_2O	0.60
TiO_2	1.03
MnO	0.14
P_2O_5	0.05
Total	99.61

Ni	235
Cu	88
Zn	72
Sr	300
Rb	19
Zr	62
Nb	5
Ba	117
Y	19

Sample KJO17

Major elements from Sigurdsson and Shepherd (1974) recalculated oxidised and volatile-free.

Trace elements from Arculus (1973).

including the cumulates.

This model can account both for the occurrence of the cumulate blocks in basaltic andesites and andesites, normally of pyroclastic association, and for the fact that the trace element chemistry indicates that only in the origin of magmas of these compositions does amphibole appear to have played a significant role. Fractionation of amphibole, calcic plagioclase and clinopyroxene, together with titanomagnetite and apatite, from basaltic andesite magmas produced the acid andesites which represent the most evolved lavas on Grenada. The use of an element of very low bulk distribution coefficient, such as Rb, as a fractionation index shows that the acid andesites represent the products of at least 85% fractional crystallisation of a parental composition with 16% MgO.

6.4 Evolution of C-series magmas

The most primitive C-series compositions show evidence in the cores of clinopyroxene phenocrysts of derivation from more primitive parents. Major element mixing calculations show a reasonably good fit between the parental M-series and C-series compositions involving approximately 20% olivine fractionation, although the magnesian clinopyroxene cores suggest the involvement of this phase also. The low Cr abundances in the C-series rocks require minor fractionation of a Cr-rich spinel with the olivine. An olivine-dominated fractionation scheme is supported by the abundances of Ni and Sc, respectively sensitive indicators of olivine and clinopyroxene fractionation, in the two series. It therefore appears probable that picritic magmas were parental to the C-series also.

The substantial olivine fractionation from these parents could result from sufficiently rapid ascent of the magmas to expand the primary phase volume of olivine more quickly than the liquid compositions

were driven out of this volume by olivine crystallisation (O'Hara, 1968). The low pressure phase relations of sample 6264, which shows olivine and clinopyroxene close to its liquidus at 2 kilobars, indicate that such olivine fractionation must have continued up to shallow depths beneath Grenada.

At shallow depths, substantial fractionation of clinopyroxene and plagioclase occurred, together with some titanomagnetite and olivine, producing basaltic andesite derivatives which crystallised amphibole. It is probable that this fractionation of amphibole with clinopyroxene and calcic plagioclase is represented in the type D olivine-free cumulates, since the minor proportion of olivine in C-series compositions would quickly disappear by reaction once amphibole crystallised. Fractionation of this assemblage results in rapid silica enrichment but little iron enrichment, which is typical of calc-alkaline suites. The basaltic andesite magmas are likely to have been highly viscous, by comparison with lavas of similar composition erupted on St. Vincent in 1971 and 1979. It is therefore highly unlikely that the low pressure fractionation in the C-series, and probably also in the M-series, resulted from gravitational settling of crystals. Crystal accumulation on the walls of conduits and small magma chambers seems a more plausible mechanism for crystal-liquid differentiation.

6.5 Activities of water and oxygen

Burnham (1979) has shown, from thermodynamic considerations, that the minimum water content of a melt in equilibrium with amphibole at low pressures is close to 3 weight percent. The presence of amphibole phenocrysts in some Grenada lavas therefore provides an immediate indication of their water content under subvolcanic conditions, although the corroded appearance of many of the amphiboles may reflect loss of

some water on eruption. A number of samples examined in this study with compositions in the 3 to 6 percent MgO range contain amphibole phenocrysts.

Using the results of major element least-squares mixing calculations from Chapter 2, and treating water as incompatible in closed-system fractionation, the presence of amphibole in sample 6177, a C-series basalt, indicates a minimum water content for a picritic parent to this series of about 1%. Similar treatment of basaltic andesite 307, which shows petrographic and isotopic affinities to the M-series basic lavas, suggests that the picritic parents to this series had a similar minimum water content. However, experimental evidence discussed in Chapter 5 indicates that crystallisation of amphibole before plagioclase reflects high water activities, which may imply water contents for some M-series parents at least a factor of two greater than the minimum estimate. The petrographic evidence from the cumulate blocks shows variable relative stabilities of plagioclase and amphibole in M-series magmas and these must reflect, at least in part, variable water contents. Small differences in the water contents of the parents will, of course, be amplified by subsequent fractionation.

Sigurdsson and Shepherd (1974) suggested that the texture of the Kick 'em Jenny scoria indicates crystallisation of amphibole after plagioclase in this magma. Using their chemical and modal data, and assuming this composition to be related to the M-series, the minimum water content of a picritic parent would be close to 1.4%.

Experimental evidence suggests that the early crystallisation of a magnetite-rich spinel phase, observed in the cumulate blocks and in the basaltic andesites, requires oxygen fugacities in excess of those defined by the synthetic NNO buffer, and perhaps close to those of the HM buffer. Although the constraints are poor, such an estimate agrees

well with that obtained by Wills (1974) using the compositions of co-existing Fe-Ti oxides in cumulate blocks from St. Kitts. The high oxygen fugacity is believed to result from the relatively high water activity of the magmas, since water would be the largest oxygen reservoir, buffering the oxygen fugacity through its dissociation.

6.6 Conclusions

(a) Both M-series and C-series Grenada magmas were derived from picritic parents produced by partial melting of a peridotite source. Some of the erupted M-series lavas may represent primary melt compositions.

(b) The source of M-series magmas had been variably contaminated by material derived from the subducted oceanic lithosphere. This slab-derived component was rich in alkali and alkaline earth elements, water, LREE, and probably also other incompatible elements.

(c) Isotopic evidence suggests that the M-series source was heterogeneous prior to subduction and addition of a slab-derived component. This component may have included a contribution from subducted sediments.

(d) The variable contamination of the M-series source produced variable water contents in the primary melts, resulting in variable degrees of olivine fractionation which correlate with the trace element chemistry and isotopic composition of Sr.

(e) The source of the C-series magmas differed in chemistry from that of the M-series prior to subduction, and was probably heterogeneous at least in Ba and Sr contents. This source appears to have been contaminated by a slab-derived component different to that involved in the M-series source. This component may have been derived from the subducted oceanic crust.

(f) The M-series magmas fractionated olivine, clinopyroxene and spinel at high pressures while the C-series parents crystallised dominantly olivine up to shallow depths, and are not represented in the Grenada rock suite. These differences may be related to differences in volatile content of the magmas, but are not fully understood. Similarly, some M-series magmas underwent substantial crystallisation at shallow depths, producing olivine-bearing cumulate assemblages, while others were erupted in an essentially liquid state from high pressures, carrying genetically unrelated peridotite nodules. The transition from Ne-normative to Hy-normative magmas resulted from the high pressure olivine-clinopyroxene-spinel fractionation rather than amphibole fractionation.

(g) The considerable low pressure fractionation suffered by the magmas of both series can be related to the genesis of the cumulate blocks. Liquids in equilibrium with the cumulate assemblages were of basaltic andesite and andesite compositions. Their viscosities were probably too high to allow the gravitational settling of crystals, crystal accumulation on the walls of conduits and small magma chambers being the most likely mechanism of differentiation. The phase relations of these crystal cumulates indicate that the activities of both water and oxygen in the subvolcanic magma bodies were high. The high water activities resulted in explosive eruptions of basaltic andesite and andesite magmas, which often sampled the cumulate assemblages.

CHAPTER 7

IMPLICATIONS OF THE GRENADA PETROGENETIC SCHEME FOR MAGMA GENESIS IN ISLAND ARCS.

The scheme presented in the preceding chapter for the genesis of Grenada magmas involves the derivation of andesitic melts from picritic parents by fractional crystallisation at high and low pressures. These primary melts were generated from a peridotitic source whose composition had been modified by addition of a component derived from the subducted lithosphere, but was probably variable prior to subduction. The applicability of this petrogenetic scheme to island arc magma genesis in the Lesser Antilles as a whole, and in other island arcs, is discussed in the following two sections.

The major element compositions of the primitive Grenada M-series rocks are, as noted by previous workers, unusual for island arc volcanics (Sigurdsson et al., 1973; Arculus, 1976) and therefore the general applicability of the Grenada petrogenetic scheme is essentially a question of whether

(a) picritic magmas are not normally involved in island arc magma genesis, or

(b) many island arc volcanic suites are picrite-parented, but only in Grenada are the parent magmas represented abundantly in the erupted products.

7.1 Implications for the Lesser Antilles arc

Brown et al. (1977) have carried out a major study of the chemistry of island arc volcanics from the Lesser Antilles. The average composition of the volcanic products determined by them is andesitic, but the relative proportions of andesitic and basaltic products is variable between islands. The southernmost islands of Grenada and St. Vincent

contain abundant basalt and basaltic andesite, but those in the centre and north of the arc contain dominantly andesite. Wills (1974) proposed that the volcanic centres of the various islands could be grouped into basic (basalt-dominated) and intermediate (andesite-dominated) centres, and suggested that these might reflect the existence of parental basaltic and andesitic melts beneath the arc. The intermediate centres, such as Mt. Pelee in Martinique, contain a higher proportion of pyroclastic products than the basic centres, but do not contain ultrabasic, olivine-bearing cumulate plutonic blocks, which appear to be restricted to the basic centres. In view of the lack of any trace element or isotopic evidence for a different source to these two parental magmas, it is likely that the different centres are a reflection of controls on the ascent and crystallisation of basic magmas.

In addition to this variation in proportions of rock types between islands, Brown et al. (1977) noted that, in general, the abundances of incompatible elements such as K, Nb and Zr increased, in rocks of a given silica content, from north to south along the arc. The southernmost islands also showed a tendency towards silica undersaturation in their basaltic rocks, culminating in the occurrence of compositions with up to about 7% normative Ne in Grenada. These features were compared with the chemical variation documented across many Pacific island arcs (Kuno, 1966; Jakes and White 1972; Whitford et al., 1979), and were ascribed by Brown et al. (1977) to regional chemical variation in the mantle above the subducted lithosphere.

The relatively undersaturated nature of the basic Grenada lavas and their resultant classification as alkaline (Arculus, 1973, 1976; Brown et al., 1977) does, rather unfortunately, give the impression that they are chemically similar to comparably undersaturated alkaline lavas from other tectonic environments. Arculus and Curran (1972), in

particular, used the Grenada suite to suggest that calc-alkaline differentiates could be produced from both tholeiitic and alkaline basaltic parents. Their conclusion is confirmed in this study, but in terms of incompatible element abundances, the Grenada basalts are not closely comparable with alkaline basalts from intra-plate environments.

Figure 7.1.1 depicts the patterns of selected incompatible elements in Grenada basalts. This plot was used by Hawkesworth et al. (1979a) in a study of Patagonian basalts and Chilean andesites. Similar plots for alkaline basalts from Kenya, Mauritius and the Azores, together with average basalts from the Sunda Arc are shown for comparison. Fractional crystallisation will not affect the relative abundances of these elements unless apatite or plagioclase is an early-crystallising phase. The M-series and C-series basalt patterns are distinct, particularly in the relative abundances of K, Rb and Sr, but neither series shows the enrichment in Nb typical of the intra-plate alkaline basalts. The incompatible element patterns of the Grenada basalts, particularly the more undersaturated M-series, are more comparable with other calc-alkaline basalts, showing enrichment of K, Rb and Sr relative to high field-strength elements. It may, therefore, be rather misleading to consider trace element indicators of 'alkalinity' together with major element indicators such as silica saturation, since they may not always be related, particularly if metasomatic processes operate extensively within the upper mantle.

The undersaturated nature of many of the M-series Grenada magmas remains to be explained. Those compositions with highest MgO and Ni are just saturated or slightly undersaturated in silica, with up to about 2% normative Ne, whereas the primitive magmas with lower MgO and Ni, and higher incompatible element concentrations, LREE enrichment and $^{87}Sr/^{86}Sr$ ratio tend to be more undersaturated, with up to 7.5% Ne.

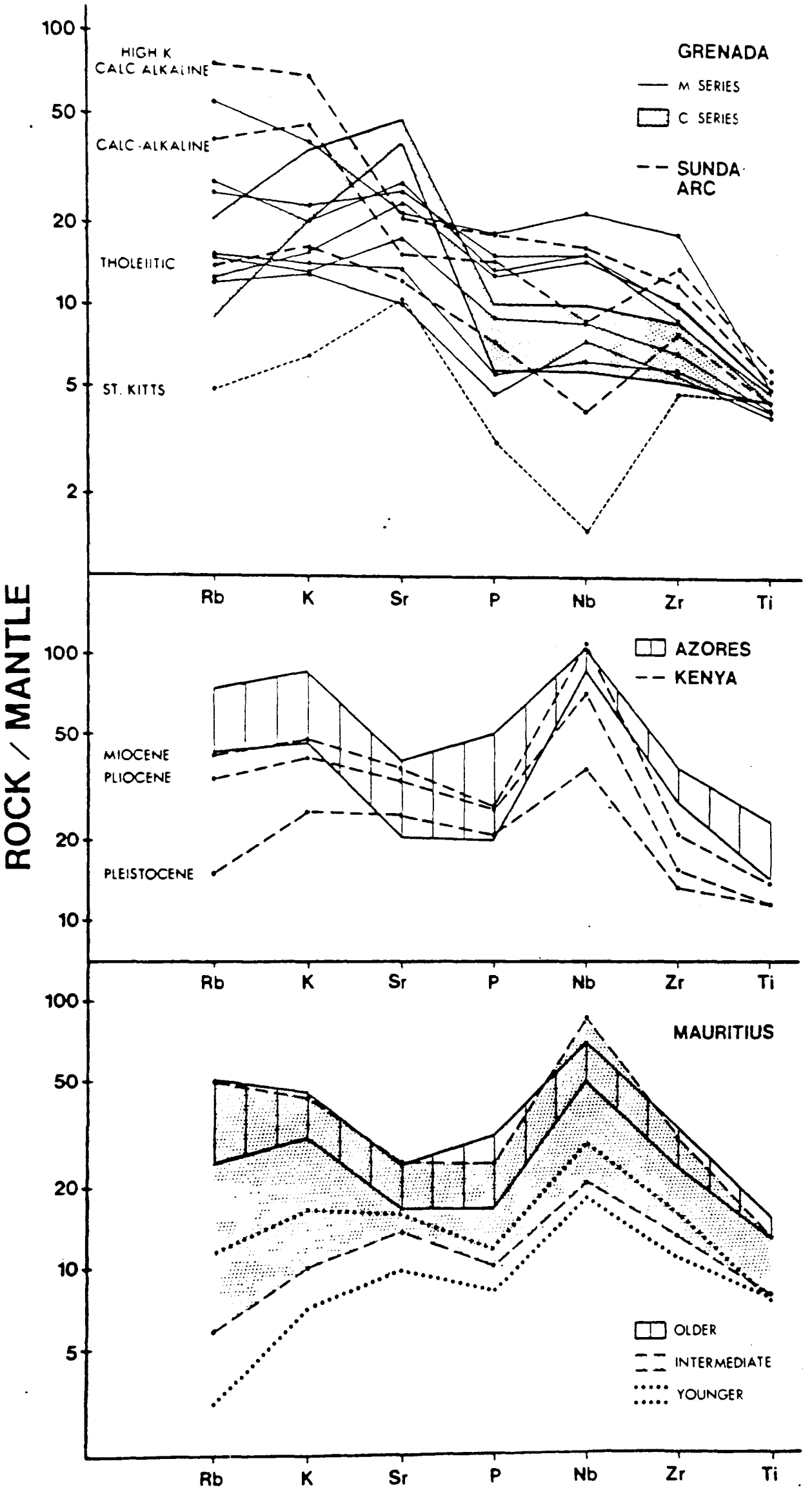
ROCK / MANTLE
100
50
20
10
5
2
HIGH K
CALC ALKALINE
CALC-ALKALINE
THOLEIITIC
ST. KITTS
GRENADA
M SERIES
C SERIES
SUNDA
ARC
Rb
K
Sr
P
Nb
Zr
Ti
100
50
20
10
MIOCENE
PLIOCENE
PLEISTOCENE
AZORES
KENYA
Rb
K
Sr
P
Nb
Zr
Ti
100
50
20
10
5
MAURITIUS
OLDER
INTERMEDIATE
YOUNGER
Rb
K
Sr
P
Nb
Zr
Ti

This difference cannot be accounted for by olivine fractionation, which would not greatly increase silica undersaturation. Fractionation of a substantial proportion of orthopyroxene together with olivine would not, however, be inconsistent with the major element chemistry, although not supported by some interpretations of the available experimental data (O'Hara, 1968).

Alternatively, the variation in silica saturation may be derived from the primary melt compositions. Variable silica saturation of the primitive melts might then reflect variations in the depth and/or degree of melting of the source peridotite. Published thermal models of the subducted lithosphere (e.g. Toksoz et al., 1971; Hsui and Toksoz, 1979) indicate that the highest temperatures in the overriding mantle wedge are some distance above the subduction zone. It is thus possible that the most contaminated mantle, closest to the subducted slab, would undergo a lower degree of melting than the relatively uncontaminated mantle at higher levels. Clearly there are several possible mechanisms which could produce the observed variation in silica saturation but, given the scatter of the chemical data and the present crude thermal models of subduction zones, there is little possibility of differentiating between them.

The C-series Grenada magmas are also slightly nepheline-normative at the assumed oxidation ratio ($Fe_2O_3/(FeO + Fe_2O_3)$) of 0.20. The relatively undersaturated nature of the Grenada magmas in comparison with those of other islands in the Lesser Antilles is probably a consequence either of a different depth of melting, or of a different degree of melting, of the mantle beneath Grenada than beneath the rest of the arc. Although increased CO_2 activity in the source region would produce more undersaturated magmas (Eggler, 1974), it is unlikely that large amounts of volatiles are present in the mantle (Eggler, 1978), or

that CO_2 is the dominant volatile species in destructive plate margin environments. O'Hara (1968) proposed that magmas generated within the pressure range 10-20 kilobars will be nepheline-normative, while those generated at high pressures will be hypersthene-normative. Green (1970), on the other hand, suggested that alkali picrites will be produced by 20 percent melting of peridotite at pressures of around 25 kilobars, with higher degrees of melting producing hypersthene-normative compositions. The occurrence of possible primary melts in Grenada but not in the central and northern islands of the Lesser Antilles is not easily reconciled with a lower degree of melting of the mantle beneath Grenada, but relatively easily explained if melting occurs at shallower depths beneath Grenada. Unfortunately, the lack of conclusive experimental determinations of the degree of silica saturation of primary partial melts of peridotite and the absence from the rock suites of the more northerly islands of primitive compositions prevents distinction of the exact cause of the relative undersaturation in silica of the basic Grenada magmas.

The major element compositions of the most primitive lavas in Dominica and St. Kitts (Wills, 1974; Baker, 1968) to the north of Grenada, show strong similarities to the Grenada C-series compositions, except for generally lower alkali contents in the more northerly suites which probably reflect regional variation in source composition. The basalts from these islands do not, however, show the distinctive incompatible element patterns, involving high Sr, of the Grenada C-series - again a function of their mantle source (Chapter 6). In St. Vincent, Graham and Thirlwall (in prep.) suggest that the basalts and basaltic andesites of the Soufriere are derivatives of highly magnesian parents, present as olivine-microphyric basalt flows with up to 12% MgO (Tomblin, 1968). These lavas are petrographically and chemically similar to the

Grenada M-series rocks.

Thus, despite the presence of undersaturated magmas in Grenada, there seems no reason why the Grenada petrogenetic scheme should not be applicable to the Lesser Antilles as a whole, although available data indicate unusual variability in incompatible trace elements and isotopic compositions in the Grenada suite. Variation in the chemistry of the magmas within and between islands is believed to be a function of the composition of their upper mantle source (Brown et al., 1977) and the degree of fractionation suffered by the primary, picritic melts during ascent.

The unusually small degree of fractionation suffered by many of the Grenada M-series magmas may have resulted from an unusual temperature distribution in the overriding mantle wedge, perhaps an "edge effect" at the junction of the Lesser Antilles destructive plate margin with a transform fault system running across northern South America (Molnar and Sykes, 1969). DeLong et al. (1975) have suggested that occurrences of undersaturated volcanics in island arcs may be related to tectonic discontinuities in the subducted plate. There is, as yet, only a poor understanding of the temperature distribution around the subducted lithosphere, but it is clear that the most recent models (e.g. Hsui and Toksoz, 1979, and references therein) do not predict the existence in the overriding mantle wedge of the temperatures close to 1400°C necessary to produce the Grenada parent magmas. An additional factor promoting the eruption of primitive magmas in Grenada, and, to a lesser extent, in St. Vincent may be a relatively high water content, since the Grenada M-series rocks show evidence of crystallisation of amphibole from magmas more primitive than those erupted on other islands. However, the effects of water on the crystallisation and ascent of magmas are, as previously stated, poorly understood.

7.2 Implications for island arcs in general

7.2.1 Nature of the slab-derived component

There is strong evidence that island arc magmas include a component derived from the subducted oceanic lithosphere, in particular their hydrous nature and their isotopic compositions of Nd and Sr. This slab-derived component may be either a melt or simply a hydrous fluid. Any partial melt produced from the subducted oceanic crust and/or overlying sediments is unlikely, however, to be able to pass through the overriding mantle wedge without reaction and it appears to be generally accepted that this mantle is the ultimate source of island arc magmas (Ringwood, 1974).

Isotopic evidence has been used to suggest that sediments have been involved in the slab-derived component of some arcs (e.g. Kay, 1977; Magaritz et al., 1978; Whitford and Jezek, 1979) but not of others, while Hawkesworth, DePaulo and co-workers have interpreted isotopic data as demonstrating the involvement of subducted oceanic crust (Hawkesworth et al., 1977, 1979a, 1979b; DePaulo and Wasserburg, 1977; DePaulo and Johnson, 1979). Rare earth evidence was used by Gill (1974) and later workers to demonstrate that many andesites cannot be direct partial melts of subducted oceanic crust. This suggests that the slab-derived component may not be contributing directly to island arc magmas. The continuous supply of subducted oceanic crust, and possibly also sediments, to the mantle, and the likely reaction of any slab-derived component with it, suggest that open-system contamination processes are likely to operate in the mantle overriding the subducted lithosphere. The effects of these may be complicated, as appears to be the case in Grenada, by pre-existing heterogeneity in the mantle. Additional difficulties in defining the nature of the slab-derived component result from a lack of understanding of the likely mineral assemblages in the

subducted lithosphere at different depths, partly the consequence of the crude thermal models.

Despite this lack of knowledge of the slab-derived component, incompatible element studies suggest that alkalis and alkaline earth elements are important components of it, together with water. The Grenada data also suggest that LREE can be mobilised from the subducted lithosphere. Further studies of incompatible element abundances in island arc volcanics may prove useful.

7.2.2 Spatial variation in the chemistry of island arc volcanics

Spatial chemical variation across the strike of island arcs is well documented (Kuno, 1966; Jakes and White, 1972) and involves an increase in incompatible element concentrations and LREE enrichment and a decrease in K/Rb ratios, at comparable silica contents with depth to the Benioff zone. Where sufficient data exist, it is, however, clear that the concentrations of compatible elements such as FeO, MgO, CaO, Ni, Cr and V are not similarly variable, which implies that the degrees of melting of the mantle and of subsequent fractionation of the magmas produced, are not greatly different at different depths to the Benioff zone. This, in turn, implies that the chemical differences between rocks of the island arc tholeiite, calc-alkaline and shoshonitic associations (Jakes and White, 1972) are a reflection of variation in the composition of their sources with depth, unless very small degrees of melting are involved.

This chemical variation in the source may result from addition of a component derived from the subducted lithosphere, or may have existed prior to subduction, at least in part, as a vertical chemical zonation of the mantle. Most tholeiitic and calc-alkaline island arc rocks have very low Nb contents and Zr/Y ratios compared with mid-ocean ridge basalts and, more strikingly, with intra-plate alkaline basalts. These

chemical features indicate derivation from depleted mantle sources. This is also indicated in island arc tholeiites by their low K contents and very high K/Rb ratios. Hawkesworth and Powell (in press) and Pearce (in press) have suggested that the relative mobility of alkaline earth elements, such as Sr, from the subducted slab, in comparison with LREE, leads to low Ce/Sr ratios in island arc basalts compared with basalts from mid-ocean ridges. The general increase in Ce/Sr ratios with increasing depth to the Benioff zone in island arcs would thus indicate either an increasing contribution of LREE from the subducted slab with depth or else a vertical chemical zonation of the overriding mantle unrelated to the subduction process. At present it is not possible to distinguish between these possibilities although, provided sediments are not involved, Nd isotopic studies might be expected to be of use in this respect.

The important feature of the chemical variation across island arcs is that magmas with similar major element compositions have widely variable incompatible element concentrations reflecting the compositions of their sources. Therefore, although the Grenada rock suite may be somewhat atypical of island arc volcanics in terms of certain trace elements, this does not invalidate the application of its major element evolution to island arc volcanic suites in general.

7.2.3 Melting and crystallisation relations

Much consideration has been given in the last decade to the influence of water on the melting of mantle peridotites in island arcs. Experiments at high water activities by Kushiro and Yoder (1968), Kushiro (1972) and Mysen and Boettcher (1975) showed that water expands the primary phase volume of olivine relative to pyroxenes, moving the initial partial melts towards more silica-rich compositions in both synthetic and natural systems. However, the exact degree of silica

saturation of these wet melts is highly controversial. Cawthorn et al. (1973b) and Green (1973) believed that the analysed compositions of the experimental melts had been highly modified by quench crystallisation, while Kushiro, Mysen and co-workers proposed that the partial melt compositions were truly andesitic or even dacitic. Subsequent studies by Nicholls and Ringwood (1973) and Nicholls (1974) demonstrated that the postulated andesitic melts could not be in equilibrium with olivine, although controversy has persisted (e.g. Mysen et al., 1974). Regardless of the uncertainty over the experimental evidence, these water-saturated experiments are clearly unrealistic when compared with the evidence from the natural magmas. Water-saturated melts at high pressures will have very high water contents, leading to massive oversaturation in water on decompression, yet most island arc basalts are demonstrably water-undersaturated at low pressures. The evidence from Grenada indicates water contents of the primary melts of 1-2 per-cent, implying very low water activities at the site of melting. This might be expected, since the maximum amount of water which can be included in hydrous minerals in an average mantle composition is about 0.4 wt.%, and large proportions of free vapour are unlikely to exist within the mantle. If water activities are low, their effects on melting behaviour will be small. Small differences in water activity at high pressures will, however, result in larger differences in activity at low pressures, producing stronger effects on low-pressure crystallisation behaviour.

It is possible that some island arc rocks, such as the so-called 'boninites', result from melting of peridotite at high water activities. Nevertheless, it is probable that the majority of primary melts in island arcs are not greatly different in composition from those which would be produced from the same sources by anhydrous melting. During ascent,

however, the relatively high water content of island arc magmas results in extensive fractionation of olivine, producing the high - Al_2O_3, high FeO/MgO derivative basalts with low Ni and Cr contents which are typical of calc-alkaline suites, and are represented in Grenada by the C-series basalts. Such extensive olivine fractionation implies picritic parental melts. The low Ni, Cr and MgO contents of basalts from islands north of St. Vincent in the Lesser Antilles are consistent with this interpretation.

7.3 Conclusions

(a) Although the incompatible element contents of the Grenada basalts suggest a more alkaline affinity than is shown by basalts from other islands in the Lesser Antilles volcanic arc, the patterns of incompatible elements of both the M- and C-series basalts are more comparable with those of other island arc basalts than with alkaline basalts from intra-plate environments.

(b) The comparatively undersaturated nature of the Grenada magmas is probably a function of the depth and/or degree of melting of their source peridotite.

(c) Basalts comparable in major element chemistry with M-series and C-series rocks from Grenada are found on the other islands of the Lesser Antilles arc. Their differences in incompatible element and isotopic characteristics reflect differences in their source compositions, rather than in the melting and crystallisation processes responsible for their production. This suggests that the Grenada model of picritic parent magmas is applicable to the other islands in the Lesser Antilles arc.

(d) The unusual presence of primitive magmas at the surface in Grenada may be a consequence of the island's position near the

end of a destructive plate margin, or of unusually high water contents of the magmas.

(e) Chemical and isotopic evidence indicates that water, alkalis, and alkaline earth elements are important constituents of the fluid or melt derived from the subducted oceanic lithosphere. This slab-derived component probably reacts with the overriding mantle wedge in an open-system contamination process.

(f) The spatial chemical variation across many island arcs suggests that basalts with differing trace element characteristics originated by similar melting and crystallisation processes. The spatial variation reflects variable contributions from the subducted slab with depth and/or pre-subduction vertical chemical zonation in the overriding mantle.

(g) The water contents of island arc magmas are probably insufficient, in most cases, for water to have had a strong effect on the melting relations of their peridotite source. They are, however, likely to be sufficiently high to have affected crystallisation behaviour at lower pressures, principally by stabilisation of olivine relative to pyroxenes. This effect will result in the production of the high - Al_2O_3 derivative basalts with low compatible trace element contents, typical of island arc volcanic suites, from picritic parent magmas.

ACKNOWLEDGEMENTS

This project could not have been initiated without the assistance of R. J. Arculus, who generously made his samples available for further study. I am also indebted to M. J. O'Hara and J. G. Fitton for their guidance of the project during their respective periods of supervision.

Professors Sir Frederick Stewart and G. Y. Craig placed the excellent research facilities of the Grant Institute at my disposal. Mr. C. Chaplin and his technical staff provided assistance throughout the work.

In the collection of data, particular thanks are due to Peter Hill and Cameron Begg for advice and assistance with the operation of the electron microprobe, and for its admirable reliability. I also wish to thank Cliff Ford and Cameron Begg for instruction and advice in the operation of the experimental equipment, and Cliff Ford and Gordon Biggar for advice on experimental techniques.

I am indebted to Michael Saunders for his instruction in chemical analysis, particularly his work in developing the analytical method for iron in experimental charges. Accurate whole-rock chemical data could not have been obtained without the X.R.F. techniques developed by Matthew Thirlwall and Godfrey Fitton, to whom I am most grateful. Matthew Thirlwall also kindly analysed the isotopic compositions of several samples.

Geoff Yarwood gave much assistance with early computing problems. The use of programs written by D. J. Humphries, C. E. Ford, M. F. Thirlwall, and R. F. Cheeney is acknowledged. Matthew Thirlwall's graph-plotting program proved to be a considerable time-saver.

Field work was greatly assisted by J. F. Tomblin and the staff of the Seismic Research Unit in Trinidad, who also provided samples for study. Many people in Grenada provided hospitality.

I wish to thank Colin Graham, Peter Jackson and many others for

stimulating discussion. Chris Hawkesworth and Mike Norry very kindly made available their unpublished data. Godfrey Fitton, Gordon Biggar, Ben Harte and Brian Upton carefully read and criticised chapters of the manuscript.

Finally, this thesis could not have been completed without the printing of photomicrographs and diagrams by Diana Baty and Karol Swanson, the patient deciphering and typing of the manuscript by Lucian Begg, the moral support of my family and friends, and the financial support of a Natural Environment Research Council research studentship.

REFERENCES

ABBEY, S. 1977. Studies in "standard samples" for use in the general analysis of silicate rocks and minerals. Part 5: 1977 edition of "usable" values. Geol. Surv. Canada. Paper 77-34.

ALLEGRE, C. J., MINSTER, J. F. 1978. Quantitative models of trace element behaviour in magmatic processes. Earth Planet. Sci. Lett. 38, 1-25.

ALLEGRE, C. J., TREUIL, M., MINSTER, J. F., MINSTER, J. B., ALBAREDE, F. 1977. Systematic use of trace elements in igneous processes; Part I: Fractional crystallisation processes in volcanic suites. Contrib. Mineral. Petrol. 60, 57-75.

ALLEN, J. C., BOETTCHER, A. L., MARLAND, G. 1975. Amphiboles in andesite and basalt: I. Stability as a function of P-T-f_{O_2}. Am. Mineral. 60, 1069-1085.

ALLEN, J. C., BOETTCHER, A. L. 1978. Amphiboles in andesite and basalt: II. Stability as a function of P-T-f_{H_2O}-f_{O_2}. Am. Mineral. 63, 1074-1087.

AOKI, K., PRINZ, M. 1974. Chromian spinels in lherzolite inclusions from Itinome-gata, Japan. Contrib. Mineral. Petrol. 46, 249-256.

ARCULUS, R. J. 1973. The alkali basalt, andesite association of Grenada, Lesser Antilles. Unpubl. Ph.D. thesis, Univ. Durham.

ARCULUS, R. J. 1974. Solid solution characteristics of spinels: pleonaste-chromite-magnetite compositions in some island-arc basalts. Carnegie Inst. Wash. Year Book 73, 322-327.

ARCULUS, R. J. 1975. Melting behaviour of two basanites in the range 10-35 kbar and the effect of TiO_2 on the olivine-diopside reactions at high pressures. Carnegie Inst. Wash. Year Book 74, 512-515.

ARCULUS, R. J. 1976. Geology and geochemistry of the alkali basalt - andesite association of Grenada, Lesser Antilles. Geol. Soc. Am. Bull. 87, 612-24.

ARCULUS, R. J. 1978. Mineralogy and petrology of Grenada, Lesser Antilles island arc. Contrib. Mineral. Petrol. 65, 413-424.

ARCULUS, R. J., CURRAN, E. B. 1972. The genesis of the calc-alkaline rock suite. Earth Planet. Sci. Lett. 15, 255-262.

ARCULUS, R. J., WILLS, K. J. A. The petrology of plutonic blocks and inclusions from the Lesser Antilles island arc. Manuscript in preparation.

ARNDT, N. T. 1977. Partitioning of nickel between olivine and ultrabasic and basic komatiite liquids. Carnegie Inst. Wash. Year Book 76, 553-557.

ARTH, J. G. 1976. Behaviour of trace elements during magmatic processes - a summary of theoretical models and their applications. J. Res. U.S. Geol. Survey 4, 41-47.

BACON, C. R., CARMICHAEL, I. S. E. 1973. Stages in the P-T path of ascending basalt magma: an example from San Quintin, Baja California. Contrib. Mineral. Petrol. 41, 1-22.

BAKER, B. H., GOLES, G. G., LEEMAN, W. P., LINDSTROM, M. M. 1977. Geochemistry and petrogenesis of a basalt-benmoreite-trachyte suite from the southern part of the Gregory Rift, Kenya. Contrib. Mineral. Petrol. 64, 303-332.

BAKER, P. E. 1963. The geology of Mt. Misery volcano, St. Kitts. Unpubl. D. Phil. thesis, Univ. Oxford.

BAKER, P. E. 1968. Petrology of Mt. Misery volcano, St. Kitts. Lithos 1, 124-150.

BASU, A. R. 1975. Hot spots, mantle plumes, and a model for the origin of ultramatic xenoliths in alkali basalts. Earth Planet. Sci. Lett. 28, 261-274.

BAXTER, A. N. 1972. Magmatic evolution of Mauritius, western Indian Ocean. Unpubl. Ph.D. thesis, Univ. Edinburgh.

BEST, M. G. 1974. Contrasting types of chromium-spinel peridotite xenoliths in basanitic lavas, western Grand Canyon, Arizona. Earth Planet. Sci. Lett. 23, 229-237.

BESWICK, A. E., CARMICHAEL, I.S.E. 1978. Constraints on mantle source compositions imposed by phosphorus and rare-earth elements. Contrib. Mineral. Petrol. 67, 317-330.

BICKLE, M. J., FORD, C. E., NISBET, E. G. 1977. The petrogenesis of peridotitic komatiites: evidence from high-pressure melting experiments. Earth Planet. Sci. Lett. 37, 97-106.

BICKLE, M. J., HAWKESWORTH, C. J., MARTIN, A., NISBET, E. G., O'NIONS, R. K. 1976. Mantle composition derived from the chemistry of ultramafic lavas. Nature 263, 577-580.

BOTTINGA, Y., KUDO, A., WEILL, D. F. 1966. Some observations on oscillatory zoning and crystallisation of magmatic plagioclase. Am. Mineral. 51, 792-806.

BRIDEN, J. C., REX, D. C., FALLER, A. M., TOMBLIN, J. F. 1979. K-Ar geochronology and palaeomagnetism of volcanic rocks in the Lesser Antilles island arc. Phil. Trans. R. Soc. Lond. A. 291, 485-528.

BRIDGEMAN, P. W. 1911. Mercury - liquid and solid under pressure. Proc. Amer. Acad. Arts Sci. 47, 388.

BROUSSE, R. 1968. La place des ultra-basites en France. Geol. Rundschau 57, 621-655.

BROWN, G. M., HOLLAND, J. G., SIGURDSSON, H., TOMBLIN, J. F., ARCULUS, R. J. 1977. Geochemistry of the Lesser Antilles volcanic island arc. Geochim. Cosmochim. Acta 41, 785-801.

BROWN, G. M., SCHAIRER, J. F. 1971. Chemical and melting relations of some calc-alkaline volcanic rocks. Geol. Soc. Am. Memoir 130, 139-157.

BURNHAM, C. W. 1975. Water and magmas: a mixing model. Geochim. Cosmochim. Acta 39, 1077-1084.

BURNHAM, C. W. 1979. The importance of volatile constituents. In: Evolution of the igneous rocks: fiftieth anniversary perspectives (H. S. Yoder, ed.) pp. 439-482. Princeton: University Press.

BURNHAM, C. W., DAVIS, N. F. 1971. The role of H_2O in silicate melts. I: P-V-T relations in the system $NaAlSi_3O_8$-H_2O to 10 kilobars and 1000°C. Am. J. Sci. 270, 54-79.

BURNHAM, C. W., DAVIS, N. F. 1974. The role of H_2O in silicate melts. II: Thermodynamic and phase relations in the system $NaAlSi_3O_8$-H_2O to 10 kilobars, 700° to 1100°C. Am. J. Sci. 274, 902-940.

BURNHAM, C. W., JAHNS, R. H. 1962. A method for determining the solubility of water in silicate melts. Am. J. Sci. 260, 721-745.

CAMPBELL, I. H. 1978. Some problems with the cumulus theory. Lithos 11, 311-323.

CAWTHORN, R. G. 1976. Melting relations in part of the system CaO-MgO-Al_2O_3-SiO_2-Na_2O-H_2O under 5 kb pressure. J. Petrology 17, 44-72.

CAWTHORN, R. G., CURRAN, E. B., ARCULUS, R. J. 1973a. A petrogenetic model for the origin of the calc-alkaline suite of Grenada, Lesser Antilles. J. Petrology 14, 327-338.

CAWTHORN, R. G., FORD, C. E., BIGGAR, G. M., BRAVO, M. S., CLARKE, D. B. 1973b. Determination of the liquid composition in experimental samples: discrepancies between microprobe analysis and other methods. Earth Planet. Sci. Lett. 21, 1-5.

CAWTHORN, R. G., O'HARA, M. J. 1976. Amphibole fractionation in calc-alkaline magma genesis. Am. J. Sci. 276, 309-329.

CHAMPNESS, P. E. 1970. Nucleation and growth of iron oxides in olivine. Mineral. Mag. 37, 790-800.

CHARLU, T. V., NEWTON, R. C., KLEPPA, O. J. 1975. Enthalpies of formation at 970°K of some compounds in the system MgO-Al_2O_3-SiO_2 from high temperature solution calorimetry. Geochim. Cosmochim. Acta 39, 1487-1497.

CHARLU, T. V., NEWTON, R. C., KLEPPA, O. J. 1978. Enthalpy of formation of some lime silicates by high-temperature solution calorimetry, with discussion of high pressure phase equilibria. Geochim. Cosmochim. Acta 42, 367-375.

CLARK, S. P. 1966. Solubility.
In: Handbook of physical constants (S. P. Clark, ed.) pp. 415-436. Geol. Soc. Am. Memoir 97.

CRAIG, J. R., SCOTT, S. D. 1974. Sulfide phase equilibria.
In: Sulfide Mineralogy (P. H. Ribbe, ed.) pp. 1-110. Washington: Mineralogical Society of America.

DANCKWERTH, P. A., NEWTON, R. C. 1978. Experimental determination of the spinel peridotite to garnet peridotite reaction in the system MgO-Al_2O_3-SiO_2 in the range 900°-1100°C and Al_2O_3 isopleths of enstatite in the spinel field. Contrib. Mineral. Petrol. 66, 189-201.

DeLONG, S. E., HODGES, F. N., ARCULUS, R. J. 1975. Ultramafic and mafic inclusions, Kanaga Island, Alaska, and the occurrence of alkaline rocks in island arcs. J. Geol. 83, 721-736.

DePAULO, D. J., JOHNSON, R. W. 1979. Magma genesis in the New Britain island arc: constraints from Nd and Sr isotopes and trace-element patterns. Contrib. Mineral. Petrol. 70, 367-379.

DePAULO, D. P., WASSERBURG, G. J. 1977. The sources of island arcs as indicated by Nd and Sr isotopic studies. Geophys. Res. Lett. 4, 465-468.

DONALDSON, C. H. 1976. An experimental investigation of olivine morphology. Contrib. Mineral. Petrol. 57, 187-213.

DONALDSON, C. H. 1978. Petrology of the uppermost mantle deduced from spinel-lherzolite and harzburgite nodules at Calton Hill, Derbyshire. Contrib. Mineral. Petrol. 65, 363-377.

DONALDSON, C. H. 1979. An experimental investigation of the delay in nucleation of olivine in mafic magmas. Contrib. Mineral. Petrol. 69, 21-32.

DONNELLY, T. W., ROGERS, J. J. W., PUSHKAR, P., ARMSTRONG, R. L. 1971. Chemical evolution of the igneous rocks of the eastern West Indies: an investigation of thorium, uranium, and potassium distributions, and lead and strontium isotopic ratios. Geol. Soc. Am. Memoir 130, 181-224.

DRAKE, M. J., WEILL, D. F. 1975. Partition of Sr, Ba, Ca, Y, Eu^{2+}, Eu^{3+}, and other REE between plagioclase feldspar and magmatic liquid: an experimental study. Geochim. Cosmochim. Acta 39, 689-712.

DUNCUMB, P., JONES, E. M. 1969. Electron probe microanalysis: an easy to use computer program for correcting quantitative data. Tube Investments Research Laboratories, Saffron Walden, Cambridge.

EGGLER, D. H. 1972a. Amphibole stability in H_2O-undersaturated calc-alkaline melts. Earth Planet. Sci. Lett. 15, 28-34.

EGGLER, D. H. 1972b. Water-saturated and undersaturated melting relations in a Paricutin andesite and an estimate of water content in the natural magma. Contrib. Mineral. Petrol. 34, 261-271.

EGGLER, D. H. 1974. Effect of CO_2 on the melting of peridotite. Carnegie Inst. Wash. Year Book 73, 215-224.

EGGLER, D. H. 1978. The effect of CO_2 upon partial melting of peridotite in the system Na_2O-CaO-Al_2O_3-MgO-SiO_2-CO_2 to 35 kb, with an analysis of melting in a peridotite - H_2O - CO_2 system. Am. J. Sci. 278, 305-343.

EGGLER, D. H., BURNHAM, C. W. 1973. Crystallisation and fractionation trends in the system andesite-H_2O-CO_2-O_2 at pressures to 10 kb. Geol. Soc. Am. Bull. 84, 2517-2532.

EGGLER, D. H., KADIK, A. A. 1979. The system $NaAlSi_3O_8$-H_2O-CO_2 to 20 kbar pressure: I. Compositional and thermodynamic relations of liquids and vapours coexisting with albite. Am. Mineral. 64, 1036-1048.

ELTHON, D., RIDLEY, W. I. 1978. Comments on: "The partitioning of nickel between olivine and silicate melt" by S. R. Hart and K. E. Davis. Earth Planet. Sci. Lett. 44, 162-164.

EUGSTER, H. P., WONES, D. R. 1962. Stability relations of the ferruginous biotite, annite. J. Petrology 3, 82-125.

EVANS, B. W., FROST, B. R. 1975. Chrome-spinel in progressive metamorphism - a preliminary analysis. Geochim. Cosmochim. Acta 39, 959-972.

FABRIES, J. 1979. Spinel-olivine geothermometry in peridotites from ultramafic complexes. Contrib. Mineral. Petrol. 69, 329-336.

FITTON, J. G., GILL, R. C. O. 1970. The oxidation of ferrous iron in rocks during mechanical grinding. Geochim. Cosmochim. Acta 34, 518-524.

FORD, C. E. 1972. Furnace design, temperature distribution, calibration and seal design in internally heated pressure vessels. In: Progress in experimental petrology. Second report, pp. 89-96. London: Natural Environment Research Council Publications, Series D, No. 2.

FORD, C. E. 1978. Platinum-iron alloy sample containers for melting experiments on iron-bearing rocks, minerals, and related systems. Mineral. Mag. 42, 271-275.

FOX, P. J., SCHREIBER, E., HEEZEN, B. C. 1971. The geology of the Caribbean crust: Tertiary sediments, granitic and basic rocks from the Aves Ridge. Tectonophysics 12, 89-109.

FREY, F. A., GREEN, D. H. 1974. The mineralogy, geochemistry and origin of lherzolite inclusions in Victorian basanites. Geochim. Cosmochim. Acta 38, 1023-1059.

FREY, F. A., PRINZ, M. 1978. Ultramafic inclusions from San Carlos, Arizona: petrologic and geochemical data bearing on their petrogenesis. Earth Planet. Sci. Lett. 38, 129-176.

FRISCH, T. 1971. Alteration of chromite in a dunite nodule from Lanzarote, Canary Islands. Lithos 4, 83-91.

GIBB, F. G. F. 1974. Supercooling and the crystallisation of plagioclase from a basaltic magma. Mineral. Mag. 39, 641-653.

GILL, J. B. 1974. Role of underthrust oceanic crust in the genesis of a Fijian calc-alkaline suite. Contrib. Mineral. Petrol. 43, 29-45.

GILL, J. B. 1978. Role of trace element partition coefficients in models of andesite genesis. Geochim. Cosmochim. Acta 42, 709-724.

GREEN, D. H. 1970. The origin of basaltic and nephelinitic magmas. Trans. Leics. Lit. and Phil. Soc. 64, 28-54.

GREEN, D. H. 1973. Experimental melting studies on a model upper mantle composition at high pressures under water-saturated and water-undersaturated conditions. Earth Planet. Sci. Lett. 19, 37-53.

GRAHAM, A. M., SAUNDERS, M. J. 1978. A rapid wet-chemical method for the determination of total iron content of experimental charges. In: Progress in experimental petrology. Fourth report, pp. 124-125. London: Natural Environment Research Council Publication tions, Series D, No. 11.

GRAHAM, A. M., THIRLWALL, M. F. Petrology of the 1979 eruption of Soufriere volcano, St. Vincent, Lesser Antilles (in preparation).

GREENBAUM, D. 1977. The chromitiferous rocks of the Troodos Ophiolite Complex, Cyprus. Econ. Geol. 72, 1175-1194.

GUNN, B. M., ROOBOL, M. J., SMITH, A. L. 1974. Petrochemistry of the Pelean-type volcanoes of Martinique. Geol. Soc. Am. Bull. 85, 1023-1030.

HAGGERTY, S. E. 1976. Opaque mineral oxides in terrestrial igneous rocks.
In: Oxide Minerals (D. Rumble, ed.) pp. 101-300. Washington: Mineralogical Society of America.

HAMILTON, D. L., ANDERSON, G. M. 1967. Effects of water and oxygen pressures on the crystallisation of basaltic magmas. In: Basalts: the Poldevaart treatise on rocks of basaltic composition (H. H. Hess and A. Poldevaart, eds.) pp. 445-482. New York : Interscience.

HANSON, G. N., LANGMUIR, C. H. 1978. Modelling of major elements in mantle-melt systems using trace element approaches. Geochim. Cosmochim. Acta 42, 725-741.

HART, S. R., BROOKS, C. K. 1974. Clinopyroxene-matrix partitioning of K, Rb, Cs, Sr and Ba. Geochim. Cosmochim. Acta 38, 1799-1806.

HART, S. R., DAVIS, K. E. 1978. Nickel partitioning between olivine and silicate melt. Earth Planet. Sci. Lett. 40, 203-219.

HARTE, B. 1977. Rock nomenclature with particular relation to deformation and recrystallisation textures in olivine-bearing xenoliths. J. Geol. 85, 279-288.

HARTE, B., GURNEY, J. J., COX, K. G. 1977. Clinopyroxene-rich sheets in garnet-peridotite: xenolith specimens from the Matsoku kimberlite pipe, Lesotho. Extended Abstr., 2nd Internat. Kimberlite Conf., Santa Fe.

HAWKESWORTH, C. J., NORRY, M. J., RODDICK, J. C., BAKER, P. E., FRANCIS, P. W., THORPE, R. S. 1979a. $^{143}Nd/^{144}Nd$, $^{87}Sr/^{86}Sr$, and incompatible element variations in calc-alkaline andesites and plateau lavas from South America. Earth Planet. Sci. Lett. 42, 45-57.

HAWKESWORTH, C. J., NORRY, M. J., RODDICK, J. C., VOLLMER, R. 1979c. $^{143}Nd/^{144}Nd$ and $^{87}Sr/^{86}Sr$ ratios from the Azores and their significance in LIL-element enriched mantle. Nature 280, 28-31.

HAWKESWORTH, C. J., O'NIONS, R. K., ARCULUS, R. J. 1979b. Nd and Sr isotope geochemistry of island arc volcanics, Grenada, Lesser Antilles. Earth Planet. Sci. Lett. 45, 237-248.

HAWKESWORTH, C. J., O'NIONS, R. K., PANKHURST, R. J., HAMILTON, P. J., EVENSEN, N. M. 1977. A geochemical study of island- arc and back-arc tholeiites from the Scotia Sea. Earth Planet. Sci. Lett. 36, 253-262.

HAWKESWORTH, C. J., POWELL, M. On the origin of andesites in the Lesser Antilles island arc. Earth Planet. Sci. Lett. (in press).

HELZ, R. T. 1973. Phase relations of basalts in their melting range at P_{H_2O} = 5 kb as a function of oxygen fugacity. Part I. Mafic phases. J. Petrology 14, 249-302.

HELZ, R. T. 1976. Phase relations of basalts in their melting ranges at P_{H_2O} = 5 kb. Part II. Melt compositions. J. Petrology 17, 139-193.

HEDGE, C. E., LEWIS, J. F. 1971. Isotopic composition of strontium in three basalt-andesite centres along the Lesser Antilles arc. Contrib. Mineral. Petrol. 32, 39-47.

HERZBERG, C. T. 1978. Pyroxene geothermometry and geobarometry: experimental and thermodynamic evaluation of some subsolidus phase relations involving pyroxenes in the system $CaO-MgO-Al_2O_3-SiO_2$. Geochim. Cosmochim. Acta 42, 945-957.

HILL, R., ROEDER, P. L. 1974. The crystallisation of spinel from basaltic liquid as a function of oxygen fugacity. J. Geol. 82, 709-729.

HOFMANN, A. W., HART, S. R. 1978. An assessment of local and regional isotopic equilibrium in the mantle. Earth Planet. Sci. Lett. 38, 44-62.

HOLLOWAY, J. R. 1973. The system pargasite-H_2O-CO_2: a model for melting of a hydrous mineral with a mixed volatile fluid. I: Experimental results to 8 kbars. Geochim. Cosmochim. Acta 37, 651-666.

HOLLOWAY, J. R. 1976. Fugacity and activity coefficients of molecular species in fluids at high pressures and temperatures. Carnegie Inst. Wash. Year Book 75, 771-775.

HOLLOWAY, J. R., BURNHAM, C. W. 1972. Melting relations of basalt with equilibrium water pressure less than total pressure. J. Petrology 13, 1-29.

HOLLOWAY, J. R., EGGLER, D. H., DAVIS, N. F. 1971. An analytical expression for calculating the fugacity and free energy of H_2O to 10,000 bars and 1300°C. Geol. Soc. Am. Bull. 82, 2639-2642.

HOLLOWAY, J. R., FORD, C. E. 1975. Fluid-absent melting of the fluoro-hydroxy amphibole pargasite to 35 kilobars. Earth Planet. Sci. Lett. 25, 44-48.

HOLLOWAY, J. R., REESE, R. L. 1974. The generation of N_2-CO_2-H_2O fluids for use in hydrothermal experimentation. I. Experimental method and equilibration calculations in the C-O-H-N system. Am. Mineral. 59, 587-597.

HSUI, A. T., TOKSOZ, M. N. 1979. The evolution of thermal structures beneath a subduction zone. Tectonophysics 60, 43-60.

IRVINE, T. N. 1965. Chromian spinel as a petrogenetic indicator. Part I, Theory. Can. J. Earth Sci. 2, 648-672.

JACKSON, P. M. Ultramafic xenoliths, and the lower crust and upper mantle beneath southern Africa. Ph.D. thesis, Univ. Edinburgh (in prep.).

JACKSON, T. A. 1970. Geology and petrology of the volcanic rocks of Carriacou. Unpubl. M.Sc. thesis, Univ. West Indies, Jamaica.

JAKES, P., WHITE, A. J. R. 1972. Major and trace element variations in volcanic rocks from island arc areas. Geol. Soc. Am. Bull. 83, 29-40.

JOHANNES, W. 1978. Melting of plagioclase in the system Ab-An-H_2O and Qz-Ab-An-H_2O at P_{H_2O} = 5 kbars, an equilibrium problem. Contrib. Mineral. Petrol. 66, 195-303.

KAY, R. W. 1977. Geochemical constraints on the origin of Aleutian magmas.
In: Island Arcs, Deep Sea Trenches and Back-Arc Basins (M. Talwani and W. C. Pitman, ed.). Washington: Am. Geophys. Union.

KERRICK, D. M., DARKEN, L. S. 1975. Statistical thermodynamic models for ideal oxide and silicate solid solutions, with application to plagioclase. Geochim. Cosmochim. Acta 39, 1431-1442.

KESSON, S. E., HOLLOWAY, J. R. 1974. The generation of N_2-CO_2-H_2O fluids for use in hydrothermal experimentation. II. Melting of albite in a multispecies fluid. Am. Mineral. 59, 598-603.

KHITAROV, N. I., KADIK, A. A., LEBEDEV, E. B. 1963. Estimate of thermal effects of separation of water from felsic melts based on data for the system albite-water. Geochem., 1963, 7, 637-649.

KORRINGA, M. K., NOBLE, D. C. 1971. Distribution of Sr and Ba between natural feldspar and igneous melt. Earth Planet. Sci. Lett. 11, 147-151.

KUNO, H. 1966. Lateral variation of basalt magma type across continental margins and island arcs. Bull. Volcanol. 29, 195-222.

KUSHIRO, I. 1972. Effect of water on the compositions of magmas formed at high pressures. J. Petrology 13, 311-334.

KUSHIRO, I., YODER, H. S. 1966. Anorthite-forsterite and anorthite-enstatite reactions and their bearing on the basalt-eclogite transformation. J. Petrology 7, 337-362.

KUSHIRO, I., YODER, H. S. 1968. Melting of forsterite and enstatite at high pressures under hydrous conditions. Carnegie Inst. Wash. Year Book 67, 153-158.

LACROIX, A. 1904. La Montagne Pelee et ses eruptions. Paris: Masson et Cie, 366 pp.

LANGMUIR, C. H., VOCKE, R. D., HANSON, G. N., HART, S. R. 1978. A general mixing equation with applications to Icelandic basalts. Earth Planet. Sci. Lett. 37, 380-392.

LEAKE, B. E. 1978. Nomenclature of amphiboles. Mineral. Mag. 42, 533-563.

LEEMAN, W. P. 1973. Partitioning of Ni and Co between olivine and basaltic liquid: an experimental study. Trans. Am. Geophys. Union 54, 1222.

LEEMAN, W. P., MA, M.-S., MURALI, A. V., SCHMITT, R. A. 1978. Empirical estimation of magnetite/liquid distribution coefficients for some transition elements. A correction. Contrib. Mineral. Petrol. 66, 429.

LEEMAN, W. P., VITALIANO, C. J., PRINZ, M. 1976. Evolved lavas from the Snake River Plain: Craters of the Moon National Monument, Idaho. Contrib. Mineral. Petrol. 56, 35-60.

LEWIS, J. F. 1964. Mineralogical and petrological studies of plutonic blocks from the Soufriere volcano, St. Vincent, West Indies. Unpubl. D. Phil. thesis, Univ. Oxford.

LEWIS, J. F. 1973. Petrology of ejected plutonic blocks of the Soufriere volcano, St. Vincent, West Indies. J. Petrology 14, 81-112.

LITTLEJOHN, A. L., GREENWOOD, H. J. 1973. Lherzolite nodules in basalts from British Columbia, Canada. Can. J. Earth Sci. 11, 1288-1308.

LOFGREN, G. 1974. An experimental study of plagioclase crystal morphology: isothermal crystallisation. Am. J. Sci. 274, 243-273.

MAALOE, S., AOKI, K. 1977. The major element composition of the upper mantle estimated from the composition of lherzolites. Contrib. Mineral. Petrol. 63, 161-173.

McALLISTER, R. H., MEYER, H.O.A., BROOKINS, D. G. 1975. "Pyroxene"-ilmenite xenoliths from the Stockdale Pipe, Kansas: chemistry, crystallography and origin. In: Physics and chemistry of the earth (L. H. Ahrens, J. B. Dawson, A. R. Duncan, A. J. Erlank, ed.). vol.9, pp. 287-293. Oxford: Pergamon.

McBIRNEY, A. R., NOYES, R. M. 1979. Crystallisation and layering of the Skaergaard intrusion. J. Petrology 20, 487-554.

MAGARITZ, M., WHITFORD, D. J., JAMES, D. E. 1978. Oxygen isotopes and the origin of high $^{87}Sr/^{86}Sr$ andesites. Earth Planet. Sci. Lett. 40, 220-230.

MALPAS, J. G. 1978. Magma generation in the upper mantle, field evidence from ophiolite suites, and application to the generation of oceanic lithosphere. Phil. Trans. R. Soc. Lond. A. 288, 527-546.

MALPAS, J. G., STRONG, D. F. 1975. A comparison of chrome-spinels in ophiolites and mantle diapirs of Newfoundland. Geochim. Cosmochim. Acta 39, 1045-60.

MARTIN-KAYE, P. H. A. 1969. A summary of the geology of the Lesser Antilles. Overseas Geol. Miner. Resour. 10, 172-206.

MENZIES, M., ALLEN, C. R. 1974. Plagioclase lherzolite - residual mantle relationships within two Eastern Mediterranean ophiolites. Contrib. Mineral. Petrol. 45, 197-213.

MERRILL, R. B., WYLLIE, P. J. 1973. Absorption of iron by platinum capsules in high pressure rock melting experiments. Am. Mineral. 58, 16-20.

MINSTER, J. F., ALLEGRE, C. J. 1978. Systematic use of trace elements in igneous processes; Part III: Inverse problem of batch partial melting in volcanic suites. Contrib. Mineral. Petrol. 68, 37-52.

MINSTER, J. F., MINSTER, J. B., TREUIL, M., ALLEGRE, C. J. 1977. Systematic use of trace elements in igneous processes; Part II: Inverse problem of the fractional crystallisation process in volcanic suites. Contrib. Mineral. Petrol. 61, 49-77.

MOLNAR, P., SYKES, L. R. 1969. Tectonics of the Caribbean and Middle American regions from local mechanisms and seismicity. Geol. Soc. Am. Bull. 80, 1639-1684.

MUELLER, R. F. 1970. Oxidative capacity of magmatic components. Am. J. Sci. 270, 236-243.

MULLER, F., KLEPPA, O. J. 1973. Thermodynamics of formation of chrome spinels. J. Inorg. Nucl. Chem. 35, 2673-2678.

MYSEN, B. O., BOETTCHER, A. L. 1975. Melting of a hydrous mantle: II. Geochemistry of crystals and liquids formed by anatexis of mantle peridotite at high pressures and high temperatures as a function of controlled activities of water, hydrogen, and carbon dioxide. J. Petrology 16, 549-593.

MYSEN, B. O., KUSHIRO, I., NICHOLLS, I. A., RINGWOOD, A. E. 1974. A possible mantle origin for andesitic magmas: discussion of a paper by Nicholls and Ringwood. Earth Planet. Sci. Lett. 21, 221-229.

NAGLE, F. 1972. Rocks from the seamounts and escarpments of the Aves Ridge.
In: Trans. Caribbean Geological Conference VI (1971) pp. 409-413. Caracas: Impreso por Cromotip.

NEEF, G., PLIMER, I. R. 1979. Ophiolite complexes on Small Nggela island, Solomon Islands. Geol. Soc. Am. Bull. 90, 136-138.

NEWHALL, D. H., ABBOT, L. H., DUNN, R. A. 1963. A redetermination of the freezing pressure of mercury using improved apparatus and techniques.
In: High pressure measurement (A. A. Giardini and E. C. Lloyd, ed.). Washington: Butterworths.

NEWTON, R. C. 1978. Experimental and thermodynamic evidence for the operation of high pressures in Archaean metamorphism.
In: Archaean Geochemistry (B. F. Windley and S. M. Naqui, ed.) pp. 221-240. Amsterdam: Elsevier.

NEWTON, R. C., CHARLU, T. V., KLEPPA, O. J. 1977. Thermochemistry of high pressure garnets and clinopyroxenes in the system CaO-MgO-Al_2O_3-SiO_2. Geochim. Cosmochim. Acta 41, 369-378.

NICHOLLS, I. A. 1974. Liquids in equilibrium with peridotitic mineral assemblages at high water pressures. Contrib. Mineral. Petrol. 45, 289-316.

NICHOLLS, I. A., RINGWOOD, A. E. 1973. Effect of water on olivine stability in tholeiites and the production of silica-saturated magmas in the island-arc environment. J. Geol. 81, 285-300.

NITSAN, U. 1974. Stability field of olivine with respect to oxidation and reduction. J. Geophys. Res. 79, 706-711.

NIXON, P. H., BOYD, F. R. 1973. Petrogenesis of the granular and sheared ultrabasic nodule suite in kimberlites.
In: Lesotho kimberlites (P. H. Nixon, ed.) pp. 48-75.
Lesotho: National Development Corporation.

NORRISH, K., HUTTON, J. T. 1969. An accurate X-ray spectrographic method for the analysis of a wide range of geological samples. Geochim. Cosmochim. Acta 33, 431-453.

NORRY, M. J., TRUCKLE, P. H., LIPPARD, S. J., HAWKESWORTH, C. J., WEAVER, S. D., MARRINER, G. F. Isotopic and trace element evidence from lavas, bearing on mantle heterogeneity beneath Kenya. Phil. Trans. R. Soc. Lond. (in press).

O'HARA, M. J. 1965. Primary magmas and the origin of basalts. Scott. J. Geol. 1, 19-40.

O'HARA, M. J. 1968. The bearing of phase equilibria studies in synthetic and natural systems on the origin and evolution of basic and ultrabasic rocks. Earth-Sci. Rev. 4, 69-133.

O'HARA, M. J. 1969. The atmospheric pressure equilibrium and fractional crystallisation of basalt-like mixtures in the $MgSiO_3$-rich part of the plane $CaSiO_3$-$MgSiO_3$-Al_2O_3 and the nature of thermal divides.
In: Progress in experimental petrology. First report, pp. 129-152. London: Natural Environment Research Council.

O'HARA, M. J. 1977. Geochemical evolution during fractional crystallisation of a periodically refilled magma chamber. Nature 266, 503-507.

O'HARA, M. J., MERCY, E. L. P., SAUNDERS, M. J. 1975. Garnet-peridotite, primary ultrabasic magma and eclogite; interpretation of upper mantle processes in kimberlite. Phys. Chem. Earth 9, 571-604.

O'NIONS, R. K., HAMILTON, P. J., EVENSEN, N. M. 1977. Variations in $^{143}Nd/^{144}Nd$ and $^{87}Sr/^{86}Sr$ ratios in oceanic basalts. Earth Planet. Sci. Lett. 34, 13-22.

ORLOVA, G. P. 1962. The solubility of water in albite melts. Internat. Geol. Rev., 1964, 6, 254-258.

ORVILLE, P. M. 1972. Plagioclase cation exchange equilibria with aqueous chloride solution at 700°C and 2000 bars in the presence of quartz. Am. J. Sci. 272, 234-272.

OSBORN, E. F. 1959. Role of oxygen pressure in the crystallisation and differentiation of basaltic magma. Am. J. Sci. 257, 609-647.

OSBORN, E. F. 1978. Changes in phase relations in response to change in pressure from 1 atm. to 10 kbar for the system Mg_2SiO_4- iron oxide - $CaAl_2Si_2O_8$ - SiO_2. Carnegie Inst. Wash. Year Book 77, 784-790.

PEARCE, J. A. Geochemical evidence for the genesis and eruptive setting of lavas from Tethyan ophiolites. Proc. Int. Ophiolite Symp., Cyprus, 1979 (in press).

PEARCE, J. A., NORRY, M. J. 1979. Petrogenetic implications of Ti, Zr, Y, and Nb variations in volcanic rocks. Contrib. Mineral. Petrol. 69, 33-47.

PHILPOTTS, A. R., SCHNETZLER, C. C. 1970. Phenocryst-matrix partition coefficients for K, Rb, Sr, and Ba, with applications to anorthosite and basalt genesis. Geochim. Cosmochim. Acta 36, 1131-1166.

PIKE, J. E. N. 1876. Pressures and temperatures calculated from chromium-rich pyroxene compositions of megacrysts and peridotite xenoliths, Black Rock Summit, Nevada. Am. Mineral. 61, 725-731.

POWELL, M. 1978. Crystallisation of low-pressure cumulate nodules from the Lesser Antilles island arc. Earth Planet. Sci. Lett. 39, 162-172.

POWELL, R. 1978. The thermodynamics of pyroxene geotherms. Phil. Trans. R. Soc. Lond. A. 288, 457-469.

PRESNALL, D. C., DIXON, S. A., DIXON, J. R., O'DONNELL, T. H., BRENNER, N. L., SCHROCK, R. L., DYCUS, D. W. 1978. Liquidus phase relations on the join diopside-forsterite-anorthite from 1 atm. to 20 kbar: their bearing on the generation and crystallisation of basaltic magma. Contrib. Mineral. Petrol. 66, 203-220.

PUSHKAR, P., STEUBER, A. M., TOMBLIN, J. F., JULIAN, G. M. 1973. Strontium isotopic ratios in volcanic rocks from St. Vincent and St. Lucia, Lesser Antilles. J. Geophys. Res. 78, 1279-1287.

REA, W. J. 1970. The geology of Montserrat, British West Indies. Unpubl. D.Phil. thesis, Univ. Oxford.

RINGWOOD, A. E. 1966. The chemical composition and origin of the earth. In: Advances in Earth Science (P. M. Hurley, ed.) pp. 287-356. Cambridge, Mass.: M.I.T. Press.

RINGWOOD, A. E. 1974. The petrological evolution of island arc systems. J. Geol. Soc. Lond. 130, 183-204.

RITCHEY, J. L., EGGLER, D. H. 1978. Amphibole stability in a differentiated calc-alkaline magma chamber: an experimental investigation. Carnegie Inst. Wash. Year Book 77, 790-793.

ROBIE, R. A., WALDBAUM, D. R. 1968. Thermodynamic properties of minerals and related substances at 298.15°K (25.0°C) and one atmosphere (1.013 bars) pressure and at higher temperatures. Bull. U.S. geol. Surv. 1259.

ROEDER, P. L., CAMPBELL, I. H., JAMIESON, H. E. 1979. A re-evaluation of the olivine-spinel geothermometer. Contrib. Mineral. Petrol. 68, 325-334.

ROEDER, P. L., EMSLIE, R. F. 1970. Olivine-liquid equilibrium. Contrib. Mineral. Petrol. 29, 275-289.

ROSS, C. S., FOSTER, M. D., MYERS, A. T. 1954. Origin of dunites and of olivine-rich inclusions in basaltic rocks. Am. Mineral. 39, 693-737.

ROWLEY, K. C. 1978. Late Pleistocene pyroclastic deposits of Soufriere Volcano, St. Vincent, West Indies. Geol. Soc. Am. Bull. 89, 825-835.

SCHNETZLER, C. C., PHILPOTTS, A. R. 1970. Partition coefficients of rare-earth elements between igneous matrix material and rock-forming mineral phenocrysts - II. Geochim. Cosmochim. Acta 34, 331-40.

SHIMIZU, N. 1974. An experimental study of the partitioning of K, Rb, Cs, Sr and Ba between clinopyroxene and liquid at high pressures. Geochim. Cosmochim. Acta 38, 1789-1798.

SHIMIZU, N., ARCULUS, R. J. 1975. Rare earth element concentrations in a suite of basanitoids and alkali olivine basalts from Grenada, Lesser Antilles. Contrib. Mineral. Petrol. 50, 231-240.

SIBLEY, D. F., VOGEL, T. A., WALKER, B. M., BYERLY, G. 1976. The origin of oscillatory zoning in plagioclase: a diffusion and growth model. Am. J. Sci. 276, 275-284.

SIGURDSSON, H., SCHILLING, J. G. 1976. Spinels in mid-Atlantic ridge basalts: chemistry and occurrence. Earth Planet. Sci. Lett. 29, 7-20.

SIGURDSSON, H., SHEPHERD, J. B. 1974. Amphibole-bearing basalts from the submarine volcano Kick 'em-Jenny in the Lesser Antilles island arc. Bull. Volcanol. 38, 891-910.

SIGURDSSON, H., TOMBLIN, J. F., BROWN, G. M., HOLLAND, J. G., ARCULUS, R. J. 1973. Strongly undersaturated magmas in the Lesser Antilles island arc. Earth Planet. Sci. Lett. 18, 285-295.

STATHAM, P. J. 1975. Quantitative X-ray energy spectrometry: the application of a Si(Li) detector to electron microprobe analysis. Unpubl. Ph.D. thesis, Univ. Cambridge.

STERN, C. R., WYLLIE, P. J. 1975. Effect of iron absorption by noble-metal capsules on phase boundaries in rock-melting experiments at 30 kilobars. Am. Mineral. 60, 681-689.

SUWA, K., YUSA, Y., KISHIDA, N. 1975. Petrology of peridotite nodules from Ndonyuo Olnchoro, Samburu district, central Kenya. Phys. Chem. Earth 9, 273-286.

SWEATMAN, T. R., LONG, J. V. P. 1969. Quantitative electron-probe microanalysis of rock-forming minerals. J. Petrology 10, 332-379.

SYKES, M. L. 1979. Hydrous mineral stabilities as a function of fluid composition: a biotite melting experiment and model for melting curves. Unpubl. M.Sc. thesis, Arizona State Univ.

TAYLOR, S. R., KAYE, M., WHITE, A. J. R., DUNCAN, A. R., EWART, A. 1969. Genetic significance of Co, Cr, Ni, Sc, and V contents of andesites. Geochem. Cosmochim. Acta 33, 275-286.

THIRLWALL, M. F. 1979. The petrochemistry of the British Old Red Sandstone volcanic province. Unpubl. Ph.D. thesis, Univ. Edinburgh.

THOMPSON, R. N. 1974. Some high-pressure pyroxenes. Mineral. Mag. 39, 768-787.

TOKSOZ, M. N., MINEAR, J. W., JULIAN, B. R. 1971. Temperature fields and geophysical effects of a downgoing slab. J. Geophys. Res. 76, 1113-1138.

TOMBLIN, J. F. 1964. The volcanic history and petrology of the Soufriere region, St. Lucia. Unpubl. D.Phil. thesis, Univ. Oxford.

TOMBLIN, J. F. 1968. Chemical analyses of volcanic rocks from the Lesser Antilles. Special Publ. 15, Seismic Research Unit, Univ. West Indies, Trinidad.

TOMBLIN, J. F. 1975. The Lesser Antilles and Aves Ridge. In: The Ocean Basins and Margins (A.E.M. Nairn, F.G. Stehli, ed.) 3, pp. 467-500. New York: Plenum.

TREUIL, M. 1973. Criteres petrologiques, geochimiques et structuraux de la genese et de la differenciation des magmas basaltiques. Exemples de l'Afar. These, Orleans.

VARNE, R. 1977. On the origin of spinel lherzolite inclusions in basaltic rocks from Tasmania and elsewhere. J. Petrology 18, 1-23.

WAGER, L. R. 1962. Igneous cumulates from the 1902 eruption of Soufriere, St. Vincent. Bull. Volcanol. 24, 93-99.

WAGER, L. R., BROWN, G. M., WADSWORTH, W. J. 1960. Types of igneous cumulates. J. Petrology 1, 73-85.

WALKER, D., KIRKPATRICK, R. J., LONGHI, J., HAYS, J. F. Crystallisation history of lunar picrite basalt sample 12002: phase equilibrium and cooling rate studies. Geol. Soc. Am. Bull. 87, 646-656.

WELLS, P. R. A. 1977. Pyroxene thermometry in simple and complex systems. Contrib. Mineral. Petrol. 62, 129-139.

WESTBROOK, G. K. 1975. The structure of the crust and upper mantle in the region of Barbados and the Lesser Antilles. Geophys. J. R. astr. Soc. 43, 201-242.

WHITFORD, D. J., JEZEK, P. A. 1979. Origin of late-Cenozoic lavas from the Banda arc, Indonesia: trace element and Sr isotope evidence. Contrib. Mineral. Petrol. 68, 141-150.

WHITFORD, D. J., NICHOLLS, I. A., TAYLOR, S. R., 1979. Spatial variations in the geochemistry of Quaternary lavas across the Sunda arc in Java and Bali. Contrib. Mineral. Petrol. 70, 341-356.

WHITNEY, J. A. 1972. The effect of reduced water fugacity on buffering of oxygen in hydrothermal experiments. Am. Mineral. 57, 1902-1908.

WILLIAMS, R. J. 1972. Activity-composition relationships in the fayalite-forsterite solid solution between 900° and 1300° at low pressures. Earth Planet. Sci. Lett. 15, 296-300.

WILLS, K. J. A. 1974. The geological history of southern Dominica, and plutonic nodules from the Lesser Antilles. Unpubl. Ph.D. thesis, Univ. Durham.

WOOD, B. J. 1978. Reactions involving anorthite and $CaAl_2SiO_6$ pyroxene at high pressures and temperatures. Am. J. Sci. 278, 930-942.

WOOD, B. J. 1979. Activity-composition relationships in $Ca(Mg,Fe)Si_2O_6$-$CaAl_2SiO_6$ clinopyroxene solid solutions. Am. J. Sci. 279, 854-875.

WOOD, B. J., BANNO, S. 1973. Garnet-orthopyroxene and orthopyroxene-clinopyroxene relationships in simple and complex systems. Contrib. Mineral. Petrol. 42, 109-124.

WRIGHT, T. L., DOHERTY, P. C. 1970. A linear programming and least squares computer method for solving petrologic mixing problems. Geol. Soc. Am. Bull. 81, 1995-2008.

WYATT, B. A. 1977. The melting and crystallisation behaviour of a natural clinopyroxene-ilmenite intergrowth. Contrib. Mineral. Petrol. 61, 1-9.

WYATT, B. A., McALLISTER, R. H., BOYD, F. R., OHASHI, Y. 1975. An experimentally-produced clinopyroxene-ilmenite intergrowth. Carnegie Inst. Wash. Year Book 74, 536-539.

YODER, H. S. 1969. Calc-alkaline andesites, experimental data bearing on the origin of their assumed characteristics. Oregon Dept. Geol. and Mineral Industries Bull. 65, 77-89.

YODER, H. S., STEWART, D. B., SMITH, J. R. 1957. Feldspars. Carnegie Inst. Wash. Year Book 56, 206-214.

YODER, H. S., TILLEY, C. E. 1962. Origin of basalt magmas: an experimental study of natural and synthetic rock systems. J. Petrology 3, 342-532.

ZIELINSKI, R. A., FREY, F. A. 1970. Gough Island: evaluation of a fractional crystallisation model. Contrib. Mineral. Petrol. 29, 242-254.

APPENDIX A

MICROPROBE ANALYSIS

A.1 Introduction

Mineral analyses were obtained using a Cambridge Instruments Microscan 5 electron microprobe. Two methods of X-ray analysis are available on the Edinburgh microprobe, using wavelength or energy dispersion. Details of each of the methods are given below. In each method standards and specimens were carbon-coated simultaneously.

A.2 Wavelength-dispersive analysis

The majority of mineral analyses from Grenada rocks were obtained by wavelength-dispersive spectrometry (WDS) using a probe current of 30 nA at 20 kV. Up to four elements may be determined in one group using this method, necessitating relocation of the electron beam for successive element groups. Although more time-consuming than energy-dispersive analysis, this method allows counting times for elements to be varied to suit the analytical precision required and yields better precision for minor and trace elements.

Some difficulty in analysis of V results from interference on VKα by TiKβ. This can be largely overcome by use of the collimator slits on the Microscan 5. This leads to a decrease in count rate which was offset by use of a 50 nA probe current for the element group Ni, Cr, Mn, V. A small correction to the raw X-ray counts produced is still required, but measurements of the V counts produced by the Ti standard made in each probe session resulted in a correction of only - 0.025% V per percent Ti.

In general, background counts were measured only on standards and on one example of each phase in each specimen, unless large compositional variation of a phase was found. Only one background position

was used for Sr because of interference from SiKβ.

Data reduction and correction were carried out using computer programs written by D. J. Humphries and Duncumb and Jones (1969). Raw X-ray counts were corrected for 'dead-time', and apparent concentrations calculated. Z.A.F. corrections of the apparent concentrations are those described by Sweatman and Long (1969). In almost all cases, apparent concentrations were calculated relative to an average of measurements on standards taken before and after those on the unknown. Rarely, the amount of machine drift necessitated the use of only one set of standard measurements. Typical precisions and detection limits are given in Table A2, and analytical conditions summarised in Table A1.

A.3 Energy-dispersive analysis

The remainder of Grenada mineral analyses and all analyses of phases in experimental charges were obtained by energy-dispersive spectrometry (EDS), using the Si(Li) Link Systems detector fitted to the Edinburgh Microscan. Analyses were obtained using a 6 nA probe current at 20 kV and 100 second livetimes, with on-line spectrum processing by a Data General Nova Computer, utilising a program written by Statham (1975). The Z.A.F. correction procedures in this program are those of Sweatman and Long (1969). Calibration of the EDS system needs to be updated only infrequently. Short-term drift is corrected by reference to a Co metal monitor.

Apart from slightly increased speed, EDS has the advantage of not requiring the relocation of analysis points. Beam location in experimental charges was assisted by use of a ratemeter with audio output which could be set to record X-rays in any energy range of interest. Minimum Al counts were used to locate olivines and pyroxenes, and minimum Fe counts to locate plagioclase feldspars.

Table A1 Wavelength-dispersive analytical conditions

Element	Line	Crystal	Angle 2θ degrees	Background	Counting time (secs) peak	background	Standard
Ca	Kα	LiF	113.09	±2	40	20	wollastonite
Si	Kα	RAP	31.66	+1.5	40	20	wollastonite
Fe	Kα	LiF	57.52	±2	40	20	Fe metal
Mg	Kα	RAP	44.50	+1.5	40	20	olivine or periclase
K	Kα	PET	50.69	±1.75	40	20	orthoclase
Na	Kα	RAP	54.25	+1.5	40	20	jadeite
Ti	Kα	PET	36.67	±2	40	20	rutile or Ti metal
Al	Kα	RAP	37.24	+1.5	40	20	corundum
Ni	Kα	LiF	48.67	±2	60 lavas 80	20 40	Ni metal
Cr	Kα lavas	Quartz LiF	40.05 69.31	±2 ±2	40	20	Cr metal
Mn	Kα	LiF	62.93	±2	40	20	Mn metal
V	Kα	Quartz	43.98	±2	40	20	V metal
Cl	Kα	PET	65.48	±2	60	20	NaCl
F	Kα	RAP	89.07	+1.5	60	20	$(Co,Zn)F_2$
Sr	Lα	PET	103.45	+2	200	200	celestite

Flow counters used for all elements.

Ni, Cr, Mn, V, Cl, F, Sr in cumulates and peridotites analysed with a probe current of 50nA. All other analyses at 30nA.

Accelerating potential of 20kV used throughout.

Cr and V analysed on Quartz with slits in.

Table A2 Precision and detection limits of typical wavelength-dispersive electron microprobe analyses

Pyroxene 06501

oxide	analysis	precision ± 2σ	detection limit
SiO_2	49.39	.284	.024
TiO_2	0.64	.048	.032
Al_2O_3	4.83	.080	.012
Cr_2O_3	0.02	.026	.019
V_2O_3	0.03	.030	.019
FeO	8.17	.196	.030
MnO	0.25	.040	.027
MgO	14.20	.132	.015
NiO	0.01	.031	.037
CaO	20.31	.306	.085
Na_2O	0.42	.045	.020
K_2O	0.02	.015	.014

Amphibole 06501

oxide	analysis	precision ± 2σ	detection limit
SiO_2	40.57	.268	.025
TiO_2	1.98	.066	.032
Al_2O_3	13.52	.129	.012
Cr_2O_3	0.02	.023	.019
V_2O_3	0.05	.018	.017
FeO	10.43	.218	.032
MnO	0.11	.034	.028
MgO	14.50	.138	.017
NiO	0.02	.051	.037
CaO	11.90	.218	.036
Na_2O	2.80	.092	.020
K_2O	0.61	.028	.014
Cl	0.14	.015	.008

Plagioclase 10502

oxide	analysis	precision ± 2σ	detection limit
SiO_2	44.23	.278	.025
TiO_2	0.00	-	.032
Al_2O_3	34.57	.184	.014
FeO	0.46	.059	.036
MgO	0.07	.020	.017
CaO	19.05	.274	.038
SrO	0.08	.024	.014
Na_2O	0.64	.048	.020
K_2O	0.00	-	.017

Formulae used:

$$\text{detection limit} = \frac{3}{m}\sqrt{\frac{R_b}{T_b}}$$

$$\text{precision} \quad \sigma = \frac{100}{T_p} \times \frac{1}{\sqrt{R_p} - \sqrt{R_b}} \quad \%$$

where m = counts sec^{-1} $\%^{-1}$

R_b = background count rate

T_b = time on background (secs)

R_p = peak count rate

T_p = time on peak (secs)

Key to mineral analysis tables

	1	- table number (referred to in text)
	07801	- probe number (last 3 characters of sample no. and analysis no.)
	E	- W = WDS analysis, E = EDS analysis
SIO2	48.13	
TIO2	1.21	
AL203	6.17	
CR203	0.69	
FEO	5.63	
MNO	0.13	
MGO	14.11	
NIO	0.00	- zero values represent elements either not analysed or, in EDS analyses, concentrations not detectable
CAO	23.83	
NA2O	0.00	
K2O	0.00	
TOTAL	99.90	

Where a probe number terminates in a letter, the letter represents a point in a grain analysed in a number of places. Successive letters represent successive points from core (no letter) to rim (highest letter)

Ferric iron has been calculated in spinels assuming 3 cations per 4 oxygens

Key to elements analysed

olivine Si*, Ti*, Al*, Cr, V, Fe*, Mn*, Mg*, Ni*, Ca*

pyroxene Si*, Ti*, Al*, V, Fe*, Mn*, Mg*, Ni, Ca*, Na*, K

amphibole Si*, Ti*, Al*, Cr, V, Fe*, Mn*, Mg*, Ni, Ca*, Na*, K*, Cl*, F

plagioclase Si*, Ti*, Al*, Fe*, Mg*, Ca*, Na*, K*, Sr

spinel Si*, Ti*, Al*, Cr*, V*, Fe*, Mn*, Mg*, Ni, Ca

glass Si*, Ti*, Al*, Cr*, Fe*, Mn*, Mg*, Ca*, Na*, K*, P*, S*, Cl*

Elements asterisked were determined in EDS analyses

Lava and peridotite analyses do not include F and Sr

Lava WDS analyses do not include V

TABLE A3.1 GRENADA LAVAS - OLIVINES

	1	2	3	4	5	6	7	8
	07801	07802	10401	10402	07301	07302	07303	07304
	E	E	E	E	W	W	W	W
SIO2	41.22	41.52	39.32	39.07	36.52	37.00	36.56	36.01
TIO2	0.00	0.00	0.00	0.00	0.01	0.02	0.03	0.05
AL2O3	0.00	0.00	0.00	0.00	0.04	0.04	0.04	0.05
CR2O3	0.00	0.00	0.00	0.00	0.00	0.01	0.02	0.03
FEO	9.14	8.75	19.33	20.23	29.61	32.05	32.78	36.09
MNO	0.14	0.23	0.43	0.51	0.87	0.88	0.97	1.18
MGO	49.14	49.07	41.39	39.87	32.96	31.03	30.30	27.27
NIO	0.39	0.45	0.00	0.00	0.02	0.03	0.05	0.06
CAO	0.20	0.12	0.35	0.24	0.19	0.21	0.24	0.20
TOTAL	100.23	100.14	100.82	99.92	100.23	101.29	101.00	100.94
MOLE PERCENT ENDMEMBERS								
FO	90.6	90.9	79.2	77.8	66.5	63.3	62.2	57.4
FA	9.4	9.1	20.8	22.2	33.5	36.7	37.8	42.6

	9	10	11	12	13	14	15	16
	15801	15801A	15802	15802A	15803	26401	26402	26402A
	W	W	W	W	W	W	W	W
SIO2	39.55	38.86	39.72	39.32	38.92	39.05	40.31	36.31
TIO2	0.00	0.01	0.00	0.00	0.00	0.02	0.00	0.00
AL2O3	0.04	0.07	0.04	0.04	0.04	0.02	0.01	0.02
CR2O3	0.00	0.01	0.00	0.00	0.00	0.00	0.00	0.00
FEO	18.18	21.19	17.64	17.59	18.03	19.88	13.49	33.20
MNO	0.41	0.62	0.37	0.38	0.42	0.46	0.19	0.46
MGO	42.59	39.59	42.84	42.60	42.19	41.21	46.32	29.33
NIO	0.05	0.03	0.06	0.03	0.06	0.04	0.11	0.09
CAO	0.26	0.30	0.26	0.28	0.27	0.17	0.15	0.28
TOTAL	101.08	100.69	100.91	100.25	99.93	100.85	100.60	99.70
MOLE PERCENT ENDMEMBERS								
FO	80.7	76.9	81.2	81.2	80.7	78.7	86.0	61.2
FA	19.3	23.1	18.8	18.8	19.3	21.3	14.0	38.8

	17	18	19	20	21	22	23	24
	26403	26404	25201	25202	25203	25204	25205	25601
	W	W	E	E	E	E	E	E
SIO2	37.77	38.83	40.31	40.70	39.85	40.51	39.65	41.46
TIO2	0.01	0.00	0.11	0.00	0.00	0.00	0.00	0.00
AL2O3	0.03	0.04	0.00	0.00	0.00	0.00	0.00	0.00
CR2O3	0.00	0.00	0.00	0.00	0.00	0.00	0.00	0.00
FEO	25.06	21.46	15.75	12.86	15.45	14.36	14.11	13.61
MNO	0.64	0.50	0.53	0.32	0.40	0.23	0.37	0.31
MGO	36.94	39.79	45.60	47.39	45.88	46.75	46.14	46.62
NIO	0.04	0.04	0.00	0.31	0.15	0.16	0.20	0.22
CAO	0.23	0.17	0.35	0.18	0.32	0.18	0.16	0.23
TOTAL	100.73	100.83	102.65	101.76	102.05	102.19	100.63	102.45
MOLE PERCENT ENDMEMBERS								
FO	72.4	76.8	83.8	86.8	84.1	85.3	85.4	85.9
FA	27.6	23.2	16.2	13.2	15.9	14.7	14.6	14.1

TABLE A3.1 GRENADA LAVAS - OLIVINES

	25	26	27	28	29	30	31	32
	25601A	25601B	25602	25603	25604A	25605	25901	25902
	E	E	E	E	E	E	E	E
SIO2	41.43	39.51	40.38	40.13	40.74	40.60	40.29	40.19
FEO	13.23	19.21	14.32	16.31	15.17	14.35	15.88	14.74
MNO	0.22	0.55	0.26	0.34	0.39	0.31	0.35	0.24
MGO	46.73	41.06	45.54	45.35	45.88	46.66	45.26	45.89
NIO	0.20	0.00	0.35	0.27	0.32	0.27	0.18	0.23
CAO	0.16	0.38	0.20	0.13	0.15	0.21	0.17	0.00
TOTAL	101.97	100.71	101.05	102.53	102.65	102.40	102.13	101.29
MOLE PERCENT ENDMEMBERS								
FO	86.3	79.2	85.0	83.2	84.4	85.3	83.6	84.7
FA	13.7	20.8	15.0	16.8	15.6	14.7	16.4	15.3

	33	34
	25903	25904
	E	E
SIO2	40.33	39.96
FEO	15.27	16.55
MNO	0.00	0.27
MGO	46.30	45.23
NIO	0.00	0.27
CAO	0.24	0.09
TOTAL	102.14	102.37
MOLE PERCENT ENDMEMBERS		
FO	84.4	83.0
FA	15.6	17.0

TABLE A3.2 GRENADA LAVAS - PYROXENES

	1	2	3	4	5	6	7	8
	07801	10401	10401A	10401B	10401C	07301	07301A	07302
	E	E	E	E	E	W	W	W
SIO2	48.13	51.92	46.95	47.98	50.23	48.86	48.23	49.85
TIO2	1.21	0.69	0.85	0.99	0.76	0.89	2.18	0.73
AL203	6.17	2.77	8.24	7.26	3.21	6.16	3.94	3.24
CR203	0.69	0.00	0.00	0.00	0.00	0.06	0.00	0.00
FEO	5.63	6.58	8.56	8.40	8.52	6.01	8.77	8.29
MNO	0.13	0.20	0.15	0.00	0.21	0.12	0.31	0.28
MGO	14.11	15.89	12.48	12.84	13.81	14.05	13.48	14.14
NIO	0.00	0.00	0.00	0.00	0.00	0.03	0.03	0.01
CAO	23.83	21.55	22.32	22.11	22.44	23.28	21.57	21.89
NA2O	0.00	0.49	0.00	0.67	0.00	0.26	0.31	0.41
K2O	0.00	0.00	0.00	0.00	0.00	0.01	0.01	0.01
TOTAL	99.90	100.09	99.55	100.25	99.18	99.73	98.85	98.86
MOLE PERCENT ENDMEMBERS								
EN	41.0	45.3	37.5	38.4	39.8	41.1	39.8	41.0
FS	9.2	10.5	14.4	14.1	13.8	9.9	14.5	13.5
WO	49.8	44.2	48.1	47.5	46.5	49.0	45.7	45.6

	9	10	11	12	13	14	15	16
	07304	07304A	15801	15801A	15802	15803	15803A	15804
	W	W	W	W	W	W	W	W
SIO2	47.93	51.68	49.95	47.95	49.99	50.71	47.17	47.35
TIO2	1.04	0.55	0.90	1.24	0.97	0.58	1.14	1.33
AL203	5.84	3.01	3.91	6.52	5.86	4.78	6.54	5.74
CR203	0.01	0.00	0.00	0.00	0.01	0.43	0.00	0.00
FEO	8.72	8.22	7.10	7.68	6.86	4.57	7.81	8.26
MNO	0.23	0.34	0.20	0.14	0.17	0.10	0.16	0.21
MGO	13.12	15.28	14.39	13.33	14.58	15.12	13.07	12.95
NIO	0.02	0.02	0.02	0.04	0.02	0.03	0.01	0.03
CAO	21.69	20.63	22.47	22.56	22.46	23.23	22.77	22.11
NA2O	0.47	0.33	0.46	0.38	0.52	0.23	0.42	0.57
K2O	0.01	0.01	0.01	0.01	0.01	0.01	0.00	0.01
TOTAL	99.09	100.06	99.41	99.86	101.45	99.79	99.10	98.56
MOLE PERCENT ENDMEMBERS								
EN	39.0	44.0	41.7	39.4	42.2	44.0	38.6	38.7
FS	14.6	13.3	11.5	12.7	11.1	7.5	13.0	13.9
WO	46.4	42.7	46.8	47.9	46.7	48.6	48.4	47.5

	17	18	19	20	21	22	23	24
	26401	26401A	26402	26403	26403A	26404	25201	25201A
	W	W	W	W	W	W	E	E
SIO2	52.73	49.13	52.14	52.31	48.59	52.38	48.37	47.55
TIO2	0.15	0.78	0.25	0.18	0.83	0.29	0.79	1.11
AL203	2.00	4.66	2.58	2.24	5.08	2.13	6.05	6.13
CR203	0.63	0.00	0.26	0.79	0.00	0.40	1.00	0.00
FEO	3.17	7.82	4.00	3.47	7.92	3.63	4.64	7.06
MNO	0.10	0.22	0.09	0.09	0.19	0.08	0.12	0.00
MGO	17.01	14.10	16.37	16.75	13.93	16.84	14.24	13.50
NIO	0.04	0.02	0.03	0.03	0.01	0.02	0.00	0.00
CAO	23.40	22.01	23.68	23.33	22.32	23.21	23.21	23.29
NA2O	0.19	0.41	0.19	0.22	0.43	0.22	0.00	0.00
K2O	0.01	0.01	0.01	0.01	0.01	0.01	0.00	0.00
TOTAL	99.42	99.17	99.60	99.35	99.33	99.13	98.42	98.64
MOLE PERCENT ENDMEMBERS								
EN	47.8	41.1	45.9	47.2	40.5	47.4	42.5	39.5
FS	5.0	12.8	6.3	5.5	12.9	5.7	7.8	11.6
WO	47.2	46.1	47.8	47.3	46.6	46.9	49.8	48.9

TABLE A3.2 GRENADA LAVAS - PYROXENES

	25	26	27	28	29	30	31	32
	25202	25203	25601	25601A	25601B	25602	25602A	25602B
	E	E	E	E	E	E	E	E
SIO2	48.33	50.87	45.87	49.79	49.69	52.89	53.01	48.79
TIO2	0.78	0.73	0.97	0.68	1.30	0.49	0.34	0.87
AL203	6.61	3.61	7.64	4.95	7.11	2.59	2.74	5.94
CR203	0.83	0.41	0.21	0.74	0.00	0.61	0.57	0.52
FEO	4.85	4.98	7.94	5.47	6.97	4.48	4.24	6.00
MNO	0.00	0.00	0.13	0.00	0.22	0.19	0.00	0.00
MGO	14.33	15.10	13.05	14.85	12.42	16.53	16.23	0.00
NIO	0.00	0.00	0.00	0.00	0.00	0.00	0.00	0.19
CAO	23.46	23.47	23.04	23.77	21.55	23.47	23.14	23.73
NA2O	0.00	0.00	0.00	0.00	1.27	0.00	0.00	0.00
P2O5	0.00	0.00	0.00	0.00	0.00	0.00	0.00	13.96
TOTAL	99.19	99.17	98.85	100.25	100.53	101.25	100.27	100.00
MOLE PERCENT ENDMEMBERS								
EN	42.3	43.4	38.3	42.4	39.0	46.0	46.1	0.0
FS	8.0	8.0	13.1	8.8	12.3	7.0	6.7	16.5
WO	49.7	48.5	48.6	48.8	48.7	47.0	47.2	83.5

	33	34	35	36	37	38	39	40
	25603	25604	25605	25901	25901A	25901B	25902	25903
	E	E	E	E	E	E	E	E
SIO2	51.95	51.82	50.91	51.97	51.64	50.79	52.06	52.57
TIO2	0.42	0.35	0.54	0.41	0.45	0.72	0.43	0.45
AL203	3.47	2.68	3.57	3.12	2.99	3.96	3.14	2.97
CR203	0.30	0.41	0.33	0.26	0.51	0.00	0.44	0.62
FEO	5.08	4.70	5.55	4.90	4.64	5.70	4.70	4.45
MNO	0.17	0.00	0.18	0.00	0.14	0.14	0.17	0.00
MGO	15.98	16.39	15.77	16.68	16.12	15.66	16.06	16.95
CAO	23.28	22.83	23.05	23.49	22.93	22.66	23.10	23.24
TOTAL	100.65	99.18	99.90	100.83	99.42	99.63	100.10	101.25
MOLE PERCENT ENDMEMBERS								
EN	44.9	46.3	44.5	45.9	45.8	44.6	45.5	46.9
FS	8.0	7.4	8.8	7.6	7.4	9.1	7.5	6.9
WO	47.0	46.3	46.7	46.5	46.8	46.3	47.0	46.2

TABLE A3.3 GRENADA LAVAS - PLAGIOCLASES

	1	2	3	4	5	6	7	8
	10401	10402	10403	07301	07302	07304	07304A	15801
	E	E	E	W	W	W	W	W
SIO2	47.20	48.24	48.87	46.83	44.38	45.07	49.67	46.34
TIO2	0.00	0.00	0.00	0.02	0.01	0.02	0.06	0.03
AL203	32.26	31.49	31.29	34.20	34.29	34.85	30.75	33.68
FEO	0.76	0.90	0.87	0.67	0.66	0.62	0.78	0.68
MGO	0.00	0.00	0.00	0.07	0.05	0.04	0.05	0.06
CAO	16.53	15.74	15.30	17.08	18.37	18.57	14.81	17.40
NA20	1.95	2.32	2.11	1.46	1.10	1.02	3.50	1.63
K20	0.14	0.11	0.14	0.04	0.02	0.04	0.18	0.07
TOTAL	98.84	98.80	98.58	100.37	98.90	100.24	99.80	99.90
MOLE PERCENT ENDMEMBERS								
AB	17.4	20.9	19.8	13.4	9.7	9.1	29.7	14.4
AN	81.7	78.4	79.3	86.4	90.1	90.7	69.4	85.2
OR	0.8	0.7	0.9	0.2	0.1	0.2	1.0	0.4

	9	10	11	12	13	14	15	16
	15802	15803A	26401	26401A	26402	26403	26403A	26404
	W	W	W	W	W	W	W	W
SIO2	47.68	50.55	45.74	49.36	48.13	44.85	48.55	46.84
TIO2	0.04	0.06	0.00	0.03	0.03	0.00	0.04	0.01
AL203	33.22	29.68	34.12	31.77	31.89	35.02	31.92	33.59
FEO	0.80	0.90	0.72	0.92	0.77	0.60	0.82	0.72
MGO	0.11	0.11	0.06	0.11	0.12	0.05	0.09	0.06
CAO	16.00	13.85	17.71	14.51	15.71	18.29	15.73	16.67
NA20	1.84	4.20	1.53	2.79	2.67	0.98	2.78	1.71
K20	0.08	0.31	0.07	0.15	0.15	0.04	0.14	0.08
TOTAL	99.75	99.67	99.95	99.65	99.48	99.83	100.06	99.68
MOLE PERCENT ENDMEMBERS								
AB	17.1	34.9	13.5	25.6	23.3	8.8	24.0	15.6
AN	82.4	63.5	86.1	73.5	75.8	91.0	75.2	83.9
OR	0.5	1.7	0.4	0.9	0.9	0.2	0.8	0.5

	17
	25601
	E
SIO2	46.74
AL203	33.16
FEO	0.97
CAO	17.12
NA20	1.93
TOTAL	99.92
MOLE PERCENT ENDMEMBERS	
AB	16.9
AN	83.1
OR	0.0

TABLE A3.4 GRENADA LAVAS - OXIDES

	1	2	3	4	5	6	7	8
	07801	07802	07803	10401	10402	10403	07303	07304
	E	E	E	E	E	E	E	E
SIO2	0.66	0.22	0.00	0.31	0.23	0.23	0.25	0.39
TIO2	0.71	0.65	0.80	5.20	4.83	5.64	6.98	13.50
AL203	18.20	17.96	19.47	8.45	10.53	8.33	7.72	2.32
CR203	43.66	43.50	44.70	0.25	0.18	0.20	0.42	0.00
V203	0.00	0.00	0.00	0.78	0.78	0.67	0.92	1.35
FE203	7.00	8.42	7.55	49.82	48.85	49.59	47.42	37.92
FEO	17.84	17.48	14.06	31.23	32.22	32.80	35.00	42.84
MNO	0.25	0.41	0.27	0.36	0.66	0.53	0.34	0.48
MGO	11.99	11.67	14.22	4.13	3.48	3.34	2.93	0.69
TOTAL	100.31	100.31	101.08	100.52	101.76	101.33	101.97	99.49

	9	10	11	12	13	14	15	16
	07305	15801	15802	15803	15804	15805	26401	26402
	E	E	E	E	E	E	E	E
SIO2	0.35	0.23	0.18	0.40	0.29	0.19	0.41	0.32
TIO2	13.15	4.86	5.40	4.88	7.43	4.71	9.24	5.23
AL203	2.50	7.83	7.66	7.52	6.28	7.87	3.75	5.45
CR203	0.34	0.29	0.24	0.29	0.13	0.00	0.17	0.00
V203	1.24	0.54	0.58	0.47	0.78	0.60	1.00	0.51
FE203	38.04	52.82	52.55	52.91	48.85	51.33	45.02	53.78
FEO	41.58	28.85	28.93	28.58	32.56	27.46	38.11	30.12
MNO	0.20	0.38	0.34	0.33	0.50	0.39	0.00	0.36
MGO	1.31	5.46	5.78	5.77	4.39	5.61	1.65	4.47
TOTAL	98.71	101.25	101.66	101.14	101.22	98.15	99.35	100.24

	17	18	19	20	21	22	23	24
	26403	26404	26405	25201	25202	25203	25205	25206
	E	E	E	E	E	E	E	E
SIO2	0.24	0.38	0.31	0.38	0.26	0.24	0.00	0.21
TIO2	5.38	6.07	5.51	5.23	0.54	4.40	1.54	2.10
AL203	4.86	7.19	6.59	9.69	22.50	10.38	10.31	10.72
CR203	3.78	0.00	0.23	6.14	36.56	9.97	28.96	27.99
V203	0.77	0.70	0.54	0.64	0.22	0.50	0.25	0.33
FE203	49.36	50.59	52.73	43.12	9.86	42.05	27.90	28.46
FEO	31.37	31.24	30.45	27.88	17.69	25.47	21.19	22.31
MNO	1.11	0.42	0.37	0.58	0.36	0.63	0.49	0.31
MGO	3.11	4.67	4.80	6.33	11.90	7.61	8.25	8.64
TOTAL	99.98	101.26	101.53	99.99	99.89	101.25	98.90	101.07

TABLE A3.4 GRENADA LAVAS - OXIDES

	25	26	27	28	29	30	31	32
	25207	25208	25209	25210	25210A	25601	25602	25603
	E	E	E	E	E	E	E	E
SIO2	0.00	0.00	0.00	0.31	0.26	0.25	0.19	0.00
TIO2	0.48	3.71	6.64	3.48	5.48	1.74	8.78	5.92
AL203	19.41	10.53	8.21	10.19	9.35	9.27	4.73	5.60
CR203	44.33	16.17	1.27	17.54	4.35	29.82	6.81	21.33
V203	0.00	0.44	0.69	0.40	0.56	0.29	0.71	0.51
FE203	7.65	37.31	47.77	35.85	46.06	27.25	41.30	32.14
FEO	17.60	24.46	29.87	24.42	27.67	23.48	32.01	28.63
MNO	0.35	0.42	0.65	0.41	0.62	0.29	0.59	0.55
MGO	11.77	7.77	5.40	7.83	6.63	7.28	5.11	5.72
TOTAL	101.59	100.81	100.50	100.43	100.98	99.67	100.23	100.40

	33	34	35	36	37	38	39	40
	25603A	25604	25605	25606	25607	25608	25901	25902
	E	E	E	E	E	E	E	E
SIO2	0.39	0.00	0.00	0.27	0.27	0.36	0.24	0.32
TIO2	8.95	0.54	0.77	6.98	8.99	7.28	0.79	4.16
AL203	4.28	14.83	7.43	5.02	4.29	4.68	17.50	5.96
CR203	7.76	40.68	32.26	15.79	8.40	14.38	37.26	34.79
V203	0.73	0.00	0.00	0.72	0.93	0.63	0.00	0.48
FE203	40.13	14.04	28.88	36.34	39.81	35.71	13.26	20.74
FEO	32.89	21.44	23.11	30.35	32.43	30.60	23.81	29.51
MNO	0.56	0.41	0.67	0.47	0.57	0.65	0.22	0.17
MGO	4.86	8.48	6.21	5.65	5.14	5.14	7.78	4.92
TOTAL	100.54	100.42	99.33	101.59	100.83	99.43	100.86	101.05

	41	42	43	44	45
	25903	25904	25904A	25905	25906
	E	E	E	E	E
SIO2	0.36	0.20	0.20	0.00	0.21
TIO2	10.88	0.35	5.12	4.86	3.01
AL203	4.97	16.13	7.66	7.66	9.84
CR203	8.59	42.44	28.31	23.94	35.81
V203	1.15	0.17	0.69	0.59	0.40
FE203	34.21	11.34	24.37	29.67	18.37
FEO	36.27	22.69	29.90	29.51	27.92
MNO	0.49	0.53	0.42	0.55	0.47
MGO	4.02	8.13	5.29	5.06	5.52
TOTAL	100.94	101.98	101.96	101.83	101.55

TABLE A4.1 GRENADA CUMULATES - OLIVINES

	1	2	3	4	5	6	7	8
	06601	07001	07002	07002A	09101	09102	09102A	09101
	W	W	W	W	W	W	W	W
SIO2	38.72	39.61	39.46	39.49	39.11	39.21	39.52	38.77
TIO2	0.00	0.02	0.00	0.01	0.01	0.02	0.01	0.03
AL2O3	0.04	0.05	0.06	0.06	0.02	0.01	0.02	0.03
CR2O3	0.01	0.01	0.01	0.00	0.00	0.00	0.00	0.01
V2O3	0.00	0.00	0.00	0.00	0.00	0.00	0.00	0.00
FEO	21.59	18.10	17.75	17.96	20.79	18.32	19.20	21.34
MNO	0.51	0.31	0.30	0.29	0.40	0.32	0.41	0.45
MGO	39.81	42.73	42.98	42.74	40.45	42.70	41.82	40.00
NIO	0.09	0.16	0.15	0.14	0.16	0.19	0.14	0.09
CAO	0.14	0.15	0.11	0.18	0.03	0.03	0.06	0.21
K2O	0.00	0.00	0.00	0.00	0.03	0.03	0.03	0.00
TOTAL	100.92	101.15	100.80	100.87	101.01	100.84	101.22	100.93
MOLE PERCENT ENDMEMBERS								
FO	76.7	80.8	81.2	80.9	77.6	80.6	79.5	77.0
FA	23.3	19.2	18.8	19.1	22.4	19.4	20.5	23.0

	9	10	11	12	13	14	15	16
	05102	16601	16601A	16601B	06501	06502	16701	16701A
	W	E	E	E	W	W	W	W
SIO2	38.65	39.07	38.64	39.65	38.78	39.82	38.43	38.33
TIO2	0.02	0.12	0.00	0.00	0.00	0.00	0.03	0.02
AL2O3	0.03	0.00	0.00	0.00	0.01	0.11	0.02	0.04
CR2O3	0.01	0.00	0.00	0.00	0.00	0.00	0.00	0.00
V2O3	0.00	0.00	0.00	0.00	0.01	0.04	0.01	0.01
FEO	21.48	21.35	20.86	20.37	20.22	19.75	21.19	21.64
MNO	0.46	0.72	0.50	0.64	0.46	0.33	0.52	0.52
MGO	39.74	38.02	39.67	39.40	40.66	40.15	40.14	39.82
NIO	0.06	0.29	0.24	0.21	0.10	0.13	0.16	0.16
CAO	0.16	0.12	0.00	0.00	0.20	0.33	0.05	0.07
TOTAL	100.62	99.69	99.91	100.27	100.45	100.66	100.55	100.60
MOLE PERCENT ENDMEMBERS								
FO	76.7	76.0	77.2	77.5	78.2	78.4	77.1	76.6
FA	23.3	24.0	22.8	22.5	21.8	21.6	22.9	23.4

	17	18	19	20	21	22	23	24
	16702	06701	06701A	06702	06703	09501	09502	09901
	W	W	W	W	W	W	W	W
SIO2	38.57	39.41	39.61	39.85	39.85	38.50	38.71	38.63
TIO2	0.04	0.01	0.01	0.02	0.01	0.00	0.01	0.00
AL2O3	0.05	0.05	0.05	0.04	0.05	0.04	0.04	0.04
CR2O3	0.01	0.00	0.00	0.00	0.00	0.00	0.01	0.01
V2O3	0.01	0.00	0.00	0.00	0.00	0.00	0.00	0.00
FEO	22.41	16.87	17.21	16.89	17.06	21.77	22.94	21.27
MNO	0.63	0.30	0.29	0.29	0.29	0.65	0.66	0.52
MGO	39.34	43.64	43.32	44.02	43.88	39.96	39.15	40.70
NIO	0.16	0.11	0.12	0.12	0.07	0.14	0.20	0.14
CAO	0.09	0.14	0.18	0.15	0.18	0.05	0.08	0.20
TOTAL	101.31	100.53	100.78	101.39	101.41	101.12	101.79	101.53
MOLE PERCENT ENDMEMBERS								
FO	75.8	82.2	81.8	82.3	82.1	76.6	75.3	77.3
FA	24.2	17.8	18.2	17.7	17.9	23.4	24.7	22.7

TABLE A4.1 GRENADA CUMULATES - OLIVINES

	25	26	27	28	29	30	31	32
	09901A	09902	09903	09401	09402	16801	10201	10202
	W	W	W	W	W	E	E	E
SIO2	38.70	38.67	39.16	38.88	38.72	38.53	39.57	39.16
TIO2	0.00	0.00	0.00	0.03	0.05	0.00	0.00	0.00
AL203	0.03	0.05	0.03	0.04	0.03	0.00	0.00	0.00
CR203	0.01	0.01	0.02	0.01	0.01	0.00	0.00	0.00
V203	0.02	0.00	0.00	0.00	0.00	0.00	0.00	0.00
FEO	21.43	21.35	21.45	21.17	20.92	22.49	20.18	20.72
MNO	0.51	0.52	0.49	0.46	0.48	0.44	0.53	0.51
MGO	40.61	40.24	40.57	40.35	40.15	39.15	41.41	40.80
NIO	0.14	0.16	0.15	0.12	0.11	0.15	0.00	0.00
CAO	0.18	0.11	0.10	0.09	0.08	0.00	0.12	0.13
TOTAL	101.62	101.11	101.96	101.16	100.55	100.76	101.81	101.32
MOLE PERCENT ENDMEMBERS								
FO	77.2	77.1	77.1	77.3	77.4	75.6	78.5	77.8
FA	22.8	22.9	22.9	22.7	22.6	24.4	21.5	22.2

	33	34	35	36	37	38	39	40
	16501	16501	16502	16503	16504	50A01	50A02	15501
	E	W	W	E	E	W	W	W
SIO2	39.32	39.39	39.67	39.32	39.00	38.59	38.34	39.22
TIO2	0.00	0.02	0.01	0.00	0.00	0.01	0.07	0.01
AL203	0.00	0.02	0.02	0.00	0.00	0.04	0.03	0.01
CR203	0.00	0.00	0.01	0.00	0.00	0.00	0.00	0.00
V203	0.00	0.01	0.03	0.00	0.00	0.00	0.00	0.00
FEO	19.47	19.24	19.13	19.47	19.39	20.68	20.94	17.90
MNO	0.46	0.43	0.45	0.46	0.48	0.47	0.46	0.36
MGO	40.93	42.19	42.18	40.93	40.06	39.64	39.56	42.28
NIO	0.00	0.21	0.22	0.00	0.25	0.14	0.16	0.06
CAO	0.00	0.13	0.12	0.00	0.14	0.13	0.12	0.17
TOTAL	100.18	101.66	101.85	100.18	99.32	99.70	99.69	100.01
MOLE PERCENT ENDMEMBERS								
FO	78.9	79.6	79.7	78.9	78.6	77.4	77.1	80.8
FA	21.1	20.4	20.3	21.1	21.4	22.6	22.9	19.2

	41	42	43
	15502	40601	40602
	W	W	W
SIO2	39.24	39.54	39.34
TIO2	0.02	0.01	0.02
AL203	0.03	0.02	0.02
FEO	17.74	17.39	16.47
MNO	0.33	0.35	0.31
MGO	42.28	42.87	43.24
NIO	0.08	0.17	0.16
CAO	0.11	0.05	0.04
TOTAL	99.84	100.40	99.60
MOLE PERCENT ENDMEMBERS			
FO	80.9	81.5	82.4
FA	19.1	18.5	17.6

TABLE A4.2 GRENADA CUMULATES - PYROXENES

	1	2	3	4	5	6	7	8
	06601	06601A	06602	06602A	06603	06603A	07001	07002
	W	W	W	W	W	W	W	W
SIO2	49.26	50.89	47.72	51.27	49.29	47.59	49.45	50.03
TIO2	0.93	0.65	1.25	0.52	1.13	1.10	0.66	0.59
AL203	5.07	3.18	6.39	3.13	4.78	6.29	5.37	5.60
CR203	0.08	0.01	0.03	0.01	0.04	0.05	0.87	0.22
V203	0.03	0.02	0.03	0.03	0.06	0.03	0.02	0.03
FEO	6.85	7.11	8.11	7.14	7.27	8.06	5.38	5.79
MNO	0.16	0.26	0.20	0.29	0.14	0.18	0.11	0.13
MGO	14.13	14.77	13.34	14.72	13.77	13.18	14.42	14.70
NIO	0.00	0.00	0.00	0.00	0.00	0.00	0.02	0.03
CAO	22.71	22.23	21.84	22.33	22.72	22.39	22.88	23.25
NA20	0.36	0.41	0.56	0.42	0.44	0.36	0.27	0.24
K20	0.02	0.02	0.05	0.03	0.03	0.02	0.02	0.02
TOTAL	99.61	99.57	99.51	99.90	99.67	99.24	99.47	100.62
MOLE PERCENT ENDMEMBERS								
EN	41.2	42.5	39.7	42.3	40.3	39.0	42.6	42.4
FS	11.2	11.5	13.6	11.5	11.9	13.4	8.9	9.4
WO	47.6	46.0	46.7	46.2	47.8	47.6	48.5	48.2

	9	10	11	12	13	14	15	16
	07002A	07003	09101	05101	05101A	05102	05103	05103A
	W	W	W	W	W	W	W	W
SIO2	50.33	49.56	51.21	50.67	50.00	49.08	47.31	50.55
TIO2	0.77	0.59	0.60	0.41	0.77	0.85	0.99	0.66
AL203	5.83	5.58	3.31	3.58	3.87	5.63	7.12	4.23
CR203	0.17	0.31	0.09	0.14	0.08	0.10	0.04	0.20
V203	0.02	0.03	0.03	0.03	0.06	0.05	0.07	0.03
FEO	5.75	5.88	6.22	7.41	7.53	6.76	7.16	5.47
MNO	0.11	0.10	0.21	0.27	0.26	0.17	0.13	0.13
MGO	14.72	14.32	15.06	14.71	14.34	14.00	12.95	15.02
NIO	0.01	0.02	0.02	0.00	0.00	0.00	0.00	0.00
CAO	23.49	23.09	22.71	21.56	21.65	23.05	23.44	23.29
NA20	0.24	0.24	0.33	0.35	0.43	0.33	0.29	0.23
K20	0.03	0.02	0.03	0.01	0.02	0.01	0.02	0.01
TOTAL	101.47	99.76	99.82	99.16	99.01	100.02	99.54	99.82
MOLE PERCENT ENDMEMBERS								
EN	42.3	41.9	43.2	42.8	42.0	40.7	38.3	43.1
FS	9.3	9.6	10.0	12.1	12.4	11.0	11.9	8.8
WO	48.5	48.5	46.8	45.1	45.6	48.2	49.8	48.1

	17	18	19	20	21	22	23	24
	16601	16602	16603	16605	24901	24901A	24901B	24902
	W	W	W	E	W	W	W	W
SIO2	52.64	52.28	53.07	52.62	49.53	49.53	50.14	51.68
TIO2	0.21	0.26	0.11	0.36	0.83	0.83	0.83	0.62
AL203	2.13	2.69	1.60	2.46	4.91	4.91	4.06	3.18
CR203	0.02	0.04	0.03	0.00	0.22	0.22	0.00	0.00
V203	0.01	0.01	0.00	0.00	0.00	0.03	0.03	0.04
FEO	6.55	6.54	6.47	7.50	6.34	7.00	7.88	7.71
MNO	0.41	0.31	0.42	0.34	0.13	0.13	0.22	0.26
MGO	15.36	15.33	15.65	15.76	14.01	14.22	14.24	14.74
NIO	0.05	0.03	0.04	0.00	0.02	0.02	0.00	0.00
CAO	22.24	21.89	22.43	20.82	23.16	22.45	21.88	21.55
NA20	0.32	0.28	0.34	0.00	0.29	0.36	0.43	0.43
K20	0.02	0.02	0.03	0.00	0.01	0.01	0.01	0.00
TOTAL	99.97	99.71	100.19	99.86	99.46	99.71	99.72	100.22
MOLE PERCENT ENDMEMBERS								
EN	43.9	44.1	44.2	45.1	40.9	41.5	41.4	42.7
FS	10.5	10.6	10.2	12.0	10.4	11.5	12.9	12.5
WO	45.6	45.3	45.5	42.8	48.7	47.1	45.7	44.8

TABLE A4.2 GRENADA CUMULATES - PYROXENES

	25	26	27	28	29	30	31	32
	06501	06502	06502A	06503	06503A	10501	10502	10503
	W	W	W	W	W	W	W	W
SIO2	49.39	51.15	48.38	49.20	49.70	48.80	48.62	48.38
TIO2	0.64	0.47	1.02	0.71	0.67	0.61	0.91	0.81
AL203	4.83	3.54	5.69	5.08	4.82	5.71	5.53	6.10
CR203	0.02	0.33	0.00	0.03	0.02	0.04	0.01	0.03
V203	0.03	0.00	0.00	0.01	0.01	0.03	0.04	0.04
FEO	8.17	5.24	7.97	6.44	6.64	7.04	7.39	7.29
MNO	0.25	0.11	0.22	0.17	0.14	0.15	0.12	0.09
MGO	14.20	15.60	13.59	14.11	14.26	13.53	13.68	13.41
NIO	0.01	0.03	0.01	0.02	0.01	0.01	0.01	0.00
CAO	20.31	22.49	21.37	22.72	22.42	22.40	22.17	22.83
NA2O	0.42	0.28	0.51	0.33	0.28	0.27	0.32	0.26
K2O	0.02	0.02	0.01	0.02	0.01	0.02	0.01	0.02
TOTAL	98.29	99.27	98.78	98.83	98.98	98.61	98.80	99.26
MOLE PERCENT ENDMEMBERS								
EN	42.5	44.9	40.7	41.4	41.8	40.3	40.5	39.6
FS	13.7	8.5	13.4	10.6	10.9	11.8	12.3	12.1
WO	43.7	46.6	46.0	48.0	47.3	47.9	47.2	48.4

	33	34	35	36	37	38	39	40
	16701	16703	16704	16705	16706	06701	06701A	06702
	W	W	W	W	W	W	W	W
SIO2	54.70	55.45	53.00	55.28	53.10	49.11	48.92	49.00
TIO2	0.05	0.06	0.16	0.07	0.19	0.84	0.80	0.86
AL203	1.05	1.04	1.67	1.29	1.82	6.09	6.09	6.00
CR203	0.03	0.05	0.13	0.02	0.13	0.15	0.43	0.33
V203	0.00	0.00	0.02	0.00	0.02	0.03	0.05	0.03
FEO	13.14	13.92	6.80	14.26	6.88	5.79	6.05	5.88
MNO	0.57	0.62	0.28	0.56	0.32	0.12	0.15	0.14
MGO	29.04	29.03	15.68	28.42	15.27	14.18	13.86	14.03
NIO	0.08	0.08	0.05	0.08	0.06	0.02	0.04	0.02
CAO	0.63	0.63	22.07	0.78	21.99	23.08	23.15	23.51
NA2O	0.01	0.00	0.35	0.00	0.53	0.28	0.31	0.28
K2O	0.02	0.01	0.01	0.01	0.02	0.00	0.00	0.00
TOTAL	99.31	100.89	100.23	100.79	100.34	99.70	99.85	100.10
MOLE PERCENT ENDMEMBERS								
EN	78.8	77.9	44.3	76.9	43.7	41.7	40.9	41.0
FS	20.0	20.9	10.8	21.6	11.0	9.6	10.0	9.6
WO	1.2	1.2	44.9	1.5	45.2	48.8	49.1	49.4

	41	42	43	44	45	46	47	48
	06703	09501	09502	09503	09504	09505	09506	10701
	W	W	W	W	W	W	W	W
SIO2	49.28	53.75	55.24	54.09	52.19	55.59	53.72	50.23
TIO2	0.75	0.10	0.04	0.07	0.38	0.02	0.08	0.64
AL203	5.64	1.48	0.74	1.51	2.43	0.79	1.07	4.85
CR203	0.13	0.16	0.03	0.02	0.11	0.00	0.13	0.23
V203	0.02	0.00	0.00	0.01	0.04	0.00	0.00	0.03
FEO	5.95	5.76	16.04	16.40	6.10	14.32	6.51	5.41
MNO	0.12	0.25	0.58	0.58	0.20	0.67	0.30	0.12
MGO	14.19	15.79	27.44	26.57	14.88	28.52	15.54	14.56
NIO	0.01	0.00	0.05	0.04	0.01	0.05	0.04	0.00
CAO	23.04	23.29	0.69	1.13	23.37	0.76	22.65	23.58
NA2O	0.28	0.36	0.01	0.03	0.40	0.02	0.34	0.24
K2O	0.01	0.00	0.00	0.01	0.00	0.00	0.01	0.00
TOTAL	99.43	100.94	100.86	100.45	100.11	100.75	100.41	99.90
MOLE PERCENT ENDMEMBERS								
EN	41.6	44.2	74.3	72.6	42.4	76.9	43.8	42.1
FS	9.8	9.0	24.4	25.1	9.7	21.6	10.3	8.8
WO	48.6	46.8	1.3	2.2	47.9	1.5	45.9	49.1

TABLE A4.2 GRENADA CUMULATES - PYROXENES

	49	50	51	52	53	54	55	56
	10701A	10702	09901	09902	09903	09904	09904A	09904B
	W	W	W	W	W	W	W	W
SIO2	50.63	50.83	52.22	52.23	51.97	52.05	51.61	50.31
TIO2	0.79	0.49	0.21	0.19	0.34	0.28	0.22	0.41
AL2O3	4.08	3.59	2.12	2.42	2.56	2.25	2.56	3.82
CR2O3	0.01	0.01	0.10	0.18	0.53	0.07	0.03	0.04
V2O3	0.04	0.03	0.00	0.00	0.02	0.02	0.02	0.02
FEO	7.81	7.64	6.28	6.28	5.53	7.06	7.01	7.36
MNO	0.28	0.24	0.23	0.26	0.18	0.29	0.29	0.21
MGO	13.91	14.17	15.91	15.87	15.80	15.06	14.96	14.16
NIO	0.00	0.01	0.01	0.01	0.00	0.02	0.01	0.01
CAO	22.25	22.46	22.47	22.23	23.10	22.41	22.60	22.97
NA2O	0.42	0.37	0.29	0.31	0.30	0.30	0.33	0.31
K2O	0.01	0.01	0.00	0.00	0.00	0.00	0.00	0.00
TOTAL	100.25	99.86	99.84	99.98	100.34	99.83	99.65	99.63
MOLE PERCENT ENDMEMBERS								
EN	40.6	41.0	44.7	44.9	44.5	42.9	42.6	40.7
FS	12.8	12.4	9.9	10.0	8.7	11.3	11.2	11.9
WO	46.7	46.7	45.4	45.2	46.8	45.8	46.2	47.4

	57	58	59	60	61	62	63	64
	09905	09906	09401	09402	13501	13502	13503	13504
	W	W	W	W	W	W	W	W
SIO2	48.76	49.90	55.05	54.79	52.60	54.38	53.79	52.72
TIO2	0.62	0.49	0.03	0.01	0.32	0.02	0.08	0.18
AL2O3	5.25	4.33	1.59	1.35	2.40	0.71	1.52	1.43
CR2O3	0.06	0.06	0.01	0.00	0.38	0.00	0.02	0.11
V2O3	0.04	0.03	0.02	0.00	0.01	0.00	0.00	0.02
FEO	7.56	7.44	13.79	14.06	4.15	16.41	16.72	7.67
MNO	0.20	0.22	0.42	0.51	0.08	0.83	0.73	0.35
MGO	13.47	13.89	28.77	28.20	16.56	26.74	26.05	15.50
NIO	0.00	0.00	0.07	0.06	0.00	0.00	0.04	0.03
CAO	23.04	22.88	0.95	0.97	23.28	0.85	1.09	21.63
NA2O	0.30	0.31	0.01	0.01	0.20	0.03	0.03	0.43
K2O	0.00	0.00	0.01	0.00	0.01	0.00	0.02	0.01
TOTAL	99.31	99.55	100.71	99.97	99.99	99.98	100.09	100.08
MOLE PERCENT ENDMEMBERS								
EN	39.3	40.3	77.4	76.7	46.5	73.1	71.9	43.8
FS	12.4	12.1	20.8	21.4	6.5	25.2	25.9	12.2
WO	48.3	47.7	1.8	1.9	47.0	1.7	2.2	44.0

	65	66	67	68	69	70	71	72
	15901	15902	15903	15904	13601	13601A	13602	16801
	E	E	E	E	E	E	E	E
SIO2	53.53	53.35	51.82	51.52	48.18	51.34	49.96	51.81
TIO2	0.14	0.19	0.32	0.42	0.88	0.41	0.66	0.51
AL2O3	0.76	1.06	1.88	2.47	7.16	3.44	5.17	3.60
CR2O3	0.00	0.00	0.00	0.00	0.42	0.00	0.83	0.16
FEO	6.83	7.31	7.65	7.69	6.24	6.14	4.82	6.60
MNO	0.31	0.29	0.53	0.46	0.14	0.18	0.00	0.21
MGO	15.81	15.92	15.37	14.57	13.00	15.18	14.85	14.67
CAO	22.17	21.79	21.32	22.48	23.29	22.94	23.53	22.29
TOTAL	99.55	99.91	98.89	99.61	99.31	99.63	99.82	99.85
MOLE PERCENT ENDMEMBERS								
EN	44.4	44.6	43.9	41.6	39.1	43.2	43.1	42.7
FS	10.8	11.5	12.3	12.3	10.5	9.8	7.8	10.8
WO	44.8	43.9	43.8	46.1	50.4	47.0	49.1	46.6

TABLE A4.2 GRENADA CUMULATES - PYROXENES

	73	74	75	76	77	78	79	80
	16802	16805	08701	08701A	08702	08703	10201	10202
	E	E	E	E	E	E	E	E
SIO2	54.82	54.96	48.78	50.46	49.89	50.27	53.20	52.11
TIO2	0.00	0.00	0.67	0.53	0.56	0.63	0.20	0.44
AL2O3	1.60	1.92	5.36	4.61	4.84	4.77	2.08	3.01
CR2O3	0.00	0.00	0.00	0.00	0.16	0.00	0.18	0.63
FEO	14.67	14.95	8.27	6.96	7.25	6.92	5.55	4.91
MNO	0.45	0.54	0.27	0.26	0.16	0.25	0.38	0.00
MGO	27.89	27.85	13.12	14.56	13.92	14.05	16.61	16.05
CAO	1.24	1.19	22.72	23.28	23.14	23.11	22.73	23.87
TOTAL	100.67	101.41	99.19	100.66	99.92	100.00	100.93	100.12
MOLE PERCENT ENDMEMBERS								
EN	75.4	75.1	38.5	41.4	40.2	40.7	46.1	45.3
FS	22.2	22.6	13.6	11.1	11.7	11.2	8.6	6.3
WO	2.4	2.3	47.9	47.5	48.0	48.1	45.3	48.4

	81	82	83	84	85	86	87	88
	10202A	16301	16302	16501	16501A	16502	16503	16505
	E	E	E	W	W	W	E	E
SIO2	51.82	46.81	49.30	51.02	51.23	53.31	50.31	51.09
TIO2	0.41	0.95	0.54	0.36	0.28	0.07	0.46	0.46
AL2O3	2.94	7.76	4.91	3.98	4.05	1.55	3.54	3.41
CR2O3	0.39	0.00	0.00	0.09	0.11	0.06	0.00	0.29
V2O3	0.00	0.00	0.00	0.02	0.00	0.00	0.00	0.00
FEO	5.59	7.86	7.75	5.97	6.14	4.89	6.55	5.96
MNO	0.23	0.27	0.20	0.19	0.20	0.23	0.22	0.13
MGO	16.08	12.78	13.68	15.15	15.18	16.85	14.28	15.06
NIO	0.00	0.00	0.00	0.05	0.01	0.03	0.00	0.00
CAO	22.86	23.10	22.86	22.93	22.67	22.20	23.25	23.27
NA2O	0.00	0.00	0.00	0.28	0.30	0.28	0.00	0.00
K2O	0.00	0.00	0.00	0.01	0.01	0.01	0.00	0.00
TOTAL	100.32	99.53	99.24	100.06	100.16	99.49	98.61	99.67
MOLE PERCENT ENDMEMBERS								
EN	45.1	37.8	39.7	43.3	43.5	47.4	41.2	42.9
FS	8.8	13.0	12.6	9.6	9.9	7.7	10.6	9.5
WO	46.1	49.1	47.7	47.1	46.7	44.9	48.2	47.6

	89	90	91	92	93	94	95	96
	50B01	50B02	50C01	50C02	15801	15802	15803	50A01
	E	E	E	E	E	E	E	W
SIO2	49.86	49.73	50.46	49.45	52.25	49.84	51.94	50.75
TIO2	0.61	0.77	0.63	0.70	0.41	0.70	0.32	0.30
AL2O3	4.61	5.31	4.89	4.86	2.72	5.27	2.72	3.42
CR2O3	0.00	0.16	0.00	0.00	0.00	0.26	0.00	0.02
V2O3	0.00	0.00	0.00	0.00	0.00	0.00	0.00	0.02
FEO	7.81	8.18	8.16	7.63	8.09	5.65	8.18	6.77
MNO	0.17	0.21	0.16	0.13	0.28	0.00	0.36	0.21
MGO	13.41	13.08	13.84	12.82	14.84	15.03	14.88	14.66
NIO	0.00	0.00	0.00	0.00	0.00	0.00	0.00	0.02
CAO	22.95	23.13	23.10	22.74	21.60	23.17	21.72	22.61
NA2O	0.00	0.00	0.00	0.00	0.00	0.57	0.00	0.32
K2O	0.00	0.00	0.00	0.00	0.00	0.00	0.00	0.02
TOTAL	99.42	100.57	101.24	98.33	100.19	100.49	100.12	99.13
MOLE PERCENT ENDMEMBERS								
EN	39.1	38.1	39.5	38.3	42.5	43.1	42.4	42.2
FS	12.8	13.4	13.1	12.8	13.0	9.1	13.1	10.9
WO	48.1	48.5	47.4	48.9	44.5	47.8	44.5	46.8

TABLE A4.2 GRENADA CUMULATES - PYROXENES

	97	98	99	100	101	102	103
	50A02	15501	15502	40601	40602	40603	40604
	W	W	W	W	W	W	W
SIO2	50.78	49.50	50.63	50.95	55.60	51.67	54.22
TIO2	0.54	0.44	0.59	0.58	0.03	0.45	0.04
AL2O3	3.39	4.59	3.98	3.80	0.78	2.81	2.17
CR2O3	0.03	0.00	0.21	0.14	0.04	0.37	0.12
V2O3	0.03	0.03	0.04	0.04	0.01	0.03	0.02
FEO	6.60	6.59	5.13	5.55	11.96	4.92	13.11
MNO	0.19	0.17	0.14	0.16	0.42	0.14	0.45
MGO	14.58	14.46	14.99	14.76	29.63	15.46	27.97
NIO	0.04	0.02	0.01	0.03	0.02	0.05	0.09
CAO	22.05	22.59	23.07	23.43	1.12	23.45	1.41
NA2O	0.32	0.32	0.29	0.24	0.02	0.19	0.02
K2O	0.02	0.02	0.02	0.01	0.02	0.00	0.02
TOTAL	98.57	98.73	99.08	99.70	99.68	99.56	99.63
MOLE PERCENT ENDMEMBERS							
EN	42.7	42.0	43.5	42.5	79.8	44.1	77.0
FS	10.8	10.7	8.4	9.0	18.1	7.9	20.2
WO	46.4	47.2	48.1	48.5	2.2	48.1	2.8

TABLE A4.3 GRENADA CUMULATES - PLAGIOCLASES

	1	2	3	4	5	6	7	8
	06601	06601A	06602	06603	06603A	09101	09102	05101
	W	W	W	W	W	W	W	W
SIO2	45.58	45.70	45.57	45.21	45.81	49.23	47.78	45.06
TIO2	0.01	0.00	0.02	0.01	0.04	0.02	0.01	0.00
AL203	34.16	34.24	34.30	34.28	33.86	31.89	32.92	33.87
FEO	0.50	0.60	0.58	0.61	1.10	0.48	0.60	0.57
MGO	0.05	0.04	0.05	0.04	0.05	0.04	0.04	0.04
CAO	18.16	18.31	18.33	18.30	17.85	14.77	16.26	18.57
SRO	0.22	0.26	0.00	0.00	0.00	0.19	0.00	0.08
NA2O	1.19	1.20	1.11	1.05	1.33	2.98	2.14	1.10
K2O	0.04	0.03	0.03	0.03	0.03	0.07	0.05	0.03
TOTAL	99.90	100.39	99.98	99.54	100.08	99.68	99.81	99.33
MOLE PERCENT ENDMEMBERS								
AB	10.6	10.6	9.9	9.4	11.9	26.7	19.2	9.7
AN	89.2	89.2	90.0	90.4	87.9	72.9	80.5	90.2
OR	0.2	0.2	0.2	0.2	0.2	0.4	0.3	0.2

	9	10	11	12	13	14	15	16
	05101A	05102	05103	05104	16602	16603	16604	16605
	W	W	W	W	W	W	W	E
SIO2	45.05	45.04	45.29	46.86	56.20	46.64	45.76	46.06
TIO2	0.00	0.00	0.00	0.02	0.01	0.02	0.00	0.00
AL203	33.81	33.77	34.06	33.00	26.60	33.27	33.52	33.23
FEO	0.59	0.77	0.58	0.56	0.66	0.63	0.39	0.50
MGO	0.05	0.09	0.05	0.04	0.08	0.05	0.03	0.00
CAO	18.38	18.37	18.20	17.08	9.89	17.24	17.98	17.69
SRO	0.08	0.11	0.09	0.18	0.17	0.16	0.18	0.00
NA2O	1.15	1.06	1.06	1.72	5.84	1.62	1.60	1.53
K2O	0.02	0.03	0.02	0.02	0.23	0.02	0.02	0.00
TOTAL	99.14	99.24	99.35	99.49	99.68	99.65	99.48	99.01
MOLE PERCENT ENDMEMBERS								
AB	10.2	9.4	9.5	15.4	51.0	14.5	13.9	13.5
AN	89.7	90.4	90.3	84.4	47.7	85.4	86.0	86.5
OR	0.1	0.2	0.1	0.1	1.3	0.1	0.1	0.0

	17	18	19	20	21	22	23	24
	16606	24901	24902	24903	06501	06502	06503	10502
	E	W	W	W	W	W	W	W
SIO2	46.22	46.05	46.09	45.91	47.54	45.03	45.17	44.23
TIO2	0.00	0.00	0.00	0.01	0.01	0.01	0.01	0.00
AL203	32.86	33.75	33.39	33.72	32.18	33.67	33.75	34.57
FEO	0.67	0.58	0.61	0.52	0.59	0.55	0.61	0.46
MGO	0.00	0.03	0.04	0.05	0.08	0.06	0.08	0.07
CAO	17.55	17.83	17.64	17.59	16.29	18.09	18.28	19.05
SRO	0.00	0.14	0.12	0.15	0.18	0.18	0.17	0.08
NA2O	1.66	1.33	1.52	1.35	2.10	1.17	1.02	0.64
K2O	0.00	0.04	0.04	0.04	0.06	0.03	0.02	0.00
TOTAL	98.96	99.74	99.47	99.34	99.04	98.79	99.11	99.10
MOLE PERCENT ENDMEMBERS								
AB	14.6	11.9	13.5	12.2	18.9	10.4	9.2	5.7
AN	85.4	87.9	86.3	87.5	80.8	89.4	90.7	94.3
OR	0.0	0.2	0.3	0.3	0.4	0.2	0.1	0.0

TABLE A4.3 GRENADA CUMULATES - PLAGIOCLASES

	25	26	27	28	29	30	31	32
	10502A	16701	16701A	16702	09501	09502	09503	09503A
	W	W	W	W	W	W	W	W
SIO2	44.22	46.58	49.15	45.41	45.48	54.91	54.29	54.74
TIO2	0.00	0.01	0.00	0.00	0.00	0.00	0.00	0.04
AL2O3	34.40	32.71	31.18	34.13	34.28	27.99	28.28	28.02
FEO	0.46	0.39	0.45	0.46	0.39	0.44	0.39	0.48
MGO	0.07	0.06	0.06	0.06	0.04	0.06	0.04	0.05
CAO	19.11	16.85	15.19	18.62	18.51	11.06	11.28	10.88
SRO	0.07	0.18	0.18	0.19	0.14	0.28	0.28	0.27
NA2O	0.57	1.86	3.09	1.08	1.03	5.31	5.08	5.30
K2O	0.00	0.02	0.04	0.02	0.04	0.17	0.17	0.17
TOTAL	98.90	98.67	99.35	99.96	99.90	100.21	99.84	99.94
MOLE PERCENT ENDMEMBERS								
AB	5.1	16.7	26.8	9.5	9.2	46.0	44.5	46.4
AN	94.9	83.2	72.9	90.4	90.6	53.0	54.5	52.6
OR	0.0	0.1	0.3	0.1	0.2	0.9	1.0	1.0

	33	34	35	36	37	38	39	40
	09504	09505	10701	10702	10702A	10703	09901	09901A
	W	W	W	W	W	W	W	W
SIO2	55.85	56.13	46.89	45.87	46.19	46.07	44.99	44.52
TIO2	0.00	0.00	0.01	0.04	0.03	0.03	0.00	0.00
AL2O3	27.23	27.34	32.93	33.57	33.55	33.41	34.03	34.30
FEO	0.37	0.40	0.62	0.59	0.52	0.59	0.50	0.63
MGO	0.06	0.05	0.05	0.05	0.05	0.05	0.05	0.04
CAO	10.25	9.93	16.98	17.49	17.57	17.65	18.70	19.06
SRO	0.23	0.26	0.17	0.21	0.20	0.20	0.14	0.15
NA2O	5.58	5.82	1.67	1.34	1.29	1.47	0.91	0.72
K2O	0.21	0.21	0.04	0.02	0.03	0.02	0.02	0.02
TOTAL	99.78	100.14	99.37	99.20	99.44	99.50	99.33	99.45
MOLE PERCENT ENDMEMBERS								
AB	49.0	50.8	15.1	12.2	11.7	13.1	8.1	6.4
AN	49.7	47.9	84.7	87.7	88.1	86.8	91.8	93.5
OR	1.2	1.2	0.2	0.1	0.2	0.1	0.1	0.1

	41	42	43	44	45	46	47	48
	09401	09402	13501	13501A	13502	13503	13503A	15901
	W	W	W	W	W	W	W	E
SIO2	47.18	48.30	55.87	60.25	56.34	54.27	55.19	57.88
TIO2	0.01	0.00	0.01	0.03	0.04	0.03	0.04	0.00
AL2O3	33.29	32.07	27.36	24.69	27.17	25.96	27.97	26.38
FEO	0.36	0.34	0.36	0.39	0.50	0.35	0.42	0.48
MGO	0.05	0.05	0.05	0.04	0.06	0.06	0.06	0.00
CAO	17.15	15.96	9.84	6.46	9.77	10.97	10.67	8.95
SRO	0.21	0.21	0.16	0.12	0.13	0.15	0.02	0.00
NA2O	1.81	2.58	5.93	7.50	5.98	7.05	5.46	6.55
K2O	0.02	0.05	0.23	0.38	0.22	0.28	0.18	0.25
TOTAL	100.09	99.56	99.81	99.86	100.21	99.12	100.00	100.49
MOLE PERCENT ENDMEMBERS								
AB	16.0	22.6	51.5	66.2	51.9	53.0	47.6	56.2
AN	83.8	77.2	47.2	31.5	46.8	45.6	51.4	42.4
OR	0.1	0.3	1.3	2.2	1.3	1.4	1.0	1.4

TABLE A4.3 GRENADA CUMULATES - PLAGIOCLASES

	49	50	51	52	53	54	55	56
	15901A	15902	15902A	13601	13601A	13602	13602A	16801
	W	E	E	E	E	E	E	E
SIO2	55.48	54.68	55.59	45.27	44.66	46.08	45.04	47.18
AL2O3	27.77	27.81	27.46	34.26	34.04	33.61	34.53	33.28
FEO	0.40	0.56	0.57	0.50	0.54	0.73	0.53	0.50
CAO	10.44	10.68	10.16	18.30	18.76	18.12	18.73	17.04
NA2O	5.00	5.40	5.55	0.96	1.27	0.75	0.58	1.23
K2O	0.22	0.14	0.17	0.00	0.00	0.00	0.00	0.00
TOTAL	99.31	99.27	99.50	99.29	99.27	99.29	99.41	99.23
MOLE PERCENT ENDMEMBERS								
AB	45.8	47.4	49.2	8.7	10.9	7.0	5.3	11.6
AN	52.9	51.8	49.8	91.3	89.1	93.0	94.7	88.4
OR	1.3	0.8	1.0	0.0	0.0	0.0	0.0	0.0

	57	58	59	60	61	62	63	64
	16801A	16802	16802A	08701	08701A	08702	16301A	16301B
	E	E	E	E	E	E	E	E
SIO2	46.92	48.20	47.21	45.58	45.57	45.63	44.53	44.02
TIO2	0.00	0.00	0.00	0.00	0.11	0.00	0.00	0.00
AL2O3	33.94	33.29	33.32	34.42	34.60	34.19	34.60	34.81
FEO	0.55	0.47	0.58	0.57	0.59	0.54	0.56	0.64
CAO	17.36	17.33	17.41	18.24	18.88	18.09	18.82	19.09
NA2O	1.32	1.97	1.81	0.84	0.59	0.98	0.94	0.76
TOTAL	100.09	101.26	100.33	99.65	100.34	99.43	99.45	99.32
MOLE PERCENT ENDMEMBERS								
AB	12.1	17.1	15.8	7.7	5.4	8.9	8.3	6.7
AN	87.9	82.9	84.2	92.3	94.6	91.1	91.7	93.3
OR	0.0	0.0	0.0	0.0	0.0	0.0	0.0	0.0

	65	66	67	68	69	70	71	72
	16302	50B01	50B02	50B03	50B03A	50B04	50C01	50C02
	E	E	E	E	E	E	E	E
SIO2	45.68	44.95	45.49	45.02	45.40	44.50	44.45	44.95
AL2O3	33.81	34.70	34.36	34.35	34.63	34.25	33.94	34.22
FEO	0.64	0.61	0.49	0.48	0.53	0.61	0.60	0.65
CAO	17.91	18.92	18.57	18.91	18.97	18.79	18.71	18.53
NA2O	0.96	0.77	0.83	0.63	0.83	0.78	0.92	0.64
TOTAL	99.00	99.95	99.74	99.39	100.36	98.93	98.62	98.99
MOLE PERCENT ENDMEMBERS								
AB	8.8	6.9	7.5	5.7	7.3	7.0	8.2	5.9
AN	91.2	93.1	92.5	94.3	92.7	93.0	91.8	94.1
OR	0.0	0.0	0.0	0.0	0.0	0.0	0.0	0.0

TABLE A4.3 GRENADA CUMULATES - PLAGIOCLASES

	73	74	75	76	77	78	79	80
	50C03	15801	15801A	15802	15803	50A01	50A02	50A02A
	E	E	E	E	E	W	W	W
SIO2	44.80	45.03	45.86	45.23	45.99	44.64	44.71	45.10
TIO2	0.00	0.00	0.15	0.00	0.00	0.01	0.01	0.00
AL203	34.72	34.07	33.58	34.51	33.38	34.01	34.02	33.81
FEO	0.64	0.59	0.58	0.61	0.69	0.52	0.52	0.54
MGO	0.00	0.00	0.00	0.00	0.00	0.05	0.05	0.06
CAO	18.90	18.24	17.86	18.22	17.49	18.13	18.29	18.05
SRO	0.00	0.00	0.00	0.00	0.00	0.16	0.17	0.14
NA2O	0.80	1.26	1.12	0.80	1.71	1.07	0.96	1.12
K2O	0.00	0.00	0.06	0.00	0.00	0.02	0.01	0.02
TOTAL	99.86	99.19	99.21	99.37	99.26	98.62	98.76	98.86
MOLE PERCENT ENDMEMBERS								
AB	7.1	11.1	10.2	7.4	15.0	9.7	8.7	10.1
AN	92.9	88.9	89.5	92.6	85.0	90.2	91.3	89.8
OR	0.0	0.0	0.4	0.0	0.0	0.1	0.1	0.1

	81	82	83	84
	15501	15502	40601	40602
	W	W	W	W
SIO2	45.21	44.99	55.22	55.24
TIO2	0.01	0.03	0.00	0.01
AL203	33.73	34.00	27.34	27.61
FEO	0.52	0.48	0.38	0.36
MGO	0.06	0.05	0.04	0.05
CAO	18.00	18.52	10.05	10.40
SRO	0.12	0.11	0.18	0.17
NA2O	1.23	1.02	5.84	5.60
K2O	0.02	0.02	0.19	0.20
TOTAL	98.89	99.23	99.26	99.64
MOLE PERCENT ENDMEMBERS				
AB	11.0	9.1	50.7	48.8
AN	88.9	90.8	48.2	50.1
OR	0.1	0.1	1.1	1.2

TABLE A4.4 GRENADA CUMULATES - AMPHIBOLES

	1	2	3	4	5	6	7	8
	06601	06601A	06602	06602A	07001	07002	09101	09102
	W	W	W	W	W	W	W	W
SIO2	42.25	41.69	41.75	41.83	40.64	41.78	43.48	42.96
TIO2	2.48	2.81	2.61	2.81	1.69	1.49	1.65	1.79
AL2O3	11.91	11.92	12.16	12.07	14.48	13.71	11.55	11.78
CR2O3	0.01	0.03	0.06	0.07	0.28	0.28	0.05	0.32
V2O3	0.06	0.07	0.06	0.07	0.07	0.04	0.03	0.07
FEO	10.77	11.00	11.17	11.82	8.56	8.31	10.37	10.57
MNO	0.18	0.16	0.18	0.20	0.09	0.07	0.20	0.21
MGO	14.86	14.50	14.44	14.37	15.35	15.99	15.17	14.90
NIO	0.00	0.00	0.00	0.00	0.05	0.05	0.05	0.03
CAO	11.62	11.75	11.53	11.57	12.35	12.12	11.59	11.71
NA2O	2.78	2.75	2.86	2.89	2.59	2.58	2.45	2.38
K2O	0.52	0.53	0.50	0.49	0.43	0.42	0.56	0.68
F	0.10	0.08	0.07	0.21	0.00	0.00	0.04	0.00
CL	0.07	0.07	0.06	0.08	0.01	0.01	0.04	0.05
TOTAL	97.62	97.35	97.45	98.49	96.61	96.85	97.23	97.46

	9	10	11	12	13	14	15	16
	09103	05101	05102	05103	16601	16602	16603	16604
	W	W	W	W	W	W	W	W
SIO2	43.86	41.87	41.36	41.20	42.96	43.87	42.94	44.67
TIO2	1.43	2.01	3.48	2.08	1.64	1.20	1.28	1.11
AL2O3	11.09	12.68	12.11	12.67	12.05	11.34	11.80	10.74
CR2O3	0.21	0.11	0.05	0.01	0.01	0.03	0.19	0.07
V2O3	0.05	0.09	0.10	0.06	0.05	0.03	0.04	0.04
FEO	10.75	11.02	11.40	11.77	11.14	11.10	11.99	10.42
MNO	0.21	0.18	0.22	0.20	0.25	0.28	0.30	0.26
MGO	15.22	14.47	14.00	13.81	14.41	14.98	14.06	15.45
NIO	0.03	0.03	0.06	0.04	0.03	0.02	0.03	0.03
CAO	11.41	11.85	11.28	11.69	11.75	11.53	11.57	11.73
NA2O	2.46	2.51	2.53	2.77	2.54	2.38	2.47	2.27
K2O	0.48	0.41	0.49	0.48	0.34	0.36	0.37	0.40
F	0.04	0.00	0.00	0.00	0.00	0.00	0.00	0.00
CL	0.05	0.04	0.04	0.04	0.02	0.02	0.02	0.04
TOTAL	97.30	97.28	97.13	96.83	97.21	97.13	97.07	97.23

	17	18	19	20	21	22	23	24
	24901	24902	24903	24904	06501	06502	06502A	06503
	W	W	W	W	W	W	W	W
SIO2	42.95	42.33	41.72	41.41	40.57	40.98	40.57	40.39
TIO2	0.87	1.47	1.77	2.01	1.98	2.73	2.06	2.26
AL2O3	11.69	12.31	12.74	12.87	13.52	12.63	13.45	13.33
CR2O3	0.01	0.02	0.03	0.01	0.02	0.30	0.01	0.03
V2O3	0.07	0.08	0.08	0.09	0.05	0.07	0.03	0.07
FEO	11.81	11.78	11.79	11.75	10.43	10.08	10.29	10.54
MNO	0.20	0.18	0.16	0.16	0.11	0.16	0.09	0.12
MGO	14.85	14.33	14.03	14.08	14.50	14.63	14.60	14.49
NIO	0.04	0.04	0.05	0.04	0.02	0.03	0.02	0.02
CAO	11.41	11.26	11.73	11.64	11.90	11.55	12.02	11.89
NA2O	2.47	2.57	2.55	2.65	2.80	2.71	2.76	2.78
K2O	0.41	0.44	0.52	0.50	0.61	0.66	0.58	0.60
CL	0.04	0.04	0.03	0.04	0.14	0.15	0.10	0.11
TOTAL	96.83	96.86	97.19	97.27	96.65	96.65	96.58	96.64

TABLE A4.4 GRENADA CUMULATES - AMPHIBOLES

	25	26	27	28	29	30	31	32
	10501	10502	10502A	16701	16702	16703	06701	06702
	W	W	W	W	W	W	W	W
SIO2	40.05	40.13	39.32	40.36	43.31	43.89	41.33	40.78
TIO2	1.86	1.61	2.02	4.13	1.30	1.01	1.64	1.93
AL203	14.48	14.24	14.84	12.22	11.30	11.18	14.04	14.48
CR203	0.06	0.05	0.05	0.05	0.20	0.05	0.33	0.18
V203	0.07	0.06	0.06	0.06	0.05	0.03	0.07	0.06
FEO	10.51	10.64	9.97	9.70	11.19	10.96	8.27	8.50
MNO	0.12	0.13	0.09	0.16	0.21	0.19	0.10	0.09
MGO	14.25	14.43	14.24	14.29	15.30	15.62	15.75	15.59
NIO	0.02	0.03	0.02	0.02	0.02	0.07	0.04	0.02
CAO	12.20	12.00	12.36	11.88	11.66	11.45	12.16	12.32
NA2O	2.64	2.71	2.65	2.40	2.39	2.40	2.67	2.70
K2O	0.50	0.45	0.51	0.99	0.55	0.50	0.49	0.53
CL	0.02	0.02	0.03	0.09	0.11	0.09	0.03	0.02
TOTAL	96.77	96.41	96.15	96.37	97.59	97.45	96.94	97.21

	33	34	35	36	37	38	39	40
	06703	09501	09502	09503	09504	10701	10702	10703
	W	W	W	W	W	W	W	W
SIO2	40.57	42.12	44.98	42.09	41.76	41.58	40.88	42.74
TIO2	1.97	3.23	0.30	2.78	3.09	2.43	3.08	2.00
AL203	14.61	11.73	10.57	11.59	11.86	12.35	12.32	11.44
CR203	0.09	0.20	0.16	0.17	0.11	0.02	0.01	0.02
V203	0.07	0.08	0.03	0.09	0.07	0.06	0.08	0.04
FEO	8.37	10.43	10.33	11.59	10.76	12.15	11.69	11.24
MNO	0.08	0.21	0.21	0.24	0.17	0.19	0.19	0.20
MGO	15.55	14.81	16.47	14.10	14.60	13.94	13.73	14.70
NIO	0.03	0.02	0.07	0.05	0.02	0.02	0.00	0.00
CAO	12.27	11.46	11.43	11.57	11.54	11.67	11.83	11.44
NA2O	2.60	2.44	2.26	2.44	2.45	2.64	2.78	2.62
K2O	0.56	0.85	0.57	0.80	0.81	0.45	0.40	0.46
CL	0.03	0.29	0.22	0.27	0.27	0.15	0.15	0.15
TOTAL	96.82	97.88	97.62	97.80	97.52	97.68	97.16	97.05

	41	42	43	44	45	46	47	48
	09901	09902	09903	09904	09905	09401	09402	13502
	W	W	W	W	W	W	W	W
SIO2	43.22	42.91	43.41	40.77	41.35	41.13	41.34	45.25
TIO2	1.21	1.43	1.35	1.78	1.71	2.41	2.49	1.03
AL203	11.47	11.43	11.28	13.44	12.43	12.74	12.65	9.67
CR203	0.42	0.37	0.45	0.13	0.11	0.32	0.19	0.02
V203	0.02	0.03	0.03	0.05	0.03	0.07	0.09	0.03
FEO	9.95	9.96	9.88	11.16	11.10	10.42	10.34	11.62
MNO	0.17	0.17	0.16	0.16	0.19	0.19	0.17	0.28
MGO	15.94	15.86	15.92	14.39	14.62	14.87	14.86	15.45
NIO	0.04	0.03	0.02	0.00	0.01	0.05	0.05	0.02
CAO	11.72	11.54	11.59	12.12	12.00	11.47	11.39	11.26
NA2O	2.44	2.52	2.51	2.53	2.52	2.62	2.57	2.21
K2O	0.38	0.39	0.35	0.48	0.41	0.57	0.63	0.51
CL	0.09	0.09	0.12	0.12	0.10	0.21	0.19	0.20
TOTAL	97.08	96.72	97.07	97.13	96.58	97.05	96.98	97.55

TABLE A4.4 GRENADA CUMULATES - AMPHIBOLES

	49	50	51	52	53	54	55	56
	13503	13503A	15901	15902	15903	13602	16801	16802
	W	W	E	E	E	E	E	E
SIO2	43.16	45.19	42.98	43.41	41.96	40.49	43.59	44.90
TIO2	1.47	1.21	3.39	2.33	2.66	1.99	1.23	0.66
AL2O3	11.49	9.40	10.91	10.73	12.16	14.95	11.46	11.70
CR2O3	0.24	0.12	0.00	0.00	0.00	0.00	0.00	0.00
V2O3	0.04	0.05	0.00	0.00	0.00	0.00	0.00	0.00
FEO	10.81	11.59	11.95	12.59	11.57	9.77	10.49	10.33
MNO	0.21	0.28	0.35	0.29	0.12	0.00	0.13	0.24
MGO	15.27	15.38	13.90	14.05	14.17	14.76	15.51	15.79
NIO	0.05	0.05	0.00	0.00	0.00	0.00	0.00	0.00
CAO	11.35	11.42	11.68	11.41	11.57	12.30	11.82	11.55
NA2O	2.59	2.14	2.13	2.14	2.29	2.12	2.40	1.90
K2O	0.37	0.51	0.47	0.49	0.42	0.43	0.55	0.50
CL	0.12	0.19	0.00	0.00	0.00	0.00	0.00	0.00
TOTAL	97.16	97.54	97.76	97.44	96.92	96.81	97.18	97.57

	57	58	59	60	61	62	63	64
	08701	08702	10201	16301	16501	16502	16504	50B01
	E	E	E	E	W	W	E	E
SIO2	40.98	40.48	44.18	42.26	42.42	41.90	41.12	41.64
TIO2	1.66	1.76	0.94	1.69	0.86	1.31	1.48	2.01
AL2O3	15.19	14.90	12.07	13.23	12.25	14.14	13.83	13.52
CR2O3	0.00	0.00	0.00	0.00	0.21	0.10	0.00	0.00
V2O3	0.00	0.00	0.00	0.00	0.04	0.05	0.00	0.00
FEO	9.92	9.81	9.39	10.23	8.77	9.10	9.75	11.79
MNO	0.00	0.00	0.23	0.18	0.14	0.16	0.18	0.23
MGO	14.89	14.56	16.36	15.22	16.12	15.74	14.45	13.69
NIO	0.00	0.00	0.00	0.00	0.06	0.08	0.00	0.00
CAO	12.61	12.50	11.70	12.41	11.88	11.98	12.42	12.10
NA2O	2.17	2.12	1.94	2.12	2.38	2.53	2.25	2.16
K2O	0.45	0.48	0.37	0.50	0.41	0.55	0.51	0.45
CL	0.00	0.00	0.00	0.00	0.07	0.07	0.00	0.06
TOTAL	97.87	96.61	97.18	97.84	95.60	97.71	95.99	97.65

	65	66	67	68	69	70	71	72
	50B03	50C02	50C03	15801	15802	15803	15804	50A01
	E	E	E	E	E	E	E	W
SIO2	41.31	42.52	41.88	41.20	41.31	41.05	41.10	42.08
TIO2	1.91	1.88	1.73	3.13	2.82	2.75	2.74	1.19
AL2O3	12.71	12.96	13.35	12.44	12.28	12.92	13.03	12.57
CR2O3	0.00	0.00	0.00	0.00	0.00	0.00	0.00	0.12
V2O3	0.00	0.00	0.00	0.00	0.00	0.00	0.00	0.04
FEO	11.74	11.59	11.28	11.93	12.07	11.48	11.70	10.07
MNO	0.17	0.21	0.15	0.20	0.28	0.32	0.21	0.15
MGO	13.80	14.60	14.00	13.72	14.64	13.65	14.25	15.25
NIO	0.00	0.00	0.00	0.00	0.00	0.00	0.00	0.05
CAO	11.69	12.17	11.77	11.40	11.50	11.67	11.57	11.76
NA2O	2.19	2.19	2.06	2.68	2.29	3.00	2.75	2.54
K2O	0.44	0.36	0.41	0.49	0.35	0.41	0.45	0.41
CL	0.09	0.05	0.05	0.11	0.11	0.06	0.08	0.00
TOTAL	96.05	98.53	96.68	97.30	97.65	97.31	97.88	96.22

TABLE A4.4 GRENADA CUMULATES - AMPHIBOLES

	73	74	75	76
	50A02	15501	15502	40601
	W	W	W	W
SIO2	40.89	41.30	40.58	42.25
TIO2	1.30	1.49	1.90	1.24
AL203	13.62	13.88	14.17	12.84
CR203	0.11	0.01	0.13	0.06
V203	0.06	0.06	0.06	0.05
FEO	10.42	9.21	9.38	9.70
MNO	0.11	0.09	0.09	0.11
MGO	14.51	15.29	14.57	15.28
NIO	0.05	0.06	0.05	0.03
CAO	11.90	11.97	11.97	11.73
NA2O	2.58	2.70	2.62	2.53
K2O	0.44	0.40	0.44	0.50
TOTAL	96.00	96.46	95.98	96.33

TABLE A4.5 GRENADA CUMULATES - OXIDES

	1	2	3	4	5	6	7	8
	06601A	06602	06602A	06603	06604	07001	07002	07003
	W	W	W	W	W	W	W	W
SIO2	0.06	0.05	0.07	0.10	0.07	0.08	0.02	0.00
TIO2	6.37	6.43	6.54	6.72	7.75	2.19	2.42	2.04
AL2O3	4.58	4.51	4.51	4.84	4.28	18.62	18.92	18.66
CR2O3	0.35	0.33	0.35	0.28	0.34	14.89	13.21	17.12
V2O3	0.47	0.50	0.47	0.28	0.38	0.28	0.31	0.28
FE2O3	52.10	52.37	52.29	51.59	50.05	31.82	32.83	30.31
FEO	31.77	32.37	31.98	30.75	32.17	23.69	22.97	22.97
MNO	0.45	0.44	0.44	0.33	0.41	0.37	0.38	0.38
MGO	3.43	3.28	3.56	4.15	3.85	8.01	8.54	8.41
NIO	0.05	0.00	0.04	0.06	0.04	0.11	0.14	0.17
CAO	0.11	0.02	0.07	0.43	0.29	0.11	0.04	0.03
K2O	0.03	0.03	0.03	0.03	0.03	0.03	0.03	0.03
TOTAL	99.79	100.34	100.37	99.56	99.65	100.20	99.82	100.39

	9	10	11	12	13	14	15	16
	07003A	07004	09101	09101A	09102	05101	05101A	05102
	W	W	W	W	W	W	W	W
SIO2	0.04	0.06	0.00	0.01	0.01	0.04	0.09	0.10
TIO2	2.21	0.20	2.73	2.71	2.43	4.81	4.82	5.36
AL2O3	19.05	17.16	5.63	5.72	5.62	7.86	7.96	7.50
CR2O3	13.90	47.08	11.58	11.85	11.59	2.84	2.31	1.34
V2O3	0.28	0.10	0.42	0.42	0.38	1.69	0.43	0.48
FE2O3	32.26	5.82	46.61	46.14	47.11	48.82	49.07	49.82
FEO	22.87	18.91	29.00	28.83	28.82	29.96	29.12	29.99
MNO	0.35	0.56	0.62	0.63	0.56	0.34	0.33	0.37
MGO	8.38	9.99	3.15	3.16	3.07	4.46	4.46	4.40
NIO	0.17	0.07	0.14	0.17	0.15	0.09	0.10	0.07
CAO	0.18	0.02	0.02	0.08	0.07	0.05	0.28	0.12
K2O	0.03	0.03	0.03	0.03	0.03	0.00	0.00	0.00
TOTAL	99.73	100.01	99.94	99.74	99.83	100.98	98.98	99.54

	17	18	19	20	21	22	23	24
	05103	16601	16601A	16602	16603	16604	16604A	16604B
	W	W	W	W	W	E	E	E
SIO2	0.04	0.00	0.05	0.01	0.11	0.00	0.39	0.00
TIO2	5.26	1.50	2.58	2.25	9.14	1.48	1.71	1.99
AL2O3	7.60	4.75	4.13	4.61	2.44	4.45	4.72	4.36
CR2O3	3.41	26.45	12.01	12.25	0.04	26.39	23.56	19.67
V2O3	0.48	0.19	0.22	0.27	0.37	0.00	0.00	0.00
FE2O3	48.17	34.54	47.86	47.54	47.99	34.43	36.87	41.37
FEO	29.98	28.13	28.88	28.26	34.57	28.29	29.69	29.37
MNO	0.35	1.06	0.66	0.82	0.54	0.70	0.90	0.90
MGO	4.47	2.79	2.94	2.94	2.67	2.67	2.50	2.40
NIO	0.12	0.06	0.12	0.13	0.14	0.00	0.00	0.00
CAO	0.01	0.00	0.08	0.12	0.16	0.00	0.00	0.00
TOTAL	99.88	99.58	99.53	99.20	98.19	98.41	100.35	100.06

TABLE A4.5 GRENADA CUMULATES - OXIDES

	25	26	27	28	29	30	31	32
	16604C	16604D	16605	16605A	24901	24902	24903	24904
	E	E	E	E	W	W	W	W
SIO2	0.00	0.21	0.19	0.00	0.07	0.04	0.06	0.03
TIO2	2.15	2.32	3.27	3.25	5.11	3.73	5.28	3.95
AL203	4.08	4.14	3.62	3.92	3.13	5.28	3.66	5.15
CR203	16.83	14.28	9.69	9.15	1.53	0.39	0.39	0.40
V203	0.00	0.00	0.00	0.00	0.59	0.53	0.41	0.53
FE203	44.53	45.80	50.12	50.17	54.07	55.79	54.70	55.47
FEO	29.29	29.60	30.15	29.88	32.16	30.67	31.88	30.80
MNO	0.73	0.77	0.48	0.43	0.37	0.32	0.35	0.34
MGO	2.64	2.56	3.02	2.91	2.34	2.80	2.74	2.82
NIO	0.00	0.00	0.00	0.00	0.04	0.04	0.06	0.04
CAO	0.00	0.00	0.00	0.00	0.13	0.01	0.03	0.02
TOTAL	100.25	99.68	100.54	99.71	99.55	99.61	99.56	99.55

	33	34	35	36	37	38	39	40
	06501	06501A	06502	06504	10501	10501A	10502	10503
	W	W	W	W	W	W	W	W
SIO2	0.06	0.05	0.09	0.08	0.05	0.09	0.08	0.10
TIO2	6.85	6.70	7.09	5.82	4.61	4.55	4.50	4.87
AL203	5.68	5.83	5.61	6.68	12.31	12.40	12.26	10.44
CR203	0.53	0.50	0.54	0.24	0.43	0.40	0.37	0.54
V203	0.57	0.54	0.56	0.45	0.49	0.51	0.49	0.48
FE203	49.43	50.12	49.22	50.32	47.81	47.74	48.03	48.61
FEO	30.99	30.97	31.32	29.93	28.65	28.36	28.49	28.95
MNO	0.38	0.39	0.40	0.37	0.29	0.27	0.25	0.30
MGO	4.35	4.43	4.35	4.29	5.61	5.76	5.69	5.23
NIO	0.08	0.06	0.07	0.05	0.09	0.09	0.07	0.09
CAO	0.01	0.01	0.03	0.25	0.00	0.04	0.00	0.03
TOTAL	98.93	99.60	99.28	98.48	100.34	100.21	100.25	99.65

	41	42	43	44	45	46	47	48
	16701	16702	06701	06702	06704	09501	09502	09503
	W	W	W	W	W	W	W	W
SIO2	0.02	0.04	0.04	0.06	0.05	0.04	0.09	0.05
TIO2	6.52	2.64	2.37	2.45	1.99	4.67	0.79	0.76
AL203	4.34	4.35	25.22	23.44	25.22	3.48	3.38	3.41
CR203	3.76	4.55	7.01	11.28	14.21	2.44	2.80	6.89
V203	0.50	0.25	0.33	0.35	0.26	0.31	0.21	0.07
FE203	48.13	56.10	32.35	30.44	26.74	54.44	60.69	57.48
FEO	31.50	29.02	21.47	22.44	20.54	30.77	28.54	27.47
MNO	0.43	0.44	0.28	0.35	0.32	0.46	0.39	0.45
MGO	3.56	3.07	10.22	9.64	10.74	2.98	1.97	2.78
NIO	0.13	0.28	0.18	0.17	0.18	0.11	0.14	0.15
CAO	0.00	0.01	0.01	0.10	0.12	0.07	0.05	0.02
TOTAL	98.99	100.45	99.49	100.72	100.37	99.77	99.15	99.53

TABLE A4.5 GRENADA CUMULATES - OXIDES

	49	50	51	52	53	54	55	56
	09504	10701	10701A	10702	09901	09902	09903	09904
	W	W	W	W	W	W	W	W
SIO2	0.00	0.04	0.06	0.05	0.11	0.14	0.05	0.06
TIO2	3.73	5.26	5.34	5.57	3.68	2.64	4.19	4.17
AL203	3.53	4.76	4.76	4.39	6.31	6.81	6.30	6.26
CR203	4.92	0.65	0.57	1.22	5.97	9.39	1.48	1.39
V203	0.29	0.51	0.51	0.54	0.33	0.25	0.42	0.45
FE203	53.88	53.96	53.34	52.83	49.37	46.98	53.32	53.26
FEO	29.82	31.66	31.81	32.01	27.94	26.60	30.30	30.38
MNO	0.45	0.39	0.38	0.42	0.47	0.45	0.43	0.40
MGO	3.07	3.06	3.01	3.01	4.26	4.35	3.43	3.37
NIO	0.16	0.04	0.05	0.04	0.21	0.19	0.13	0.10
CAO	0.00	0.15	0.01	0.00	0.22	0.43	0.01	0.00
TOTAL	99.85	100.48	99.85	100.07	98.85	98.24	100.07	99.83

	57	58	59	60	61	62	63	64
	09401	09402	13501	13502	13502A	13601	13602	13603
	W	W	W	W	W	E	E	E
SIO2	0.04	0.07	0.03	0.19	0.08	0.00	0.26	0.37
TIO2	4.88	4.86	5.04	1.87	1.89	3.02	5.16	5.09
AL203	6.40	5.30	5.00	3.43	3.43	6.50	5.15	4.90
CR203	5.10	1.16	11.01	10.02	9.98	16.17	2.74	2.62
V203	0.57	0.40	0.49	0.28	0.26	0.43	0.47	0.61
FE203	47.69	52.87	43.61	51.24	51.05	39.65	51.43	49.98
FEO	30.30	30.23	30.61	29.54	29.14	28.56	28.75	30.70
MNO	0.42	0.34	0.51	0.65	0.69	0.31	0.45	0.42
MGO	3.73	3.49	3.59	2.17	2.10	3.83	5.04	3.58
NIO	0.15	0.19	0.10	0.10	0.14	0.00	0.00	0.00
CAO	0.01	0.16	0.07	0.01	0.10	0.00	0.00	0.00
TOTAL	99.28	99.06	100.07	99.51	98.87	98.45	99.45	98.27

	65	66	67	68	69	70	71	72
	16802	08701	08702	08703	16301	16302	16501	16501
	E	E	E	E	E	E	E	W
SIO2	0.26	0.48	0.28	0.27	0.23	0.42	0.28	0.00
TIO2	1.39	4.55	4.78	4.55	4.00	4.50	4.39	1.48
AL203	6.73	15.19	14.55	12.45	8.89	7.50	6.69	10.60
CR203	10.95	0.57	0.42	0.29	0.27	0.33	1.87	13.72
V203	0.43	0.59	0.65	0.62	0.65	0.45	0.00	0.16
FE203	48.93	44.11	45.47	48.11	51.92	52.42	51.48	42.48
FEO	27.76	29.19	29.75	29.70	30.03	30.69	30.63	24.82
MNO	0.51	0.31	0.43	0.35	0.37	0.35	0.32	0.49
MGO	3.92	6.13	5.78	5.40	4.15	4.09	3.57	5.77
NIO	0.00	0.00	0.00	0.00	0.00	0.00	0.00	0.16
CAO	0.00	0.00	0.00	0.00	0.00	0.00	0.00	0.04
TOTAL	100.87	101.12	102.11	101.74	100.51	100.75	99.23	99.72

TABLE A4.5 GRENADA CUMULATES - OXIDES

	73	74	75	76	77	78	79	80
	16502	16503	16504	16505	50B01	50B02	50C01	50C02
	E	E	E	E	E	E	E	E
SIO2	0.28	0.33	0.00	0.31	0.00	0.30	0.34	0.29
TIO2	4.39	1.98	2.02	4.12	5.20	4.98	4.97	5.01
AL2O3	6.69	10.64	9.10	6.64	5.55	5.63	5.14	5.78
CR2O3	1.87	9.07	10.01	2.27	0.24	0.17	0.34	0.34
V2O3	0.00	0.00	0.00	0.00	0.61	0.71	0.76	0.77
FE2O3	51.48	44.71	46.16	51.93	54.27	53.51	54.77	53.75
FEO	30.63	26.06	25.97	30.34	30.76	31.84	31.52	31.36
MNO	0.32	0.36	0.53	0.36	0.23	0.37	0.28	0.19
MGO	3.57	5.51	5.07	3.68	3.98	3.32	3.78	3.89
TOTAL	99.23	98.66	98.87	99.65	100.84	100.83	101.90	101.39

	81	82	83	84	85	86	87	88
	15802	15803	15804	15805	50A01	50A02	15501	15502
	E	E	E	E	W	W	W	W
SIO2	0.31	0.32	0.20	0.25	0.05	0.04	0.03	0.08
TIO2	7.81	8.12	8.51	8.62	2.86	3.23	3.38	3.76
AL2O3	5.56	6.17	6.69	6.50	9.21	8.98	8.60	8.14
CR2O3	0.87	0.78	0.59	0.44	4.53	7.80	9.80	6.65
V2O3	1.06	0.74	0.89	1.02	0.34	0.34	0.35	0.43
FE2O3	47.56	47.50	45.89	46.35	49.62	46.01	44.09	46.28
FEO	34.21	33.37	33.66	33.97	27.49	27.72	28.56	28.86
MNO	0.65	0.32	0.40	0.45	0.36	0.41	0.46	0.43
MGO	3.45	4.55	4.37	4.39	4.67	4.77	4.31	4.10
NIO	0.00	0.00	0.00	0.00	0.14	0.11	0.10	0.11
CAO	0.00	0.00	0.00	0.00	0.06	0.04	0.03	0.13
TOTAL	101.49	101.87	101.20	102.01	99.33	99.45	99.72	98.98

	89	90	91	92	93	94	95	96
	40601	40603	40501	40602	40603	40603A	40604	40605
	W	W	E	E	E	E	E	E
SIO2	0.02	0.01	0.29	0.00	0.22	0.27	0.33	0.35
TIO2	0.51	0.30	0.49	0.88	0.26	0.37	0.74	0.99
AL2O3	13.51	10.84	13.79	0.70	10.73	10.89	5.14	3.20
CR2O3	27.47	23.19	27.65	2.18	23.71	23.54	29.86	25.27
V2O3	0.28	0.07	0.00	0.44	0.00	0.25	0.33	0.31
FE2O3	25.34	34.15	24.61	63.73	34.48	33.87	30.36	37.24
FEO	25.11	23.53	26.13	30.29	24.22	24.80	29.79	29.82
MNO	0.86	0.60	0.81	0.34	0.65	0.58	0.84	1.03
MGO	4.98	5.60	4.76	0.75	5.83	5.65	1.70	1.60
NIO	0.14	0.28	0.00	0.00	0.00	0.00	0.00	0.00
CAO	0.00	0.05	0.00	0.00	0.00	0.00	0.00	0.00
TOTAL	98.23	98.72	98.53	99.33	100.11	100.23	99.09	99.81

TABLE A4.5 GRENADA CUMULATES - OXIDES

	97	98	99	100	101	102	103	104
	40606	40607	40608	40609	40610	40611	40611A	40612
	E	E	E	E	E	E	E	E
SIO2	0.22	0.42	0.23	2.61	0.00	0.29	0.26	0.33
TIO2	0.69	0.74	0.54	1.47	0.46	0.45	0.72	0.44
AL203	1.07	0.55	14.73	2.13	13.51	8.25	6.09	8.33
CR203	26.52	2.41	31.58	1.45	34.30	33.71	30.76	33.68
V203	0.42	0.41	0.32	0.43	0.19	0.17	0.00	0.28
FE203	38.23	62.56	22.99	56.22	21.41	25.13	29.35	25.69
FEO	29.41	30.55	23.95	32.01	24.49	29.57	30.01	27.09
MNO	0.86	0.38	0.32	0.42	0.40	1.02	1.13	0.57
MGO	1.22	0.66	7.32	2.32	6.39	2.28	1.57	4.15
TOTAL	98.64	98.78	101.98	99.05	101.15	100.92	99.89	100.55

	105	106
	40613	40614
	E	E
SIO2	0.23	0.34
TIO2	0.63	0.48
AL203	14.02	0.57
CR203	37.56	4.66
V203	0.00	0.57
FE203	16.80	62.31
FEO	23.15	30.76
MNO	0.00	0.36
MGO	7.70	0.82
TOTAL	100.08	100.87

TABLE A5.1 GRENADA PERIDOTITES - OLIVINES

	1	2	3	4	5	6	7	8
	23101	23102	23103	23104	23105	23301	23302	23303
	E	E	E	E	E	E	E	E
SIO2	41.09	40.93	41.49	41.01	41.66	40.88	40.97	40.61
TIO2	0.00	0.00	0.00	0.00	0.00	0.00	0.00	0.11
FEO	9.92	9.79	10.14	9.32	8.64	9.76	9.87	9.36
MNO	0.00	0.18	0.00	0.20	0.13	0.00	0.12	0.24
MGO	47.83	48.64	48.53	48.69	49.40	48.63	48.07	48.67
NIO	0.27	0.43	0.44	0.30	0.34	0.30	0.48	0.30
CAO	0.08	0.00	0.00	0.17	0.19	0.11	0.10	0.16
TOTAL	99.19	99.97	100.60	99.69	100.36	99.68	99.61	99.45
MOLE PERCENT ENDMEMBERS								
FO	89.6	89.9	89.5	90.3	91.1	89.9	89.7	90.3
FA	10.4	10.1	10.5	9.7	8.9	10.1	10.3	9.7

	9	10	11	12	13	14	15	16
	23305	23306	23307	23308	23203	23204	23205	23206
	W	W	W	W	E	E	E	E
SIO2	40.91	41.22	40.82	40.71	41.06	41.46	40.96	41.24
AL2O3	0.02	0.02	0.02	0.03	0.00	0.00	0.00	0.00
CR2O3	0.00	0.00	0.04	0.08	0.00	0.00	0.00	0.00
FEO	9.61	9.94	9.65	9.90	8.99	9.50	9.68	9.68
MNO	0.13	0.12	0.16	0.17	0.00	0.16	0.14	0.00
MGO	48.26	48.49	48.14	48.00	48.76	49.91	48.93	48.31
NIO	0.40	0.42	0.35	0.30	0.38	0.56	0.30	0.36
CAO	0.03	0.04	0.11	0.13	0.15	0.00	0.00	0.00
TOTAL	99.36	100.25	99.28	99.33	99.34	101.59	100.01	99.59
MOLE PERCENT ENDMEMBERS								
FO	90.0	89.7	89.9	89.6	90.6	90.4	90.0	89.9
FA	10.0	10.3	10.1	10.4	9.4	9.6	10.0	10.1

	17	18	19	20	21	22	23	24
	23206A	23207	23207A	23210	23211	23212	23213	12201
	E	E	E	W	W	W	W	E
SIO2	41.40	41.50	41.10	40.79	41.25	40.82	40.65	40.86
TIO2	0.00	0.00	0.00	0.01	0.00	0.01	0.01	0.00
AL2O3	0.00	0.00	0.00	0.05	0.04	0.03	0.01	0.00
CR2O3	0.00	0.00	0.00	0.00	0.03	0.04	0.00	0.00
V2O3	0.00	0.00	0.00	0.00	0.00	0.00	0.00	0.00
FEO	9.61	9.74	9.74	9.78	8.87	8.63	9.76	10.96
MNO	0.00	0.00	0.00	0.11	0.09	0.12	0.12	0.11
MGO	48.70	49.49	49.40	48.55	49.08	49.21	48.43	46.47
NIO	0.44	0.43	0.43	0.41	0.30	0.25	0.39	0.51
CAO	0.00	0.00	0.13	0.00	0.10	0.10	0.00	0.24
TOTAL	100.15	101.16	100.80	99.71	99.76	99.20	99.37	99.15
MOLE PERCENT ENDMEMBERS								
FO	90.0	90.1	90.0	89.8	90.8	91.0	89.8	88.3
FA	10.0	9.9	10.0	10.2	9.2	9.0	10.2	11.7

TABLE A5.1 GRENADA PERIDOTITES - OLIVINES

	25	26	27	28	29	30	31	32
	12202	12203	12301	12302	12303	12306	23701	23702
	E	E	E	E	E	E	E	E
SIO2	41.43	41.38	41.16	41.74	41.17	41.02	41.70	41.27
FEO	8.97	8.35	9.66	9.13	9.78	9.95	10.10	10.12
MNO	0.00	0.00	0.22	0.23	0.27	0.00	0.17	0.18
MGO	48.12	48.44	47.57	48.13	47.43	47.59	49.24	49.60
NIO	0.40	0.41	0.41	0.00	0.36	0.32	0.53	0.48
CAO	0.00	0.12	0.00	0.15	0.00	0.12	0.00	0.00
TOTAL	98.92	98.70	99.02	99.38	99.01	99.00	101.74	101.65
MOLE PERCENT ENDMEMBERS								
FO	90.5	91.2	89.8	90.4	89.6	89.5	89.7	89.7
FA	9.5	8.8	10.2	9.6	10.4	10.5	10.3	10.3

	33	34	35
	23601	23602	23603
	W	W	W
SIO2	41.42	41.51	41.45
TIO2	0.01	0.00	0.00
AL203	0.01	0.02	0.02
CR203	0.01	0.02	0.05
FEO	9.72	8.71	8.58
MNO	0.15	0.17	0.12
MGO	48.32	49.37	49.21
NIO	0.54	0.39	0.36
CAO	0.01	0.09	0.10
TOTAL	100.20	100.28	99.88
MOLE PERCENT ENDMEMBERS			
FO	89.9	91.0	91.1
FA	10.1	9.0	8.9

TABLE A5.2 GRENADA PERIDOTITES - PYROXENES

	1	2	3	4	5	6	7	8
	23101	23101A	23101B	23102	23103	23104	23105	23106
	E	E	E	E	E	E	E	E
SIO2	56.78	57.96	57.52	53.74	54.47	53.32	53.07	57.62
TIO2	0.00	0.00	0.00	0.11	0.00	0.15	0.18	0.00
AL2O3	1.96	1.36	1.13	2.13	1.47	3.08	2.83	0.80
CR2O3	0.16	0.14	0.00	0.61	0.40	1.01	0.65	0.12
FEO	6.73	6.51	6.40	3.35	3.41	3.03	3.28	6.31
MNO	0.17	0.12	0.14	0.00	0.14	0.12	0.00	0.15
MGO	34.38	34.56	34.45	19.37	19.23	17.25	17.65	34.52
NIO	0.13	0.00	0.00	0.00	0.00	0.00	0.00	0.00
CAO	0.36	0.34	0.29	20.13	21.14	21.47	21.74	0.22
TOTAL	100.67	100.99	99.93	99.44	100.26	99.43	99.40	99.74
MOLE PERCENT ENDMEMBERS								
EN	89.5	89.9	90.1	54.2	52.9	50.2	50.3	90.3
FS	9.8	9.5	9.4	5.3	5.3	4.9	5.2	9.3
WO	0.7	0.6	0.5	40.5	41.8	44.9	44.5	0.4

	9	10	11	12	13	14	15	16
	23106A	23301	23301A	23302	23302A	23303	23303	23304
	E	E	E	E	E	E	E	E
SIO2	57.81	53.09	53.13	57.51	57.38	57.38	57.38	53.66
TIO2	0.00	0.18	0.15	0.00	0.00	0.00	0.00	0.00
AL2O3	0.96	2.27	2.18	0.78	0.87	0.92	0.92	2.06
CR2O3	0.00	1.14	0.55	0.11	0.21	0.00	0.00	0.64
FEO	6.35	3.09	3.20	6.28	6.54	6.32	6.32	2.61
MNO	0.15	0.12	0.12	0.12	0.16	0.15	0.15	0.00
MGO	34.56	16.62	16.43	34.25	34.56	34.47	34.47	17.06
NIO	0.00	0.00	0.00	0.00	0.00	0.15	0.15	0.00
CAO	0.24	22.72	23.28	0.51	0.31	0.41	0.41	24.02
TOTAL	100.07	99.23	99.04	99.57	100.03	99.80	99.80	100.05
MOLE PERCENT ENDMEMBERS								
EN	90.2	47.9	47.0	89.8	89.9	90.0	90.0	47.7
FS	9.3	5.0	5.1	9.2	9.5	9.3	9.3	4.1
WO	0.5	47.1	47.9	1.0	0.6	0.8	0.8	48.2

	17	18	19	20	21	22	23	24
	23307	23308	23308B	23310	23311	23312	23313	23314
	E	E	E	W	W	W	W	W
SIO2	54.55	52.56	51.72	56.90	57.53	54.58	50.45	53.22
TIO2	0.00	0.33	0.55	0.05	0.04	0.09	0.19	0.12
AL2O3	1.20	2.68	3.31	1.41	0.74	1.97	5.26	2.67
CR2O3	0.41	0.63	0.51	0.15	0.21	0.98	1.61	0.78
V2O3	0.00	0.00	0.00	0.00	0.00	0.06	0.02	0.02
FEO	2.26	4.19	5.15	6.46	6.24	3.03	3.12	2.74
MNO	0.00	0.11	0.00	0.15	0.15	0.11	0.06	0.11
MGO	17.68	16.35	15.47	33.97	34.21	17.86	16.91	17.51
NIO	0.00	0.00	0.00	0.09	0.09	0.03	0.08	0.07
CAO	24.29	23.13	23.13	0.35	0.21	21.40	20.58	21.83
NA2O	0.00	0.00	0.00	0.01	0.00	0.42	0.44	0.28
K2O	0.00	0.00	0.00	0.01	0.00	0.01	0.01	0.02
TOTAL	100.39	99.98	99.84	99.56	99.42	100.54	98.73	99.38
MOLE PERCENT ENDMEMBERS								
EN	48.6	46.3	44.2	89.8	90.4	51.1	50.5	50.4
FS	3.5	6.7	8.3	9.6	9.2	4.9	5.2	4.4
WO	48.0	47.1	47.5	0.7	0.4	44.0	44.2	45.2

TABLE A5.2 GRENADA PERIDOTITES - PYROXENES

	25	26	27	28	29	30	31	32
	23201	23201A	23202	23202A	23203	23204	23206	23206A
	E	E	E	E	E	E	E	E
SIO2	57.80	57.84	57.84	57.00	57.72	49.10	51.14	49.65
TIO2	0.10	0.00	0.00	0.00	0.00	0.29	0.19	0.29
AL2O3	0.45	0.82	1.63	1.66	0.73	7.44	6.22	6.72
CR2O3	0.00	0.00	0.19	0.13	0.11	2.83	1.72	2.39
FEO	6.74	6.64	6.50	6.49	6.21	3.82	3.36	3.89
MNO	0.11	0.11	0.00	0.00	0.15	0.00	0.00	0.00
MGO	34.88	35.08	34.37	34.37	34.75	15.23	16.11	15.78
NIO	0.00	0.13	0.00	0.00	0.00	0.00	0.00	0.00
CAO	0.30	0.25	0.17	0.22	0.36	20.55	21.29	20.47
TOTAL	100.38	100.87	100.70	99.87	100.03	99.25	100.03	99.19
MOLE PERCENT ENDMEMBERS								
EN	89.7	90.0	90.1	90.0	90.3	47.4	48.4	48.3
FS	9.7	9.6	9.6	9.5	9.1	6.7	5.7	6.7
WO	0.6	0.5	0.3	0.4	0.7	45.9	46.0	45.0

	33	34	35	36	37	38	39	40
	23207	23208	23208A	23209	23212	23213	23214	23215
	E	E	E	E	W	W	W	W
SIO2	57.29	49.66	49.86	57.30	57.49	49.84	50.03	57.23
TIO2	0.00	0.15	0.19	0.00	0.04	0.28	0.30	0.01
AL2O3	1.41	7.71	6.76	1.46	0.94	6.79	6.79	1.45
CR2O3	0.28	2.15	2.76	0.28	0.14	2.07	1.29	0.18
V2O3	0.00	0.00	0.00	0.00	0.00	0.06	0.05	0.02
FEO	6.43	3.48	3.61	6.42	6.35	3.79	3.68	6.43
MNO	0.00	0.00	0.00	0.00	0.12	0.05	0.07	0.11
MGO	34.55	15.51	15.19	34.65	34.01	15.92	16.09	33.91
NIO	0.00	0.00	0.00	0.00	0.10	0.08	0.09	0.09
CAO	0.25	20.76	20.69	0.40	0.42	19.52	20.05	0.34
NA2O	0.00	0.00	0.51	0.00	0.03	0.69	0.59	0.02
K2O	0.00	0.00	0.00	0.00	0.01	0.00	0.00	0.02
TOTAL	100.21	99.42	99.57	100.51	99.67	99.11	99.04	99.80
MOLE PERCENT ENDMEMBERS								
EN	90.1	47.9	47.3	89.9	89.8	49.6	49.4	89.8
FS	9.4	6.0	6.3	9.3	9.4	6.6	6.3	9.6
WO	0.5	46.1	46.3	0.7	0.8	43.7	44.3	0.7

	41	42	43	44	45	46	47	48
	23216	23217	12201R	12202R	12203	12204	12205	12206
	W	W	E	E	E	E	E	E
SIO2	52.15	57.58	51.70	48.72	55.14	57.38	54.63	55.08
TIO2	0.15	0.05	0.65	0.94	0.15	0.00	0.00	0.11
AL2O3	4.11	0.72	3.60	6.75	0.80	0.49	0.64	0.60
CR2O3	1.27	0.11	0.24	0.56	0.27	0.00	0.14	0.27
V2O3	0.04	0.00	0.00	0.00	0.00	0.00	0.00	0.00
FEO	3.02	6.54	4.94	5.70	2.54	8.31	2.65	2.54
MNO	0.09	0.11	0.00	0.00	0.00	0.25	0.00	0.00
MGO	17.33	34.25	15.77	13.75	17.70	33.23	17.61	17.85
NIO	0.05	0.06	0.00	0.14	0.00	0.00	0.00	0.00
CAO	20.97	0.27	23.54	23.25	23.83	0.43	23.78	24.10
NA2O	0.41	0.03	0.00	0.00	0.00	0.00	0.00	0.00
K2O	0.03	0.00	0.00	0.00	0.00	0.00	0.00	0.00
TOTAL	99.63	99.72	100.44	99.84	100.43	100.09	99.45	100.55
MOLE PERCENT ENDMEMBERS								
EN	50.8	89.9	44.5	40.9	48.8	87.0	48.7	48.8
FS	5.0	9.6	7.8	9.5	3.9	12.2	4.1	3.9
WO	44.2	0.5	47.7	49.6	47.2	0.8	47.2	47.3

TABLE A5.2 GRENADA PERIDOTITES - PYROXENES

	49	50	51	52	53	54	55	56
	12207	12208	12301	12302	12303	12304	12305	12306
	E	E	E	E	E	E	E	E
SIO2	57.10	57.42	57.43	57.57	54.05	53.92	52.92	52.22
TIO2	0.00	0.00	0.00	0.00	0.14	0.00	0.00	0.00
AL2O3	0.36	0.45	1.52	1.45	1.55	2.13	2.66	3.00
CR2O3	0.00	0.15	0.11	0.22	1.17	1.17	1.34	1.16
FEO	7.96	8.14	6.56	6.61	3.27	3.22	2.98	2.86
MNO	0.20	0.21	0.26	0.19	0.00	0.00	0.00	0.00
MGO	33.60	34.04	35.30	34.46	18.59	17.92	17.48	17.30
NIO	0.00	0.23	0.00	0.00	0.27	0.00	0.00	0.00
CAO	0.52	0.30	0.32	0.34	21.51	21.11	22.48	22.53
TOTAL	99.84	100.94	101.60	100.84	100.55	99.47	99.86	99.07
MOLE PERCENT ENDMEMBERS								
EN	87.2	87.7	89.9	89.7	51.8	51.3	49.5	49.3
FS	11.6	11.8	9.5	9.7	5.1	5.2	4.7	4.6
WO	1.2	0.5	0.6	0.6	43.1	43.5	45.8	46.1

	57	58	59	60	61	62	63	64
	12307	23701	23702	23703R	23601	23602	23603	23604
	E	E	E	E	W	W	W	W
SIO2	56.36	57.05	56.81	51.41	57.40	57.49	57.37	51.74
TIO2	0.00	0.00	0.00	0.65	0.03	0.03	0.02	0.13
AL2O3	2.47	1.26	1.49	3.29	1.37	0.68	0.38	4.41
CR2O3	0.68	0.00	0.27	0.19	0.10	0.13	0.04	0.78
V2O3	0.00	0.00	0.00	0.00	0.01	0.00	0.00	0.03
FEO	6.59	6.41	6.59	5.24	6.29	6.20	6.27	2.97
MNO	0.21	0.00	0.14	0.00	0.20	0.18	0.22	0.09
MGO	34.11	34.61	34.37	15.68	34.10	34.31	34.47	17.24
NIO	0.00	0.00	0.00	0.00	0.10	0.11	0.07	0.14
CAO	0.26	0.23	0.17	23.06	0.44	0.35	0.47	21.81
NA2O	0.00	0.00	0.00	0.00	0.01	0.00	0.00	0.36
K2O	0.00	0.00	0.00	0.00	0.01	0.01	0.02	0.00
TOTAL	100.78	99.56	99.84	99.52	100.06	99.50	99.34	99.69
MOLE PERCENT ENDMEMBERS								
EN	89.6	90.2	90.0	44.6	89.9	90.2	89.9	49.9
FS	9.9	9.4	9.7	8.4	9.3	9.1	9.2	4.8
WO	0.5	0.4	0.3	47.1	0.8	0.7	0.9	45.3

	65	66
	23605	23606
	W	W
SIO2	52.19	51.77
TIO2	0.15	0.09
AL2O3	3.71	4.43
CR2O3	1.46	1.32
V2O3	0.04	0.04
FEO	2.71	3.27
MNO	0.10	0.10
MGO	17.23	16.80
NIO	0.09	0.04
CAO	21.10	21.35
NA2O	0.51	0.39
K2O	0.01	0.01
TOTAL	99.28	99.62
MOLE PERCENT ENDMEMBERS		
EN	50.3	49.4
FS	4.5	5.4
WO	44.7	45.2

TABLE A5.3 GRENADA PERIDOTITES - SPINELS

	1	2	3	4	5	6	7	8
	23303A	23304	23305	23305A	12201	12202	12203	12302
	W	W	W	W	E	E	E	E
SIO2	0.02	0.00	0.06	0.40	0.34	0.26	0.00	0.18
TIO2	0.21	0.20	0.71	0.87	0.33	0.14	0.00	0.62
AL203	19.95	20.26	13.70	17.42	12.83	13.12	13.49	23.01
CR203	40.97	40.48	44.56	40.03	50.73	51.07	50.25	36.88
V203	0.16	0.17	0.18	0.18	0.32	0.31	0.41	0.30
FE203	9.55	9.62	10.34	11.09	8.50	8.59	8.97	10.04
FEO	17.07	17.16	17.28	18.05	16.50	16.16	16.46	18.41
MNO	0.43	0.41	0.48	0.45	0.44	0.15	0.44	0.00
MGO	11.55	11.48	10.63	11.28	12.04	12.32	11.55	12.03
NIO	0.12	0.12	0.12	0.14	0.00	0.00	0.00	0.00
CAO	0.00	0.01	0.02	0.03	0.00	0.00	0.00	0.00
TOTAL	100.05	99.92	98.07	99.96	102.02	102.12	101.57	101.47

	9	10
	12303	23703
	E	E
SIO2	0.26	0.00
TIO2	0.16	0.25
AL203	16.13	23.54
CR203	47.02	40.21
V203	0.21	0.00
FE203	9.88	8.18
FEO	14.37	16.01
MNO	0.17	0.00
MGO	13.75	13.30
TOTAL	101.95	101.49

TABLE A6.1 EXPERIMENTAL OLIVINES

	1	2	3	4	5	6	7	8
	R23101	R23102	R23103	R23104	R23105	R23201	R23202	R24101
	E	E	E	E	E	E	E	E
SIO2	39.65	39.56	39.32	39.53	39.51	40.44	39.55	40.56
FEO	18.20	18.12	17.79	16.10	16.14	14.60	17.68	12.67
MNO	0.48	0.55	0.49	0.34	0.40	0.42	0.50	0.29
MGO	43.28	42.94	43.41	44.57	44.75	45.73	43.47	47.54
NIO	0.00	0.00	0.00	0.24	0.25	0.00	0.00	0.00
CAO	0.25	0.34	0.30	0.31	0.20	0.29	0.33	0.43
TOTAL	101.86	101.51	101.31	101.09	101.25	101.48	101.53	101.49
MOLE PERCENT ENDMEMBERS								
FO	80.9	80.9	81.3	83.2	83.2	84.8	81.4	87.0
FA	19.1	19.1	18.7	16.8	16.8	15.2	18.6	13.0

	9	10	11	12	13	14	15	16
	R24102	R24103	R24104	R24105	R24106	R24201	R24301	R24302
	E	E	E	E	E	E	E	E
SIO2	39.38	40.11	40.20	39.47	39.71	39.46	39.32	40.11
FEO	17.41	14.94	14.08	14.45	15.20	17.23	17.13	14.68
MNO	0.47	0.37	0.28	0.32	0.40	0.55	0.40	0.28
MGO	43.68	45.69	46.31	45.72	45.45	44.08	43.54	45.89
NIO	0.00	0.00	0.16	0.17	0.00	0.15	0.00	0.27
CAO	0.26	0.32	0.22	0.31	0.32	0.30	0.24	0.26
TOTAL	101.20	101.43	101.25	100.44	101.08	101.77	100.63	101.49
MOLE PERCENT ENDMEMBERS								
FO	81.7	84.5	85.4	84.9	84.2	82.0	81.9	84.8
FA	18.3	15.5	14.6	15.1	15.8	18.0	18.1	15.2

	17	18	19	20	21	22	23	24
	R25101	R25102	R31101	R31102	R31103	R31104	R31201	R31202
	E	E	E	E	E	E	E	E
SIO2	41.07	41.23	40.47	40.93	39.97	39.77	39.54	40.07
TIO2	0.00	0.00	0.00	0.11	0.00	0.00	0.00	0.00
AL2O3	0.00	0.00	0.00	0.00	0.00	0.00	0.00	0.25
FEO	8.30	8.34	14.70	13.71	15.71	15.42	16.87	12.71
MNO	0.00	0.28	0.31	0.20	0.42	0.41	0.50	0.23
MGO	49.93	50.40	46.06	46.18	44.93	44.77	43.70	46.48
NIO	0.00	0.00	0.20	0.00	0.00	0.14	0.15	0.15
CAO	0.36	0.39	0.19	0.47	0.28	0.30	0.32	0.54
TOTAL	99.66	100.64	101.93	101.60	101.31	100.81	101.08	100.43
MOLE PERCENT ENDMEMBERS								
FO	91.5	91.5	84.8	85.7	83.6	83.8	82.2	86.7
FA	8.5	8.5	15.2	14.3	16.4	16.2	17.8	13.3

TABLE A6.1 EXPERIMENTAL OLIVINES

	25	26	27	28	29	30	31	32
	R31301	R31302	R31303	R31304	R31305	R31306	R31307	R32101
	E	E	E	E	E	E	E	E
SIO2	39.40	39.08	40.43	41.03	40.86	40.80	40.58	41.40
FEO	17.44	19.02	12.60	12.60	11.90	12.56	15.30	10.66
MNO	0.36	0.42	0.19	0.23	0.13	0.24	0.26	0.19
MGO	43.29	41.93	47.02	47.33	47.73	47.10	44.49	48.37
NIO	0.00	0.14	0.00	0.00	0.24	0.13	0.18	0.26
CAO	0.28	0.30	0.20	0.33	0.23	0.09	0.23	0.21
TOTAL	100.77	100.89	100.44	101.52	101.09	100.92	101.04	101.09
MOLE PERCENT ENDMEMBERS								
FO	81.6	79.7	86.9	87.0	87.7	87.0	83.8	89.0
FA	18.4	20.3	13.1	13.0	12.3	13.0	16.2	11.0

	33	34	35	36	37	38	39	40
	R32102	R33101	R33102	R33103	R33104	R33105	R33202	R33203
	E	E	E	E	E	E	E	E
SIO2	41.28	40.66	40.86	41.29	40.58	41.31	40.79	40.33
TIO2	0.00	0.00	0.00	0.00	0.12	0.00	0.00	0.00
FEO	12.07	10.78	12.16	11.36	13.98	12.53	14.52	13.75
MNO	0.15	0.12	0.24	0.22	0.25	0.00	0.33	0.27
MGO	47.92	47.97	46.59	48.06	45.09	46.89	45.45	44.67
NIO	0.26	0.28	0.23	0.26	0.26	0.00	0.18	0.00
CAO	0.24	0.28	0.28	0.32	0.39	0.25	0.25	0.39
TOTAL	101.92	100.09	100.36	101.51	100.67	100.98	101.52	99.41
MOLE PERCENT ENDMEMBERS								
FO	87.6	88.8	87.2	88.3	85.2	87.0	84.8	85.3
FA	12.4	11.2	12.8	11.7	14.8	13.0	15.2	14.7

	41	42	43	44	45	46	47	48
	R33301	R33302	R35101	R35102	R35103	R35201	R35202	R39101
	E	E	E	E	E	E	E	E
SIO2	41.10	41.55	39.77	40.76	40.18	39.94	40.74	39.51
TIO2	0.00	0.00	0.00	0.00	0.00	0.00	0.00	0.11
AL2O3	0.00	0.00	0.00	0.00	0.00	0.27	0.00	0.00
FEO	13.14	12.14	16.80	12.24	17.28	17.66	13.79	15.98
MNO	0.14	0.13	0.48	0.22	0.41	0.49	0.28	0.34
MGO	46.54	47.29	43.66	47.53	43.19	42.68	46.47	44.78
NIO	0.00	0.00	0.00	0.15	0.00	0.14	0.22	0.00
CAO	0.25	0.35	0.44	0.30	0.35	0.60	0.36	0.29
TOTAL	101.17	101.46	101.15	101.20	101.41	101.78	101.86	101.01
MOLE PERCENT ENDMEMBERS								
FO	86.3	87.4	82.2	87.4	81.7	81.2	85.7	83.3
FA	13.7	12.6	17.8	12.6	18.3	18.8	14.3	16.7

TABLE A6.1 EXPERIMENTAL OLIVINES

	49	50	51	52	53	54	55	56
	R39102	R39201	R39202	R39301	R43102	R43103	R49101	R49102
	E	E	E	E	E	E	E	E
SIO2	39.79	40.52	41.31	39.84	40.26	40.26	40.87	40.98
FEO	17.23	11.72	11.42	13.54	14.38	14.38	10.53	10.44
MNO	0.43	0.28	0.32	0.28	0.23	0.23	0.37	0.28
MGO	43.97	48.11	48.73	46.02	46.21	46.21	48.19	48.26
NIO	0.00	0.41	0.55	0.00	0.00	0.00	0.00	0.00
CAO	0.39	0.28	0.22	0.27	0.39	0.39	0.16	0.27
TOTAL	101.81	101.32	102.55	99.95	101.47	101.47	100.12	100.23
MOLE PERCENT ENDMEMBERS								
FO	82.0	88.0	88.4	85.8	85.1	85.1	89.1	89.2
FA	18.0	12.0	11.6	14.2	14.9	14.9	10.9	10.8

	57	58	59	60	61	62	63	64
	R49103	R50102	R50105	R51101	R52101	R52201	R52202	R52301
	E	E	E	E	E	E	E	E
SIO2	40.55	40.36	40.55	40.34	41.03	37.87	37.73	39.29
FEO	11.70	13.65	13.70	14.68	10.44	27.00	26.98	20.55
MNO	0.30	0.26	0.21	0.28	0.22	0.66	0.35	0.46
MGO	47.20	45.48	45.92	45.01	47.57	34.46	34.82	40.53
NIO	0.13	0.00	0.00	0.00	0.37	0.00	0.00	0.00
CAO	0.20	0.19	0.15	0.21	0.18	0.23	0.22	0.26
TOTAL	100.08	99.94	100.53	100.52	99.81	100.22	100.10	101.09
MOLE PERCENT ENDMEMBERS								
FO	87.8	85.6	85.7	84.5	89.0	69.5	69.7	77.9
FA	12.2	14.4	14.3	15.5	11.0	30.5	30.3	22.1

	65	66	67	68	69	70	71	72
	R52302	R53101	R53102	R53103	R53104	R53201	R61101	R61102
	E	E	E	E	E	E	E	E
SIO2	39.41	37.02	37.23	37.38	36.58	38.88	40.66	40.64
TIO2	0.00	0.11	0.00	0.00	0.13	0.00	0.00	0.00
FEO	20.64	31.05	30.70	31.02	30.59	20.70	11.51	11.46
MNO	0.49	0.74	0.59	0.64	0.64	0.42	0.00	0.24
MGO	39.98	31.67	32.41	32.06	31.65	40.34	48.52	47.96
NIO	0.00	0.00	0.00	0.00	0.00	0.00	0.00	0.29
CAO	0.28	0.36	0.30	0.31	0.30	0.29	0.20	0.21
TOTAL	100.80	100.95	101.23	101.41	99.89	100.63	100.89	100.80
MOLE PERCENT ENDMEMBERS								
FO	77.5	64.5	65.3	64.8	64.8	77.6	88.3	88.2
FA	22.5	35.5	34.7	35.2	35.2	22.4	11.7	11.8

TABLE A6.1 EXPERIMENTAL OLIVINES

	73	74	75	76	77	78	79	80
	R61103	R61104	R64102	R65101	R65102	R65201	R82101	R88101
	E	E	E	E	E	E	E	E
SIO2	40.47	40.49	38.43	38.56	38.19	39.47	39.12	38.30
TIO2	0.00	0.00	0.00	0.00	0.00	0.00	0.18	0.00
AL203	0.00	0.00	0.00	0.35	0.00	0.37	1.17	0.44
FEO	11.61	11.53	23.22	27.72	27.38	20.92	26.80	26.97
MNO	0.27	0.20	0.27.	0.48	0.47	0.42	0.69	0.59
MGO	47.69	48.08	37.68	34.06	34.68	39.43	33.27	33.78
NIO	0.00	0.14	0.00	0.14	0.00	0.00	0.00	0.00
CAO	0.21	0.20	0.52	0.69	0.65	0.43	0.68	0.76
TOTAL	100.25	100.64	100.12	102.00	101.37	101.04	101.91	100.84
MOLE PERCENT ENDMEMBERS								
FO	88.0	88.1	74.3	68.7	69.3	77.1	68.9	69.1
FA	12.0	11.9	25.7	31.3	30.7	22.9	31.1	30.9

TABLE A6.2 EXPERIMENTAL CLINOPYROXENES

	1	2	3	4	5	6	7	8
	R31101	R31102	R31103	R35101	R35102	R35103	R35104	R35105
	E	E	E	E	E	E	E	E
SIO2	49.78	49.77	50.45	52.18	49.94	52.50	51.93	49.79
TIO2	0.86	0.76	0.67	0.48	0.76	0.49	0.55	0.77
AL203	5.12	5.20	5.37	2.80	5.25	2.83	2.73	5.80
CR203	1.10	0.76	0.96	0.46	1.02	0.46	0.50	0.54
FEO	4.73	5.30	4.26	4.90	5.17	4.94	4.79	5.64
MNO	0.00	0.00	0.00	0.00	0.00	0.11	0.00	0.00
MGO	14.56	15.12	15.25	16.28	14.76	16.40	16.25	14.40
CAO	23.70	23.45	22.69	23.71	23.36	23.39	23.90	23.98
TOTAL	99.85	100.36	99.65	100.81	100.26	101.12	100.65	100.92
MOLE PERCENT ENDMEMBERS								
EN	42.5	43.3	44.9	45.1	42.8	45.6	45.0	41.4
FS	7.7	8.5	7.0	7.6	8.4	7.7	7.4	9.1
WO	49.7	48.2	48.0	47.2	48.7	46.7	47.6	49.5

	9	10	11	12	13	14	15	16
	R51102	R51102	R51102	R51201	R51202	R51203	R52101	R52102
	E	E	E	E	E	E	E	E
SIO2	48.96	48.89	49.41	51.23	51.02	51.09	49.31	48.35
TIO2	0.89	0.86	0.89	0.91	0.79	0.76	0.95	1.19
AL203	6.15	6.55	6.23	5.72	5.51	5.54	5.98	6.53
CR203	0.52	0.47	0.42	0.21	0.18	0.23	0.12	0.29
FEO	5.23	5.26	5.27	6.69	6.86	6.42	6.19	7.03
MNO	0.23	0.16	0.00	0.25	0.26	0.27	0.00	0.21
MGO	14.32	14.94	14.76	15.22	16.08	15.38	14.50	13.19
CAO	22.54	22.52	22.93	20.56	20.30	20.69	21.42	22.37
TOTAL	98.84	99.65	99.91	100.79	101.00	100.38	98.47	99.16
MOLE PERCENT ENDMEMBERS								
EN	42.8	43.8	43.2	45.1	46.6	45.4	43.5	39.7
FS	8.8	8.7	8.6	11.1	11.1	10.6	10.4	11.9
WO	48.4	47.5	48.2	43.8	42.3	43.9	46.1	48.4

	17	18	19	20	21	22	23	24
	R52103	R52201	R52202	R52203	R52301	R52302	R52303	R52304
	E	E	E	E	E	E	E	E
SIO2	49.45	48.47	47.81	49.41	52.38	49.70	48.32	49.20
TIO2	1.19	1.34	1.20	0.93	0.47	0.73	1.00	0.80
AL203	6.55	7.75	6.80	6.47	2.68	5.33	6.05	5.55
CR203	0.35	0.21	0.00	0.15	0.21	0.23	0.31	0.00
FEO	6.54	7.66	8.26	7.83	8.17	8.01	9.03	8.47
MNO	0.15	0.20	0.30	0.34	0.43	0.24	0.33	0.32
MGO	14.60	13.95	13.65	15.15	16.06	14.20	13.34	14.05
CAO	21.68	19.98	20.26	19.51	19.47	20.87	20.28	20.43
TOTAL	100.51	99.56	98.28	99.79	99.87	99.31	98.66	98.82
MOLE PERCENT ENDMEMBERS								
EN	43.1	42.8	41.6	45.1	46.4	42.1	40.4	42.0
FS	10.8	13.2	14.1	13.1	13.2	13.3	15.4	14.2
WO	46.0	44.0	44.3	41.8	40.4	44.5	44.2	43.9

TABLE A6.2 EXPERIMENTAL CLINOPYROXENES

	25	26	27	28	29	30	31	32
	R53102	R53103	R53104	R53105	R53201	R53202	R53205	R53206
	E	E	E	E	E	E	E	E
SIO2	51.17	49.35	53.23	49.21	48.91	51.80	48.96	51.23
TIO2	0.73	0.99	0.32	0.96	1.13	0.45	1.17	0.72
AL203	3.11	6.06	0.82	7.17	6.34	2.65	5.93	3.60
CR203	0.00	0.00	0.13	0.16	0.15	0.11	0.12	0.17
FEO	6.67	10.47	7.49	10.28	7.40	8.34	8.39	9.45
MNO	0.48	0.33	0.54	0.42	0.19	0.35	0.30	0.46
MGO	15.21	14.46	15.43	13.90	14.03	16.93	14.02	16.84
NIO	0.00	0.00	0.18	0.14	0.00	0.00	0.15	0.00
CAO	22.04	17.66	21.87	17.07	21.34	18.61	20.70	17.17
NA2O	0.47	0.00	0.00	0.00	0.00	0.00	0.00	0.00
TOTAL	99.88	99.32	100.01	99.31	99.49	99.24	99.74	99.64
MOLE PERCENT ENDMEMBERS								
EN	43.7	43.8	43.6	43.5	41.9	48.4	41.7	48.8
FS	10.8	17.8	11.9	18.1	12.4	13.4	14.0	15.4
WO	45.5	38.4	44.5	38.4	45.8	38.2	44.3	35.8

	33	34	35	36	37	38	39	40
	R54101	R63101	R63102	R63103	R63105	R64101	R64103	R64205
	E	E	E	E	E	E	E	E
SIO2	51.42	49.89	49.78	50.59	50.94	49.90	50.79	50.86
TIO2	0.78	0.95	0.92	0.58	0.64	0.82	0.73	0.63
AL203	2.17	5.64	5.34	4.32	4.13	4.79	4.12	4.21
CR203	0.00	0.14	0.00	0.22	0.13	0.25	0.22	0.25
FEO	8.75	6.97	7.69	7.07	7.63	7.61	7.47	7.02
MNO	0.53	0.21	0.23	0.22	0.17	0.23	0.00	0.17
MGO	13.90	13.97	13.90	14.63	14.64	13.96	14.54	14.64
NIO	0.00	0.00	0.00	0.00	0.00	0.00	0.16	0.00
CAO	21.27	21.51	21.10	21.57	21.30	21.23	21.81	22.17
NA2O	0.53	0.00	0.00	0.00	0.00	0.00	0.00	0.00
TOTAL	99.35	99.28	98.96	99.20	99.58	98.79	99.84	99.95
MOLE PERCENT ENDMEMBERS								
EN	40.8	41.9	41.6	42.9	42.8	41.7	42.3	42.4
FS	14.4	11.7	12.9	11.6	12.5	12.7	12.2	11.4
WO	44.8	46.4	45.4	45.5	44.7	45.6	45.6	46.2

	41	42	43	44	45	46	47	48
	R65101	R65102	R65103	R65201	R65202	R65203	R65301	R65302
	E	E	E	E	E	E	E	E
SIO2	51.28	51.59	52.14	51.88	49.38	51.25	49.74	50.92
TIO2	0.57	0.63	0.54	0.52	0.93	0.59	0.74	0.64
AL203	3.90	4.66	3.30	3.05	5.43	3.42	5.11	4.64
CR203	0.27	0.17	0.00	0.37	0.13	0.15	0.29	0.26
FEO	5.89	8.17	8.11	4.96	8.63	7.51	7.33	7.33
MNO	0.00	0.22	0.46	0.00	0.17	0.27	0.00	0.21
MGO	14.80	13.99	15.38	15.68	13.76	14.97	14.18	14.10
CAO	22.62	20.63	21.30	22.96	21.37	21.62	22.49	22.43
TOTAL	99.33	100.06	101.23	99.42	99.80	99.78	99.88	100.53
MOLE PERCENT ENDMEMBERS								
EN	43.1	41.9	43.6	44.8	40.5	43.1	41.2	41.1
FS	9.6	13.7	12.9	8.0	14.3	12.1	11.9	12.0
WO	47.3	44.4	43.4	47.2	45.2	44.8	46.9	47.0

TABLE A6.2 EXPERIMENTAL CLINOPYROXENES

	49	50	51	52	53	54	55	56
	R68101	R68102	R68103	R68201	R68202	R68203	R69201	R70102
	E	E	E	E	E	E	E	E
SIO2	51.04	48.35	51.13	50.13	49.46	52.34	52.36	50.28
TIO2	0.45	0.91	0.67	0.63	0.60	0.52	0.35	0.91
AL203	3.95	6.56	4.16	5.43	5.96	2.75	3.34	4.04
CR203	0.30	0.24	0.17	0.38	0.35	0.00	0.46	0.00
FEO	4.98	8.34	6.88	6.44	6.72	7.69	4.61	8.83
MNO	0.12	0.00	0.12	0.12	0.12	0.31	0.00	0.18
MGO	15.37	14.05	15.11	14.36	14.24	15.65	16.01	14.02
CAO	23.17	21.66	23.01	23.06	22.87	21.57	23.13	21.56
TOTAL	99.38	100.11	101.25	100.55	100.52	100.83	100.26	99.82
MOLE PERCENT ENDMEMBERS								
EN	44.1	41.0	42.6	41.6	41.3	44.1	45.5	40.7
FS	8.0	13.6	10.9	10.5	10.9	12.2	7.3	14.4
WO	47.8	45.4	46.6	48.0	47.7	43.7	47.2	45.0

	57	58	59	60	61	62	63	64
	R70103	R70201	R70202	R72102	R72103	R72104	R72202	R72203
	E	E	E	E	E	E	E	E
SIO2	48.97	50.23	48.68	50.89	49.15	50.71	48.44	49.20
TIO2	0.70	0.70	0.73	0.55	0.88	0.72	1.00	0.80
AL203	4.74	3.96	5.44	4.18	4.99	4.63	5.40	6.10
CR203	0.16	0.00	0.23	0.28	0.27	0.00	0.00	0.32
FEO	8.13	7.85	8.70	9.00	8.50	7.65	8.13	7.34
MNO	0.00	0.25	0.20	0.24	0.17	0.31	0.17	0.17
MGO	13.65	14.65	13.62	13.57	13.50	15.02	13.60	13.87
CAO	21.37	21.76	21.99	20.94	21.53	22.03	21.92	22.03
TOTAL	97.72	99.40	99.59	99.65	98.99	101.07	98.66	99.83
MOLE PERCENT ENDMEMBERS								
EN	40.7	42.2	39.7	40.3	40.0	42.7	40.1	41.0
FS	13.6	12.7	14.2	15.0	14.1	12.2	13.4	12.2
WO	45.8	45.1	46.1	44.7	45.9	45.1	46.5	46.8

	65	66	67	68	69	70	71	72
	R72204	R72205	R72206	R73101	R73102	R73103	R73104	R73201
	E	E	E	E	E	E	E	E
SIO2	48.98	49.56	48.81	49.68	50.37	51.03	51.93	49.47
TIO2	0.64	0.67	0.94	0.65	0.53	0.62	0.47	0.86
AL203	5.62	5.01	4.91	4.90	4.42	3.32	3.38	5.24
CR203	0.26	0.00	0.00	0.11	0.27	0.00	0.43	0.28
FEO	7.29	7.61	8.43	7.05	6.52	7.41	4.78	7.02
MNO	0.00	0.25	0.00	0.18	0.00	0.24	0.00	0.11
MGO	14.19	14.35	13.93	14.65	14.61	15.08	16.22	13.94
CAO	21.83	21.69	21.83	22.00	22.52	21.51	22.95	21.98
TOTAL	98.78	99.14	98.85	99.22	99.24	99.21	100.16	98.50
MOLE PERCENT ENDMEMBERS								
EN	41.8	41.9	40.6	42.6	42.4	43.5	45.8	41.4
FS	12.0	12.5	13.8	11.5	10.6	12.0	7.6	11.7
WO	46.2	45.6	45.7	45.9	47.0	44.6	46.6	46.9

TABLE A6.2 EXPERIMENTAL CLINOPYROXENES

	73	74	75	76	77	78	79	80
	R73301	R73302	R74101	R74102	R74201	R74202	R74203	R74301
	E	E	E	E	E	E	E	E
SIO2	51.44	49.41	49.48	49.06	51.56	50.21	50.06	51.06
TIO2	0.56	0.77	0.90	0.96	0.37	0.65	0.91	0.39
AL2O3	3.41	5.32	4.70	4.93	3.03	4.18	4.68	4.01
CR2O3	0.35	0.31	0.00	0.13	0.27	0.00	0.00	0.47
FEO	6.08	6.43	8.38	8.08	4.99	7.62	8.99	5.68
MNO	0.00	0.16	0.17	0.25	0.00	0.26	0.29	0.13
MGO	15.25	14.23	13.97	13.68	16.16	14.66	13.73	14.73
CAO	22.50	22.66	21.26	22.07	22.81	21.97	21.23	22.91
TOTAL	99.59	99.29	98.86	99.16	99.19	99.55	99.89	99.38
MOLE PERCENT ENDMEMBERS								
EN	43.8	41.7	41.1	40.1	45.7	42.2	40.3	42.8
FS	9.8	10.6	13.8	13.3	7.9	12.3	14.8	9.3
WO	46.4	47.7	45.0	46.6	46.4	45.5	44.8	47.9

	81	82	83	84	85	86	87	88
	R74302	R74303	R81101	R81102	R81103	R81104	R81301	R81302
	E	E	E	E	E	E	E	E
SIO2	50.94	51.60	53.05	50.84	51.82	50.96	51.90	52.16
TIO2	0.41	0.32	0.52	0.89	0.56	0.64	0.57	0.61
AL2O3	3.50	3.61	3.76	2.67	3.77	2.55	3.28	3.32
CR2O3	0.63	0.28	0.13	0.13	0.15	0.23	0.18	0.23
FEO	5.11	5.64	9.22	11.02	8.17	7.95	6.99	6.99
MNO	0.20	0.00	0.60	0.79	0.47	0.47	0.33	0.34
MGO	15.65	14.85	14.85	13.52	15.26	15.04	15.36	15.09
CAO	23.15	23.17	18.57	19.80	19.01	20.31	19.90	19.57
NA2O	0.00	0.00	0.59	0.00	0.00	0.00	0.00	0.00
TOTAL	99.59	99.47	101.29	99.66	99.21	98.15	98.51	98.31
MOLE PERCENT ENDMEMBERS								
EN	44.5	42.8	44.5	39.8	45.5	44.1	45.7	45.6
FS	8.2	9.1	15.5	18.2	13.7	13.1	11.7	11.9
WO	47.3	48.0	40.0	41.9	40.8	42.8	42.6	42.5

	89	90	91	92	93	94	95	96
	R81303	R82101	R82102	R82103	R82104	R82201	R82202	R82203
	E	E	E	E	E	E	E	E
SIO2	53.13	51.15	51.88	52.08	52.34	51.66	52.02	51.47
TIO2	0.27	0.62	0.57	0.40	0.48	0.70	0.68	0.56
AL2O3	1.47	4.00	2.60	1.77	3.47	1.79	2.67	3.05
CR2O3	0.14	0.18	0.25	0.00	0.00	0.14	0.34	0.00
FEO	7.01	7.47	6.22	9.28	7.89	9.71	8.38	6.35
MNO	0.42	0.25	0.43	0.72	0.46	0.60	0.50	0.57
MGO	15.73	14.78	15.48	15.74	14.74	14.38	15.26	15.76
CAO	21.65	20.53	21.58	19.61	19.27	19.97	19.37	21.66
TOTAL	99.82	98.98	99.01	99.60	98.65	98.95	99.22	99.42
MOLE PERCENT ENDMEMBERS								
EN	44.7	43.8	44.9	44.9	44.6	42.1	45.0	45.2
FS	11.2	12.4	10.1	14.9	13.4	15.9	13.9	10.2
WO	44.2	43.8	45.0	40.2	41.9	42.0	41.1	44.6

TABLE A6.2 EXPERIMENTAL CLINOPYROXENES

	97	98	99	100	101	102	103	104
	R82301	R82302	R83102	R83103	R83104	R83301	R83302	R83303
	E	E	E	E	E	E	E	E
SIO2	51.99	51.09	51.87	51.58	51.73	52.71	52.82	52.81
TIO2	0.48	0.64	0.72	0.66	0.55	0.51	0.37	0.42
AL203	3.09	4.20	3.14	3.91	2.48	1.93	2.40	1.95
CR203	0.14	0.26	0.00	0.14	0.00	0.00	0.13	0.26
FEO	7.87	7.64	10.45	9.74	8.39	7.47	6.38	6.73
MNO	0.37	0.48	0.48	0.38	0.41	0.47	0.46	0.51
MGO	15.87	14.79	15.09	13.91	14.66	15.22	16.04	17.34
CAO	20.18	19.75	17.69	18.25	19.98	20.84	21.22	19.81
TOTAL	99.99	98.85	99.44	98.57	98.20	99.15	99.82	99.83
MOLE PERCENT ENDMEMBERS								
EN	45.6	44.5	44.8	42.8	43.5	44.3	46.0	49.0
FS	12.7	12.9	17.4	16.8	14.0	12.2	10.3	10.7
WO	41.7	42.7	37.8	40.4	42.6	43.6	43.7	40.3

	105	106	107	108	109	110	111	112
	R83201	R83202	R83203	R83204	R88101	R88102	R90101	R90102
	E	E	E	E	E	E	E	E
SIO2	51.43	51.15	52.73	51.61	52.08	52.12	52.92	52.28
TIO2	0.72	0.50	0.37	0.55	0.64	0.47	0.21	0.38
AL203	3.11	3.19	1.50	2.42	3.07	2.90	0.73	2.35
CR203	0.00	0.23	0.21	0.15	0.23	0.22	0.11	0.16
FEO	6.50	7.86	6.88	6.46	7.35	7.94	6.97	7.54
MNO	0.31	0.42	0.56	0.52	0.34	0.43	0.59	0.47
MGO	15.44	14.87	16.70	16.47	15.28	14.61	15.98	14.91
CAO	21.10	19.70	20.00	20.16	19.78	20.42	21.28	20.60
TOTAL	98.61	97.92	98.95	98.34	98.77	99.11	98.79	98.69
MOLE PERCENT ENDMEMBERS								
EN	45.1	44.5	47.8	47.6	45.5	43.3	45.4	43.9
FS	10.6	13.2	11.0	10.5	12.3	13.2	11.1	12.5
WO	44.3	42.3	41.1	41.9	42.3	43.5	43.5	43.6

	113	114	115	116
	R90103	R92101	R92102	R92104
	E	E	E	E
SIO2	50.47	50.83	51.54	50.91
TIO2	1.01	0.69	0.65	0.72
AL203	2.67	5.12	5.34	3.20
CR203	0.11	0.00	0.20	0.21
FEO	8.98	7.55	7.54	9.01
MNO	0.57	0.43	0.32	0.47
MGO	13.61	14.88	14.23	13.69
NIO	0.00	0.00	0.18	0.00
CAO	21.09	19.26	18.27	20.28
NA2O	0.00	0.00	0.86	0.00
TOTAL	98.51	98.76	99.13	98.49
MOLE PERCENT ENDMEMBERS				
EN	40.3	45.1	45.0	41.1
FS	14.9	12.9	13.4	15.2
WO	44.8	42.0	41.6	43.7

TABLE A6.3 EXPERIMENTAL PLAGIOCLASES

	1	2	3	4	5	6	7	8
	R31302	R31303	R31304	R31305	R33101	R35102	R35104	R39101
	E	E	E	E	E	E	E	E
SIO2	48.03	48.11	47.99	49.36	52.98	48.45	48.91	48.33
TIO2	0.00	0.00	0.00	0.00	0.22	0.11	0.16	0.00
AL2O3	32.62	32.68	32.54	31.75	28.76	31.35	31.69	31.32
FEO	0.79	0.92	0.73	0.83	0.84	0.91	0.68	0.79
MGO	0.00	0.00	0.00	0.00	0.21	0.49	0.00	0.00
CAO	16.72	16.27	16.57	15.76	14.28	16.59	15.95	15.18
NA2O	2.06	2.05	1.81	2.33	3.41	2.25	1.85	2.61
K2O	0.00	0.00	0.00	0.00	0.23	0.00	0.09	0.11
TOTAL	100.22	100.03	99.64	100.03	100.93	100.15	99.33	98.34
MOLE PERCENT ENDMEMBERS								
AB	18.2	18.6	16.5	21.1	29.8	19.7	17.3	23.6
AN	81.8	81.4	83.5	78.9	68.9	80.3	82.2	75.8
OR	0.0	0.0	0.0	0.0	1.3	0.0	0.6	0.7

	9	10	11	12	13	14	15	16
	R39102	R39103	R52102	R52103	R52201	R52202	R53102	R53105
	E	E	E	E	E	E	E	E
SIO2	49.87	48.12	49.42	50.31	54.11	54.26	54.00	54.80
TIO2	0.18	0.00	0.00	0.00	0.00	0.00	0.00	0.00
AL2O3	29.36	32.35	31.13	31.40	27.70	27.81	28.53	27.36
FEO	1.09	1.00	0.60	0.57	0.73	0.70	0.69	0.74
MGO	0.52	0.00	0.00	0.00	0.00	0.00	0.00	0.00
CAO	14.29	16.20	15.11	15.08	11.01	11.29	11.73	10.92
NA2O	2.62	2.25	2.62	2.86	4.89	4.68	4.55	4.77
K2O	0.15	0.00	0.12	0.00	0.14	0.17	0.10	0.24
TOTAL	98.08	99.92	99.00	100.22	98.58	98.91	99.60	98.83
MOLE PERCENT ENDMEMBERS								
AB	24.7	20.1	23.7	25.6	44.2	42.4	41.0	43.5
AN	74.4	79.9	75.6	74.4	55.0	56.6	58.4	55.0
OR	0.9	0.0	0.7	0.0	0.8	1.0	0.6	1.4

	17	18	19	20	21	22	23	24
	R53106	R54101	R54103	R54104	R63101	R63104	R63105	R63107
	E	E	E	E	E	E	E	E
SIO2	52.81	52.99	53.22	53.94	47.81	46.92	48.27	47.16
TIO2	0.00	0.00	0.00	0.00	0.14	0.00	0.00	0.00
AL2O3	29.06	28.64	28.57	27.88	31.70	32.79	31.23	32.46
FEO	0.29	0.93	0.77	0.85	0.99	0.88	1.16	0.99
CAO	12.09	11.73	11.77	11.31	16.56	16.93	15.41	16.65
NA2O	3.94	4.74	4.17	5.02	1.97	1.72	2.22	2.06
K2O	0.09	0.00	0.09	0.14	0.13	0.00	0.10	0.14
TOTAL	98.28	99.03	98.59	99.14	99.30	99.24	98.39	99.46
MOLE PERCENT ENDMEMBERS								
AB	36.9	42.2	38.9	44.2	17.6	15.5	20.6	18.1
AN	62.6	57.8	60.6	55.0	81.7	84.5	78.8	81.0
OR	0.6	0.0	0.6	0.8	0.8	0.0	0.6	0.8

TABLE A6.3 EXPERIMENTAL PLAGIOCLASES

	25	26	27	28	29	30	31	32
	R64102	R64201	R64202	R65102	R65201	R65202	R70101	R70103
	E	E	E	E	E	E	E	E
SIO2	46.41	46.88	45.47	49.54	47.33	47.16	48.61	47.47
TIO2	0.00	0.11	0.00	0.14	0.16	0.00	0.39	0.12
AL2O3	32.52	31.98	33.28	31.01	31.14	32.13	29.00	32.47
FEO	1.13	1.09	1.03	1.31	1.21	1.31	2.46	1.14
MGO	0.00	0.00	0.00	0.00	0.30	0.00	0.90	0.00
CAO	17.03	16.42	17.87	15.05	16.38	16.53	13.96	16.75
NA2O	1.49	1.85	1.29	2.51	1.81	1.66	2.67	1.44
K2O	0.15	0.00	0.00	0.23	0.08	0.10	0.35	0.11
TOTAL	98.73	98.33	98.94	99.79	98.41	98.89	98.34	99.50
MOLE PERCENT ENDMEMBERS								
AB	13.5	16.9	11.6	22.9	16.6	15.3	25.2	13.4
AN	85.6	83.1	88.4	75.8	82.9	84.1	72.7	86.0
OR	0.9	0.0	0.0	1.4	0.5	0.6	2.2	0.7

	33	34	35	36	37	38	39	40
	R70104	R72101	R74101	R74102	R74104	R74105	R74106	R81101
	E	E	E	E	E	E	E	E
SIO2	46.30	50.95	46.03	47.16	47.86	45.56	49.05	52.10
TIO2	0.00	0.16	0.00	0.16	0.00	0.00	0.00	0.00
AL2O3	32.82	28.54	32.36	31.90	31.55	33.03	31.68	29.74
FEO	1.23	1.49	1.29	1.03	1.52	1.12	0.94	0.76
MGO	0.00	0.44	0.00	0.00	0.00	0.00	0.00	0.00
CAO	16.85	13.47	16.80	16.03	15.81	17.26	15.56	13.23
NA2O	1.49	3.85	1.26	1.78	2.32	1.45	2.81	3.69
K2O	0.11	0.25	0.20	0.14	0.18	0.00	0.17	0.19
TOTAL	98.80	99.15	97.94	98.20	99.24	98.42	100.21	99.71
MOLE PERCENT ENDMEMBERS								
AB	13.7	33.6	11.8	16.6	20.8	13.2	24.4	33.2
AN	85.6	65.0	87.0	82.6	78.2	86.8	74.6	65.7
OR	0.7	1.4	1.2	0.9	1.1	0.0	1.0	1.1

	41	42	43	44	45	46	47	48
	R81102	R82101	R82102	R82103	R82104	R82105	R83101	R83102
	E	E	E	E	E	E	E	E
SIO2	51.56	54.62	55.89	56.06	57.42	52.31	55.19	53.92
TIO2	0.00	0.00	0.00	0.00	0.20	0.24	0.18	0.00
AL2O3	30.24	27.18	26.62	27.32	25.97	27.95	25.28	28.25
FEO	0.76	1.05	0.66	0.49	0.58	1.07	0.98	0.51
MGO	0.00	0.00	0.31	0.00	0.00	0.63	0.00	0.00
CAO	13.42	10.70	10.17	10.05	8.51	12.84	9.12	11.12
NA2O	3.29	4.98	5.40	5.32	6.05	3.86	5.09	5.01
K2O	0.11	0.23	0.25	0.19	0.35	0.22	0.38	0.17
TOTAL	99.38	98.76	99.30	99.43	99.08	99.14	96.22	98.98
MOLE PERCENT ENDMEMBERS								
AB	30.5	45.1	48.3	48.4	55.1	34.9	49.0	44.5
AN	68.8	53.5	50.2	50.5	42.8	63.8	48.6	54.5
OR	0.7	1.4	1.5	1.1	2.1	1.3	2.4	1.0

TABLE A6.3 EXPERIMENTAL PLAGIOCLASES

	49	50	51	52	53	54	55	56
	R83103	R83104	R83201	R83202	R83203	R83205	R83206	R90101
	E	E	E	E	E	E	E	E
SIO2	55.49	55.20	51.79	52.14	54.47	52.93	53.83	50.15
TIO2	0.14	0.00	0.18	0.00	0.00	0.13	0.00	0.00
AL203	26.39	27.36	28.55	29.84	28.48	29.05	29.01	30.54
FEO	0.80	0.56	0.89	0.63	0.67	0.67	0.65	0.73
MGO	0.30	0.00	0.21	0.00	0.00	0.00	0.00	0.00
CAO	9.70	10.26	12.65	13.38	11.35	12.19	11.91	14.30
NA2O	5.43	5.44	3.26	4.04	4.85	3.78	4.29	3.33
K2O	0.32	0.19	0.30	0.11	0.16	0.18	0.15	0.13
TOTAL	98.57	99.01	97.83	100.14	99.98	98.93	99.84	99.18
MOLE PERCENT ENDMEMBERS								
AB	49.4	48.4	31.2	35.1	43.2	35.5	39.1	29.4
AN	48.7	50.5	66.9	64.3	55.9	63.3	60.0	69.8
OR	1.9	1.1	1.9	0.6	0.9	1.1	0.9	0.8

	57
	R90102
	E
SIO2	51.85
AL203	30.07
FEO	0.59
CAO	12.82
NA2O	3.50
K2O	0.13
TOTAL	96.96
MOLE PERCENT ENDMEMBERS	
AB	32.8
AN	66.4
OR	0.8

TABLE A6.4 EXPERIMENTAL AMPHIBOLES

	1	2	3	4	5	6	7
	R54101	R54104	R54105	R54108	R83302	R83303	R83304
	E	E	E	E	E	E	E
SIO2	42.95	42.18	42.22	41.29	42.30	42.02	41.75
TIO2	1.73	1.88	1.93	1.91	2.26	2.22	2.19
AL2O3	12.19	13.21	12.77	13.51	12.80	13.37	13.77
FEO	11.14	12.08	11.44	13.40	9.80	9.81	11.04
MNO	0.19	0.16	0.29	0.28	0.27	0.20	0.23
MGO	15.26	13.92	13.90	12.93	14.60	14.54	13.70
CAO	10.86	11.43	11.30	11.19	11.48	11.38	11.20
NA2O	2.15	2.74	2.23	2.39	2.09	1.93	2.06
K2O	0.32	0.32	0.29	0.41	0.34	0.33	0.45
CL	0.04	0.00	0.00	0.00	0.00	0.00	0.00
TOTAL	96.83	97.92	96.37	97.31	95.94	95.80	96.39

TABLE A6.5 EXPERIMENTAL OXIDES

	1	2	3	4	5	6	7	8
	R23101	R31102	R31103	R32101	R39201	R43101	R51101	R52101
	E	E	E	E	E	E	E	E
SIO2	0.00	0.00	0.00	0.00	0.00	0.00	0.48	0.34
TIO2	0.68	0.35	1.84	0.74	0.56	0.54	0.59	0.77
AL2O3	9.03	9.99	9.93	23.54	15.88	15.09	17.92	21.68
CR2O3	33.96	31.89	29.11	34.01	41.95	42.52	43.11	34.60
V2O3	0.00	0.00	0.00	0.00	0.00	0.00	0.19	0.20
FE2O3	25.10	27.72	28.47	11.84	10.25	12.24	7.62	10.49
FEO	21.93	20.20	20.35	16.64	24.07	18.04	17.09	20.12
MNO	0.39	0.53	0.65	0.00	0.32	0.23	0.25	0.00
MGO	6.84	7.88	8.50	12.53	6.71	10.35	12.00	10.39
CAO	0.32	0.34	0.56	0.27	0.22	0.38	0.00	0.00
TOTAL	98.26	98.90	99.41	99.58	99.96	99.39	99.24	98.59

	9	10	11	12	13	14	15	16
	R53201	R54101	R54102	R54103	R61103	R65102	R70201	R70202
	E	E	E	E	E	E	E	E
SIO2	0.86	0.41	0.43	0.35	0.36	0.61	0.40	0.22
TIO2	3.95	4.30	4.51	5.35	0.66	8.11	2.85	2.91
AL2O3	9.29	6.51	6.80	4.94	18.39	6.46	9.14	9.05
CR2O3	14.04	0.00	0.64	0.00	39.84	0.24	0.28	0.56
V2O3	0.55	0.42	0.49	0.58	0.31	0.79	0.28	0.28
FE2O3	35.13	52.57	51.79	52.03	10.88	44.39	54.30	54.74
FEO	28.60	32.37	32.39	33.33	17.28	33.99	27.18	27.38
MNO	0.25	0.53	0.31	0.46	0.39	0.32	0.25	0.00
MGO	5.36	2.38	2.84	2.15	11.90	3.79	5.49	5.49
TOTAL	98.03	99.49	100.20	99.19	100.01	98.72	100.17	100.63

TABLE A6.6 EXPERIMENTAL GLASSES

	1	2	3	4	5	6	7	8
	R49101	R49102	R49103	R50201	R50202	R50203	R51201	R51202
	E	E	E	E	E	E	E	E
SIO2	50.39	49.70	49.96	52.41	53.34	52.11	53.04	52.89
TIO2	0.84	0.70	0.82	0.74	0.77	0.64	0.71	0.87
AL203	17.03	16.75	17.10	15.90	15.85	15.75	16.61	17.04
CR203	0.00	0.00	0.00	0.00	0.00	0.19	0.00	0.00
FEO	6.88	6.54	6.80	7.40	7.15	7.46	6.97	6.97
MNO	0.00	0.12	0.00	0.24	0.23	0.21	0.12	0.28
MGO	5.73	5.41	5.98	4.99	4.67	5.14	4.04	3.87
CAO	9.80	10.04	10.05	8.54	8.35	8.77	7.52	7.71
NA20	2.44	2.74	2.60	3.86	3.25	3.79	4.07	3.91
K20	0.81	0.84	0.78	0.89	0.86	0.87	0.93	0.93
TOTAL	93.92	92.84	94.09	94.97	94.47	94.93	94.01	94.47

	9	10	11	12	13	14	15	16
	R51301	R51302	R52301	R52302	R54101	R54102	R54103	R54105
	E	E	E	E	E	E	E	E
SIO2	52.68	51.32	51.77	52.76	54.60	54.39	55.00	54.79
TIO2	0.79	0.82	0.83	0.83	0.78	0.68	0.44	0.42
AL203	15.75	15.61	16.54	17.86	16.83	15.61	17.85	17.87
FEO	6.75	7.19	7.16	6.53	6.20	6.90	5.57	5.52
MNO	0.14	0.22	0.19	0.19	0.21	0.33	0.28	0.23
MGO	4.56	5.04	3.55	3.13	3.12	3.90	1.58	1.72
CAO	8.09	8.42	7.80	6.65	6.09	6.54	6.04	6.10
NA20	3.94	3.70	3.71	4.15	4.71	4.15	4.76	4.57
K20	0.88	0.81	0.88	1.03	1.22	1.10	1.11	1.07
TOTAL	93.58	93.13	92.43	93.13	93.76	93.60	92.63	92.29

	17	18	19	20	21	22	23	24
	R54106	R62201	R62202	R62203	R62204	R62205	R62301	R62302
	E	E	E	E	E	E	E	E
SIO2	54.85	47.14	47.24	47.14	47.35	47.09	46.33	46.06
TIO2	0.44	0.96	0.90	0.91	0.87	0.86	0.83	0.91
AL203	17.90	16.05	15.61	16.07	15.73	15.67	15.77	15.19
CR203	0.00	0.00	0.00	0.00	0.00	0.00	0.11	0.00
FEO	5.87	9.51	9.34	9.33	9.33	9.40	10.28	10.09
MNO	0.16	0.29	0.17	0.33	0.32	0.13	0.00	0.14
MGO	1.60	6.39	6.26	6.06	6.27	6.23	6.20	6.59
CAO	6.11	12.94	12.76	12.96	12.96	13.07	12.48	13.46
NA20	4.78	2.49	2.29	1.93	2.31	1.89	1.90	1.62
K20	1.10	0.75	0.64	0.78	0.72	0.75	0.64	0.52
TOTAL	92.81	96.52	95.21	95.51	95.86	95.09	94.54	94.58

TABLE A6.6 EXPERIMENTAL GLASSES

	25	26	27	28	29	30	31	32
	R62303	R62304	R62305	R63201	R63202	R63203	R63204	R63205
	E	E	E	E	E	E	E	E
SIO2	45.43	45.64	46.20	46.83	47.34	46.58	46.82	46.13
TIO2	0.84	0.85	0.84	0.81	0.96	0.94	0.84	0.92
AL203	15.01	15.69	15.46	15.76	16.05	15.79	15.65	15.77
CR203	0.00	0.00	0.00	0.00	0.00	0.00	0.15	0.14
FEO	10.35	10.54	9.08	9.33	9.23	9.37	9.44	9.49
MNO	0.13	0.00	0.00	0.27	0.28	0.20	0.17	0.12
MGO	6.75	6.01	5.82	6.33	6.58	6.31	6.29	6.19
CAO	14.06	12.41	13.01	12.77	12.87	12.79	12.74	12.75
NA20	1.83	1.88	2.04	1.60	2.21	2.05	2.38	2.28
K20	0.56	0.80	0.66	0.72	0.71	0.65	0.67	0.72
TOTAL	94.96	93.82	93.11	94.42	96.23	94.68	95.15	94.51

	33	34	35	36	37	38	39	40
	R67101	R67102	R67105	R67201	R69202	R72301	R72302	R72303
	E	E	E	E	E	E	E	E
SIO2	47.73	46.68	46.91	46.42	45.97	45.18	45.13	46.38
TIO2	0.96	0.87	0.86	0.80	0.96	0.88	0.85	0.83
AL203	15.21	15.35	14.93	15.97	17.01	15.63	15.22	15.68
CR203	0.13	0.00	0.00	0.00	0.00	0.00	0.00	0.00
FEO	10.94	10.75	10.59	9.70	9.84	11.89	12.02	11.56
MNO	0.11	0.17	0.20	0.13	0.00	0.15	0.00	0.15
MGO	5.66	5.66	5.71	6.03	4.94	5.69	5.71	5.25
CAO	12.24	12.33	12.11	12.66	10.54	12.15	12.12	11.76
NA20	2.53	2.43	2.77	2.33	3.17	2.00	2.67	2.64
K20	0.72	0.70	0.71	0.68	0.93	0.72	0.79	0.73
TOTAL	96.23	94.94	94.79	94.72	93.36	94.29	94.51	94.98

	41	42	43	44	45	46	47	48
	R72304	R76101	R76102	R76103	R77101	R77102	R77103	R78101
	E	E	E	E	E	E	E	E
SIO2	45.74	48.66	48.31	48.02	46.52	46.36	46.39	46.54
TIO2	0.82	0.86	0.99	0.97	0.93	0.91	0.98	0.91
AL203	15.59	16.35	16.53	16.08	15.71	15.79	15.94	16.00
CR203	0.00	0.00	0.00	0.00	0.15	0.00	0.00	0.11
FEO	11.18	6.86	7.06	6.95	9.55	9.31	9.54	9.67
MNO	0.14	0.15	0.15	0.00	0.30	0.23	0.16	0.11
MGO	5.67	6.68	6.72	6.36	6.46	5.93	6.34	6.50
CAO	12.04	13.56	13.32	13.49	12.77	12.74	12.69	12.77
NA20	2.69	2.42	2.46	1.56	1.88	2.08	2.22	2.47
K20	0.74	0.74	0.67	0.72	0.69	0.67	0.67	0.72
CL	0.00	0.00	0.08	0.05	0.00	0.00	0.00	0.00
TOTAL	94.61	96.28	96.29	94.20	94.96	94.02	94.93	95.80

TABLE A6.6 EXPERIMENTAL GLASSES

	49	50
	R78102	R78103
	E	E
SIO2	46.51	46.39
TIO2	0.78	0.87
AL2O3	15.98	15.77
FEO	9.09	9.23
MNO	0.17	0.11
MGO	6.14	6.23
CAO	12.69	12.73
NA2O	1.84	1.95
K2O	0.67	0.70
TOTAL	93.87	93.98

APPENDIX B

WHOLE ROCK ANALYSIS

B.1 Production of whole rock powders

Most of the samples from the collection of Arculus (1973) were obtained as splits of powders. The remainder together with the samples collected in 1978 by the writer, were prepared for analysis at Edinburgh.

Where possible, samples weighing more than 500 grams were used to ensure representative sampling of the whole rock compositions. After removal of weathered surfaces, the samples were split using a Cutrock Engineering hydraulic splitter, then washed in deionised water. The samples were then crushed using a Sturtevant jaw crusher which was thoroughly cleaned with acetone before each operation, and flushed prior to each crushing session with surplus Grenada rock fragments to minimise contamination from previously crushed rocks.

After reduction of particle size to less than 5 mm by the crusher, the samples were split by 'coning and quartering'. A portion of the crushed rock was then ground in a Tema tungsten carbide swing mill to < 100 mesh and dried in an oven at 110^{o}C for at least 24 hours prior to analysis. Replicate analyses of sample 6127 in Table B4 provide an estimate of the sample homogeneity. Grinding probably oxidises some of the iron in the samples (Fitton and Gill, 1970) and produces contamination by Co and W, but the latter two elements were not analysed in this study.

B.2 Analytical procedure

Major and trace elements were determined by X-ray fluorescence spectrometry using the Philips PW 1450/20 spectrometer at Edinburgh. Full details of the techniques used are given by Thirlwall (1979) and only a short summary thereof is presented here.

B.2.1 Major elements - preparation

Major element analyses were carried out on fused glass discs prepared by a method similar to that of Norrish and Hutton (1969). Just over 1 gram of sample was ignited at 1100°C for 30 minutes and, after cooling, a lithium tetraborate - lithium oxide - lanthanum oxide flux was added in a fixed sample:flux ratio. Sample and flux were then fused for 20 minutes at 1100°C and cooled to a glass. The small weight loss during fusion was then made up by addition of more flux to make up the constant sample:flux weight ratio. The mixture was then refused, mixed thoroughly, and cast into a disc.

Ignition of samples prior to fusion generates a loss of ignition (LOI) value which is a combination of the weight loss due to loss of volatile constituents and the weight gain due to oxidation of ferrous iron. The generally fresh state of the analysed rocks is reflected in their low, or even negative, LOI values. However, petrographic examination shows that some secondary alteration is common and it was therefore decided not to carry out additional determinations of ferrous and ferric iron to those of Tomblin (1968) on Grenada samples, but to analyse only total iron contents. Similarly, it is considered unlikely that the H_2O contents of the rocks represent those of the original magmas due to loss of volatiles on eruption and limited post-eruptive alteration. Therefore the analysis of all rocks on an oxidised and dry basis produces an internally consistent data set, the analysis total providing an additional analytical check of constant total oxides.

B.2.2 Trace elements - preparation

Trace elements were analysed using pressed pellets of approximately 7 g of powder, this weight having been calculated by J. G. Fitton (pers. comm., 1978) to give absorption of 99% of NbK radiation in a matrix of very low absorption. Some of the Arculus samples were slightly smaller

than this (4 to 7 g), but analysis of a 4 g sample of 6127 (Table B4) shows that this has not significantly affected the trace element concentrations determined.

B.2.3 Major element analysis

Major elements (Na, Mg, Al, Si, P, K, Ca, Ti, Mn, Fe) were determined using a Cr-anode X-ray tube in an evacuated X-ray path. The presence of the heavy absorber La in the flux produces samples with closely similar mass absorption coefficients, and the major element analyses were therefore not corrected for mass absorption differences between samples. Calibrations were based on international standards, including USGS and CRPG standards.

B.2.4 Trace element analysis

Sc, V, Cu, Ba and La were analysed using a Cr-anode tube, and Ni, Zn, Th, Rb, Sr, Y, Zr, Nb, Cr, Ce, Sm and Nd using a W-anode tube, in an evacuated X-ray path. In addition, Ti was determined together with each group of trace elements. Agreement of TiO_2 values is generally good, but some discrepancies occur. Possible explanations for these are discussed by Thirlwall (1979). Mass absorption coefficients were calculated for each sample on the basis of the major element analysis. Calibrations were based on international standards and synthetic spiked standards (Table B1)

B.2.5 Analytical conditions

Analytical conditions are listed in Table B2. Interferences between analytical lines, and their treatment, are summarised in Table B3. It was found that the interference of CrKα on the Ce background resulted in Ce values significantly lower than those determined using isotope dilution methods, by Shimizu and Arculus (1975) and Hawkesworth et al. (1979), in samples whose Cr contents exceeded about 500 ppm.

	Sc	V	Cu	Ba	La	Ni	Zn	Th	Rb	Sr	Y	Zr	Nb	Cr	Ce	Sm	Nd	TiO_2
SY3	*				*			*			*		*		*	*	*	
GSN					*			*								*	*	
PCC1				*	*	*		*			*	*	*	*	*	*	*	
UBN	x	x	x	x	x	*		*			*	*	*	*	*	*	*	
JB1													*					
JG1													*				*	
GSP1					*										*	*	*	
T1	*				*			*	*		*		*		*	*	*	
GH							*											
FKN	x	x	x	x	x		*	*	*		*	*	*		*	*	*	
DRN	x	x	x	x	x			*					*		*	*	*	
	GA, BR, G2, AGV1 and BCR1 used for all elements																	
INTSGA2		*			*				*				*	*	*		*	*
INTSGB2	*	*			*	*	*				*			*				*
INTSBA2		*				*							*	*	*		*	*
INTSBB2	*	*			*	*	*				*	*		*				*
INTSGA3		*				*								*				*
INTSGB3	*	*				*								*				*
INTSBA3		*				*								*				*
INTSBB3	*	*				*								*				*
INTSGA4		*				*								*				*
INTSGB4		*				*								*				*
INTSBA4		*				*								*				*
INTSBB4		*				*								*				*
INTSG		*				*							x	*		x		*
INTSB		*				*							x	*		x		*
INTSA		*				*	x	x	x	x	x	x	x	*	x	x	x	*

Table B1 Standards used in trace element calibrations.

* = omitted by program

x = omitted by not including in run

(from Thirlwall, 1979)

Table B2 XRF analytical conditions

(from Thirlwall, 1979)

Line	Crystal	kV	mA	Collimator	Counter	Background offset 2θ°	Lower Level	Window
SiK_α	PE	50	45	C	F	+ 4.40	25%	60%
AlK_α	PE	60	45	C	F	- 5.75	25%	60%
FeK_α	LiF200	50	45	F	F	- 1.63	20%	60%
MgK_α	TlAP	60	45	C	F	+ 2.70	25%	50%
CaK_α	LiF200	50	30	F	F	- 3.00	25%	60%
NaK_α	TlAP	60	45	C	F	- 2.25	30%	50%
KK_α	LiF200	50	45	F	F	- 4.55	25%	60%
TiK_α	LiF200	50	45	F	F	+ 4.74	30%	50%
MnK_α	LiF200	60	45	F	F	- 1.00	15%	70%
PK_α	Ge	50	45	C	F	+ 3.14	35%	40%
ScK_α	LiF200	60	45	F	F	- 1.59	25%	60%
VK_α	LiF220	60	45	F	F	- 2.62	30%	50%
CuK_α	LiF200	60	45	C	F	+ 1.01	39%	26%
BaL_{β_2}	LiF220	60	45	F	F	+ 1.75	15%	60%
LaL_{α_1}	LiF200	60	45	C	F	- 1.08	30%	50%
NiK_α	LiF200	60	45	F	F	+ 1.33	25%	50%
ZnK_α	"	60	45	F	F	+ 0.80	25%	50%
ThL_{α_1}	"	90	30	F	FS	-	20%	60%
RbK_α	"	90	30	F	FS	+ 2.09	20%	60%
SrK_α	"	90	30	F	FS	-	20%	60%
YK_α	"	90	30	F	FS	+ 0.48	20%	60%
ZrK_α	"	90	30	F	FS	-	20%	60%
NbK_α	"	90	30	F	FS	- 0.40	20%	60%
CrK_α	"	60	45	F	F	+ 1.44 - 0.74	15%	60%
CeL_{β_1}	"	60	45	F	F	-	15%	60%
SmL_{α_1}	"	60	45	F	FS	- 0.48	20%	60%
NdL_{α_1}	"	60	45	F	F	- 1.34	15%	60%
TiK_β	"	60	45	F	F	- 1.54	30%	50%
CaK_β	"	60	45	F	F	-	25%	60%

Crystals

PE = Pentaerythritol,
Ge = Germanium,
TlAP = Thallium acid phthalate
LiF = Lithium Fluoride

Collimators

C = coarse, F = fine

Counters

F = gas flow proportional counter
FS = flow counter and scintillation counter

Table B3

Interferences on chosen analytical lines and backgrounds.

Line	Interference	Approx extent of Interference	Correction made
Mn K_α	Cr K_β	Unimportant for Cr <1500 ppm	None
P K_α	Ca K_β (2nd order)	Unimportant for CaO <20%	Narrow energy window
Mg K_α	Ca K_α (3rd order)	? 0.1% MgO for 20% CaO	None
Sc K_α	Ca K_β	1 ppm. Sc per % CaO	Regression
V K_α	Ti K_β	180 ppm. V per % TiO_2	Regression
La $L\alpha_1$	Ti K_α	5 ppm. La per % TiO_2	Regression
Ti K_β	Ba $L\beta_3$	0.00004 % TiO_2 per ppm. Ba	Yes
	V K_α	0.0004 % TiO_2 per ppm. V	Yes
Ni K_α	Y K_α (2nd order)	Unimportant for Y <400 ppm.	Narrow energy window
Y K_α	Rb K_α	0.22 ppm. Y per ppm. Rb	Regression
Zr K_α	Sr K_α	0.07 ppm. Zr per ppm. Sr	Regression
Nb K_α	La K_α (2nd order)	0.01 ppm. Nb per ppm. La	Regression
	Y K_β	Unimportant for Y <1000 ppm.	None
	U $L_{\beta 2,4}$	Unimportant for U<50 ppm.	None
Cr K_α	V K_β	0.05 ppm. Cr per ppm. V	Regression
Ce L_{β_1}	Nd $L\alpha_1$	Probably unimportant?	None
Nd $L\alpha_1$	Ce L_{β_1}	0.01 ppm. Nd per ppm. Ce	Regression
Sm $L\alpha_1$	Ce L_{β_2}	0.02 ppm. Sm per ppm. Ce	Regression
Cu background	Hf $L\alpha_1$	Unimportant for Zr <800 ppm	None
	Zr K_α (2nd order)		
Y, Zr, Nb backgrounds	U, Th	Unimportant for <500 ppm U, Th	None
Ce, Nd background	Cr K_α	Unimportant for Cr <800 ppm	None

(from Thirlwall, 1979)

A correction was therefore applied to both samples and standards using analyses of synthetic interference standards. The corrected Ce values are in good agreement with the isotope dilution results (Table B8).

B.2.6 Reproducability, repeatability, precision and accuracy

The analyses of sample 6127 in Table B4 provide a combined estimate of the reproducability of disc and pellet preparation and of repeatability and precision of analyses. Additional reproducability, repeatability and precision data are presented in Table B5 and B6 (from Thirlwall, 1979). Accuracy is estimated, by analysis of standard samples, in Table B7. Comparisons of trace element data from this study with those from other studies of the same samples are presented in Table B8.

Table B4

Replicate analyses of sample 6127

	6127/1	6127/2	6127/3	6127/4**
SiO_2	48.986	48.974	48.937	
Al_2O_3	16.761	16.696	16.729	
Fe_2O_3	10.301	10.274	10.259	
MgO	6.258	6.284	6.212	
CaO	12.626	12.640	12.587	
Na_2O	2.435	2.328	2.326	
K_2O	1.007	1.004	1.009	
TiO_2	0.986	0.982	0.983	
MnO	0.160	0.175	0.170	
P_2O_5	0.182	0.182	0.180	
LOI	0.37	0.37	0.34	
Ni	52.1	51.2	51.2	50.9
Cr	71.0	68.1	70.0	66.9
V	308.1	302.1	306.3	309.3
Sc	36.1	35.5	36.9	33.5
Cu	150.4	151.3	150.3	153.0
Zn	60.8	60.2	60.8	60.1
Sr	1145.2	1140.0	1136.7	1145.0
Rb	12.2	11.7	12.5	11.7
Zr	73.9	76.6	75.2	77.2
Nb	5.3	5.4	5.0	4.7
Ba	434.2	429.1	424.4	435.7
Th	5.1	5.6	5.4	6.3
La	18.7	20.7	21.0	19.9
Ce	42.5	40.7	39.2	39.1
Nd	24.0	25.4	24.1	24.3
Sm	8.6	6.9	8.6	11.0
Y	24.5	24.6	24.1	25.5
TiO_2CR	1.010	1.003	1.012	0.995
TiO_2W	1.027	1.034	1.046	1.017

**sample weight reduced from 7g to 4g in 6127/4

Table B5 Reproducability of disc and pellet production

Six discs and six pellets of sample MT45

Data from Thirlwall (1979)

	mean	$\pm 2\sigma$
SiO_2	54.529	0.342
Al_2O_3	15.589	0.114
Fe_2O_3	8.248	0.101
MgO	6.743	0.069
CaO	8.023	0.025
Na_2O	3.317	0.104
K_2O	1.356	0.011
TiO_2	1.281	0.007
MnO	0.115	0.016
P_2O_5	0.347	0.004
LOI	1.542	0.100
Ni	138.3	0.8
Cr	289.8	4.0
V	167.0	4.6
Sc	24.4	0.4
Cu	49.9	1.2
Zn	67.9	1.1
Sr	601.1	4.5
Rb	17.3	0.9
Zr	249.1	1.5
Nb	12.4	0.9
Ba	543.6	8.5
Th	10.6	2.3
La	31.1	2.1
Ce	73.3	2.3
Nd	34.1	1.7
Sm	8.8	4.6
Y	25.8	0.8
TiO_2CR	1.309	0.036
TiO_2W	1.331	0.016

Table B6 Analytical Precision/Repeatability data. (from Thirlwall, 1979)

	G2		AGV1		DTS1	
	Mean	± 2σ	Mean	± 2σ	Mean	± 2σ
SiO_2	69.32	0.210	59.62	0.240	40.57	0.146
Al_2O_3	15.48	0.058	17.12	0.062	0.40	0.006
Fe_2O_3	2.74	0.015	6.92	0.035	8,93	0.036
MgO	0.84	0.038	1.59	0.030	49.89	0.253
CaO	1.92	0.010	4.96	0.020	0.17	0.002
Na_2O	4.30	0.060	4.37	0.124	0.11	0.057
K_2O	4.49	0.014	2.96	0.013	(-0.02)	0.001
TiO_2	0.49	0.004	1.06	0.006	0.02	0.002
MnO	0.03	0.010	0.10	0.009	0.13	0.008
P_2O_5	0.13	0.005	0.48	0.007	0.01	0.003

16 CYCLES PER SAMPLE

	SR6		S32		JB1	
	Mean	± 2σ	Mean	± 2σ	Mean	± 2σ
Sc	15.7	0.4	21.7	0.6	26.2	0.5
V	162.7	3.1	133.1	4.5	194.0	2.8
Cu	29.9	0.5	22.2	1.0	53.9	0.8
Ba	893.7	7.0	408.2	4.1	554.1	5.7
La	44.9	2.0	30.6	2.8	40.2	2.0
TiO_2CR	0.73%	0.003	1.18%	0.003	1.27%	0.007%

19 CYCLES PER SAMPLE

	MT45	
	Mean	± 2σ
Ni	138.9	1.5
Zn	68.6	1.7
Th	4.6	2.2
Rb	16.7	1.2
Sr	603.6	2.0
Y	25.5	0.5
Zr	249.8	1.7
Nb	12.7	1.1
Cr	290.0	1.7
Ce	71.7	3.8
Sm	8.7	2.8
Nd	34.1	1.6
TiO_2W	1.34%	0.014

12 CYCLES

Oxides in wt.%; trace elements in p.p.m.

G2, AGV1, DTS1 and JB1 are international standards

S32, MT45 are samples from the present study

SR6 is a basaltic andesite from the volcano Stromboli, Italy

Table B7 Analytical Accuracy

Analyses of standard samples run as unknowns, not included in calibrations, compared with values from Abbey (1977). Major elements in wt.%, trace elements in ppm. (from Thirlwall, 1979)

Major elements: sample GS-N

	SiO_2	Al_2O_3	Fe_2O_3*	MgO	CaO	Na_2O	K_2O	TiO_2	MnO	P_2O_5
XRF	66.09	14.81	3.82	2.30	2.45	3.60	4.687	0.662	0.060	0.269
Abbey (1977)	65.98	14.71	3.75	2.31	2.51	3.78	4.64	0.68	0.06	0.28

	XRF						Abbey (1977)					
	DR-N	FK-N	UB-N	W1	SY2	TB	DR-N	FK-N	UB-N	W1	SY2	TB
Sc	34	0	14	37	6	21	-	-	-	?35	?7	13.5
V	224	2	68	264	50	121	220	-	75	240	50	105
Cu	44	4	20	102	3	32	52	?3	30	110	4	50
Ba	398	198	40	175	460	777	380	?210	?45	160	460	720
La	20	2	3	12	67	51	-	-	-	?12	?85	?56

		Ni	Zn	Th	Rb	Sr	Y	Zr	Nb	Cr	Ce	Sm	Nd
XRF	W1	74	84	2	22	196	24	107	9	128	19	3	11
	SY2	11	260	427	226	270	124	288	37	9	157	13	72
	TB	44	98	19	189	164	33	188	20	107	103	7	43
Abbey (1977)	W1	78	86	2	21	190	25	105	?10	120	?23	?4	15
	SY2	10	250	?370	220	270	130	270	?25	10	?210	?16	?70
	TB	40	95	?19	180	155	?39	175	-	80	?115	?9	-

Table B8

Comparison of XRF data with other published analyses

	Th		La		Ce		Nd		Sm	
	XRF	INAA	XRF	ID	XRF	ID	XRF	ID	XRF	ID
43	2.8	2.45	9.6	-	21.5	19.0	7.0	10.8	2.1	2.85
225B	6.6	-	17.6	17.6	42.5	41.2	21.6	22.4	7.9	4.72
239	4.7	-	34.6	-	36.5	33.9	21.5	21.8	3.5	5.28
266	11.6	-	27.3	27.3	56.4	53.0	24.2	28.8	6.3	6.19
286	12.5	9.01	28.8	-	58.5	52.4	23.0	25.0	4.9	5.26
314	8.4	8.40	25.5	21.4	48.8	45.4	20.6	22.8	3.0	4.93
380	5.7	-	20.7	18.3	35.1	41.5	20.6	24.3	4.4	5.51
449	3.7	5.10	17.2	-	32.7	31.4	13.0	16.7	7.5	3.93
450	2.6	-	10.4	8.59	20.1	20.9	11.8	14.6	0.4	3.61
454	0.0	-	7.8	8.19	18.7	20.8	10.7	14.5	5.8	3.64
500	1.5	1.25	6.1	5.52	14.2	13.5	4.7	8.96	3.0	2.49
507	1.1	1.65	6.4	-	19.8	15.8	6.8	11.0	7.7	3.07
509	9.8	10.6	32.7	-	58.0	57.4	24.2	29.3	8.2	5.78

ID analyses from Shimizu and Arculus (1975) and Hawkesworth et al. (1979b)

INAA analyses from Minster and Allegre (1978)

Table B9

Whole-rock analyses

@1 = M-series

@2 = C-series

@3 = Evolved lavas

All samples are from the collection of Arculus (1973), except those prefixed 6- which were collected in this study, and those prefixed X- which are from the U.W.I. collection in Trinidad.

The U.W.I. samples were not analysed for trace elements.

	43@1	100@3	109@2	114@1	121@1	214@3	225B@2	230@2	239@2
SIO2	46.51	59.71	52.08	47.85	47.43	60.45	49.16	52.03	47.38
AL2O3	13.46	17.00	18.89	15.08	15.36	16.81	17.15	17.64	16.68
FE2O3	10.25	6.19	8.54	10.05	10.40	5.60	9.83	8.39	10.51
MGO	13.83	2.66	4.31	12.63	12.50	2.97	5.76	4.68	6.45
CAO	11.66	6.79	8.82	9.86	10.14	7.06	12.73	10.50	13.49
NA2O	2.24	4.37	4.00	1.75	1.74	4.12	2.84	3.48	2.36
K2O	0.443	1.681	1.312	0.571	0.544	1.529	1.037	1.456	1.033
TIO2	0.891	0.571	1.022	0.915	0.939	0.521	0.992	0.822	0.996
MNO	0.179	0.147	0.149	0.181	0.186	0.122	0.143	0.139	0.175
P2O5	0.122	0.201	0.406	0.225	0.225	0.192	0.190	0.232	0.172
TOTAL	99.59	99.31	99.53	99.12	99.46	99.38	99.84	99.36	99.26
LOI	0.07	0.82	1.42	0.76	1.94	0.36	0.35	0.34	0.05
NI	317.0	25.4	53.9	346.7	320.4	27.6	46.6	33.8	43.2
CR	1012.9	49.4	43.2	658.2	660.7	63.9	64.8	40.1	70.4
V	265.1	130.5	244.8	242.9	244.9	115.8	317.6	243.1	315.9
SC	40.5	12.3	18.6	33.2	35.2	13.0	33.3	20.5	35.0
CU	76.6	51.0	33.1	41.9	50.4	57.3	340.1	81.3	134.1
ZN	69.0	48.3	105.5	72.6	74.0	51.1	116.5	57.0	63.3
SR	350.4	627.1	761.2	456.5	461.9	768.7	1179.7	1034.5	1133.1
RB	12.3	57.1	42.5	12.3	9.7	59.7	10.8	27.8	15.3
ZR	54.2	164.3	153.8	85.6	86.2	149.9	80.2	111.4	68.0
NB	4.2	12.7	15.8	6.6	7.5	11.1	5.7	8.1	3.8
BA	153.0	570.8	541.1	301.3	291.7	563.4	367.2	451.7	365.8
TH	2.8	17.5	18.6	9.4	9.3	17.7	6.6	12.9	4.7
LA	9.6	28.2	36.6	18.0	17.1	27.3	17.6	27.2	34.6
CE	21.5	55.5	67.0	42.3	40.7	49.3	42.5	47.7	36.5
ND	7.0	20.4	29.9	17.8	16.6	19.0	21.6	22.5	21.5
SM	2.1	1.2	10.2	6.7	3.1	1.5	7.8	9.7	3.5
Y	18.2	19.1	22.6	20.4	21.9	13.8	18.9	18.9	20.1
TIO2CR	0.895	0.567	1.044	0.962	0.991	0.508	1.028	0.899	0.984
TIO2W	0.920	0.581	1.055	0.987	1.011	0.507	1.038	0.889	0.991

	262@1	265@1	266@1	274@3	282@1	286@1	306@1	307@3	310A@3
SIO2	47.08	53.20	44.88	62.69	49.79	45.76	47.96	56.96	55.93
AL2O3	13.40	16.72	14.47	18.14	17.82	15.02	15.14	17.16	16.70
FE2O3	10.11	7.59	10.48	5.38	10.17	10.51	10.35	7.25	7.32
MGO	14.83	7.85	12.12	1.88	6.70	11.78	9.92	3.88	3.42
CAO	10.31	9.33	13.08	4.64	9.35	12.62	12.61	7.55	6.97
NA2O	2.14	2.83	2.32	3.67	3.45	1.94	2.15	4.12	3.57
K2O	0.497	0.950	0.730	1.779	1.158	0.639	0.806	1.521	0.922
TIO2	0.814	0.731	1.080	0.552	0.766	0.979	1.015	0.731	0.659
MNO	0.167	0.148	0.186	0.415	0.175	0.182	0.167	0.162	0.177
P2O5	0.141	0.124	0.336	0.143	0.148	0.294	0.169	0.224	0.185
TOTAL	99.48	99.47	99.67	99.29	99.52	99.72	100.27	99.56	99.85
LOI	0.87	0.43	0.84	1.90	2.59	0.44	0.43	1.28	1.27
NI	409.4	129.1	234.2	27.2	119.5	219.1	178.9	48.0	91.1
CR	1090.3	383.8	612.8	45.1	320.6	454.4	500.0	104.9	242.6
V	240.3	143.5	295.2	97.1	164.2	285.4	303.9	159.7	192.3
SC	37.5	22.6	33.9	13.4	40.5	29.2	43.8	18.1	32.4
CU	95.6	44.2	89.4	62.1	33.3	55.8	125.5	45.1	46.5
ZN	74.4	55.2	76.2	46.7	76.3	80.1	70.1	64.5	66.1
SR	328.0	371.4	678.5	569.3	550.2	727.7	588.8	478.7	325.4
RB	10.6	45.3	20.8	86.4	20.4	22.8	12.3	45.1	39.1
ZR	60.4	88.7	95.8	154.6	66.9	83.9	70.7	167.6	80.8
NB	4.9	7.6	10.4	12.3	5.2	10.4	6.3	12.5	7.2
BA	158.4	213.0	346.1	920.0	290.1	379.9	214.5	467.3	254.6
TH	3.9	5.1	11.6	14.9	5.4	12.5	1.4	13.0	5.7
LA	8.4	12.4	27.3	22.4	10.7	28.8	9.4	25.6	11.0
CE	20.8	25.3	56.4	38.2	23.3	58.5	24.5	50.0	18.5
ND	4.6	11.4	24.3	15.5	11.9	23.0	14.1	21.9	7.7
SM	7.0	5.8	6.3	0.0	3.0	4.8	8.1	4.1	7.8
Y	18.1	18.9	22.0	14.9	17.6	21.4	20.5	23.1	19.0
TIO2CR	0.854	0.622	1.113	0.505	0.793	0.993	1.084	0.712	0.839
TIO2W	0.855	0.747	1.113	0.522	0.797	0.994	1.096	0.736	0.832

	311@1	313D@1	313L@3	314&1	319@1	333A@1	333B@2	334@3	337@2
SIO2	51.61	54.22	61.59	45.99	51.70	52.80	48.87	61.70	53.75
AL203	16.86	16.42	17.57	14.41	14.84	17.69	16.56	17.53	17.57
FE203	8.03	8.15	5.17	10.42	8.65	7.85	10.22	5.12	7.86
MGO	8.48	5.28	2.28	12.07	10.05	7.36	6.46	2.32	4.08
CAO	10.39	8.98	6.19	12.86	9.48	9.20	12.74	5.83	10.01
NA2O	2.79	3.97	4.25	1.67	2.91	2.92	2.51	4.35	3.71
K2O	0.789	0.927	1.607	0.493	0.889	0.891	1.121	1.623	1.562
TIO2	0.803	0.806	0.508	1.044	0.760	0.777	0.980	0.481	0.765
MNO	0.152	0.209	0.079	0.177	0.135	0.154	0.161	0.098	0.152
P2O5	0.097	0.275	0.210	0.280	0.207	0.125	0.179	0.219	0.235
TOTAL	100.01	99.23	99.45	99.41	99.61	99.76	99.80	99.27	99.70
LOI	0.20	0.41	0.46	2.30	1.52	0.50	0.17	0.68	0.52
NI	115.9	58.6	N.D.	236.2	272.5	21.5	52.3	21.9	30.6
CR	301.2	133.4	N.D.	613.8	564.9	45.9	78.1	26.6	33.1
V	207.9	194.5	N.D.	290.2	205.7	98.4	288.7	90.2	208.4
SC	37.6	29.5	N.D.	34.2	26.5	15.8	33.9	8.7	17.5
CU	60.7	57.1	N.D.	117.5	45.2	40.1	114.3	10.1	162.9
ZN	58.1	76.9	N.D.	74.1	50.6	63.1	68.7	25.9	39.9
SR	320.4	611.7	N.D.	620.5	537.4	571.4	1156.9	687.7	1021.8
RB	25.5	41.1	N.D.	10.0	21.3	30.6	14.5	50.8	30.9
ZR	69.3	129.4	N.D.	96.0	113.0	107.1	75.0	189.9	127.7
NB	5.9	13.5	N.D.	9.8	10.8	11.9	3.9	13.3	9.2
BA	221.3	386.1	N.D.	369.6	429.2	405.5	380.1	653.8	498.1
TH	1.6	7.4	N.D.	8.5	10.0	7.8	7.9	22.0	13.0
LA	6.3	33.6	N.D.	25.5	38.4	26.0	21.4	30.1	29.1
CE	19.0	65.1	N.D.	48.8	37.1	41.9	41.1	58.9	53.5
ND	7.7	26.1	N.D.	20.8	23.3	19.5	22.7	24.0	25.6
SM	3.2	4.1	N.D.	2.8	8.8	5.6	8.3	4.6	6.2
Y	17.1	21.1	N.D.	20.5	26.0	23.4	19.5	16.3	18.8
TIO2CR	0.833	0.785	N.D.	1.036	0.821	0.643	0.939	0.464	0.792
TIO2W	0.847	0.801	N.D.	1.056	0.826	0.673	0.940	0.475	0.803

	375&1	376@1	380@2	381&3	398@1	400@1	412@3	413@1	421&1
SIO2	46.38	46.27	48.32	57.03	54.98	55.22	58.77	47.46	47.72
AL203	13.81	13.16	18.39	17.04	16.05	16.46	17.10	14.86	14.84
FE203	10.40	10.55	10.91	7.30	7.74	7.54	6.54	10.06	10.09
MGO	13.23	14.13	4.99	3.13	6.76	6.04	3.30	10.02	10.06
CAO	12.12	11.36	12.21	7.97	8.10	8.64	7.02	12.62	12.66
NA2O	2.07	1.72	2.39	4.20	3.59	3.67	4.02	2.31	2.41
K2O	0.431	0.629	1.158	1.836	1.256	1.217	1.712	0.791	0.808
TIO2	0.931	0.942	0.973	0.748	0.694	0.697	0.730	1.022	1.036
MNO	0.171	0.190	0.170	0.115	0.173	0.152	0.131	0.172	0.168
P2O5	0.111	0.208	0.219	0.241	0.172	0.189	0.222	0.172	0.188
TOTAL	99.65	99.17	99.74	99.60	99.50	99.83	99.54	99.49	99.97
LOI	0.71	0.53	0.76	0.79	0.80	1.17	0.32	0.11	0.28
NI	263.5	417.0	33.4	20.9	154.8	89.9	29.0	163.2	172.1
CR	763.7	1093.6	10.8	32.6	426.6	196.4	57.0	455.4	499.2
V	292.6	268.0	341.8	188.9	172.9	170.5	141.6	278.4	291.7
SC	44.7	32.1	24.3	17.3	23.3	20.1	16.0	40.4	40.5
CU	93.6	84.4	148.0	21.7	94.4	55.9	69.4	100.5	100.7
ZN	68.9	70.4	70.0	31.1	64.1	72.6	55.9	67.6	67.1
SR	328.8	650.6	1236.5	966.1	522.5	555.1	452.0	582.8	582.9
RB	10.7	9.0	16.5	39.2	34.7	35.4	51.4	14.3	11.0
ZR	52.1	77.5	81.2	164.9	125.4	129.3	169.5	73.3	77.6
NB	4.8	9.7	6.8	11.7	8.4	10.4	12.1	8.2	7.3
BA	131.1	465.3	410.9	629.2	449.8	437.2	482.5	225.0	273.2
TH	2.5	7.7	5.7	17.3	13.0	14.3	15.0	5.6	5.2
LA	4.5	22.0	20.7	31.4	27.7	25.6	25.8	10.4	12.5
CE	17.5	43.9	35.1	66.4	44.5	41.3	49.7	24.7	30.2
ND	5.6	14.6	20.7	27.9	19.3	17.8	20.1	12.4	12.7
SM	4.4	4.2	4.3	4.8	2.0	4.2	4.2	3.4	7.3
Y	18.9	19.9	25.0	20.3	21.8	21.0	21.7	20.3	20.7
TIO2CR	0.958	0.971	1.008	0.749	0.630	0.656	0.734	1.006	1.026
TIO2W	0.987	0.962	1.003	0.762	0.669	0.674	0.748	1.021	1.061

	447@3	449@1	450@2	454@2	457@1	464@3	468@1	487A@2	500@1
SIO2	60.89	46.22	47.17	47.42	46.65	62.65	46.12	48.92	46.55
AL203	16.18	14.79	15.58	15.67	13.48	16.78	13.27	17.60	13.82
FE203	5.76	9.90	11.30	11.17	10.27	4.96	10.27	9.79	10.01
MGO	3.37	12.57	7.06	7.07	14.36	2.07	15.96	5.61	14.42
CAO	5.40	12.02	14.43	14.37	10.75	7.37	10.55	11.98	10.96
NA20	3.59	2.37	2.12	2.16	2.07	4.00	1.98	2.84	2.00
K20	1.727	0.419	0.515	0.641	0.425	1.639	0.436	1.173	0.411
TIO2	0.591	0.898	0.963	0.965	0.869	0.473	0.886	1.061	0.879
MNO	0.109	0.181	0.183	0.171	0.174	0.157	0.174	0.175	0.171
P205	0.196	0.197	0.124	0.126	0.099	0.202	0.123	0.187	0.102
TOTAL	99.80	99.58	99.45	99.76	99.16	100.29	99.76	99.34	99.31
LOI	3.88	-0.07	0.43	0.47	-0.08	3.20	-0.05	-0.14	-0.34
NI	27.6	256.2	44.5	48.8	379.9	54.4	459.6	36.3	340.6
CR	52.1	582.0	74.7	74.9	1060.9	107.6	1040.6	43.4	1000.9
V	109.4	252.1	333.6	333.1	247.3	89.6	216.6	288.3	259.8
SC	12.6	33.0	43.5	46.0	36.6	11.0	33.1	28.8	37.8
CU	24.7	78.9	145.2	178.7	75.4	15.1	76.7	136.5	80.4
ZN	30.5	71.8	74.2	61.7	79.5	61.1	70.7	57.4	70.5
SR	563.7	454.9	1022.4	1016.5	267.4	615.0	313.3	890.9	255.7
RB	76.4	12.0	5.6	7.1	11.2	80.1	12.1	18.3	9.7
ZR	164.3	62.8	46.3	48.7	55.6	154.4	54.4	81.9	52.4
NB	13.1	5.8	3.8	4.3	5.3	14.0	5.9	7.2	5.0
BA	621.4	205.5	252.5	255.6	128.0	660.7	158.5	350.5	110.5
TH	16.6	3.7	2.6	N.D.	4.2	26.3	6.1	2.7	1.5
LA	27.0	17.2	10.4	7.8	5.1	33.6	6.1	15.3	6.1
CE	45.5	32.7	20.1	18.7	13.3	57.0	19.7	33.5	14.2
ND	17.2	13.0	11.9	10.7	5.0	20.0	6.7	21.0	4.7
SM	5.5	7.5	0.4	5.8	2.5	1.8	2.8	2.2	3.0
Y	14.7	18.7	20.8	20.9	17.5	14.6	16.9	29.0	18.1
TIO2CR	0.535	0.899	0.917	0.981	0.897	0.462	0.821	0.965	0.925
TIO2W	0.562	0.906	0.957	0.995	0.901	0.490	0.869	0.967	0.917

	507@1	509@1	607@2	607@1	610@1	610@2	612@2	615@2	615@1
SIO2	47.13	45.57	49.79	45.88	45.10	47.29	48.99	46.96	47.36
AL203	14.00	12.71	18.79	12.49	12.53	15.57	16.76	16.16	13.42
FE203	10.03	10.52	10.29	10.38	10.45	11.14	10.30	10.59	10.04
MGO	13.33	14.10	4.43	14.47	15.28	7.45	6.26	7.57	12.79
CAO	11.53	11.38	10.95	12.21	12.29	13.87	12.63	14.53	11.63
NA20	2.06	2.40	3.50	1.88	1.93	1.97	2.43	1.82	2.07
K20	0.363	1.253	0.675	1.102	0.537	1.027	1.007	1.005	0.746
TIO2	0.828	1.074	0.918	1.134	0.919	0.852	0.986	0.966	0.877
MNO	0.159	0.177	0.173	0.171	0.179	0.187	0.160	0.172	0.177
P205	0.103	0.404	0.211	0.300	0.229	0.178	0.182	0.196	0.145
TOTAL	99.54	99.59	99.72	100.01	99.45	99.52	99.70	99.96	99.27
LOI	0.28	0.25	0.32	0.59	0.33	0.38	0.37	1.56	0.02
NI	343.6	330.2	35.3	359.1	388.6	55.0	52.1	55.0	354.5
CR	897.9	991.2	32.0	1020.7	943.4	108.2	71.0	108.3	1019.3
V	281.7	270.9	260.8	286.7	261.6	307.5	308.1	313.4	264.5
SC	38.7	31.3	20.7	36.8	34.6	40.0	36.1	36.3	40.2
CU	99.5	104.3	83.3	88.0	85.4	190.5	150.4	87.9	49.7
ZN	73.5	71.9	83.0	69.7	69.8	59.1	60.8	63.6	71.5
SR	354.8	567.6	499.9	529.3	676.7	1395.6	1145.2	1232.9	572.5
RB	4.7	44.8	12.1	26.7	12.3	13.9	12.2	18.8	11.9
ZR	51.4	176.5	84.2	100.5	71.7	63.9	73.9	79.5	63.2
NB	3.6	14.8	6.6	18.9	6.8	3.5	5.3	4.6	6.8
BA	182.6	453.2	255.6	386.0	283.8	335.6	434.2	345.0	214.1
TH	1.1	9.8	4.4	9.2	9.2	4.7	5.1	6.2	3.0
LA	6.4	32.7	13.8	23.5	17.2	18.2	18.7	14.9	8.0
CE	19.8	58.0	25.2	42.8	34.6	40.2	42.5	37.3	24.5
ND	6.9	24.2	13.4	16.3	12.1	22.4	24.0	20.4	9.5
SM	7.6	8.1	5.5	5.2	5.8	7.7	8.6	5.8	4.2
Y	21.5	19.3	23.4	19.5	17.6	20.8	24.5	21.4	18.6
TIO2CR	0.852	1.111	0.843	1.158	0.950	0.882	1.010	0.938	0.879
TIO2W	0.844	1.100	0.865	1.163	0.946	0.895	1.027	0.932	0.898

	6177@2	6186@1	6257@1	6259@1	6264@2
SIO2	51.07	47.09	48.07	47.25	48.05
AL2O3	17.93	13.43	14.73	14.79	16.04
FE2O3	9.01	9.99	9.72	10.13	10.77
MGO	5.78	12.65	12.00	13.10	6.61
CAO	10.66	12.38	11.00	11.09	13.44
NA2O	2.87	2.02	2.35	1.08	2.43
K2O	1.074	0.752	0.633	0.425	0.739
TIO2	0.843	0.779	0.956	0.928	0.890
MNO	0.155	0.161	0.169	0.174	0.159
P2O5	0.230	0.219	0.168	0.121	0.240
TOTAL	99.62	99.47	99.81	99.08	99.37
LOI	0.78	0.94	-0.37	-0.10	0.25
NI	43.8	245.9	234.2	316.4	62.3
CR	98.1	723.0	571.4	857.2	146.2
V	250.7	250.4	249.3	267.8	308.7
SC	26.5	30.6	30.7	34.9	34.8
CU	46.0	86.4	32.2	67.9	75.1
ZN	83.1	61.3	71.5	70.0	70.0
SR	645.4	654.9	387.5	287.0	1431.7
RB	22.0	22.5	14.4	8.4	9.4
ZR	100.7	73.7	77.0	57.6	77.8
NB	6.3	6.7	7.2	4.3	5.0
BA	322.7	295.6	192.7	134.1	353.0
TH	5.5	10.3	3.4	1.5	5.6
LA	19.4	22.9	8.8	4.0	22.3
CE	32.1	40.9	22.0	14.3	54.6
ND	21.9	17.1	7.6	3.2	26.7
SM	5.9	5.8	5.3	5.0	6.8
Y	26.0	18.2	18.8	18.8	21.8
TIO2CR	0.890	0.776	0.926	0.951	0.922
TIO2W	0.894	0.800	0.958	0.976	0.941

	X28024@1	X28035@1	X28054@3	X28070@3	X28071@2	X28072@1
SIO2	47.52	44.89	58.23	54.49	46.64	47.25
AL2O3	14.63	13.01	16.96	18.45	16.05	13.59
FE2O3	9.84	10.92	6.80	8.08	12.29	10.78
MGO	11.94	14.24	2.85	3.62	6.35	15.24
CAO	11.07	12.29	7.35	8.40	14.21	8.71
NA2O	2.54	2.02	4.14	4.08	1.69	1.78
K2O	0.660	0.453	1.956	0.999	0.896	0.254
TIO2	0.980	0.841	0.692	0.743	0.695	0.898
MNO	0.174	0.222	0.101	0.131	0.204	0.177
P2O5	0.164	0.186	0.227	0.264	0.174	0.075
TOTAL	99.51	99.06	99.32	99.24	99.40	98.75
LOI	-0.17	0.38	0.30	1.07	1.19	1.66

APPENDIX C

EXPERIMENTAL METHOD

C.1 Pressure

Horizontally-mounted, internally-heated, argon gas pressure vessels, similar to those described by Ford (1972), were used for all experiments. Pressures were measured using a manganin cell connected to a Harwood Carey-Foster bridge capable of reading to better than 4 bars. Pressures were measured during experiments by pumping the main pressure line to the desired pressure, opening the valve to the pressure vessel, and re-measuring the pressure. This procedure is believed to involve a total uncertainty of ±100 bars.

The pressure scale was calibrated using a mercury cell, in November 1976. The freezing point of mercury is a fixed point on the pressure scale (Bridgeman, 1911) which was located by Newhall et al. (1963) at 7565.4 ± 51.7 bars. The pressure calibration in 1976 bracketed this point at 7590 ± 30 bars (C. Begg, pers. comm.). Pressure variations measured during runs were small, and pressures are believed to be accurate to ±200 bars.

C.2 Temperature

10 mm internal diameter furnaces, wound with Kanthal or molybdenum wire, were employed, the molybdenum-wound furnaces being used only for runs at temperatures in excess of 1175°C. Capsules were loaded into a Mo sample container with close-fitting lid to promote as even a thermal profile as possible along the length of the charges.

Temperatures were measured using Pt-$Pt_{87}Rh_{13}$ thermocouples. In the Kanthal furnaces, a single, centrally-positioned thermocouple was used; the uncertainty in temperature measurement is believed to be within ±5°C (Ford, 1972). Because of the large size of the buffer capsules,

RUN DATA

Run No	Time hrs min	Comp	% H_2O In melt	P Kbar	T °C	Crystals %	FGC	Buffer	a_{H_2O}	-log fo_2 bars	Phases	Notes
182	3.50	43	2.68	2	1250	2	OAD	NNO	0.41	- 7.34	ol,sp,gl	
191	2.30	43	1.20	2	1225	4	OAD	NNO	0.14	- 8.09	ol,sp,gl	
192	2.30	43	2.61	2	1225	4	OAD	NNO	0.43	- 7.59	ol,sp,gl	
193	2.30	311	1.09	2	1225	0	OAD	NNO	0.08	- 8.31	gl	
201	2.00	43	1.06	2	1250	2	OAD	NNO	0.10	- 7.94	ol,sp,gl	
201	2.00	43	2.68	2	1250	2	OAD	NNO	0.41	- 7.34	ol,sp,gl	
211	2.00	43	1.07	2	1255	4	OAD	NNO	0.11	- 8.17	ol,sp,gl	
212	2.00	43	2.58	2	1225	4	OAD	NNO	0.42	- 7.59		Sample capsule failed
221	1.30	43	2.83	2	1250	2	OAD	NNO	0.44	- 7.31	ol,sp,gl	
231	1.40	43	1.03	2	1200	10	OAD	NNO	0.11	- 8.44	ol,sp,gl	Fe analysis
232	1.40	43	2.58	2	1200	6	OAD	NNO	0.44	- 7.85	ol,sp,gl	
233	1.40	311	1.09	2	1200	0	OAD	NNO	0.09	- 8.57	gl	Fe analysis
241	2.00	43	1.05	2	1175	10	OAD	NNO	0.12	- 8.71	ol,sp,gl	
242	2.00	43	2.56	2	1175	8	OAD	NNO	0.46	- 8.13	ol,sp,gl	
243	2.00	311	1.10	2	1175	0	OAD	NNO	0.09	- 8.83	ol,sp,gl	Close to liquidus
251	1.35	43	1.06	2	1275	2	OAD	NNO	0.09	- 7.72	ol,sp,gl	
252	1.35	43	2.75	2	1275	1	OAD	NNO	0.38	- 7.10	ol,sp,gl	Close to liquidus, Fe analysis
271	1.45	114	1.05	2	1225	3	OAD	NNO	0.09	- 8.27	ol,sp,gl	
271	1.45	114	2.84	2	1225	2	OAD	NNO	0.41	- 7.61	ol,sp,gl	
281	1.45	114	1.05	2	1250	2	OAD	NNO	0.08	- 8.04	ol,sp,gl	
282	1.45	114	2.91	2	1250	1	OAD	NNO	0.39	- 7.36	ol,sp,gl	Fe analysis
291	2.20	114	1.02	2	1200	6	OAD	NNO	0.09	- 8.55	ol,sp,gl	
292	2.20	114	2.83	2	1200	4	OAD	NNO	0.43	- 7.87	ol,sp,gl	
301	1.45	114	1.02	2	1275	0	OAD	NNO	0.07	- 7.83	gl	
302	1.45	114	2.96	2	1275	0	OAD	NNO	0.36	- 7.13	gl	Fe analysis

Run No	Time hrs min	Comp	% H_2O In melt	P Kbar	T °C	Crystals %	FGC	Buffer	a_{H_2O}	-log fo_2 bars	Phases	Notes
311	2.00	43	1.04	2	1150	10	OAD	NNO	0.12	- 9.01	ol,cpx,pl,gl	
312	2.00	43	2.51	2	1150	8	OAD	NNO	0.46	- 8.43	ol,sp,gl	
313	2.00	311	1.11	2	1150	6	OAD	NNO	0.10	- 9.12	ol,pl,sp,gl	
321	2.05	114	1.02	2	1175	6	OAD	NNO	0.09	- 8.82	ol,pl,sp,gl	
322	2.05	114	2.82	2	1175	4	OAD	NNO	0.44	- 8.15	ol,sp,gl	Fe analysis
323	2.05	311	3.01	2	1175	0	OAD	NNO	0.43	- 8.16	ol,sp, gl	Near liquidus
331	2.25	114	1.01	2	1150	10	OAD	NNO	0.09	- 9.12	ol,pl,sp,gl	
332	2.25	114	2.80	2	1150	8	OAD	NNO	0.45	- 8.44	ol,sp,gl	
333	2.25	311	2.71	2	1150	2	OAD	NNO	0.43	- 8.46	ol,sp,gl	
341	1.30	43	1.08	2	1300	1	OAD	NNO	0.08	- 7.52	sp,gl	
342	1.30	43	2.85	2	1300	0	OAD	NNO	0.34	- 6.90		Sample capsule failed
351	3.00	43	1.04	2	1125	12	OAD	NNO	0.12	- 9.32	ol,cpx,pl,gl	Fe analysis
352	3.00	43	2.53	2	1125	10	OAD	NNO	0.47	- 8.73	ol,cpx,pl,sp,gl	
353	3.00	114	1.02	2	1125	10	OAD	NNO	0.10	- 9.42		Sample capsule failed
361	3.15	114	1.02	2	1125	10	OAD	NNO	0.10	- 9.42	ol,pl,sp,gl	
371	2.00	43		4	1275		OAD	NNO				Sample capsule failed
372	2.00	43		4	1275		OAD	NNO				Sample capsule failed
373	2.00	114	1.02	4	1275	0	OAD	NNO	0.05	- 7.95	sp,gl	Close to liquidus
381	1.50	43	1.10	4	1275	2	OAD	NNO	0.07	- 7.80	ol,sp,gl	
382	1.50	43	2.57	4	1275	0	OAD	NNO	0.23	- 7.25	ol,gl	sp?
391	4.00	43	1.07	2	1125	12	OAD	NNO	o.13	- 9.29	ol,cpx,pl,sp,gl	
392	4.00	114	1.41	2	1125	8	OAD	NNO	0.16	- 9.19	ol,pl,sp,gl	cpx?
393	4.00	311	1.10	2	1125	6	OAD	NNO	0.09	- 9.43	ol,pl,sp,gl	
401	4.10	43	1.20	2	1100	18	OAD	NNO	0.16	- 9.53	ol,cpx,pl,sp,gl	
402	4.10	114	1.49	2	1100	18	OAD	NNO	0.18	- 9.47	ol,pl,sp,gl	cpx?

Run No	Time hrs min	Comp	% H_2O In melt	P Kbar	T °C	Crystals %	FGC	Buffer	a_{H_2O}	-log fo_2 bars	Phases	Notes
403	4.10	311	1.09	2	1100	14	OAD	NNO	0.09	- 9.76	ol,cpx,pl,sp,gl	
411	2.25	43	1.08	4	1250	2	OAD	NNO	0.07	- 8.03	ol,sp,gl	
422	4.10	311	3.00	2	1125	6	GN+W	NNO	0.45	- 8.75		Buffer dry
431	4.20	43	2.98	2	1125	12	GN+W	NNO	0.58	- 8.64	ol,cpx,pl,sp,gl	
432	4.20	114	2.99	2	1125	10	GN+W	NNO	0.50	- 8.71	ol,pl,sp,gl	cpx?
433	4.20	311	2.99	2	1125	8	GN+W	NNO	0.44	- 8.76	ol,pl,sp,gl	
441	3.40	43	3.00	2	1150	10	GN+W	NNO	0.58	- 8.33		Sample capsule failed
442	3.40	114	2.99	2	1150	8	GN+W	NNO	0.49	- 8.40	ol,sp,gl	
443	3.40	311	2.99	2	1150	4	GN+W	NNO	0.44	- 8.45	ol,sp,gl	Fe analysis
451	4.00	43	1.07	2	1150	14	GN	NNO	0.13	- 8.99	ol,cpx,sp,gl	1300° for 20 mins
452	4.00	114	1.35	2	1150	10	GN	NNO	0.15	- 8.91	ol,sp	"
471	3.45	313D	2.96	2	1150	0	GN+W	NNO	0.44	- 8.45	gl	1200° for 30 mins
472	3.45	313D	5.09	2	1150	0	GN+W	NNO	0.88	- 8.15	gl	"
473	3.45	311	5.00	2	1150	0	GN+W	NNO	0.83	- 8.17	gl	"
481	4.30	311	4.97	2	1125	2	GN+W	NNO	0.82	- 8.49	ol,sp,gl	1175° for 30 mins
482	4.30	313D	2.93	2	1125	0	GN+W	NNO	0.44	- 8.76	gl	"
483	4.30	313D	4.98	2	1125	0	GN+W	NNO	0.84	- 8.48	gl	"
491	4.40	311	4.97	2	1100	4	GN+W	NNO	0.82	- 8.82	ol,sp,gl	1150° for 30 mins
492	4.40	313D	2.94	2	1100	0	GN+W	NNO	0.45	- 9.08	gl	"
493	4.40	313D	4.95	2	1100	0	GN+W	NNO	0.83	- 8.81	gl	"
501	5.00	311	4.91	2	1075	8	GN+W	NNO	0.80	- 9.16	ol,sp,gl	"
502	5.00	313D	2.98	2	1075	2	GN+W	NNO	o.46	- 9.40	cpx,gl	"
503	5.00	313D	4.96	2	1075	0	GN+W	NNO	0.83	- 9.13	gl	"
511	5.30	311	5.01	2	1050	15	GN+W	NNO	0.83	- 9.49	ol,cpx,sp,gl	"
512	5.30	313D	2.98	2	1050	5	GN+W	NNO	0.47	- 9.74	ol,cpx,gl	"

Run No	Time hrs min	Comp	% H_2O In melt	P Kbar	T °C	Crystals %	FGC	Buffer	a_{H_2O}	-log fo_2 bars	Phases	Notes
513	5.30	313D	4.96	2	1050	2	GN+W	NNO	0.83	- 9.49	cpx,gl	1150° for 30 mins
521	6.00	311	4.99	2	1025	20	GN+W	NNO	0.81	- 9.87	ol,cpx,pl,sp,gl	"
522	6.00	313D	3.00	2	1025	12	GN+W	NNO	0.47	-10.10	ol,cpx,pl,gl	"
523	6.00	313D	4.95	2	1025	4	GN+W	NNO	0.83	- 9.86	ol,cpx,sp,gl	" Opaque sp
531	6.30	313D	2.91	2	1000	20	GN+W	NNO	0.45	-10.50	ol,cpx,pl,gl	1100° for 30 mins
532	6.30	313D	4.92	2	1000	14	GN+W	NNO	0.82	-10.24	ol,cpx,sp,gl	"
541	6.30	313D	4.96	2	975	18	GN+W	NNO	0.82	-10.63	cpx,pl,amph,sp,gl	"
551	5.00	313D	3.03	2	1050	15	GN+W	NNO	0.48	- 9.73	ol,cpx,pl,gl	
552	5.00	311	4.93	2	1050	15	GN+W	NNO	0.80	- 9.51	ol,cpx,pl,sp,gl	
561	4.40	313D	2.89	2	1050	15	GN+W	HM	0.45	- 4.97	ol,cpx,pl,sp,gl	
571	4.30	311	2.99	2	1100	12	GN+W	NNO	0.45	- 9.08	ol,pl,sp,gl	
591	3.45	311	4.97	2	1150	0	GN+W	HM	0.83	- 3.40	ol,sp,gl	Close to liquidus
601	4.30	311	4.94	2	1125	2	GN+W	HM	0.81	- 3.73	ol,sp,gl	1150° for 20 mins
611	4.20	311	4.98	2	1100	4	GN+W	HM	0.82	- 4.03	ol,sp,gl	
612	4.20	313D	2.97	2	1100	0	GN+W	HM	0.46	- 4.29	sp,gl	
613	4.20	313D	4.96	2	1100	0	GN+W	HM	0.84	- 4.02	sp,gl	
621	4.15	43	1.00	2	1150	12	GN	NNO	0.11	- 9.04	ol,cpx,pl,sp,gl	
622	4.15	6264	1.00	2	1150	0	GN	HM	0.08	- 4.37	gl	
623	4.15	6264	2.96	2	1150	0	GN+W	HM	0.46	- 3.66	gl	
631	6.40	6264	1.07	2	1125	10	GN	**	0.10	**	cpx,pl,gl	
632	6.40	6264	2.99	2	1125	0	GN+W	**	0.47	**	gl	
641	7.30	6264	1.17	2	1100	25	GN	**	0.11	**	ol,cpx,pl,gl	
642	7.30	6264	3.06	2	1100	10	GN+W	**	0.49	**	cpx,pl,gl	
651	9.00	6264	0.93	2	1075	35	GN	**	0.08	**	ol,cpx,pl,sp,gl	
652	9.00	6264	2.94	2	1075	25	GN+W	**	0.47	**	ol,cpx,pl,gl	

Run No	Time hrs min	Comp	% H_2O In melt	P Kbar	T °C	Crystals %	FGC	Buffer	a_{H_2O}	-log fo_2 bars	Phases	Notes
653	9.00	6264	4.47	2	1075	15	GN+W	**	0.75	**	cpx	
661	8.30	6264	3.99	2	1100	6	GN+W	**	0.66	**	cpx,gl	
662	8.30	6264	4.99	2	1100	0	GN+W	**	0.87	**	gl	
671	10.10	6264	2.90	2	1112	0	GN+W	**	0.46	**	gl	
672	10.10	6264	3.98	2	1112	0	GN+W	**	0.65	**	gl	
673	10.10	6264	4.98	2	1112	0	GN+W	**	0.87	**	gl	
681	5*	6264	3.16	2	1087	20	GN+W	**	0.51	**	cpx,pl,gl	
682	5*	6264	4.03	2	1087	10	GN+W	**	0.67	**	cpx,pl,gl	
683	5*	6264	5.01	2	1087	5	GN+W	**	0.88	**	cpx,gl	
691	10.30	6264	2.97	2	1062	40	GN+W	**	0.48	**	ol,cpx,pl,sp,gl	
692	10.30	6264	3.95	2	1062	30	GN+W	**	0.66	**	cpx,pl,gl	
693	10.30	6264	5.03	2	1062	25	GN+W	**	0.88	**	cpx,gl	
701	11.05	6264	3.97	2	1050	35	GN+W	**	0.66	**	ol,cpx,pl,sp,gl	
702	11.05	6264	5.03	2	1050	30	GN+W	**	0.88	**	cpx,pl,sp,gl	
711	6.00	6264	1.03	4	1150	5	GN	**	0.06	**	cpx,pl,gl	
721	7.10	6264	0.99	4	1125	15	GN	**	0.06	**	cpx,pl,gl	
722	7.10	6264	3.06	4	1125	5	GN+W	**	0.33	**	cpx,gl	
723	7.10	6264	3.98	4	1125	0	GN+W	**	0.45	**	gl	
731	6.55	6264	3.04	4	1100	20	GN+W	**	0.33	**	cpx,pl,gl	
732	6.55	6264	4.06	4	1100	10	GN+W	**	0.46	**	cpx,gl	
733	6.55	6264	4.93	4	1100	3	GN+W	**	0.59	**	cpx,gl	
741	8.00	6264	3.12	4	1075	30	GN+W	**	0.35	**	cpx,pl,gl	
742	8.00	6264	4.00	4	1075	20	GN+W	**	0.46	**	cpx,gl	
743	8.00	6264	4.87	4	1075	15	GN+W	**	0.57	**	cpx,gl	
751	12.50	6264	3.04	4	1050	35	GN+W	**	0.34	**	cpx,pl,gl	

Run No	Time hrs min	Comp	% H_2O In melt	P Kbar	T °C	Crystals %	FGC	Buffer	a_{H_2O}	-log fo_2 bars	Phase	Notes
752	12.50	6264	3.84	4	1050	25	GN+W	**	0.44	**	cpx,pl,gl	
753	12.50	6264	4.84	4	1050	20	GN+W	**	0.57	**	cox,pl,gl	
761	8.20	6264	0.99	4	1175	0	GN	**	0.06	**	gl	
771	8.25	6264	2.99	4	1150	0	GN+W	**	0.32	**	gl	
781	8.40	6264	4.98	4	1125	0	GN+W	**	0.60	**	gl	
791	8.20	313D	3.01	4	1100	2	GN+W	**	0.32	**	cpx,gl	
792	8.20	313D	4.04	4	1100	0	GN+W	**	0.45	**	gl	
801	9.15	313D	3.02	4	1075	10	GN+W	**	0.32	**	cpx,pl,gl	
802	9.15	313D	4.06	4	1075	3	GN+W	**	0.46	**	cpx,gl	
803	9.15	313D	4.99	4	1075	1	GN+W	**	0.57	**	cpx,gl	Close to liquidus
811	20.30	313D	3.00	4	1050	15	GN+W	**	0.32	**	cpx,pl,gl	
812	20.30	313D	4.00	4	1050	10	GN+W	**	0.45	**	cpx,pl,gl	
813	20.30	313D	4.97	4	1050	5	GN+W	**	0.57	**	cpx,gl	
821	25.05	313D	3.15	4	1025	20	OAD	**	0.34	**	ol,cpx,pl,gl	
822	25.05	313D	4.00	4	1025	15	GN+W	**	0.45	**	cpx,gl	
823	25.05	313D	4.49	4	1025	10	GN+W	**	0.50	**	cpx,gl	
831	24.00	313D	3.15	4	1000	22	OAD	**	0.34	**	ol,cpx,pl,amph,gl	
832	24.00	313D	3.92	4	1000	16	GN+W	**	0.44	**	cpx,pl,amph,gl	
833	24.00	313D	4.97	4	1000	10	GN+W	**	0.57	**	cpx,pl,amph,gl	
841	8.40	313D	3.77	2	1000	16	GN+W	NNO	0.62	-10.35	ol,cpx,gl	1075° for 30 mins
851	10.00	313D	4.00	2	987	18	GN+W	NNO	0.65	-10.54	ol,cpx,gl	"
861	7.00	313D	3.93	2	875	20	GN+W	NNO	0.63	-10.74	ol,cpx,pl,gl	"
871	6.20	311	4.92	2	1075	8	GN+W	NNO	0.80	- 9.16	ol,sp,gl	
881	8.40	313D	4.03	2	1000	20	GN+W	NNO	0.65	-10.34	ol,cpx,pl,gl	
882	8.40	313D	4.91	2	1000	15	GN+W	NNO	0.82	-10.24	ol,cpx,pl,gl	
891	13.15	313D	5.77	2	1000		W	NNO	1.00	-10.22	cpx,gl	

Run No.	Time hrs min	Comp	% H_2O In melt	P Kbar	T °C	Crystals %	FGC	Buffer	a_{H_2O}	-log fo_2 bars	Phases	Notes
901	13.15	313D	5.79	2	975		W	NNO	1.00	-10.62	cpx,amph,pl,sp,gl	
911	24.36	313D	5.88	4	1025	8	GN+W	**	0.71	**	cpx,gl	
912	24.35	313D	6.92	4	1025	5	GN+W	**	0.84	**	cpx,gl	
921	24.35	313D	6.01	4	1000	10	GN+W	**	0.73	**	cpx,gl	
922	24.35	313D	6.75	4	1000	8	GN+W	**	0.82	**	cpx,gl	

Note: Run 68 switched off by cooling water failure at between 3 and 7 hours

the high-temperature runs required 10 mm internal diameter Mo-wound furnaces. Ford (1972) found that the sharply-crested thermal profile of Mo-wound furnaces resulted in steeper thermal gradients than in the Kanthal-wound type. This was partially overcome in this study by spacing the furnace windings more closely at the ends of the sample container and further apart at its centre. Temperatures in the Mo-wound furnaces were measured by two thermocouples spaced 8-10 mm apart, the shorter thermocouple being positioned approximately 4 mm from the base of the sample container and the longer one near the centre. Of 22 runs in this furnace assembly, 55% showed temperature differences between the thermocouples of less than 3°C, 91% showed differences of less than 7°C, and the remaining two, runs 29 and 38, showed differences of 14°C and 11°C respectively. These data indicate that approximately 90% of runs in the Mo-wound furnaces involve a temperature uncertainty of less than ±10°C.

Temperature scales were calibrated prior to this study on the melting points of sodium chloride and gold (Ford, 1972).

C.3 Containers and iron exchange

2 mm internal diameter platinum-iron alloy sample containers (Ford, 1972) were used in this study. The distribution of iron through the capsule wall, as shown by microprobe studies of sectioned capsules, is not uniform after the capsule preparation, but longer soaking times in preparation lead to the tubing becoming brittle and unworkable. The microprobe analyses also show variation in the alloy composition along the capsule. Average capsule iron contents are given in Table C.2, from determinations by microprobe 10 microns in from the capsule surface.

Total iron contents of selected charges were determined by a colourimetric method (Graham and Saunders, 1978), and by electron

Table C2

Iron contents of capsules used

batch	mix	$\%H_2$ in gas	wt. % Fe
4	3:1	2.0	7.1
5	3:1	1.5	2.5
6	2:1	1.8	5.7
7	3:1	3.0	6.5
8	5:1	11.5	9.5
9	5:1	21.0	11.7
10	5:1	5.0	7.1
11	5:1	7.5	6.7
12	5:1	3.0	5.9
13	5:1	5.0	6.7
14	5:1	12.5	not analysed
15	5:1	8.0	"
16	5:1	10.0	"
17	5:1	10.0	"
18	5:1	9.5	"
19	5:1	9.5	"

mix = weight ratio of fired sodium metasilicate to magnetite

$\%H_2$ = percentage H_2 in CO_2-H_2 gas mix in furnace

microprobe analysis (all-glass charges only). Results are listed in Table C.3. Some variation in the amounts of iron exchange in these runs is believed to result from the variability in the iron distribution in the capsule walls, and from small variations in the weight ratio of capsule to charge. The amounts of iron exchange nevertheless represent a considerable improvement on those to be expected from use of platinum containers. The data in Table C.4 demonstrate the excellent reproducability and the accuracy of the colourimetric iron determinations.

Synthetic buffer assemblages were enclosed in 3 mm internal diameter Pt tubing. All capsules were tested for leaks prior to loading into the furnaces by immersion in a silicone oil bath at 110°-120°C for 10 seconds. Because of weight changes due to reaction with the NNO and HM buffers, the sample capsules could not be checked for weight changes after runs. Integrity of the sample capsule was therefore determined by audible escape of vapour on opening and/or consistency of experimental results. Buffered sample capsules which had ruptured were always found to contain very abundant quench amphibole crystals.

C.4 Control of melt water contents

C.4.1 Method

It is possible to calculate the weight percent of water dissolved in the melt phase in the experiments by carrying out all runs in the presence of a vapour phase. In order to produce vapour-present, water-undersaturated conditions, the water must be diluted in the vapour by the presence of another volatile component - in this case CO_2 or a mixture of CO_2 and N_2.

The following parameters must be known to calculate the melt water content: P, T, % crystals in the charge, weights of starting materials,

Table C3

Colourimetric determination of total iron in experimental charges

SAMPLE	WT. %H_2O approx.	CAPSULE batch	%Fe	T (^oC)	RUN TIME hrs. min.	Fe_2O_3	AVERAGE OF	INITIAL Fe_2O_3 (XRF)
413	4	6	5.7	1200	24.00	8.96	4	10.06
413	4	7	6.5	1300	24.00	10.36	2	10.06
413	4	6	5.7	1300	24.00	10.10	2	10.06
262	4	7	6.5	1200	24.00	8.99	4	10.11
43	1	7	6.5	1200	1.40	9.43	1	10.25
311	1	7	6.5	1200	1.40	6.62	1	8.03
43	3	7	6.5	1175	2.00	9.50	1	10.25
43	3	10	7.1	1275	1.35	8.71	1	10.25
114	1	10	7.1	1250	1.45	10.04	1	10.05
114	3	10	7.1	1275	1.45	10.72	1	10.05
114	3	8	9.5	1175	2.05	11.35	1	10.05
43	1	11	6.7	1125	3.00	10.02	1	10.25
114	1	10	7.1	1275	2.00	8.98	1	10.05
311	3	12	5.9	1150	3.40	6.73	1	8.03

Table C3

Determination of total iron in all-glass charges by electron microprobe

SAMPLE	WT. %H_2O approx.	CAPSULE batch	T (^oC)	RUN TIME hrs.min.	FeO*	AVERAGE OF	INITIAL FeO* (XRF)
6264	1	16	1150	4.15	9.38	5	9.80
"	3	16	1150	4.15	10.05	5	"
"	3	16	1125	6.40	9.37	5	"
"	3	18	1112	10.10	10.76	3	"
"	4	18	1112	10.10	9.70	1	"
"	4	18	1125	7.10	11.66	4	"
"	3	19	1175	8.20	6.96	3	"
"	4	19	1150	8.25	9.47	3	"
"	5	19	1125	8.40	9.33	3	"

FeO* = total iron calculated as FeO

Table C4

Reproducability of colourimetric total iron determinations

Sample 262 run in capsule batch 7 for 24 hours at 1200°C

weight % Fe_2O_3	8.98
	8.90
	9.06
	9.01
	8.82

413 rock powder		265 rock powder
10.03	weight % Fe_2O_3	7.68
10.03		7.57
10.03		7.51

Accuracy of colourimetric total iron determinations

USGS Standard BCR-1

weight % Fe_2O_3	13.36	13.52 (Abbey, 1977)
	13.29	
	13.28	

their water contents, and the effective molecular weight of the melt. The last of these parameters is necessary to extrapolate the albite-water molecular solubility model of Burnham and Davis (1971, 1974) into the complex natural system. It is calculated according to the rules laid down by Burnham (1979), who has demonstrated (Burnham, 1975, 1979) that the albite-water data are applicable to a wide range of natural magma compositions.

Burnham and Davis (1971) derived a numerical expression for partial molar volume of water in albite melt which can be applied to the relationship:

$$\mu_{H_2O} - \mu^{o}_{H_2O} = \int_{P^o}^{P} \bar{V}^{melt}_{H_2O} = RT \ln (f^{melt}_{H_2O} / f^{o\ melt}_{H_2O}).$$

where $\mu^{o\ melt}_{H_2O}$ is the chemical potential of water in albite melt at a reference state pressure P^o.

This relationship can, as Burnham and Davis (1974) described, be applied to lower melt water contents than those at which reliable solubility data exist by using the fugacity rather than the chemical potential, since

$$f^{melt}_{H_2O} = \text{constant} \times (X^{melt}_{H_2O})^2 \text{ for } X^{melt}_{H_2O} < 0.5.$$

A convenient reference state can be calculated, for the temperature and water mole fraction of interest, from the albite water solubility surface in P-T-X_{H_2O} space, because $f^{melt}_{H_2O} = f^{o}_{H_2O}$ at saturation. Values for $f^{o}_{H_2O}$ at the reference state pressure can be obtained from the expression of Holloway et al. (1971), the solubility of albite in the vapour being negligible under the conditions of interest here (Clark, 1966).

The fugacity (and activity) of water in the vapour phase can be calculated from the mole fraction of water in the vapour, assuming some mixing model for the fluid species. Equation of activities (or fugacities

at the same standard state) then allows calculation of the melt water content. The vapour phase was generated by the breakdown of the fluid-generating compounds oxalic acid dihydrate (OAD) and guanidine nitrate (GN), described by Holloway and Reese (1974), together with deionised water. A third-order polynomial surface was fitted to the albite-water solubility data of Burnham and Jahns (1962), Orlova (1962) and Khitarov et al. (1963) and incorporated into a computer program which calculates the proportions of rock powder, FGC, and water required to produce a chosen melt water content. The routine is listed in Table C.5.

It is necessary to know the amount of water added to the charge as combined H_2O in the dried rock powder. All starting compositions were therefore analysed for water after drying at 110°C. Samples were ignited with a lead oxide-lead chromate flux, in a silica tube through which nitrogen was passed. The nitrogen was dried prior to entering the tube by passing over magnesium perchlorate, and the evolved water from the sample removed from the nitrogen in another tube of the same substance. This tube was weighed, and the weights corrected for blanks to determine the water content of the sample. Results are given in Table C6, together with an analysis of USGS standard PCC-1, from which it can be seen that both reproducability and accuracy of the method are good.

It is also necessary to know the percentage of crystals in the charge during the run since, in the absence of hydrous phases, the solid fraction of the charge contains no water. Examination of fragments of the charge in reflected light was not considered to be a reliable method of estimating the crystallinity, since primary and quench crystals were often difficult to distinguish, and the proportion of primary crystals was often very variable between fragments. A least-squares method of determining the mode of the charge was not feasible in most cases because

Table C5

```
      SUBROUTINE AMGFUG
C     THIS ROUTINE CALCULATES MELT-VAPOUR EQUILIBRIA FOR
C     FLUID GENERATING COMPOUNDS BY EQUATING FUGACITIES OF
C     H2O IN THESE PHASES USING EXPRESSIONS FROM BURNHAM & DAVIS
C     (1974) AND A POLYNOMIAL SURFACE FITTED TO THE SOLUBILITY
C     DATA FOR ALBITE-H2O
      DIMENSION WG(3),WF(3),Y(3,3),CP(2)
      DATA WG/18.02,44.01,28.02/,WF/126.07,195.89,122.11/,Y/2,2,0,0,2,
     *  0,1,1,2/
      CALL FPRMPT('M. WT ON 8(O):',14)
      CALL RDR(WR)
      CALL FPRMPT('ROCK WT% H2O:',13)
      CALL RDR(WC)
      CALL FPRMPT('MG WATER ADDED:',15)
      CALL RDR(WA)
      CALL FPRMPT('%CRYSTALLINITY:',15)
      CALL RDI(IXN)
      CALL RDI(IXX)
      CALL FPRMPT('MELT H2O REQD:',14)
      CALL RDR(XW)
      CALL FPRMPT('PRESSURE:',9)
      CALL RDR(PN)
      CALL RDR(PX)
      CALL FPRMPT('TEMP(C):',9)
      CALL RDI(LN)
      TN=FLOAT(LN)
      CALL RDI(LX)
      TX=FLOAT(LX)
      CALL FPRMPT('COMPOUND USED:',14)
      CALL RDI(M)
      IF(M.GT.1)GO TO 3
      WRITE(6,100)
  100 FORMAT('1','H2O FROM OXALIC ACID DIHYDRATE')
      GO TO 5
    3 IF(M.GT.2) GO TO 4
      WRITE(6,150)
  150 FORMAT('1','H2O FROM SILVER OXALATE + WATER')
      GO TO 5
    4 WRITE(6,200)
  200 FORMAT('1','H2O FROM GUANIDINE NITRATE')
    5 WRITE(6,300) WR,WC,WA
  300 FORMAT(' ',' MOLECULAR WT. OF ROCK ON 8(O) BASIS= ',F6.2,/,
     *' WT.%H2O IN ROCK= ',F4.2,/,' MG WATER ADDED= ',F4.2)
C     CALCULATE MOLE FRACTION H2O IN MELT
      A=XW/WG(1)
      B=(100-XW)/WR
      XM=A/(A+B)
      IFLAG=0
C     SET MOLE FRACTION TO 0.400 IF LESS
      XR=XM
      IF(XM.GE..400) GO TO 10
      IFLAG=1
      XM=.400
   10 P=PN
      IXT=IXN
      T=TN
      DO 45 IN=1,10
      IF(IXT.GT.IXX) GO TO 50
      DO 40 I=1,50
      IF(P.GT.PX) GO TO 42
      WRITE(6,400) P,IXT,XW
  400 FORMAT('0',4X,'PRESSURE(KBARS)',F4.2,8X,'%CRYSTALLINITY',I4,8X,
     *'WT% H2O IN MELT',F3.1,/,/,10X,'TEMPERATURE (C)',13X,'H2O FUGA
     *CITY (KBARS)',12X,'F(H2O) IN MELT (KBARS)',12X,'WT OF COMPOUND
     *(MG)')
      DO 30 J=1,30
      IF(T.GT.TX) GO TO 35
      TR=T/1000.
C     FIND REFERENCE STATE PRESSURE FROM POLYNOMIAL SURFACE FOR
C     H2O SOLUBILITY IN ALBITE MELTS
      PR=-19.383+46.039*TR+43.070*XM+2.5387*TR*TR-219.03*TR*XM+112.67*X
     *  M*XM-14.668*TR**3+96.209*TR*TR*XM+25.757*TR*XM*XM-59.419*XM**3
C     EVALUATE CHEMICAL POTENTIAL INTEGRAL
      TK=T+273.16
```

```
      DO 15 N=1,2
      IF(N.EQ.2) GO TO 13
      A=P
      GO TO 14
   13 A=PR
   14 CP(N)=A*(.21855E+3+.8807E-1*TK+.2792E-3*TK*TK-.4756E-7*TK**3+
     *  A*(.146-.2324E-1*TK-.1888E-5*TK*TK)+A*A*(.373+.9113E-3*TK)-.02
     *  366*A**3)
   15 CONTINUE
      CS=CP(1)-CP(2)
C     CALCULATE FUGACITY OF H2O IN MELT
      PRB=1000.*PR
      CALL FFIND(PRB,T,FPR)
      E=CS/(1.987*TK)
      FW=FPR*EXP(E)
C     INTERPOLATE FOR MOLE FRACTION LESS THAN 0.400
      IF(IFLAG.NE.1) GO TO 20
      FW=FW*XR**2/XM**2
   20 PB=1000.*P
      CALL FFIND(PB,T,F)
      IF(FW.GT.F) GO TO 21
C     CALCULATE FUGACITY OF H2O IN VAPOUR
C     MOLES H2O FROM ROCK AND COMPOUND
      A=10.*WC/(100.*WG(1))+WA/WG(1)
C     MOLES H2O IN MELT
      C=0.1*XR*(100.-WC)*(100.-IXT)/(100.*WR*(1.-XR))
C     SOLVE FOR WEIGHT OF COMPOUND
      R=Y(2,M)+Y(3,M)
      S=(R*FW/F-Y(1,M)*(1.-FW/F))/(WF(M)*(1.-FW/F))
      W=(A-C)/S
      GO TO 22
   21 W=0.0
   22 L=IFIX(T)
      WRITE(6,500) L,F,FW,W
  500 FORMAT(' ',13X,I4,26X,F5.3,26X,F5.3,26X,F6.3)
      T=T+25.
   30 CONTINUE
   35 P=P+1.0
      T=TN
   40 CONTINUE
   42 IXT=IXT+5
      P=PN
   45 CONTINUE
   50 RETURN
      END
```

```
      SUBROUTINE FFIND (P,T,F)
C     CALCULATES THE FUGACITY OF H2O AS A FUNCTION OF T IN
C     HUNDREDS OF DEGS. C AND THE NATURAL LOG OF P IN BARS.
C     FUGACITY IS EXPRESSED IN KILOBARS
C     THE FUGACITY SURFACE IS BASED ON DATA FROM BURNHAM ET AL.
C     G.S.A. SPECIAL PAPER 132 (1969) & EXTRAPOLATIONS OF ENTROPY
C     AS DESCRIBED IN TEXT.
      DIMENSION ASUR(10,10),BSUR(7,7)
C     INITIALISE DATA FOR EQUATION 1A
      DATA ASUR/.2404363E+3,.40251743E+2,-.20492157E+2,.51978665E+1,-.
     *  45593073E+0,.18603499E-1,.69041712E-3,-.29348712E-3,.10133819
     *  E-4,-.11850884E-6,-.20399566E+3,.44413768E+0,.73369812E+0,-.1
     *  434373E+1,.17967607E+0,-.16068242E-1,.13651886E-2,.12268376E-
     *  4,-.47178569E-6,0.0E+0,.56354153E+2,-.14172324E+1,.19960306E+
     *  1,-.69877588E-1,.2076289E-2,.51592538E-3,-.21844329E-3,.80842
     *  913E-6,2*0.0,-.51933662E+1,-.65394046E+0,-.28011093E+0,.38709
     *  756E-1,-.40077198E-2,.26448622E-3,.80581407E-5,3*0.0,-.221369
     *  9E+0,.17945226E+0,-.10991622E-1,-.40929613E-3,.22780769E-3,-.
     *  17277994E-4,4*0.0,.43084433E-1,-.46564539E-2,.29055971E-2,-.2
     *  8066826E-3,.14476891E-5,5*0.0,.58575071E-2,-.16183106E-2,-.451
     *  11259E-4,.11821168E-4,6*0.0,-.13645878E-2,.12647929E-3,-.42861
     *  278E-5,7*0.0,.94066685E-4,-.22137638E-5,8*0.0,-.23475399E-5,9*
     *  0.0/
C     INITIALISE DATA FOR EQUATION 1B
      DATA BSUR/-.58941754E+3,.25601052E+3,-.34136353E+2,.2461294E+1,-
     *  .13672236E+0,.47382371E-2,-.73301562E-4,.92181745E+2,-.7364193
     *  7E+2,.76739565E+1,-.19824998E+0,.22493531E-2,.49567134E-5,0.0,
     *  .2776936E+2,.85962024E+1,-.11019954E+1,.19699329E-1,-.160326E-
     *  3,2*0.0,-.9946835E+1,-.89458899E-1,.68578768E-1,-.56455773E-3,
     *  3*0.0,.11108507E+1,-.42131257E-1,-.16246151E-2,4*0.0,-.5194721
     *  6E-1,.19724351E-2,5*0.0,.81845377E-3,6*0.0/
```

```
      C     TRANSFORM P TO LN(P) & T TO 0.01*T
            XP=ALOG(P)
            XT=T*0.01
      C     CALCULATE FUGACITY AT T,P
            F=0.0
      C     CHECK T FOR EQ. 1A OR 1B. USE 1B IF T>950 DEG C
            IF(T.GT.950.0) GO TO 3
            NI=10
            DO 2 J=1,10
            JJ=J-1
            DO 1 I=1,NI
            II=I-1
          1 F=F+ASUR(I,J)*XT**II*XP**JJ
          2 NI=NI-1
            F=EXP(F)/1000.0
            GO TO 7
          3 NI=7
            DO 5 J=1,7
            JJ=J-1
            DO 4 I=1,NI
            II=I-1
          4 F=F+BSUR(I,J)*XT**II*XP**JJ
          5 NI=NI-1
            F=EXP(F)/1000.0
          7 RETURN
            END
```

Table C6

Determination of water (H_2O+) in starting materials

composition	weight % H_2O+
43	0.42
	0.36
114	0.71
	0.76
311	0.32
	0.35
313D	0.43
	0.43
6264	0.40
	0.42
	0.47

USGS PCC-1	4.66

(value quoted by Abbey (1977) is 4.64)

of the quench modification of liquid compositions, and therefore crystallinity was estimated visually from the crushed charge. Although this produces only an approximate crystallinity for the charge, the calculation of water content is not particularly sensitive to this parameter at the degrees of crystallisation considered in this study, as shown in the following section, and this procedure is not believed to introduce substantial errors.

In the same way that the weights of starting materials can be calculated for a desired melt water content, the computation can be reversed to calculate the water content of any melt given the weights of starting materials, allowing correction of original estimates of crystallinity, pressure and temperature. The routine for this calculation is listed in Table C.7.

C.4.2 Errors in the calculations

A possibly significant error could be introduced into the calculations by deviation of the OAD from its stoichiometric formula. The water content of the batch of OAD used was therefore determined, in collaboration with C. M. Graham. A weighed amount of OAD was equilibrated in a large capsule at approximately 750°C and 1 kbar and then extracted and pierced under vaccuum in the hydrogen extraction line at S.U.R.R.C., East Kilbride. The water was frozen into a cold trap and then passed over hot uranium to convert it to hydrogen, the volume of which was measured in a calibrated manometer. The results showed one mole of OAD to contain excess water, so that its breakdown produces 2.19 rather than 2 moles of water.

Errors in calculated melt water contents will arise from uncertainties in the input parameters to the computer routines, and the effects of these are shown in Table C.8. Pressures and temperatures are taken as ± 100 bars and ± 15°C respectively, while weights are

Table C7

```
      SUBROUTINE AMGWET
C      THIS ROUTINE CALCULATES MELT WATER CONTENTS IN WATER
C      UNDERSATURATED RUNS USING BURNHAM MODEL, WITH RUN
C      CONTENTS LOADED ACCORDING TO 'GASFUG' CALCULATIONS.
C         INPUT DATA (FREE FORMAT) AS: RUN NO.,P(KBAR),T(C),%
C      CRYSTALS,F.G. COMPOUND CODE,ROCK WT,ESTIMATED WT.% H2O
C      WT. OF ROCK,ROCK WT.% H2O,WT. OF H2O, WT. OF F.G.C.,
C      BUFFER CODE (NNO=1,HM=2,UNBUFFERED=0).
C       RUN NO.,%CRYSTALS,FGC CODE, BUFFER CODE ARE INTEGER,OTHERS REAL
C      TERMINATE DATA SET BY NEGATIVE RUN NO.
      DIMENSION WG(3),WF(3),Y(3,3),CP(2)
      DATA WG/16.02,44.01,28.02/,WF/129.50,195.89,122.11/,Y/2.19,2,0,0,
     *  2,0,1,1,2/
      WRITE(6,1000)
    5 CALL RDI(IRUN)
      IF(IRUN.LT.0) GO TO 500
      CALL RDR(P)
      CALL RDR(T)
      CALL RDI(IXT)
      CALL RDI(M)
      CALL RDR(WR)
      CALL RDR(XW)
      CALL RDR(RW)
      CALL RDR(WC)
      CALL RDR(WW)
      CALL RDR(CW)
      CALL RDI(IBUF)
      IFLAG=0
      IORD=1
      XWIN=XW
C     CALCULATE MOLE FRACTION H2O IN MELT
   10 A=XW/WG(1)
      B=(100-XW)/WR
      XM=A/(A+B)
      IFLAG=0
C     SET MOLE FRACTION TO 0.400 IF LESS
      XR=XM
      IF(XM.GE..400) GO TO 12
      IFLAG=1
      XM=.400
   12 TR=T/1000.
C     FIND REFERENCE STATE PRESSURE FROM POLYNOMIAL SURFACE FOR
C     H2O SOLUBILITY IN ALBITE MELTS
      PR=-15.383+46.039*TR+43.070*XM+2.5387*TR*TR-219.03*TR*XM+112.67*X
     *  M*XM-14.668*TR**3+96.209*TR*TR*XM+25.757*TR*XM*XM-55.419*XM**3
C     EVALUATE CHEMICAL POTENTIAL INTEGRAL
      TK=T+273.16
      DO 15 N=1,2
      IF(N.EQ.2) GO TO 13
      A=P
      GO TO 14
   13 A=PR
   14 CP(N)=A*(.21855E+3+.8807E-1*TK+.2792E-3*TK*TK-.4756E-7*TK**3+
     *  A*(.146-.2324E-1*TK-.1888E-5*TK*TK)+A*A*(.373+.9113E-3*TK)-.02
     *  366*A**3)
   15 CONTINUE
      CS=CP(1)-CP(2)
C     CALCULATE FUGACITY OF H2O IN MELT
      PRB=1000.*PR
      CALL FFIND(PRB,T,FPR)
      E=CS/(1.987*TK)
      FW=FPR*EXP(E)
C     INTERPOLATE FOR MOLE FRACTION LESS THAN 0.400
      IF(IFLAG.NE.1) GO TO 20
      FW=FW*XR**2/XM**2
   20 PB=1000.*P
      CALL FFIND(PB,T,F)
      AH2O=FW/F
C     MOLES H2O AVAILABLE
      A=(RW*WC/100.+WW)/WG(1)+CW*Y(1,M)/WF(M)
C     MOLES H2O IN MELT
      C=RW/WR*XR*(100-IXT)/100/(1-XR)
C     CALCULATE FH2O IN VAPOUR PHASE
      VAPM=(Y(2,M)+Y(3,M))*CW/WF(M)
      FH2OV=(A-C)*F/(A-C+VAPM)
      IF(FH2OV.GT.FW) GO TO 70
```

```
      IF(IFLAG2) 55,52,53
   52 IFLAG2=-1
      GO TO 55
   53 IFLAG2=-1
      IORD=IORD+1
   55 XW=XW-1./10.**IORD
      GO TO 80
   70 IF(IFLAG2) 72,73,75
   72 IFLAG2=1
      IORD=IORD+1
      GO TO 75
   73 IFLAG2=1
   75 XW=XW+1./10.**IORD
   80 IF(IORD.EQ.4) GO TO 100
      GO TO 10
  100 IF(IBUF.EQ.0) GO TO 150
      IF(IBUF.EQ.2) GO TO 110
      FO2=9.36-24930./TK+0.046*(987.17*P-1)/TK
      GO TO 120
  110 FO2=13.966-24634./TK+0.019*(987.17*P-1)/TK
  120 FO2=FO2+ALOG10(AH2O)
      GO TO 200
  150 FO2=1000.
  200 WRITE(6,1020) IRUN,P,T,XWIN,IXT,XW,AH2O,FO2
      GO TO 5
  500 RETURN
 1000 FORMAT('1',10X,'RUN NO.',7X,'P (KBAR)',6X,'T (DEG C)',6X,
     *  'NOMINAL % H2O',3X,'% CRYSTALS',4X,'REAL % H2O',7X,
     *  'A(H2O)',9X,'LOG (FO2)')
 1020 FORMAT('0',12X,I3,11X,F3.1,11X,F6.1,11X,F4.1,11X,I2,11X,F5.2,11X,
     *  F4.2,11X,F6.2)
      END
```

Table C8 Effects of uncertainties in input parameters on calculated melt water contents

Run 811

P kbar	T °C	%crystals	mol. wt. of rock	wt. of rock mg.	rock $\%H_2O$	wt. of H_2O mg.	wt. of FGC mg.	$\%H_2O$ in melt wt.
4.0	1050	15	308.1	13.855	0.43	0.420	1.830	3.00
3.9	1050	15	308.1	13.855	0.43	0.420	1.830	2.97
4.0	1035	15	308.1	13.855	0.43	0.420	1.830	3.01
4.0	1050	25	308.1	13.855	0.43	0.420	1.830	3.12
4.0	1050	15	328.1	13.855	0.43	0.420	1.830	2.88
4.0	1050	15	308.1	13.875	0.43	0.420	1.830	3.00
4.0	1050	15	308.1	13.855	0.40	0.420	1.830	2.99
4.0	1050	15	308.1	13.855	0.43	0.430	1.830	3.03
4.0	1050	15	308.1	13.855	0.43	0.420	1.840	3.00

believed to be accurate to better than 0.01 mg. Effective molecular weights may be in error because of an uncertainty in the X.R.F. data, but this is very small. The dominant uncertainty comes from the change in composition of the melt, and therefore of molecular weight, at increasing degrees of crystallisation. However, the change in molecular weight considered in Table C.8 is greater than the difference between the molecular weights of samples 311, 313D, and 6264, so that the effect of this uncertainty on the calculations is small. The effective molecular weight changes at $X_{H_2O}^{melt} > 0.5$, but only the 6 and 7 percent water runs on sample 313D exceeded this limit and this will not have changes the effective molecular weight significantly.

More significant errors in the water contents may arise from assumptions made in the calculation method. It has been assumed that CO_2 and N_2 are insoluble in the melt phase. The results of Kesson and Holloway (1974) indicate that this is a reasonable assumption for N_2, but it is probable that CO_2 is slightly soluble, particularly in the more basic compositions 311, 114, and 43. Slight CO_2 solubility will lead to lower $X_{H_2O}^{fluid}$ values and therefore higher $X_{H_2O}^{melt}$ but, in the absence of published accurate determinations of CO_2 solubility in basaltic melts at low pressures, no correction can be made.

It has also been assumed that H_2O, CO_2, and N_2 mix ideally in the fluid phase. Calculations of activity coefficients in C-H-O fluid systems based on the modified Redlich-Kwong equation of state (MRK) (Holloway, 1976) indicate that such fluids are close to ideality at low pressures and high temperatures. It was therefore assumed that CO_2 and H_2O mix ideally (i.e. $a_{H_2O} = X_{H_2O}$) and, in view of the lack of evidence to the contrary, that this is also the case for N_2-bearing fluids.

Recently published data on activity coefficients in H_2O-CO_2 fluids

(Kadik and Eggler, 1979) indicate that these fluids deviate substantially from ideality under the experimental conditions of this study. These data, derived from experiments in the system albite-H_2O-CO_2, show decreasing values of the activity coefficient γ_{H_2O} with increasing $X_{H_2O}^{fluid}$, and are not in good agreement with the coefficients calculated from the MRK. They therefore suggest that the melt water contents calculated in this study are too low. The differences between the ideal and non-ideal cases will depend on $\gamma_{H_2O}^{fluid}$, which is not precisely known, and on the melt:fluid ratio in the charge, but selected examples in Table C.9 show that the differences can be substantial. However, in view of the lack of agreement on the values of γ_{H_2O} in H_2O-CO_2 fluids, and the lack of data with which to check MRK-based calculations for the N_2-bearing system, it was decided to retain the ideal mixing assumption. The possible underestimation of melt water contents will not affect the conclusions reached in Chapter 5.

Table C9

Effects of non-ideal mixing in the fluid phase on calculated melt water contents

Run no.	P	T	nominal $\%H_2O$	calculated $\%H_2O$ ideal	calculated $\%H_2O$ non-ideal
313	2.0	1150	1.0	1.11	1.16
811	4.0	1050	3.0	3.00	4.24

Activity coefficients estimated from 3kbar data of Eggler and Kadik (1979).

APPENDIX D

LIST OF SAMPLES STUDIED

1. ANALYSED LAVAS

Number	Centre	Description	Grid Ref.
6073	SW	C-series basalt; reworked volcs., Prickly Pt.	11593N 61457W
6078	MMM	M-series basalt; flow NE of Beausejour	12061N 61451W
6103	SEM	M-series basalt; block in river, Birch Grove	12068N 61404W
6104	SEM	C-series basalt; " " " "	
6127	MSC	C-series basalt; block from flow, Crayfish	12302N 61413W
6155	MGF	C-series basalt; flow W of Marigot	12077N 61450W
6157	MGF	M-series basalt; flow at road SW of Concord	12070N 61447W
6158	MGF	C-series basalt; flow SW of Grand Roy	12078N 61450W
6177	MGF	C-series basalt; loose block, Concord Valley	12070N 61433W
6186	SW	M-series basalt; flow, L'Anse aux Epines	12006N 61453W
6252	MGF	M-series basalt; flow SE of Belvidere	12076N 61410W
6256	MSC	M-series basalt; flow, Riviere Sallee	12120N 61368W
6257	MMM	M-series basalt; block from flow, Vendome	12049N 61427W
6259	MMM	M-series basalt; flow, Mount Gay	12037N 61446W
6264	MMM	C-series basalt; block from flow, Fontenoy	12046N 61452W
U.W.I. specimens			
X28024	MMM	M-series basalt; lava flow, Vendome	12049N 61426W
X28035	RS	M-series basalt; scoria fall, Lake Antoine	12112N 61369W
X28054	MGF	Evolved lava; flow, Brisant	12061N 61453W
X28070	MMM	Evolved lava; block in reworked, Constantine	12048N 61432W
X28071	SEM	C-series basalt; flow E of St. James	12068N 61395W
X28072	RS	C-series basalt; scoria fall, Pilot Hill	12075N 61374W

Details of all other samples analysed are to be found in Arculus (1973)

Centres:
- SW southwest Grenada
- MMM Mt. Maitland - Mt. Moritz
- SEM South East Mountain
- MSC Mt. St. Catherine
- MGF Mt. Granby - Fedon's Camp
- RS Recent Scoria

2. ANALYSED CUMULATES

Number	Type	Occurrence	Grid Ref.
6051	B	In reworked volcanics, Prickly Point	11593N 61457W
6065	B	"	"
6066	B	"	"
6067	A	"	"
6070	A	"	"
6087	D	In reworked volcanics, road at Dothan	12082N 61447W
6091	B	"	"
6094	C	"	"
6099	A-D (composite)	"	"
6102	A	"	"
6105	B	Loose block in river, Birch Grove	12068N 61404W
6107	B	"	"
6135	E	Loose block in river, Upper Concord Valley	12070N 61433W
6136	D	"	"
6159	D	Nodule in andesite clast, reworked volcs., Dothan	12082N 61447W
6163	D	In reworked volcanics, road at Dothan	"
6165	A	"	"
6166	D	"	"
6167	C	"	"
6168	C	"	"
6249	B	Loose block in river, Birch Grove	12068N 61404W
U.W.I. specimens			
X28150A	B	?In reworked volcanics, SE of Corinth	12019N 61406W
X28150B	D	"	"
X28150C	D	"	"
X28155	B	" , N of Calivigny	12015N 61435W
X28158	B	" , Morne Jaloux	12018N 61436W
X28406	C	In reworked volcanics, road at Dothan	12082N 61447W

3. OTHER CUMULATES STUDIED

Number	Type	Occurrence	Grid Ref.
6018	A	In mudflow, West Base	12004N 61464W
6019	B	"	"
6023	D	"	"
6042	F	In reworked volcanics, Prickly Point	11593N 61457W
6044	ol-cpx mesocumulate	"	"
6045	A	"	"
6048	A	"	"
6050	B	"	"
6052	B	"	"
6054	D	"	"
6056	D	"	"
6058	B	"	"
6060	D	"	"
6068	D	"	"
6072	B	"	"
6081	G	In reworked volcanics, road at Dothan	12082N 61447W
6085	F	"	"
6088	D	"	"
6089	D	"	"
6092	D	"	"
6093	D	"	"
6096	D	"	"
6097	D	"	"
6098	amph-cpx mesocumulate	"	"
6101	B	"	"
6106	D	Loose block in river, Birch Grove	12068N 61404W
6138	amph-cpx mesocumulate	Loose block in river, Upper Concord Valley	12070N 61433W
6140	D	"	"
6142	D	"	"
6144	F	"	"
6154	B	In mudflow, Calivigny Estate	12011N 61432W
6160	B	In reworked volcanics, road at Dothan	12082N 61447W
6162	D	"	"
6164	D	"	"
6174	A	"	"

3. (continued)

Number	Type	Occurrence	Grid Ref.
6210	D	In ?mudflow, Kendace Point, Carriacou	12776N 61261W
6211	D	"	"
6212	D	"	"
6213	D	"	"
6215	D	"	"
6222	B	In ?mudflow, Point Cistern, Carriacou	12286N 61299W
6225	G	"	"
6227	D	"	"
6228	D	"	"
6229	D	"	"
6248	D	Loose block in river, Birch Grove	12068N 61404W
6250	D	"	"

4. PERIDOTITE NODULES

Number	Occurrence	Grid Ref.
6122	In microphyric, M-series basalt scoria, Grenville	12073N 61374W
6123	"	"
6231 to 6243 (incl.)	"	"